



# Exploration at the high-energy frontier: ATLAS Run 2 searches investigating the exotic jungle beyond the Standard Model

The ATLAS Collaboration

The Large Hadron Collider is at the high-energy frontier of particle physics, having produced proton–proton collisions during Run 2, from 2015 to 2018, at an unprecedented centre-of-mass energy of 13 TeV. The ATLAS experiment has a broad programme to thoroughly explore this uncharted territory, to seek out new exotic particles predicted by theories that boldly go beyond the Standard Model. Although the Standard Model has been very successful, it leaves many questions unanswered, prompting novel ideas about particles that could be hiding in the data, waiting to be discovered by intrepid explorers. These include dark-matter candidates, hidden-sector particles, new vector resonances, leptoquarks, and vector-like quarks, to name a few examples. Searches for new particles are reported here, with the exception of searches for supersymmetry or extended Higgs sectors as these are the subjects of separate reports.

# Contents

<b>1</b>	<b>Introduction</b>	<b>3</b>
<b>2</b>	<b>Tools and methods</b>	<b>3</b>
2.1	The ATLAS detector	3
2.2	Data and Monte Carlo samples	4
2.3	Object reconstruction and identification	5
2.4	Useful kinematic variables	7
2.5	Analysis strategy	8
2.6	Statistical interpretation	9
<b>3</b>	<b>Compositeness</b>	<b>9</b>
3.1	Excited quarks	10
3.2	Excited leptons	11
<b>4</b>	<b>Additional vector bosons</b>	<b>12</b>
4.1	Resonant searches	12
4.2	Contact interactions	22
<b>5</b>	<b>Additional leptons</b>	<b>23</b>
5.1	Type-I seesaw	23
5.2	Left–right symmetric model	24
5.3	Type-III seesaw	26
<b>6</b>	<b>Vector-like lepton and quarks</b>	<b>28</b>
6.1	Vector-like leptons	28
6.2	Vector-like quarks	29
<b>7</b>	<b>Leptoquarks</b>	<b>39</b>
7.1	Searches for LQs with exclusive third-generation couplings	40
7.2	Searches for LQs with cross-generational couplings	44
<b>8</b>	<b>Charged-lepton flavour violation</b>	<b>49</b>
8.1	Lepton flavour violation in $Z$ boson decay	50
8.2	Lepton flavour violation in the decay of a heavy $Z'$	51
<b>9</b>	<b>Hidden sectors leading to long-lived neutral particles</b>	<b>52</b>
9.1	Search for dark-photon jets	52
9.2	Searches for long-lived scalars or pseudoscalars in the decay of a Higgs-like boson	54
<b>10</b>	<b>Dark-matter candidates</b>	<b>57</b>
10.1	Vector or axial-vector portal	58
10.2	Vector portal with a dark Higgs boson	60
10.3	Higgs portal	61
10.4	Pseudoscalar portal	65
10.5	Comparison with direct-detection experiments	71
10.6	Strongly coupled hidden sector	74

<b>11 Long-lived multi-charged or highly ionizing particles</b>	<b>75</b>
<b>12 Extra dimensions, gravitons and quantum black holes</b>	<b>77</b>
12.1 Gravitons in the ADD and RS scenarios	77
12.2 Gravitons in the clockwork gravity model	79
12.3 Quantum black holes	81
<b>13 Summary and conclusions</b>	<b>81</b>

## 1 Introduction

The Large Hadron Collider (LHC) [1] at CERN stands at the forefront of particle physics investigation, providing a wealth of collision data and unprecedented centre-of-mass energy. During Run 2, from 2015 to 2018,  $140 \text{ fb}^{-1}$  of  $\sqrt{s} = 13 \text{ TeV}$  proton–proton collision data were collected by the ATLAS experiment. These data were thoroughly scrutinized by the ATLAS Collaboration to search for hints of physics beyond the Standard Model (SM).

While describing a vast amount of data with excellent precision, the SM leaves many questions open. Answers to these can be sought in the data, and this report considers the following. Are the known fermions really fundamental or are they composed of even smaller constituents? Could there be new vector bosons? Are the tiny masses of the neutrinos simply due to seemingly unnaturally small Yukawa couplings, or are they explained by mechanisms involving additional heavy neutral leptons? Why are there three families of leptons and quarks – could there be new vector-like fermions or even leptoquarks? Could there be entire sectors that are ‘dark’, with new particles hidden from the interactions of the SM and which interact with it only through a heavy or feebly coupled mediator? Is dark matter a particle from such a dark sector? Could there be particles that are even more exotic, e.g. highly charged particles or magnetic monopoles? And why is the gravitational coupling so small compared to the electroweak scale – could it be an artefact of extra dimensions which have not yet been observed?

After a section introducing the common methods and tools used in the analyses, this report covers each of the questions above in a dedicated section, showing how the ATLAS Collaboration analysed the Run 2 data in its quest for answers. Besides these searches for exotic phenomena, searches for supersymmetry or additional Higgs bosons, as well as precision measurements of SM particles and their interactions, have also been pursued and are reviewed in other reports.

## 2 Tools and methods

### 2.1 The ATLAS detector

The ATLAS detector [2] at the LHC covers nearly the entire solid angle around the collision point.<sup>1</sup> It consists of an inner tracking detector surrounded by a thin superconducting solenoid, electromagnetic and

---

<sup>1</sup> ATLAS uses a right-handed coordinate system with its origin at the nominal interaction point (IP) in the center of the detector and the  $z$ -axis along the beam pipe. The  $x$ -axis points from the IP to the center of the LHC ring, and the  $y$ -axis points upwards. Polar coordinates  $(r, \phi)$  are used in the transverse plane,  $\phi$  being the azimuthal angle around the  $z$ -axis. The pseudorapidity is defined in terms of the polar angle  $\theta$  as  $\eta = -\ln \tan(\theta/2)$ . Angular distance is measured in units of  $\Delta R \equiv \sqrt{(\Delta\eta)^2 + (\Delta\phi)^2}$ .

hadron calorimeters, and a muon spectrometer incorporating three large superconducting air-core toroidal magnets.

The inner-detector system (ID) is immersed in a 2 T axial magnetic field and provides charged-particle tracking in the range  $|\eta| < 2.5$ . The high-granularity silicon pixel detector covers the vertex region and typically provides four measurements per track, the first hit normally being in the insertable B-layer (IBL) installed before Run 2 [3, 4]. It is followed by the silicon microstrip tracker (SCT), which usually provides eight measurements per track. These silicon detectors are complemented by the transition radiation tracker (TRT) which is made of straws filled with a Xenon- or Argon-gas-based mixture and which enables radially extended track reconstruction up to  $|\eta| = 2.0$ . The TRT also provides electron identification information based on the fraction of hits (typically 30 in total) above a higher energy-deposit threshold corresponding to transition radiation.

The calorimeter system covers the pseudorapidity range  $|\eta| < 4.9$ . Within the region  $|\eta| < 3.2$ , electromagnetic calorimetry is provided by barrel and endcap high-granularity lead/liquid-argon (LAr) calorimeters, with an additional thin LAr presampler covering  $|\eta| < 1.8$  to correct for energy loss in material upstream of the calorimeters. Hadron calorimetry is provided by the steel/scintillator-tile calorimeter, segmented into three barrel structures within  $|\eta| < 1.7$ , and two copper/LAr hadron endcap calorimeters. The solid angle coverage is completed with forward copper/LAr and tungsten/LAr calorimeter modules optimized for electromagnetic and hadronic energy measurements respectively.

Surrounding the calorimeter system is the muon spectrometer (MS), which comprises separate trigger and high-precision tracking chambers measuring the deflection of muons in a magnetic field generated by the superconducting air-core toroidal magnets. The field integral of the toroids ranges between 2.0 and 6.0 T m across most of the detector. Three layers of precision chambers, each consisting of layers of monitored drift tubes (MDT), cover the region  $|\eta| < 2.7$ , complemented by cathode-strip chambers (CST) in the forward region, where the background is highest. The muon trigger system covers the range  $|\eta| < 2.4$  with resistive-plate chambers (RPC) in the barrel, and thin-gap chambers (TGC) in the endcap regions.

Interesting events are selected by the first-level trigger system implemented in custom hardware, followed by selections made by algorithms implemented in software in the high-level trigger [5]. The first-level trigger accepts events from the 40 MHz bunch crossings at a rate below 100 kHz, which the high-level trigger further reduces in order to record events to disk at about 1 kHz.

An extensive software suite [6] is used in data simulation, in the reconstruction and analysis of real and simulated data, in detector operations, and in the trigger and data acquisition systems of the experiment.

## 2.2 Data and Monte Carlo samples

The analyses described in this report, when not specified otherwise, are based on the full Run 2 dataset collected by ATLAS between 2015 and 2018. The data sample is selected by requiring good conditions for the beams and the ATLAS detector and corresponds to an integrated luminosity of  $140.1 \pm 1.2 \text{ fb}^{-1}$  [7], with some analyses included in this report using a preliminary value of  $139.0 \pm 2.4 \text{ fb}^{-1}$  [8]. Various triggers are used to select the data, depending on the analysis. For example, the lowest unpre-scaled-trigger thresholds during Run 2 were at a  $p_T$  of 420 GeV for a single small- $R$  jet [9], 140 GeV for a single photon [10], and varied between 20 and 26 GeV for a single electron or muon [11], while the lowest unpre-scaled-trigger threshold for missing transverse momentum varied between 70 and 110 GeV [12].



Monte Carlo (MC) samples, which are used to model signal and background events, were produced using a variety of generators, depending on the process of interest. For the signal samples, unless specified, the generator used was either PYTHIA 8 [13, 14], MADGRAPH5\_AMC@NLO [15] or POWHEG BOX v2 [16–18], with PYTHIA 8 being used in all cases to model the parton shower, hadronization and underlying event. The decays of  $b$ - and  $c$ -hadrons were performed consistently with the EVTGEN 1.2.0 decay package [19], except for processes modelled using SHERPA [20]. To account for additional proton–proton interactions (pile-up) in the same and neighbouring bunch crossings, a number of inelastic  $pp$  interactions, generated with PYTHIA 8.186 using the NNPDF2.3LO PDF set [21] and the ATLAS A3 set of tuned parameters [22], were superimposed on the hard-scattering events. The simulated events were weighted so that the distributions of the average number of collisions per bunch crossing in simulation match those in data. The generated MC samples were passed through either a full ATLAS detector simulation [23] using GEANT4 [24] or a fast simulation which relies on a parameterization of the calorimeter response [25]. The simulated events were weighted so that the distributions of the average number of collisions per bunch crossing in simulation match those in data and are processed with the same reconstruction algorithms as data.

### 2.3 Object reconstruction and identification

Various algorithms are used to reconstruct the objects in the events. They were improved during Run 2, bringing better identification efficiency, background rejection, measurement accuracy or precision. Object reconstruction algorithms used in most analyses discussed in this report are reviewed briefly here.

#### Tracks

Track reconstruction [26, 27] in the inner detector is seeded from combinations of hits found in the pixel and SCT detectors. These seeds are used to initiate a search for additional hits along the track candidate’s trajectory in an iterative procedure using a Kalman filter. Since hits can be shared by multiple tracks, an ambiguity-resolving step then follows, and the remaining tracks are then extrapolated to the TRT detector to form an ‘inside-out’ track collection. An ‘outside-in’ reconstruction is also available, which instead extrapolates TRT track segments back into the silicon detectors, using silicon hits that were not selected by the inside-out algorithm. Tracks are required to have a transverse momentum  $p_T > 0.5$  GeV,  $|\eta| < 2.5$ , and an origin compatible with the interaction region, ensured by imposing constraints on their transverse ( $d_0$ ) and longitudinal ( $z_0$ ) impact parameters. They must also satisfy good-quality criteria related to their number of silicon hits (or missing silicon hits, when some hits are expected but not seen along their trajectory). This algorithm is not efficient in reconstructing tracks from the highly displaced vertices predicted in some models of exotic long-lived particles. A dedicated large-radius tracking (LRT) algorithm is employed in these cases: it uses as inputs the hits omitted by standard tracking algorithms and imposes looser requirements, notably on  $d_0$  and  $z_0$  [28].

#### Vertices

From the collision vertices, whose iterative-reconstruction seed positions are based on the beam spot position and which are reconstructed from at least two tracks, the primary vertex [29] is selected as the one with the highest  $\Sigma p_T^2$  of the associated tracks. Analysed events are required to possess a primary vertex (PV).

#### Jets

Jets, made of collimated showers of hadrons, are reconstructed in the detector by using algorithms that seek to identify them by clustering together different types of inputs. Input constituents considered in jet reconstruction can be inner-detector tracks, calorimeter energy deposits, or a combination of

these. The calorimeter energy-deposit inputs are called topological clusters; they are formed as groups of contiguous calorimeter cells with an energy deposit significantly above the noise level [30]. The algorithm most commonly used by ATLAS in Run 2 is the particle-flow algorithm, which exploits both types of constituents [31]: to improve the accuracy of the charged-hadron measurement, this algorithm computes their momenta from inner-tracker information only, and retains the calorimeter energy-deposit measurements for the determination of neutral-particle energies. These constituents are in turn grouped into jets using the anti- $k_t$  algorithm [32, 33] with either a small ( $R = 0.4$ ) or large ( $R = 1.0$ ) radius parameter value. While the small- $R$  jets are commonly used by analyses concerned with quark- and gluon-initiated jets, large- $R$  jets are usually considered for so-called boosted topologies, where the decay products of a  $W/Z/H$  boson or a top quark are collimated. The jets' energies and directions are then corrected by a calibration procedure [34]. In special cases, a variable- $R$  algorithm [35] is also employed, in which the radius parameter's value depends on the  $p_T$  of the constituents being clustered. A different type of jet is used in some analyses to take advantage of boosted topologies without having to explicitly reconstruct large- $R$  jets from low-level inputs. They are called reclustered jets and are constructed by the anti- $k_t$  algorithm, using small- $R$  jets as inputs.

Jets compatible with noise bursts, beam-induced background or cosmic rays are usually discarded [36], and to reduce the effect of pile-up interactions, a jet-vertex-tagger (JVT) algorithm is usually applied to track information to select jets originating from the PV [37].

### ***b*-tagged jets**

Jets originating from  $b$ -quarks can be tagged by exploiting the long lifetime of  $b$ -hadrons. A multivariate algorithm [38–40] is used, based on the impact parameters of displaced tracks and the properties of vertices in the jets. Operating points are defined for different targeted efficiencies as measured in simulated  $t\bar{t}$  samples.

### **Large- $R$ jet tagging**

Jets originating from heavy resonances (top,  $W$ ,  $Z$  or  $H$ ) decaying into hadrons can be identified as such by using a variety of techniques based on substructure information. In the case of top-tagging, a deep neural network (DNN) [41] that uses a large number of jet-substructure variables as input is often employed, with operating points defined similarly to those for  $b$ -tagged jets.

### **Photons**

Photons can reach the calorimeters directly or convert into  $e^+e^-$  in the material composing the detector. They are reconstructed [42] from clusters of energy deposits in the electromagnetic calorimeter, along with information from inner-detector tracks which is used to classify them either as converted, if the cluster is matched to a reconstructed conversion vertex, or as unconverted, if there is no match between the cluster and a conversion vertex or an electron track. Based on observables which reflect the shape of the electromagnetic shower in the calorimeter, loose or tight identification criteria are used to separate the photon candidates from background. Isolation criteria based on calorimeter and/or inner-detector information are also applied to avoid contamination such as from neutral-hadron decays into almost-collinear photon pairs.

### **Electrons**

Electrons are reconstructed by matching a cluster of energy deposits in the electromagnetic calorimeter to an inner-detector track which is identified as originating from the primary vertex via impact parameter selections [43]. Loose, medium or tight identification criteria based, for example, on the cluster's shape are applied depending on the desired levels of purity and background rejection [42].

### **Muons**

Muon reconstruction is usually based on the presence of a PV-compatible inner-detector track that is

matched to a track reconstructed in the muon spectrometer. The two tracks are combined to better determine the muon kinematics [44]. Identification criteria are applied, with their tightness depending on the targeted signal-to-background ratio.

For both electrons and muons, a veto is usually imposed on the nearby presence of additional significant calorimeter energy deposits and/or tracking activity: these isolation selections aim to remove non-prompt leptons coming, for example, from heavy-flavour decays.

### **Tau leptons**

Hadronically decaying  $\tau$ -leptons ( $\tau_{\text{had}}$ ) are reconstructed from energy clusters in the calorimeters that are matched to inner-detector tracks [45–47], according to any of five categories: one matched track with zero, one or more neutral particles; and three matched tracks with zero or more neutral particles. Selections are then made on the reconstructed electric charge of the  $\tau$ -lepton, which must have an absolute value of one, and on the output score of an identification algorithm based on a recurrent neural network [48]. Leptonically decaying  $\tau$ -leptons are usually identified as muons or electrons.

### **Missing transverse momentum**

The missing transverse momentum  $E_{\text{T}}^{\text{miss}}$  is defined as the magnitude of  $\mathbf{p}_{\text{T}}^{\text{miss}}$ , which is the negative vectorial sum of the transverse momenta of the objects identified in the event, including a so-called *soft term* which takes into account the remaining soft particle tracks from the PV which are not matched to any object [49]. When only a subset of objects is used and no soft term is added, the  $E_{\text{T}}^{\text{miss}}$  is denoted by  $H_{\text{T}}^{\text{miss}}$ .

The missing transverse momentum's significance,  $S_{E_{\text{T}}^{\text{miss}}}$ , is a variable which can be used to discriminate between the events in which the reconstructed  $E_{\text{T}}^{\text{miss}}$  originates from weakly interacting particles and the events in which the  $E_{\text{T}}^{\text{miss}}$  is consistent with resolution effects and inefficiencies in particle measurements. The value of  $S_{E_{\text{T}}^{\text{miss}}}$  can be approximated by  $E_{\text{T}}^{\text{miss}}/\sqrt{H_{\text{T}}}$  (event-level significance), where  $H_{\text{T}}$  is the scalar sum of the transverse momenta from all the reconstructed objects, or can be computed in a more detailed way (object-level significance) by considering the expected resolution and mismeasurement likelihood of all the objects that enter the  $E_{\text{T}}^{\text{miss}}$  reconstruction, as detailed in Ref. [50].

## **2.4 Useful kinematic variables**

Kinematic variables are used to increase the signal-to-background ratio or to preferentially select some types of backgrounds in order to study them in more detail. Some of them are used by multiple analyses discussed in this report and are therefore briefly described here.

### **Invariant masses**

The invariant mass of a two-body system,  $m_{XY}$  (where  $X$  and  $Y$  can be jets ( $j$ ),  $b$ -tagged jets ( $b$ ), top-quark candidates ( $t$ ), light charged leptons ( $\ell = e, \mu$ ) or photons ( $\gamma$ ), for example), is especially useful when resonances are expected. Since  $\tau$  decays involve at least one neutrino, the collinear approximation (which is well realized at large momenta) is normally used: the neutrinos produced in the  $\tau$  decays are assumed to travel in the same direction as the visible  $\tau$ -decay products and to be the only source of  $E_{\text{T}}^{\text{miss}}$ , providing information to estimate the  $p_{\text{T}}$  of the  $\tau$ -lepton and making it possible to compute a collinear invariant mass,  $m_{X\tau}^{\text{col}}$ . When reconstructing the mass of a resonance decaying into a pair of  $\tau$ -leptons, a technique called the missing mass calculator (MMC) [51] is sometimes used. This technique is based on the maximization of a likelihood that replaces the assumptions of the collinear approximation with a requirement that the decay products are consistent with the mass and decay kinematics of a  $\tau$ -lepton. This accurately reconstructs the mass of the original resonance without the limitations of the collinear approximation.

### Transverse masses

When part of the decay consists of  $E_T^{\text{miss}}$ , computing the transverse mass of the visible object  $X$  and the  $E_T^{\text{miss}}$  can be helpful:  $m_T(X, E_T^{\text{miss}}) = \sqrt{2p_T^X E_T^{\text{miss}} (1 - \cos \phi_{XE_T^{\text{miss}}})}$ . The  $m_T(\ell, E_T^{\text{miss}})$  variable can be particularly helpful in discriminating against the presence of a leptonically decaying  $W$  boson from  $W$ +jets or  $t\bar{t}$  background processes. The leptonic transverse mass,  $m_{T2}$  [52, 53], is instead based on two visible leptons and  $E_T^{\text{miss}}$ . It assumes that the leptons come from the two-body decay of a pair of identical particles into a visible one and an invisible one. For dileptonic  $t\bar{t}$  events, the  $m_{T2}$  distribution has an endpoint at the  $W$  boson mass, while higher values are expected for the signal. The leptonic asymmetric transverse mass [54, 55],  $am_{T2}$ , is a variation on  $m_{T2}$ , and is based on one lepton only and can be used to reduce the background from dileptonic  $t\bar{t}$  events in which one of the leptons is missed. The contranverse mass ( $m_{CT}$ ) [56] can also be used in the search for heavy pair-produced particles decaying semi-visibly and to reduce of the  $t\bar{t}$  background.

### Scalar sums of transverse momenta

The scalar sum of the transverse momenta of some objects (denoted by  $S_T^{\text{objects}}$  or  $H_T^{\text{objects}}$  below, with the objects considered specified) can also be useful in discriminating between more energetic signal events and the background. When this sum runs over all selected objects and also includes the  $E_T^{\text{miss}}$  value, it is called the effective mass,  $m_{\text{eff}}$ , because it would be correlated with the mass scale of the initially produced heavy ‘beyond the SM’ (BSM) particles whose decay would have led to the measured objects.

## 2.5 Analysis strategy

For each analysis, one or more signal regions (SRs) are defined by a set or sets of event selections that usually optimize the statistical significance of the signal relative to the expected background. A SR can be defined as a list of requirements on reconstructed objects or kinematic variables, or be based on the output of more sophisticated machine-learning algorithms taking these as inputs. Although machine-learning techniques have been used for quite some time in particle physics, their use has increased recently, helping to improve object tagging and signal event selection, as reviewed in Ref. [57]. Once a SR is defined, a reliable way to estimate the expected background along with its associated systematic uncertainties must be devised. Only when this full strategy is in place is the data in the SR unblinded to perform the actual search. There are several ways to estimate the background in a given SR, the choice of method depending on the process of interest and the expected associated uncertainties: using MC simulations only, which is often chosen for sources of background which are expected to contribute only a small proportion of the events in the SR; using MC simulations of events whose yields or distribution shapes are corrected to data in control regions (CRs), a selection of events orthogonal to the SR where a given type of background is enhanced relative to the others and the signal contribution is expected to be small; or in a fully data-driven way, especially useful for events whose simulation might be difficult or unreliable. Validation regions (VRs), which are selected to be close but orthogonal to both the SRs and CRs and should have small expected signal contributions, are also defined sometimes in order to validate the background estimation strategy prior to the unblinding. Some common data-driven background estimation methods used by multiple analyses presented in this report are described in more detail below.

If the signal is expected to peak over a smooth SM background distribution, such as in searches for narrow resonances in an invariant-mass distribution, the background in the SR can often be estimated directly, by fitting a parametric function to the data itself [58]. The functional form chosen for the fit of the background should minimize the number of free parameters while being flexible enough to minimize a *spurious signal*

(the number of signal events extracted from a signal-plus-background fit performed on a background-only distribution) and allowing a signal to be extracted if present.

Another data-driven technique is known as the ABCD (or 2D-sideband) method. In the most straightforward implementation of the ABCD method, the background in the targeted signal region, A, is estimated from the amounts of data in three contiguous control regions, B, C, and D. Regions B and D are each built by inverting one of the selection criteria used to define the signal region. In contrast, region C is built by inverting both of these criteria simultaneously. The method relies on the assumptions that the two criteria used in constructing the regions are uncorrelated for background events and that the signal contamination in the control regions is minor. If this is the case, then the background in the SR, A, can be predicted from the background-enriched regions via  $N_A = N_D \times N_B / N_C$ .

The contribution from *fake* objects in the SR, such as a jet being falsely reconstructed as a lepton, a  $\tau$ -lepton or a photon, can be evaluated in a fully data-driven way via two different methods: the matrix method and the fake-factor method [59]. In the matrix method, the numbers of targeted objects (e.g. leptons) in the SR passing the nominal identification or a loosened identification are counted separately. They are linked to the numbers of true or fake targeted objects by a matrix of the efficiencies for a true or fake object to satisfy the loosened or nominal criteria, which can be measured in dedicated data CRs. Inversion of this matrix can thus provide an estimate of the number of fake objects in the SR. In the fake-factor method, the probability of a fake object to pass the SR identification requirements, derived in a fake-enriched CR, is applied to events found in a region similar to the SR but in which the object identification requirements are relaxed.

## 2.6 Statistical interpretation

In order to test for the presence of new physics, templates for both the background and signal, obtained through MC simulations or data-driven methods, are compared with the data. Unless indicated otherwise, a binned maximum-likelihood fit is used, while the variable (or variables) being fitted depends on the specific analysis. Several regions may be fitted simultaneously, including the signal regions and control regions. Systematic uncertainties are included as nuisance parameters [60] with either log-normal or Gaussian constraints.

When no significant deviation from the expected background is observed in a search, constraints on various signal models that would produce an excess are extracted at 95% confidence level (CL) using the  $CL_s$  method [61] with a profile likelihood ratio as the test statistic. The asymptotic approximation to the test statistic's distribution is usually assumed [62] when extracting expected limits, except in cases where it is seen to fail (e.g. due to low statistical precision), in which case pseudo-experiments are generated.

## 3 Compositeness

In pursuit of the elementary constituents of matter, physicists since the late 1800s have delved into matter at progressively smaller scales, proving that what were at first deemed elementary, in turn atoms, nuclei and nucleons, were in fact composed of even smaller constituents. The SM currently considers, in line with the experimental results so far, that the leptons and quarks are indeed the elementary particles, but could their three generations be explained by yet smaller constituents? – i.e. could they too be composite? With the unprecedented centre-of-mass energy of the LHC, it is indeed possible to probe even smaller scales in order to see whether they have an internal structure. A tell-tale signature of compositeness would

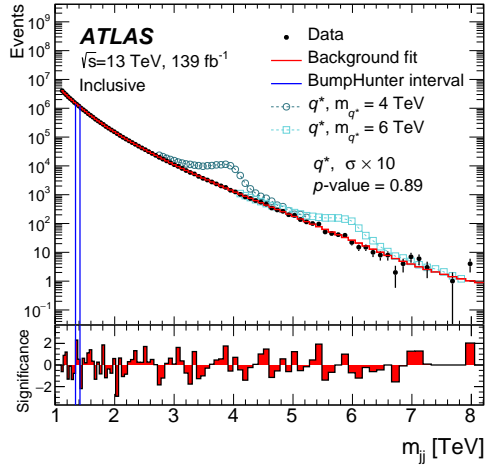


Figure 1: Distribution of  $m_{jj}$  in the inclusive search for excited quarks [64]. The vertical lines indicate the most discrepant  $m_{jj}$  interval identified, for which the  $p$ -value is stated in the figure. Two example  $q^*$  resonances are also shown, with an enhanced cross section for visibility.

be the existence of excited states at higher masses [63]. These excited states could be produced at the LHC through known gauge interactions (GI), for example the production of an excited quark  $q^*$  through a gluonic excitation  $qg \rightarrow q^*$ , or through a four-fermion contact interaction (CI), for example the production of an excited lepton  $\ell^*$  through  $q\bar{q} \rightarrow \ell^*$ . The decay of these excited states can proceed in similar ways: through a GI (e.g.  $q^* \rightarrow gq$ ,  $q^* \rightarrow \gamma q$  or  $\ell^* \rightarrow W\nu$ ), or through a CI (e.g.  $\ell^* \rightarrow q\bar{q}\ell$  or  $q^* \rightarrow q\bar{q}q$ ).

### 3.1 Excited quarks

The existence of a  $q^*$  in the GI model could be revealed by observing a resonance of the type  $q^* \rightarrow gq$  in the dijet invariant mass distribution, i.e. a peak above the smoothly falling QCD multijet background. A search for such excited quarks was performed [64] by scanning the  $m_{jj}$  distribution from 1.1 to 8 TeV. The lower bound on  $m_{jj}$  is motivated by the fact that the events must pass the trigger selection, which requires a single, high- $p_T$  small- $R$  jet, and that lower values of  $m_{q^*}$  were excluded in Run 1 [65] or by previous experiments [66]. Events are further selected by requiring two small- $R$  jets with  $p_T > 150$  GeV, separated by an azimuthal angle of at least  $\Delta\phi(j_1, j_2) = 1.0$  and a rapidity difference of at most  $y^* = (y_{j_1} - y_{j_2})/2 = 0.6$ . This selection was used to search inclusively for excited quarks, and a specific search for excited  $b$ -quarks was also performed. The latter also requires the presence of at least one  $b$ -tagged jet and imposes a  $|\eta| < 2.0$  requirement on each of the two jets, but allows  $y^*$  values up to 0.8.

The signal model assumes that the excited quarks are spin-1/2 particles, have the same couplings as SM quarks, and that the compositeness scale is  $m_{q^*}$ . Two scenarios are considered:  $q^*$  comprising both  $u^*$  and  $d^*$  or being only a  $b^*$ . The SM background is dominated by QCD multijet events and is estimated in each bin by fitting a parametric function of the type  $f(x) = p_1(1-x)^{p_2}x^{p_3+p_4 \ln x}$  in a sliding window over  $m_{jj}$ . The uncertainty in the fitted parameters is taken as a systematic uncertainty of the background estimation, along with an uncertainty concerning the choice of fitting function, and another related to the amount of spurious signal. The  $m_{jj}$  distribution is shown for the inclusive search in Figure 1 for the data and two examples of an excited quark signal.



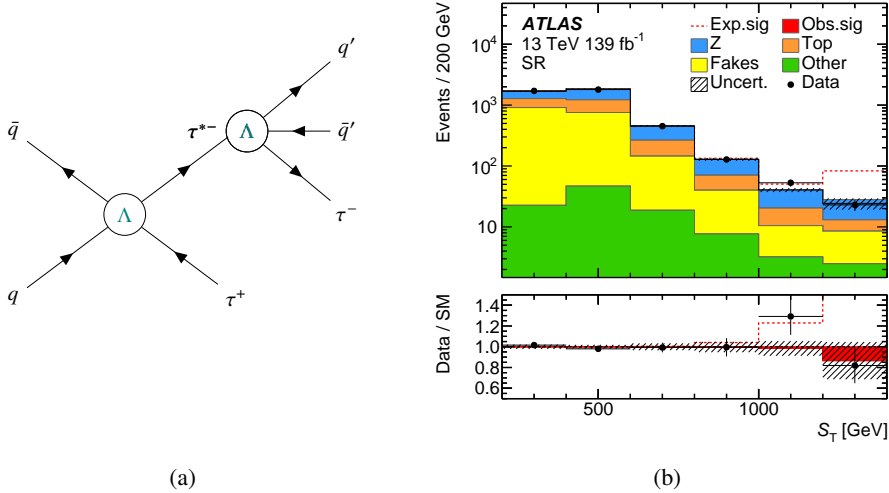


Figure 2: (a) Production and decay of an excited  $\tau$ -lepton via a contact interaction with a compositeness scale  $\Lambda$  and (b)  $S_T$  distribution in the signal region for data compared to the estimated background contribution with its uncertainty and an example signal ( $m_{\tau^*} = 1.5$  TeV,  $\Lambda = 10$  TeV) with a nominal signal strength (Exp.) and with the signal strength extracted from the fit to the data (Obs.) [69].

Since no significant excess is seen, a lower limit on the excited quark's mass is set at  $m_{q^*} = 6.7$  TeV in the inclusive search, while for the specific  $b^*$  search, the limit is set at 3.2 TeV. These correspond to compositeness length scales below  $3.0 \times 10^{-5}$  fm and  $6.2 \times 10^{-5}$  fm, respectively.

### 3.2 Excited leptons

Searches for excited electrons and muons have been performed by ATLAS, using a partial Run 2 dataset and the Run 1 dataset, respectively [67, 68]. A more recent addition is a search for excited  $\tau$ -leptons,  $\tau^*$ , assuming that they are produced and decay through a CI, as shown in Figure 2(a), leading to a final state comprising two  $\tau$ -leptons and two jets (the signal model includes all the quark flavours that are kinematically allowed). These four objects are used to compute an  $S_T$  value which is exploited in a search which focuses on hadronic  $\tau$  decays [69].

The analysis is based on a di- $\tau$  trigger. The SR requires the events to have exactly two  $\tau_{\text{had}}$  of opposite electric charge which are well separated in  $\Delta R$ . There must also be at least two small- $R$  jets with high  $p_T$  and no reconstructed electron or muon. The main background,  $Z(\rightarrow \tau\tau)$ +jets, is suppressed by requiring  $m_{\tau\tau}^{\text{col}} > 110$  GeV. For each  $\tau_{\text{had}}$ , the ratio of the visible-decay  $p_T$  to the total  $p_T$  is usually positive for signal, while it can become negative for fake  $\tau_{\text{had}}$  because now the  $E_T^{\text{miss}}$  points in a random direction; requiring this ratio to exceed a minimum value reduces the fake- $\tau_{\text{had}}$  background. Finally, the scalar sum of the  $p_T$  of the two  $\tau_{\text{had}}$ , denoted by  $L_T$ , is required to be larger than 140 GeV. The major remaining backgrounds are  $Z(\rightarrow \tau\tau)$ +jets,  $t\bar{t}$  and single-top events, and events with jets falsely reconstructed as  $\tau_{\text{had}}$ .

The  $Z(\rightarrow \tau\tau)$ +jets and top-related background yields are extracted using dedicated CRs. For the  $Z(\rightarrow \tau\tau)$ +jets background, the CR is built by requiring a  $Z$ -compatible  $m_{\tau\tau}^{\text{col}}$  and inverting the selection on  $L_T$ . For the top-related events, the CR requires one  $\tau_{\text{had}}$  with high  $p_T$  up to 450 GeV, along with at least

four jets amongst which two must be  $b$ -tagged, and a large  $E_T^{\text{miss}}$  to avoid fakes. Finally, the fake-factor method is used to estimate the fake background. The main sources of systematic uncertainty in the final background estimation are the top-related background modelling and the  $\tau$ -lepton energy scale.

As shown in Figure 2(b), good agreement between the data and the estimated background is observed in the SR. A lower limit is hence set on the excited  $\tau$ -lepton's compositeness scale. For  $\Lambda = m_{\tau^*}$ , the limit obtained is at 4.6 TeV.

## 4 Additional vector bosons

Multiple BSM theories predict the existence of new vector bosons, which are naturally predicted in theories with an extended gauge sector. A typical historical benchmark is the Sequential Standard Model (SSM) [70], in which the new  $Z'$  boson has the same fermion couplings as its SM counterpart: it can hence be searched for as a resonance in the invariant mass distribution of fermion pairs in a variety of leptonic and hadronic final states (the same can also apply to a new SSM  $W'$  boson). A  $Z'_\psi$  vector boson can also be predicted by an  $E_6$ -motivated Grand Unification model [71]. Other models predict  $Z'$  bosons which decay into top quarks with a large branching ratio, such as the colour-singlet boson predicted in the topcolour-assisted-technicolour model [72, 73], making the search for a resonance in the  $m_{tt}$  invariant mass spectrum particularly interesting. The  $Z'$  and  $W'$  can also be the nearly mass-degenerate heavy vector triplet (HVT) members of a new  $SU(2)$  gauge group [74]. This scenario includes a wider range of phenomena because the new bosons can decay into diboson final states. The SSM also appears as a particular benchmark within the HVT coupling space.

These resonances can be searched for in two-body final states or in production modes with other associated jets or leptons, or in the case of a new vector colouron [75] (a massive version of the gluon, predicted in gauge extensions of QCD), in a pair of dijet resonances. If the new vector boson's mass is higher than the  $pp$  collision centre-of-mass energy, its effects can still be seen and then interpreted in terms of contact interactions, which are the focus of other dedicated searches. All of these searches are reviewed in this section, and the limits set on the  $Z'$  and  $W'$  bosons are summarized in Table 1. Some other, specific models of new vector bosons are covered later: the left–right symmetric model in Section 5, lepton-flavour-violating  $Z'$  decays in Section 8, and a simplified model of dark-matter production through a  $Z'$ , in Section 10.

### 4.1 Resonant searches

#### 4.1.1 Two-body final states with quarks or leptons

The dijet resonance analysis discussed in Section 3.1 can also be used to search for either a SSM  $Z'$  or  $W'$ . A two- $b$ -tags channel is also defined for the  $Z'$  search, which differs from the previously described  $b^*$  search only by requiring one extra  $b$ -tagged jet. The best constraints on these models, however, come from the search in the leptonic final states described below, as shown in Table 1.

In the  $Z' \rightarrow \ell\ell$  search [76], where  $\ell = \{e, \mu\}$ , the  $m_{\ell\ell}$  spectrum above 225 GeV is probed after selecting events with at least two same-flavour (SF) leptons.<sup>2</sup> The muon channel also requires the two muons to be

<sup>2</sup> If more than two leptons of the same-flavour are found, the highest- $p_T$  ones are used. If both an  $ee$  pair and a  $\mu\mu$  pair are found, the  $ee$  pair is kept because it has better mass resolution and signal efficiency.



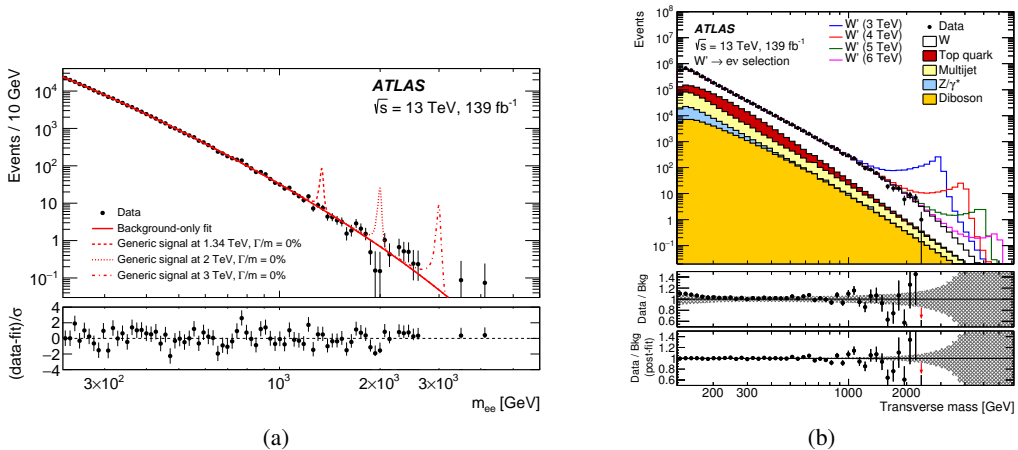


Figure 3: (a) Dielectron invariant mass spectrum used in the search for a  $Z'$  resonance [76] compared to the fitted background template and some generic signal examples, and (b) transverse mass of the electron- $E_T^{\text{miss}}$  system in the  $W'$  search [77] compared to the background expectation and example  $W'$  signals.

of opposite sign, a requirement which is not made in the electron channel because of the larger charge misidentification rate at high  $p_T$  and the fact that a wrong charge assignment in the electron channel would not impact the calorimetric measurement of the electron's momentum. The lower bound on  $m_{\ell\ell}$  is imposed to avoid the  $Z$  boson peak region, because the background estimate is (as in the dijet resonance search) obtained by fitting a functional form to the data in the SR, in this case  $f_{\ell\ell}(m_{\ell\ell}) = f_{\text{BW},Z}(m_{\ell\ell})(1-x^c)^b x^{\sum_{i=0}^3 p_i \log(x)^i}$ , where  $x = m_{\ell\ell}/\sqrt{s}$ ,  $b$  and  $p_i$  are free parameters with independent values for the  $ee$  and  $\mu\mu$  channels,  $c$  is fixed to 1 (for  $ee$ ) or  $1/3$  (for  $\mu\mu$ ), and  $f_{\text{BW},Z}(m_{\ell\ell})$  is a Breit–Wigner function with the mass and width of the  $Z$  boson. Uncertainties in the MC background modelling are propagated into the estimation of the spurious signal, which is taken as a systematic uncertainty of the background estimation. The distribution of  $m_{\ell\ell}$  in the electron channel data is compared with the background fit and some example signals in Figure 3(a). No significant deviation of the data from the background fit is observed. The same also applies to the muon channel, which is, however, slightly less sensitive due to poorer signal resolution.

In the  $W' \rightarrow \ell\nu$  search [77], the presence of exactly one electron or muon is required in the SR, along with a large value of  $E_T^{\text{miss}}$  and of  $m_T(\ell, E_T^{\text{miss}})$ , which is used as the final discriminating variable. The background is dominated by the Drell–Yan (DY) production of  $W$  bosons, but also contains some contributions from  $t\bar{t}$ , single-top, diboson,  $Z/\gamma^*$  and multijet processes. The backgrounds involving true leptons are evaluated using MC simulations; in the  $t\bar{t}$  and diboson cases, to compensate for the limited number of events at high  $m_T$ , the smoothly falling  $m_T$  distribution from the MC simulation is fitted using functional forms and extrapolated to high values. The contribution from fake leptons from multijet processes, more important in the electron channel, is evaluated with a matrix method. No significant deviation of the data from the fitted background's  $m_T$  spectrum is observed, neither in the electron channel (shown in Figure 3(b)) nor in the muon channel, whose sensitivity is, as in the  $Z'$  search, slightly worse than in the electron channel due to poorer resolution.

Analyses with  $\tau$ -leptons in the final state can be important in the search for new  $W'$  or  $Z'$  bosons and are particularly relevant in scenarios with enhanced third-generation couplings. A search for  $W' \rightarrow \tau\nu$  using the full Run 2 dataset was very recently made public [78]. The data agree with the expected background's

$m_T(\tau_{\text{had-vis}}, E_T^{\text{miss}})$  distribution within uncertainties, which are dominated by the number of data events for masses above 2 TeV. The search for a  $Z' \rightarrow \tau\tau$  has only been performed with a partial Run 2 dataset [79] recorded between 2015 and 2016.

Another analysis performs a generic search for simple two-body resonances and is based on anomaly detection techniques [80]. This approach considers resonances decaying into a pair of jets (which could be  $b$ -tagged) or a combination of one jet and one lepton (or photon). A simple preselection of events with at least one jet and at least one lepton is performed, and an unsupervised machine-learning method based on an autoencoder is used to find events with kinematic properties that are likely to be different from the bulk of preselected data events. A total of nine independent statistical analyses using different two-body invariant mass combinations are used to look for excesses above the SM background, which in each case is obtained using a parametric fit. No significant excess is found in any of the combinations, with the largest deviation being seen at a mass of 4.9 TeV when using the  $m_{j\mu}$  statistical analysis. The sensitivity of this search is poorer than in dedicated approaches but it remains interesting due to its very general, model-independent approach, which can guide more sensitive, dedicated searches.

#### 4.1.2 Diboson final states

Six searches in ATLAS consider final states with two bosons, and all of them can be interpreted in the context of additional vector gauge bosons, either  $Z'$  or  $W'$ . They can be classified into two subclasses with common characteristics: final states without ( $VV$ ) or with ( $VH$ ) Higgs bosons, where  $V$  is a  $W$  or  $Z$  boson. In addition to vector gauge bosons, several analyses in ATLAS look for scalar resonances in diboson final states such as  $H\gamma$ ,  $Z\gamma$  or  $ZZ$ ; these analyses are included in a different report.

The two  $VH$  searches consider a final state with a Higgs boson decaying into two  $b$ -quarks: a fully hadronic final state [81] and a leptons+jets final state [82].

The fully hadronic analysis considers events with no light leptons and two large- $R$  jets, well separated in rapidity. The leading (highest- $p_T$ ) jet is considered to be the Higgs candidate, while the subleading jet is considered to be the  $V$  boson candidate. Two independent channels are built, aimed at final states with either a  $W$  or a  $Z$  boson. The jets are identified (tagged) as coming from a Higgs,  $W$  or  $Z$  boson according to their mass, the number of tracks, and the  $D_2$  variable [83]. The latter is defined as a ratio of two-point to three-point energy correlation functions based on the jet's constituents and is expected to peak at values below one for heavy hadronic resonances. In each channel, events with one tagged candidate  $V$  boson and one tagged candidate  $H$  boson are categorized into SRs. Two independent categories are built in each channel according to the number (one or two) of  $b$ -tagged jets associated with the large- $R$  Higgs candidate jet. The invariant mass of the two large- $R$  jets is used in the statistical analyses. In both categories and in both channels, the background in the signal regions is obtained using a data-driven method. The initial template is obtained from a third category with no  $b$ -tagged jet associated with the Higgs candidate. The final template in the 1-tag and 2-tag categories is obtained using a combination of a multidimensional kinematic reweighting, based on a boosted decision tree (BDT), and normalization corrections. The BDT is trained on data from a dedicated CR with relaxed identification criteria for the boson candidates. The same region is used to obtain the normalization correction between the 0-tag category and the 1-tag or 2-tag categories. Finally, the estimated background is smoothed using a functional-form fit. Two independent statistical analyses are done, one for each  $V$  boson final state associated with the equivalent  $V'$  hypothesis. Agreement in both channels and both categories is good after a background-only fit.

The leptons+jets analysis uses two complementary selections aimed at different  $p_T$  regimes: a resolved selection with at least two jets, one of them  $b$ -tagged, and a merged selection with a large- $R$  jet with at least one associated  $b$ -tagged variable- $R$  track-jet. Both selections are divided according to the number of  $b$ -tagged jets or associated  $b$ -tagged variable- $R$  track-jets, respectively, into 1-tag and 2-tag categories. The pair of  $b$ -tagged jets or the  $b$ -tagged jet and the leading non- $b$ -tagged jet (for the 2-tag and 1-tag categories, respectively) are chosen in the resolved selection as the Higgs candidate and are required to have an invariant mass close to the Higgs boson mass. In the merged selection, the Higgs candidate is chosen as the leading large- $R$  jet that has least one associated  $b$ -tagged jet and a mass close to that of the Higgs boson. If an event passes both the resolved and merged selection, it is classified as resolved. Events from the two selections are then classified into six categories by looking at the number of light leptons in the event: zero, one, or two. The 0-lepton channel requires a large amount of  $E_T^{\text{miss}}$  and imposes additional kinematic selections based on the relationships between the  $E_T^{\text{miss}}$  and the jets in the event. The 1-lepton channel requires events to have one light lepton and a significant amount of  $E_T^{\text{miss}}$  and imposes additional selections sensitive to the presence of a  $W$  boson in the event, e.g. on the  $m_T(\ell, E_T^{\text{miss}})$  variable. Finally, the 2-lepton channel requires an event to have two same-flavour leptons, and additional selections, designed to select events with a  $Z$  boson in the final state, are imposed on the dilepton system. For each combination of the number of leptons and number of  $b$ -tagged jets, and separately for the merged and resolved categories, a signal region is built by imposing a very tight selection around the Higgs boson mass. In contrast, events with slightly lower or higher  $m_H$  values are kept as control regions in the 0-lepton and 1-lepton channels. In the 2-lepton resolved category, a CR is defined using events with two different flavour leptons, while the 2-lepton merged category has no corresponding CR. Two independent statistical analyses are built to search for events consistent with either a  $Z'$  or a  $W'$  hypothesis, with the former using the 0-lepton and 2-lepton channels and the latter using the 0-lepton and 1-lepton channels. The invariant mass of the  $VH$  candidate is used in the 0- and 2-lepton channels, while the transverse mass of the  $VH$  candidate is used in the 1-lepton channel. All templates for background and signal are obtained from MC samples, with the small multijet background in some regions obtained using a data-driven template method [84]. Agreement between data and the SM background expectation after a background-only fit is found to be good in all regions.

In the absence of significant excesses, cross-section limits are set as a function of the mass of the new gauge boson ( $W'$  or  $Z'$ ). Such limits from an HVT signal hypothesis are shown in Figure 4 for the quark–quark annihilation (qqA) production mode. The two searches have similar sensitivity for the  $W'$  case, but the leptons+jets search dominates across the whole mass range for a  $Z'$  hypothesis.

The four  $VV$  searches cover the large variety of  $WW$  and  $WZ$  final states, since each boson can decay either hadronically or leptonically.

The semileptonic  $VV$  search [85] considers three separate channels, named according to the number of leptons: zero, one, or two. The 0-lepton channel targets the  $ZV$  final state and requires events to have a large amount of  $E_T^{\text{miss}}$  and no leptons in addition to at least one large- $R$  jet or two small- $R$  jets. The 1-lepton channel, aimed at the  $WV$  final state, has the same jet requirements but selects events with a significant amount of  $E_T^{\text{miss}}$  and exactly one lepton. Finally, the 2-lepton channel, also dedicated to the  $ZV$  final state, requires a pair of same-flavour leptons with an  $m_{\ell\ell}$  value close to the  $Z$  boson mass. Each channel considers the two  $V$  hypotheses separately. The hadronic boson candidate is identified using the leading large- $R$  jet, with a mass window close to the  $V$  boson mass considered. If no large- $R$  jet candidate is found, an attempt is made to reconstruct a hadronic candidate using pairs of small- $R$  jets. The dijet system formed from the two leading jets is used as a candidate if its  $m_{jj}$  is consistent with that of the  $V$  boson considered. The selected events are classified into a large number of signal regions using three criteria. The first criterion uses the  $D_2$  variable to separate events according to the reconstruction quality

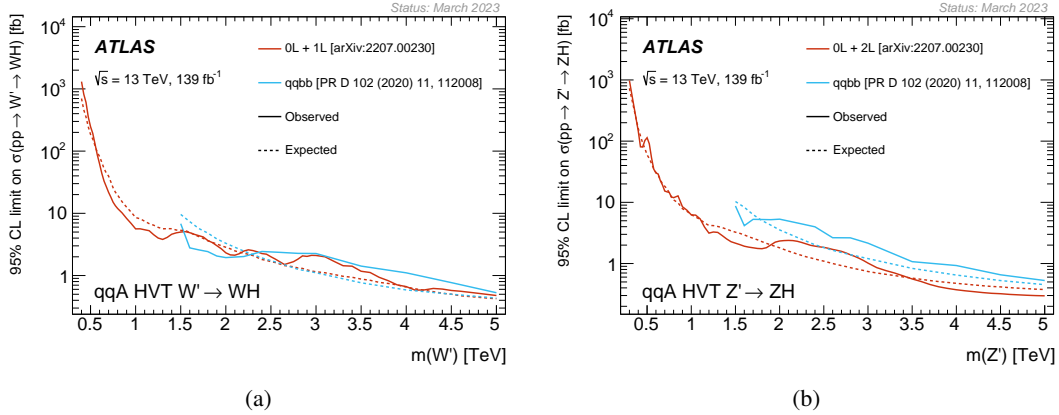


Figure 4: Upper limits on the production cross section of new gauge bosons, (a)  $W'$  or (b)  $Z'$  decaying into a  $VH$  final state from the (red) leptons+jets [82] and (blue) fully hadronic [81] analyses. The HVT model is used to define the signal hypothesis.

of the hadronic  $V$  candidate. The second criterion aims to separate vector-boson fusion (VBF) events from events produced by other processes and uses a recurrent neural network to separate events into these two categories. The final criterion is based on the number of variable- $R$  track-jets associated with the hadronic  $V$  candidate. A total of 40 SRs are defined across the three channels. CRs rich in  $t\bar{t}$ ,  $W$ +jets, and  $Z$ +jets background processes are defined in the 0-lepton, 1-lepton, and 2-lepton channels, respectively. The statistical analysis utilizes either the diboson invariant mass or the transverse mass of the  $VV$  final state (for the 0-lepton channel only) in all SRs and CRs, with most background and signal templates obtained using MC samples. The multijet background, which is non-negligible in the 1-lepton channel, is estimated using a template method. The data are found to be in good agreement with the background expectation. This search has better sensitivity than any other ATLAS analysis when considering new gauge bosons decaying into  $VV$  final states. The other three analyses [86–88], considering fully leptonic or fully hadronic final states, are included in the summary plots below but not described further.

With no significant excesses, cross-section limits are set as a function of the mass of the new gauge boson ( $W'$  or  $Z'$ ). Limits for an HVT signal hypothesis are shown in Figure 5 for the two possible final states,  $WZ$  and  $WW$ , and separately for the two possible production modes, VBF and qqA. The semileptonic search described in this section dominates the sensitivity for most of the mass range considered.

### 4.1.3 Final states with heavy quarks

Searches with top quarks in the final state are particularly relevant for models with preferred couplings to the third generation. A hadronic  $Z' \rightarrow t\bar{t}$  [89] search is employed to set limits on a leptophobic  $Z'$  from a topcolour-assisted-technicolour model, which falls in that category. This search selects events with two top-tagged large- $R$  jets, which are required to be back-to-back in the  $(\eta, \phi)$  plane. A selection based on the rapidity separation between the two jets is imposed in order to reject events with large rapidity separation, which are dominated by  $t$ -channel events from multijet production and represent a significant background. The selected events are separated into two signal regions, according to the number of  $b$ -tagged variable- $R$  track-jets (one or two) associated with the selected large- $R$  jets. The statistical analysis employs the

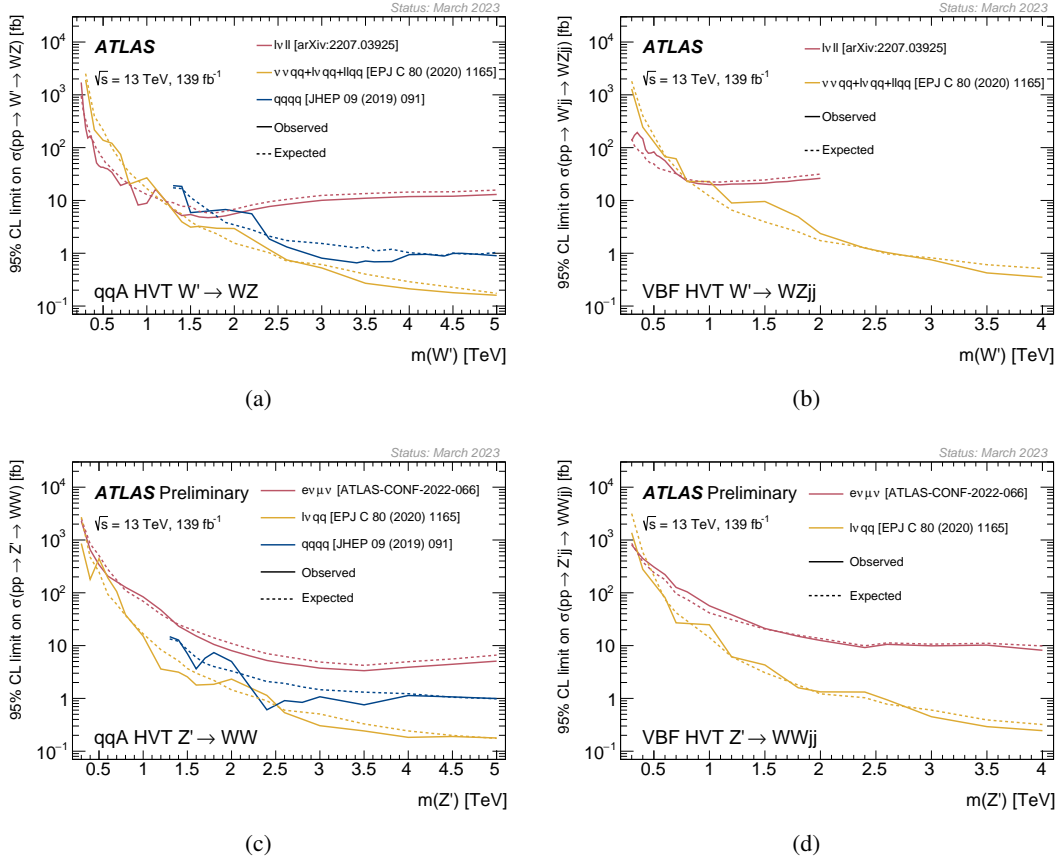


Figure 5: Upper limits on the production cross section of new gauge bosons, (a,b)  $W'$  or (c,d)  $Z'$  decaying into a (yellow)  $VV$  semileptonic final state [85], (red) leptonic final state [87, 88], or (blue) hadronic final state [86]. The HVT model is used to define the signal hypothesis. The qqA and VBF production modes are considered separately.

invariant mass of the two leading large- $R$  jets as the discriminating variable. The background distribution is obtained in situ in each signal region using a parametric function fitted to data. A background fit shows good agreement between data and MC simulation in both regions, as can be seen in Figure 6.

The same argument can be used to justify a  $W'$  search in the  $W' \rightarrow tb$  final state [90], which considers both the hadronic (0-lepton) and lepton+jets (1-lepton) channels. The 0-lepton channel selects events with exactly one top-tagged large- $R$  jet back-to-back with a  $b$ -tagged jet. Such a pair is used to reconstruct the  $W'$  boson. Events are classified into two categories according to the presence of additional  $b$ -tagged jets inside the top-tagged large- $R$  jet. A total of three SRs are defined, with 12 additional regions (6 per category), built by relaxing or inverting the  $b$ -tagging or top-tagging criteria utilized to estimate the main background, from QCD multijet production. This background is estimated using an ABCD method. The  $W' \rightarrow tb$  search uses an eight-region variant, with two SRs per category. The 1-lepton channel selects events with exactly one lepton (electron or muon), a significant amount of  $E_T^{\text{miss}}$ , two or three additional jets, and exactly one or two  $b$ -tagged jets. Events are classified according to the numbers of jets and  $b$ -tagged jets. Additional kinematic selections are imposed to reduce the major backgrounds ( $t\bar{t}$  and  $W$ +jets) and define four SRs, one per category. Additional cuts based on the same variables are used to build CRs and VRs to control or validate those major backgrounds. The  $W'$  candidate is reconstructed using the lepton,

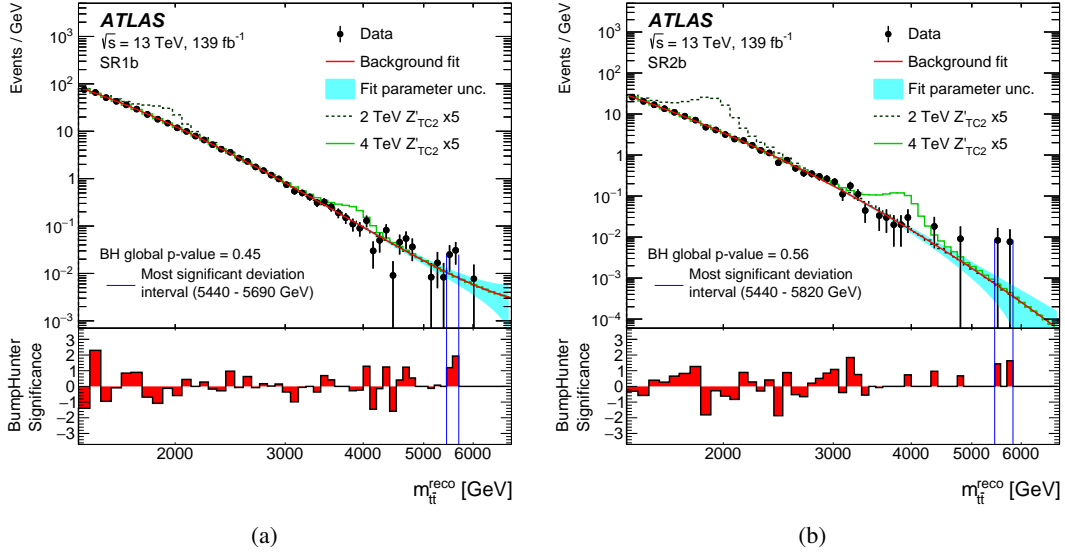


Figure 6: Distributions, in the two SRs of the  $Z' \rightarrow t\bar{t}$  analysis [89], of the invariant mass of the two leading large- $R$  jets. The fit of the parametric function to the data is shown in both regions, together with the distributions of two benchmark signal hypotheses with different masses.

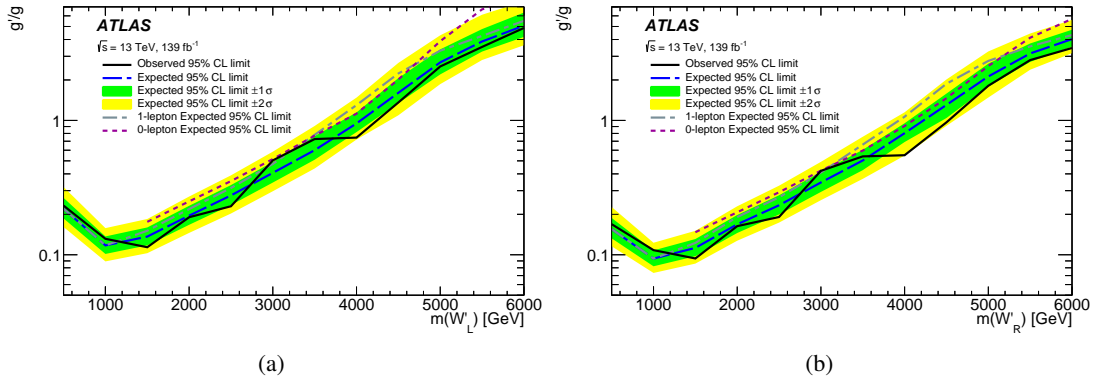


Figure 7: Two-dimensional limits in the mass vs coupling plane for the production of a  $W'$  decaying into  $tb$  [90], for (a) left-handed and (b) right-handed hypothesis.

the  $E_{\text{T}}^{\text{miss}}$ , and a combination of jets that satisfy constraints based on the top quark and  $W$  boson masses. The final statistical analysis combines the two channels, with seven SRs and two CRs. Using the invariant mass of the  $W'$  candidate as the discriminating variable, a background fit shows good agreement between the data and the SM background prediction. Limits are obtained for a leptophobic  $W'$  model in which the coupling of the  $W'$  to quarks is a free parameter. Both the left-handed and right-handed  $W'$  chiralities are considered. Two-dimensional limit plots in the coupling vs mass plane are shown in Figure 7.

A second  $Z' \rightarrow t\bar{t}$  search is done to address a more extreme case in which the  $Z'$  couples exclusively to top quarks [91]. In this context, the  $Z'$  is produced primarily through associated production with two additional



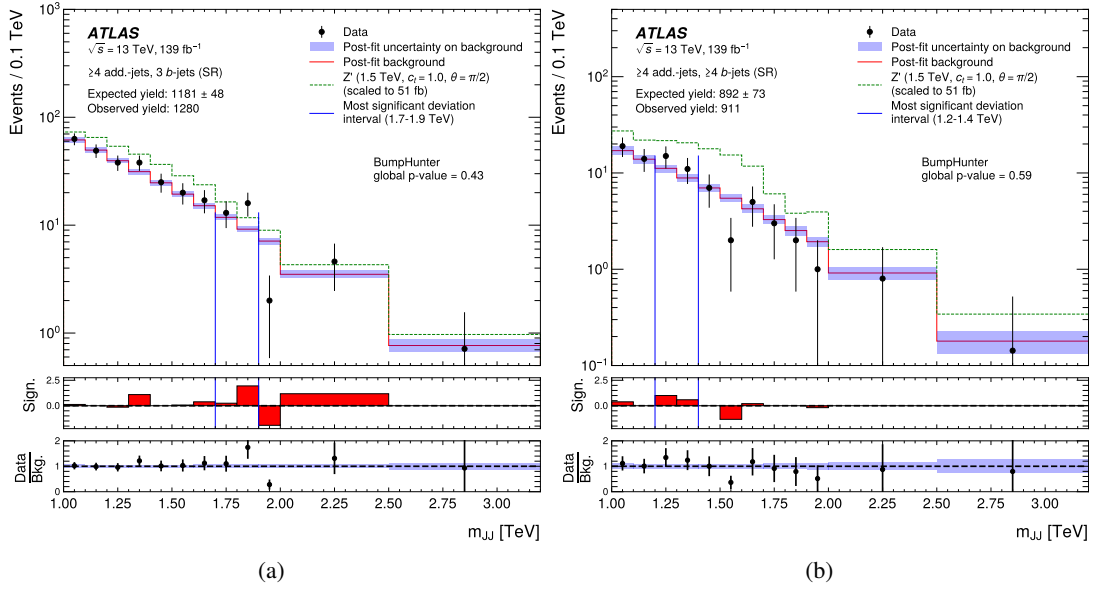


Figure 8: Distributions, in the two most sensitive SRs of the  $t\bar{t}Z' \rightarrow t\bar{t}t\bar{t}$  analysis [91], of the invariant mass of the two leading large- $R$  jets. They are shown after a background-only fit to data. The distribution for one benchmark signal hypothesis is also shown.

top quarks, thus composing a  $t\bar{t}Z' \rightarrow t\bar{t}t\bar{t}$  final state. Depending on the exact parameters of the model, final states of the type  $tjZ'$  and  $tWZ'$  can also be relevant and are considered in the analysis. This search selects events with exactly one lepton (electron or muon), at least two large- $R$  jets, with the two leading ones used to reconstruct the  $Z'$  candidate, and at least two additional small- $R$  jets not overlapping the selected large- $R$  jets. Events must also have at least two  $b$ -tagged jets, which can overlap the large- $R$  jets or be counted as additional jets. Six regions with at least three  $b$ -tagged jets and classified according to the numbers of jets and  $b$ -tagged jets are used as SRs. The background in each SR is estimated using a data-driven method. The shape of the initial background template is obtained using a parametric function fit in a region with two  $b$ -tagged jets and two small- $R$  jets, and extrapolated into the SR using factors obtained from MC simulations. The invariant mass of the reconstructed  $Z'$  candidate is used in the statistical analysis, and a background-only fit shows good agreement with the data in each of the SRs, as can be seen in Figure 8 for the two most sensitive SRs.

A third and final  $Z'$  analysis considers an associated production scenario similar to the one in the previous search, in this case involving  $b$ -quarks [92]. The analysis selects events with at least three  $b$ -tagged jets, with asymmetric  $p_T$  cuts, corresponding to the  $bbZ' \rightarrow b\bar{b}b\bar{b}$  topology. Additional kinematic cuts on the rapidity separation between the two leading jets help to differentiate between signal events and the main background, coming from QCD multijet production. The background estimate is obtained in situ in the SR using the functional decomposition method [93] and shows good agreement between the data and the SM background estimate. The search sets limits using a model that includes lepton-universality violation (LUV) and third-generation exclusive couplings in the quark sector.

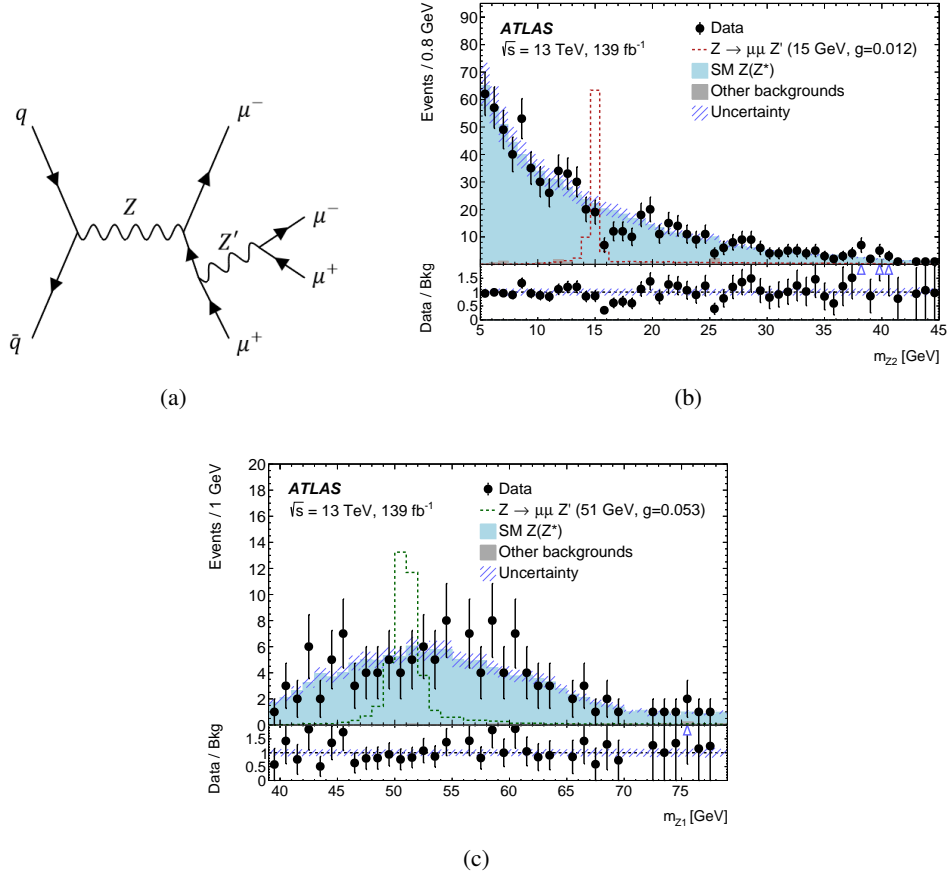


Figure 9: (a) Feynman diagram of  $Z'$  production through radiation in a Drell–Yan process, and the (b)  $m_{Z_2}$  and (c)  $m_{Z_1}$  spectra from the  $\mu\mu Z' \rightarrow 4\mu$  analysis [94] with signal examples at 15 GeV and 51 GeV, respectively.

#### 4.1.4 Many-body final states

Although simple final states are the target of many searches, more complicated configurations are useful in looking for  $Z'$  or  $W'$  bosons in specific models where simpler searches do not have enough sensitivity. The  $\mu\mu Z' \rightarrow 4\mu$  analysis [94] targets one such scenario, in which a  $Z'$  couples exclusively to second- and third-generation leptons. Because of this, they cannot be produced in the usual way and appear in final states with multiple leptons. An example of such a production mode and corresponding final state can be seen in Figure 9(a). The search selects events with four muons with kinematics compatible with producing a pair of muons with a large invariant mass ( $Z_1$ ) and an extra pair of opposite-sign muons ( $Z_2$ ), which follow the expected signature. Both pairs of muons are used to look for heavy resonances with relatively high-mass  $Z'$  signals appearing as a peak in the invariant mass distribution of  $Z_1$  and low-mass ones appearing as a peak in the invariant mass distribution of  $Z_2$ . The background is estimated using a fake-factor method. A parameterized deep neural network (pDNN) [95] is used to further separate signal and background and to define the final signal regions, with the final cut depending on the signal hypothesis. Agreement between the data and the SM prediction is excellent for most of the mass range, and is shown in Figures 9(b) and 9(c) for two different mass hypotheses.



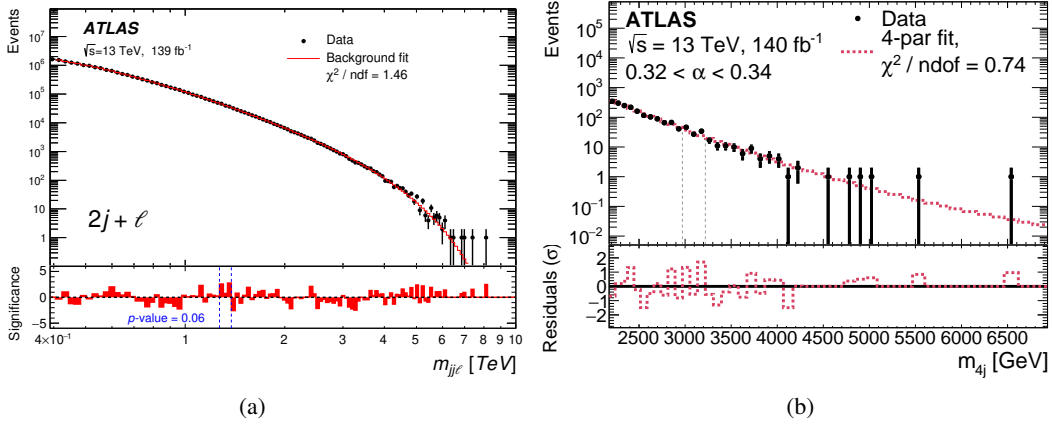


Figure 10: Distributions of two of the relevant invariant masses in the (a) multi-body search [96] and (b) the  $Y \rightarrow XX \rightarrow jjjj$  analysis [98]. The background estimate obtained using a parametric fit is shown in both cases.

Another scenario in which simple final states may prove insufficient arises when dealing with complex decay chains that follow the production of a new  $Z'$  or  $W'$  boson. More than two objects coming from the heavy resonance must be considered in this context. The analysis described in Ref. [96] constructs a single SR by selecting events with at least one isolated lepton (electron or muon) and a pair of jets. The background is then estimated in situ by using a parametric function to fit the data. Four fully independent statistical analyses are defined for four different invariant masses:  $m_{jj\ell}$ ,  $m_{jj\ell\ell}$ ,  $m_{j\ell\ell}$ , and  $m_{bb\ell}$ . The largest deviation of the data from the fitted background is found in the  $m_{jj\ell}$  analysis at a mass around 1.3 TeV and has a local significance of  $3.5\sigma$  ( $1.5\sigma$  global), but otherwise the data agrees well with the predicted SM background. Figure 10(a) shows one of the relevant distributions. A similar analysis tackles the simpler scenario of a dijet resonance, arising from a  $W'$  or  $Z'$ , produced in association with a light charged lepton [97]. It follows a similar strategy and looks for excesses in the  $m_{jj}$  distribution of such events. In this case, no significant disagreement with the SM prediction is found.

A fourth analysis of multi-body final states, which considers fully hadronic scenarios with two pairs of jets arising from a single heavy resonance, was also completed recently [98]. This analysis reconstructs events with two pairs of jets that are required to have similar invariant masses, corresponding to a scenario of the type  $Y \rightarrow XX \rightarrow jjjj$ , and uses a single SR. Additional kinematic requirements are imposed to reduce the multijet background. Two different distributions are used for the statistical analysis: the average dijet invariant mass and the invariant mass of the tetra-jet system. A total of six independent statistical analyses are defined for those two variables and three ranges of the  $\alpha$  parameter, defined as the ratio of those masses. The background is obtained by fitting a parametric function directly to the data in the SR in those six scenarios, and good agreement is found. One of the distributions is shown in Figure 10(b).

#### 4.1.5 Summary of lower limits on the masses of $Z'$ and $W'$ resonances

For most of the analyses described in this section, limits are set on the production of  $Z'$  or  $W'$  bosons. Table 1 summarizes the lower limits placed on the mass in the various models.

Table 1: 95% CL lower mass limits obtained in various analyses for different models predicting new heavy vector bosons  $W'$  and  $Z'$  (see the text for more details).

$V'$	Analysis final state	Observed lower limit on $m_{V'}$ [TeV]
$Z'_{\text{SSM}}$	$bb$	2.7
	$ee + \mu\mu$	5.1
$W'_{\text{SSM}}$	$qq$	4.0
	$e\nu + \mu\nu$	6.0
	$\tau\nu$	5.0
$Z'_{\psi}$	$ee + \mu\mu$	4.5
$Z'_{\text{TC2}}$	$t\bar{t}$	3.9
$Z'_{\text{LUV}}$	$b\bar{b}b\bar{b}$	1.45
$W'_R (g'/g = 1.0)$	$tb$	4.6
$W'_{\text{HVT}}$ (model A)	$WZ \rightarrow XXqq$	3.9
$W'_{\text{HVT}}$ (model B)	$WZ \rightarrow XXqq$	4.3
$W'_{\text{HVT}}$ (model C)	$WZ \rightarrow \ell\nu\ell\ell$	3.4
$Z'_{\text{HVT}}$ (model A)	$WW \rightarrow \ell\nu qq$	3.5
$Z'_{\text{HVT}}$ (model B)	$WW \rightarrow \ell\nu qq$	3.9

## 4.2 Contact interactions

Searches complementary to those for resonances, and looking for broad excesses in the tails of invariant mass distributions, are performed as a test for a four-fermion contact interaction (CI) approximating new physics at a scale  $\Lambda$  with coupling  $g^*$ . The value of  $\Lambda$  can be much higher than the  $pp$  collision centre-of-mass energy, extending the sensitivity of the LHC to mass scales well beyond its direct reach.

In the dilepton final state [99], the same selection criteria as the ones reported for the resonant search (see Section 4.1.1) are used, and the background is fitted with the same functional form, but only considering the data in a low  $m_{\ell\ell}$  region which forms the CR. The fitted function is then used to extrapolate to the expected number of background events in a single inclusive bin at high  $m_{\ell\ell}$  which forms the SR. The boundaries of the CR and the SR are optimized for sensitivity for each of the four scenarios considered: a CI with constructive or destructive interference with the SM, in the  $ee$  and  $\mu\mu$  channels. An example is shown in Figure 11(a) for the  $ee$  constructive interference channel, where a slight but non-significant excess is seen. Lower limits are set on  $\Lambda$  for various assumptions about the chirality of the quarks and leptons in the  $qq\ell\ell$  interaction. Combining the two lepton channels, they are as high as 35.8 (28.8) TeV in the constructive (destructive) interference scenario.

A more specific  $bs\ell\ell$  CI, inspired by lepton-flavour anomalies [100], is the target of another search [101], with independent  $ee$  and  $\mu\mu$  spectra drawn for the cases in which there is no  $b$ -tagged jet or exactly one  $b$ -tagged jet in the event, the latter being shown in Figure 11(b) for the dimuon case. The background in this case is estimated using CRs, built at lower  $m_{\ell\ell}$  values for the  $Z$ +jets background and by selecting two  $b$ -tagged jets for the top-related backgrounds. As in the leptonic  $W'$  search discussed in Section 4.1.1, some fit-based extrapolations are needed to populate the higher-mass bins of the background samples. The

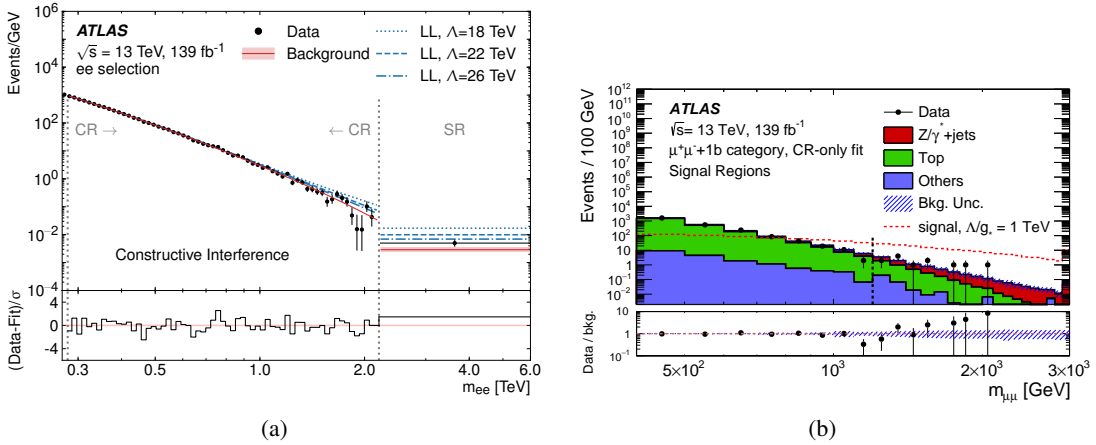


Figure 11: Distribution of  $m_{\ell\ell}$  in the CR (where the data is fitted) and the SR (where the background estimate is an extrapolation from the fit) of the  $qql\ell$  CI search [99], shown for (a) the  $ee$  channel with constructive interference, and (b) the  $bsl\ell$  search [101] in the  $\mu\mu$  channel with one  $b$ -tagged jet, where the region to the right of the dashed vertical line needs some fit-based extrapolation for the top background.

fake leptons are estimated using a matrix method. Values of  $\Lambda/g^*$  smaller than 2.0 (2.4) TeV are excluded in the  $ee$  ( $\mu\mu$ ) channel.

A similar approach can be followed to construct a non-resonant hadronic search [102], which was completed using a partial Run 2 dataset recorded between 2015 and 2016.

## 5 Additional leptons

The origin of the non-zero neutrino masses, brought to light by the observation of neutrino oscillations [103, 104], is not known. While Yukawa couplings can be invoked, their extremely small values compared to the other fermionic masses appear unnatural. One solution is the seesaw mechanism, which introduces a neutrino mass matrix containing Majorana mass terms and tiny neutrino mass eigenvalues which are due to the existence of heavier BSM particles. Several such seesaw theories exist depending on their field contents [105], classified into Type-I with right-handed neutrinos, Type-II with a scalar triplet, and Type-III with fermion triplets. Searches for heavy leptons in the context of these theories have been performed in multiple final states [106–111], as reviewed in this section.

### 5.1 Type-I seesaw

In the Type-I seesaw mechanism, the heavy Majorana neutrinos  $N$  couple to SM particles through their mixing with the light left-handed neutrinos of flavour  $\alpha = \{e, \mu, \tau\}$ , the size of the mixing being determined by the dimensionless coefficient  $V_{\alpha N}$ .

Due to the Majorana nature of the heavy neutrino, a same-sign (SS) dilepton final state can be created, for example in the scattering of  $W$  bosons, as shown in Figure 12(a). This signature was exploited to search for these new particles for non-zero values of  $V_{\mu N}$  [106]. Besides requiring the presence of exactly

two SS muons, the vector-boson scattering (VBS) production signature is exploited by requiring two jets with a large rapidity separation and a high  $m_{jj}$ . To reject background events,  $b$ -tagged jets are vetoed and the  $E_T^{\text{miss}}$  significance is required to be small. The SR is binned in subleading-muon  $p_T$ , and the shape of this distribution is exploited to enhance the sensitivity. The two main background processes, VBS  $W^\pm W^\pm jj$  and  $WZ$  production, are estimated via CRs which reverse the  $E_T^{\text{miss}}$  significance or third-lepton veto requirement, respectively. The fake-muon background is evaluated with the fake-factor method. Since the data agree with the background expectations within statistically dominated uncertainties, upper limits are set on  $|V_{\mu N}|^2$  as a function of the heavy neutrino mass  $m_N$ , as shown in Figure 12(c).

A complementary search is also conducted for lower values of  $m_N$  and  $|V_{\alpha N}|^2$  [107], focusing on production via  $W \rightarrow N\ell_\alpha$  where the heavy neutrino subsequently decays as  $N \rightarrow \ell_\beta\ell_\gamma\nu_\gamma$  (via a  $W^*$ ) or as  $N \rightarrow \nu_\beta\ell_\gamma\ell_\gamma$  (via a  $Z^*$ ), where  $\alpha, \beta, \gamma = e$  or  $\mu$  (see Figure 12(b)). For the low values of  $m_N$  and  $|V_{\alpha N}|^2$  probed in this search, the heavy neutrino is long-lived, leading to a displaced vertex (DV) of two charged leptons ( $\ell_\beta\ell_\gamma$  or  $\ell_\gamma\ell_\gamma$ ). The secondary vertexing is run on standard and LRT tracks using a procedure drawing inspiration from Ref. [112] and requiring the selected DVs to have exactly two leptons of opposite sign, and no additional tracks. The SR events are selected by requiring the presence of such a DV and one additional prompt lepton  $\ell$ , with a combined invariant mass  $40 < m_{\text{DV}+\ell} < 90$  GeV, and a reconstructed  $m_N$  below 20 GeV, where the  $m_N$  calculation uses the known  $W$  mass, assumes massless charged leptons, and takes the  $N$  flight direction to be the vector connecting the  $pp$  collision PV to the DV. Further selections are applied to suppress the cosmic-ray muon background (by removing DVs with back-to-back muons), the  $ee$  background from interactions with material in the inner detector (by removing DVs found in regions with detector material), the background from  $J/\Psi$  or other heavy-flavour decays (by setting a lower bound on  $m_{\text{DV}}$ ), the random-lepton-crossing background (by requiring the prompt lepton and displaced lepton with the same flavour to have opposite charge), and the  $Z \rightarrow \ell\ell$  background (by removing events in which the prompt lepton and the displaced lepton with the same flavour have a mass compatible with a  $Z$  boson). After these selections, the random-crossing background dominates; it is estimated in a data-driven way by using a CR at higher  $m_N$  and utilizing the fact that opposite-sign leptons and same-sign leptons should be equally probable in the DVs for this source of background. In all the lepton flavour combinations probed, between 0.2 and 2.8 background events are predicted in the SR, with 0 to 2 events observed in the data. Figure 12(d) shows the excluded parameter space in the same plane as used in the prompt heavier-neutrino search discussed above, illustrating the complementary coverage of the two analyses.

## 5.2 Left–right symmetric model

Type-I and Type-II models can also be included in larger left–right symmetric models (LRSM) [113–115] whose aim is to explain the broken parity symmetry of the SM weak interaction. In these models, right-handed counterparts to the  $W$  and  $Z$  bosons can be introduced along with the right-handed heavy neutrinos  $N_R$ . A search for such Majorana or Dirac neutrinos and right-handed  $W$  gauge bosons ( $W_R$ ) has been performed [108], looking for the Keung–Senjanović process [115] with a semileptonic final state  $W_R \rightarrow \ell N_R \rightarrow \ell\ell q\bar{q}'$  ( $\ell = \{e, \mu\}$ ), as shown in Figure 13(a). Majorana and Dirac heavy neutrinos will differ in that the Majorana neutrinos will produce same-sign leptons half of the time. For  $m(W_R) \gg m(N_R)$ , the  $N_R$  decay products will be merged, due to a Lorentz boost, into a large- $R$  jet. Two sets of SRs are therefore defined: one for the resolved decay of the  $N_R$ , and one for the boosted regime.

In the resolved regime, different SRs are defined for opposite-sign (OS) or same-sign (SS) electron and muon pairs. Since a high-mass  $W_R$  is targeted, high values are required for the  $p_T$  of the two leading jets, their  $m_{jj}$ , and the  $H_T$  computed from these jets and leptons. A high value of  $m_{\ell\ell}$  is also required, to

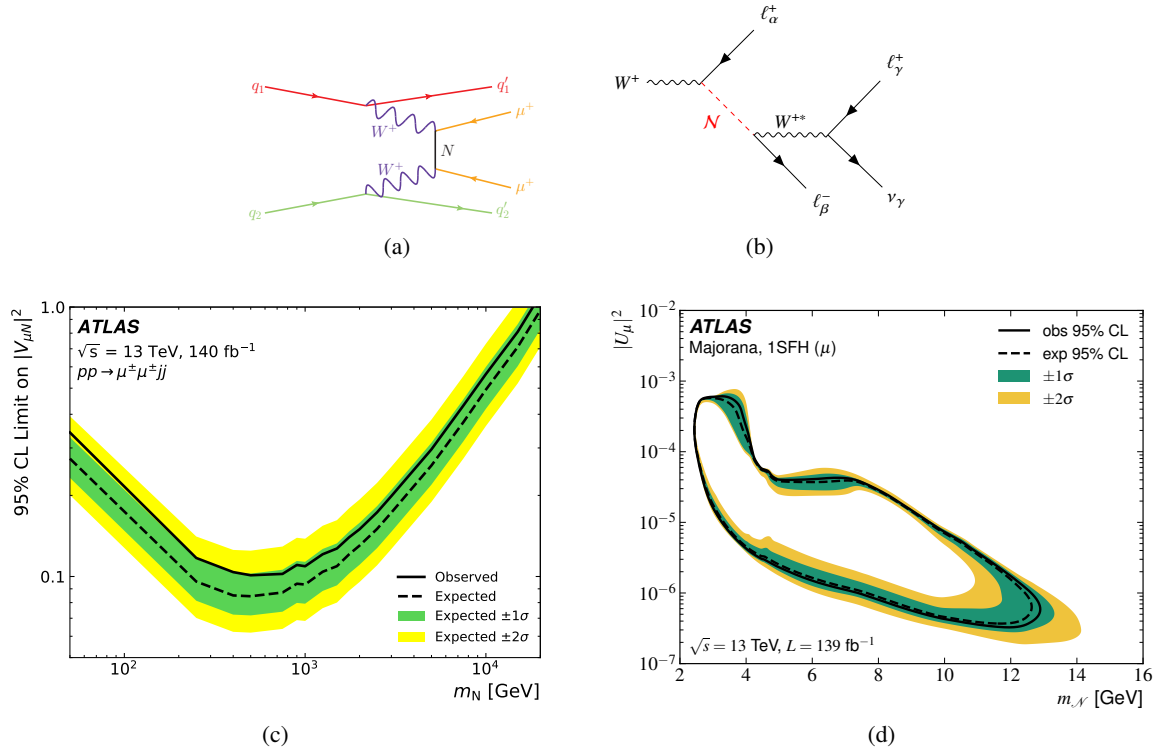


Figure 12: Examples (a,b) of the production and decay of the heavy neutrinos and (c,d) limits set on the heavy Majorana neutrino mixing element  $|V_{\mu N}|^2$  (also shown here as  $|U_\mu|^2$ ) as a function of  $m_N$  in a Type-I seesaw mechanism by (a,c) the same-sign  $WW$  scattering search [106] and (b,d) the displaced dilepton vertex search [107].

suppress the  $Z$ +jets background, and, for SS leptons, the dileptonic angular separation must not be too large, to avoid a mismodelled region of the phase space for the diboson background. The SRs are binned in either  $m_{\ell\ell jj}$  (OS case with  $m(W_R) > m(N_R)$ ),  $m_{jj}$  (OS case with  $m(W_R) < m(N_R)$ ), or  $H_T$  (SS case), to increase the sensitivity. CRs to constrain the main leptonic background processes ( $Z$ +jets,  $t\bar{t}$  and diboson) are built either at lower  $m_{\ell\ell}$  values or with opposite-flavour leptons, with the non-prompt-lepton background estimated with a fake-factor method. In the boosted channel, one of the leptons must be well separated from the large- $R$  jet in azimuth and one is likely to be inside the large- $R$  jet – while such a muon can still be readily identified, this may not be the case for an electron whose associated calorimeter energy clusters are embedded in the jet. Therefore, besides a  $2\mu$  and a  $2e$  SR with a high  $m_{\ell\ell}$ , a  $1e$  SR is also defined. In the electron SRs, the  $W$ +jets background is suppressed by imposing an upper bound on  $E_T^{\text{miss}}$  and additionally, in the  $1e$  SR, by imposing a lower bound on the polar angle of the electron from an assumed  $W$  boson decay in this boson's rest frame (with respect to the boson's flight direction in the laboratory frame). Furthermore, in the  $1e$  SR, the  $\gamma$ +jets and dijet contributions are reduced by selecting events in which the  $\eta$  difference between the jet and the electron is not too large. Finally, in order to suppress the  $t\bar{t}$  background,  $b$ -tagged jets are vetoed in all SRs and, in the  $2\mu$  channel, the  $p_T$  of the dimuon system is required to be large. The SRs are binned in the reconstructed  $W_R$  mass, with  $m(W_R) > 3$  TeV being the SR, and lower values being used as CRs to estimate the background. Other CRs are used in the  $1e$  SR, at lower polar angle, to estimate  $W$ +jets background, or with a looser electron identification, to estimate fakes.

In all SRs, the data agree with the background expectations within uncertainties, the background MC

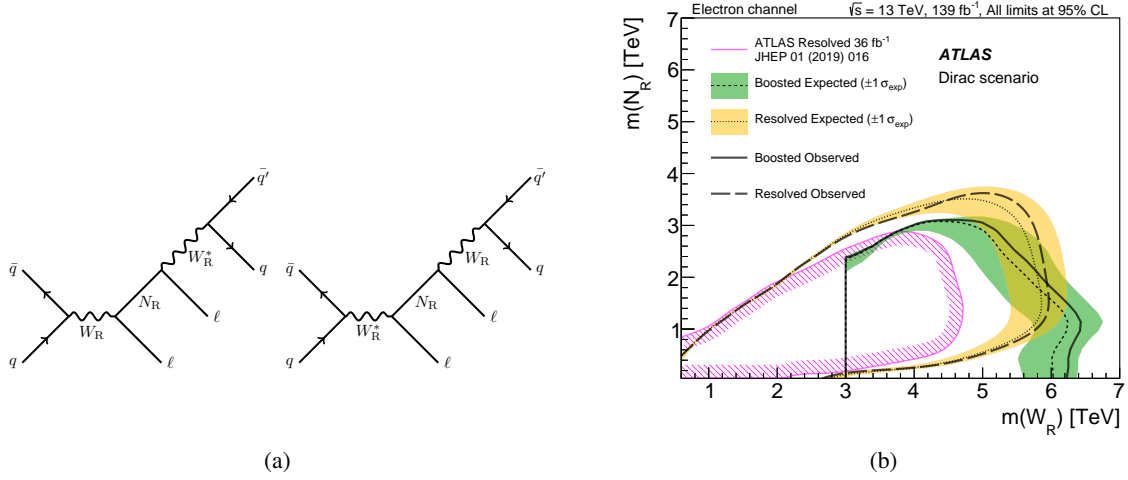


Figure 13: (a) Diagrams of the Keung–Senjanović process with different mass orderings and an off-shell  $W_R^*$ . (b) Limits obtained in the resolved and boosted channels of the analysis searching for left–right symmetric model  $W_R$  and  $N_R$  [108] in the case of a Dirac neutrino in the electron channel.

sample size being one of the dominant systematic uncertainties in the SS SRs, while modelling uncertainties become important for the other SRs. Limits in the plane of  $m(N_R)$  versus  $m(W_R)$  are shown for the Dirac scenario in the electron channel in Figure 13(b), which illustrates the complementarity of the resolved and boosted SRs. Similar limits are obtained in the muon channel and for a Majorana scenario.

### 5.3 Type-III seesaw

The minimal Type-III seesaw model described in Ref. [116] is the target of searches in multilepton final states [109, 110]. This model introduces a single fermionic triplet containing one neutral Majorana lepton  $N$  and two oppositely charged leptons  $L^\pm$ , which are degenerate in mass<sup>3</sup> and decay into a SM lepton (with which they mix with coupling  $V_\alpha$  where  $\alpha = \{e, \mu, \tau\}$ ) and a  $W, Z$  or Higgs boson. The dominant production mechanism is shown with an example decay in Figure 14(a).

The two-lepton search [109] is based on two SRs, with either SS or OS leptons ( $e$  or  $\mu$ ) having either the same or different flavours and a large  $m_{\ell\ell}$ , and with at least two jets with an invariant mass compatible with a  $W$  boson. Large values are also required for the  $p_T$  of the dijet system and of the dilepton system, for the significance of the  $E_T^{\text{miss}}$  and for  $H_T + E_T^{\text{miss}}$ , where  $H_T$  is based on the leptons. Finally, to suppress the  $t\bar{t}$  background, no  $b$ -tagged jet is allowed to be present in the final state and, in the OS SRs, the  $E_T^{\text{miss}}$  must point away from the leptons. The remaining dominant backgrounds,  $t\bar{t}$  in the OS SRs and dibosons in the SS SRs, are estimated from CRs built mainly by reversing the  $b$ -tagged veto and  $m_{jj}$  requirements, respectively. The fake-lepton background contribution is estimated via a fake-factor method. The SRs are binned in  $H_T + E_T^{\text{miss}}$  to improve the sensitivity.

The three- and four-lepton searches [110] are also divided into various SRs. In the three-lepton channel, three SRs are defined and all require a large  $E_T^{\text{miss}}$  significance. The first one targets a dileptonic  $Z$  boson in

<sup>3</sup> There could be a small mass-splitting due to radiative corrections which does not affect the phenomenology.

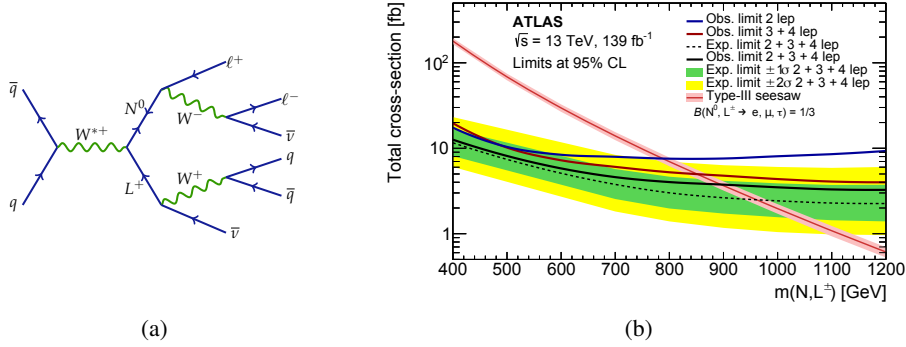


Figure 14: (a) The dominant production mechanism for Type-III seesaw heavy leptons with an example of their decay and (b) the limits placed on their mass in the various channels and their combination [109, 110].

the decay chain, and assumes that the SM boson coming from the other heavy lepton decays hadronically. It thus requires an opposite-sign same-flavour (OSSF) lepton pair compatible with the  $Z$  boson mass, along with a large tri-lepton mass and large  $m_T(\ell, E_T^{\text{miss}})$  for the two leading leptons, whose angular separation is also constrained. A complementary SR vetoes the presence of a  $Z$  boson candidate, requiring large values of  $H_T$ ,  $E_T^{\text{miss}}$  and the scalar sum of the  $p_T$  of the SS leptons, with an upper bound placed on the dijet invariant mass to reduce the diboson contribution. Finally, the last three-lepton SR targets leptonically decaying EW bosons, thus requiring a low jet multiplicity, and a lower bound on the summed scalar  $p_T$  of the leptons and on the OSSF lepton pair's invariant mass. Requirements are also placed on the transverse mass and angular separation of the two leading leptons, as in the  $Z$  SR. Since diboson production is the main background in the three-lepton channel, a CR is defined by selecting events with two jets and a low value of  $m_T(\ell_2, E_T^{\text{miss}})$ , where  $\ell_2$  is the subleading lepton.

The four-lepton channel is divided into two SRs, according to the sum of the electric charges of the leptons ( $q = 0$  or  $|q| = 2$ ), both requiring a large value of the four-lepton invariant mass and of  $H_T + E_T^{\text{miss}}$ . In the  $q = 0$  SR, which has more background to suppress, further selections are made: a  $b$ -tagged-jet veto, a  $Z$  boson veto and the requirement of a high  $E_T^{\text{miss}}$  significance. Two CRs are built to estimate the diboson and rare top backgrounds for the  $q = 0$  SR, the first at lower four-lepton mass and the second by inverting the  $b$ -jet veto. The background due to charge misidentification in the  $|q| = 2$  channel is estimated by correcting the simulation with factors derived in a  $Z \rightarrow ee$  CR. The fake-lepton background contributions are obtained via a fake-factor method. The data are found to agree well with the expected background's post-fit distributions of three-lepton transverse mass and  $H_T + E_T^{\text{miss}}$ , which are the discriminating variables used in the likelihood fit in the three- and four-lepton channels respectively.

The data in all channels are found to agree with the estimated background within uncertainties, which are dominated by the number of data events. The two-, three- and four-lepton channels are used, individually and in combination, to derive lower limits on the mass of the heavy leptons, as shown in Figure 14(b). The exclusion region reaches a mass of 910 GeV. A general, model-independent search for excesses in three- or four-lepton final states has also been performed [111] and is interpreted in terms of this model as well. However, due to the more general nature of this search in comparison with the targeted SRs described above, its sensitivity to this particular model is lower.



## 6 Vector-like lepton and quarks

One of the best-known open questions in the SM concerns the origin of the huge difference between the electroweak scale,  $\sim 250$  GeV, (as well as the Higgs boson’s mass itself) and the Planck scale,  $\sim 10^{19}$  GeV. Many possible solutions have been proposed for defining a new mechanism that cancels out radiative corrections to the Higgs boson mass without fine-tuning [117]. Although a chiral fourth generation of fermions is strongly disfavoured by Higgs boson measurements and electroweak precision data [118–120], the presence of vector-like leptons and quarks is much less constrained, since these can have electroweak-singlet masses that dominate the mass contributions from their Yukawa couplings to the Higgs boson [121]. Discovery of vector-like partners of the SM fermions could shed light on their mass and mixing patterns.

Vector-like quarks (VLQ) are colour-triplet fermions and are common in models that use a new strongly interacting sector to resolve the fine-tuning problem. In these models, the Higgs boson would be a pseudo Nambu–Goldstone boson [122] of a spontaneously broken global symmetry. The composite Higgs model [123–125] is a particular realization of this idea.

Vector-like leptons (VLL) are colour-singlet fermions. They often appear in phenomenological models motivated by string theory [126, 127] or large extra dimensions [128]. They also appear in weak-scale supersymmetry [129–131], where the mass of the lightest Higgs scalar boson can be raised by introducing new vector-like heavy chiral supermultiplets with large Yukawa couplings.

This section focuses on the searches for these two types of particles in ATLAS. It discusses one VLL result and a large part of the extensive search programme for VLQs.

### 6.1 Vector-like leptons

In a scenario with a pure VLL doublet  $L' = (\nu'_\tau, \tau')$ , this doublet comprises two fermions of approximately equal mass that couple only to the third generation of SM leptons [132]. In such a scenario the VLL production cross section is dominated by the  $pp \rightarrow \nu'_\tau \tau'$  process, with a rate approximately four times larger than for other possible combinations, such as  $pp \rightarrow \nu'_\tau \bar{\nu}'_\tau$  or  $pp \rightarrow \tau'^+ \tau'^-$ . The  $\nu'_\tau$  decays exclusively into  $W^+ \tau^-$ , while the  $\tau'$  can decay into  $Z \tau$  or  $H \tau$ , with the former dominating for low masses. To cover this wide range of possibilities in the most efficient way, VLLs are searched for [133] in final states containing at least two charged light leptons,  $e^\pm$  or  $\mu^\pm$ , zero or more  $\tau$ -leptons decaying hadronically, and a significant amount of  $E_T^{\text{miss}}$ . To maximize the sensitivity to the different final states, seven independent boosted decision trees [134] are trained in seven different categories of events based on the numbers of reconstructed light leptons and  $\tau$ -leptons. Thirty-four kinematic and topological variables for each event are used to train the BDTs, achieving good separation between signal and background samples. Seven SRs are then defined using the corresponding BDT’s output score in each category. In addition to the SRs, three CRs are used to normalize the dominant background processes ( $t\bar{t} + Z$ ,  $WZ$ , and  $ZZ$ ), and a final CR is used to assess the fake- $\tau$  background originating from gluon-initiated jets and pile-up.

The statistical analysis uses the BDT score in the signal regions, and the event yield in the CRs. Templates for signal and background processes are obtained from MC simulations. The fake contribution is estimated using the fake-factor method. The result of a background-only fit in all of the SRs is shown in Figure 15 together with a fit to one of the SRs, corresponding to a selection of two same-sign same-flavour light leptons and one  $\tau$ -lepton (2L SSSF,  $1\tau$ ). Since no significant excess is found, upper limits are set on



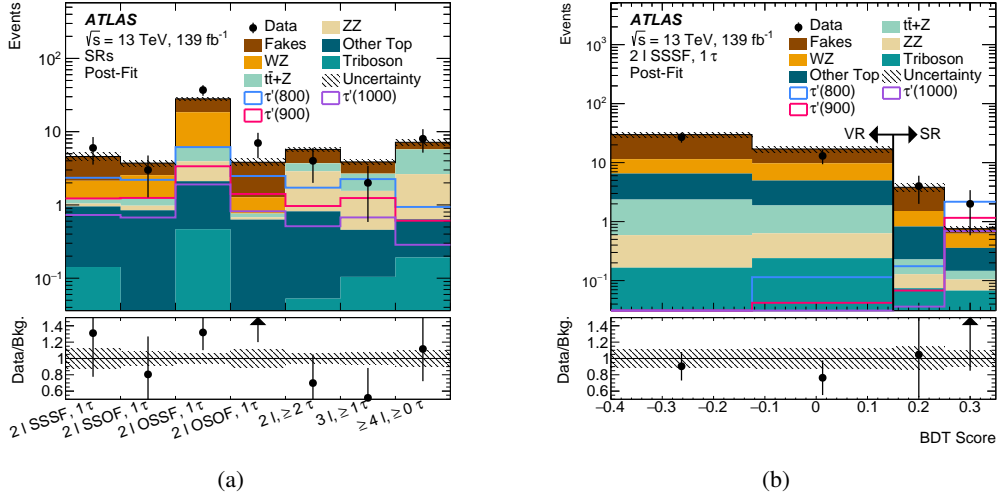


Figure 15: (a) The post-fit yield for all of the signal regions and (b) BDT score distribution for one of the signal regions used in the search for vector-like  $\tau$ -leptons [133]. Distributions of data, background, and pre-fit simulated signal are shown.

the combined production cross section of the three VLL processes considered. Masses below 900 GeV (970 GeV) are observed (expected) to be excluded for the doublet model used as a benchmark.

## 6.2 Vector-like quarks

Vector-like quarks may appear in one of seven possible multiplets: singlets ( $T^{2/3}$ ) or ( $B^{1/3}$ ); doublets ( $X^{5/3}, T^{2/3}$ ), ( $T^{2/3}, B^{-1/3}$ ) or ( $B^{-1/3}, Y^{-4/3}$ ); or triplets ( $X^{5/3}, T^{2/3}, B^{-1/3}$ ) or ( $T^{2/3}, B^{-1/3}, Y^{-4/3}$ ) where the superscript represents the charge of the new particle. The  $T$  and  $B$  quarks have the same charge as the SM top and bottom quarks but different masses, while the up-type  $X$  quarks and down-type  $Y$  quarks have non-standard isospins. Most analyses described in this report consider only the singlet and doublet scenarios containing only  $T$  and  $B$ .

Light VLQs, with masses below  $\sim 1$  TeV, would be produced mostly in pairs at the LHC via the strong interaction, illustrated in Figure 16 for a  $T$  quark. However, this process is kinematically suppressed for higher masses, and electroweak single production (also illustrated in Figure 16) becomes important and can dominate depending on the VLQ coupling strength. Searching for pair-produced VLQs is a relatively model-independent approach, as the pair-production cross section depends only on the assumed mass of the VLQ. At the same time, single production has the advantage of providing direct constraints on the coupling of VLQs to SM quarks. In most models, VLQs couple preferentially to third-generation quarks and can decay through many different channels involving  $W$ ,  $Z$ , or  $H$  bosons. The relative couplings, and therefore branching fractions, for the different decay modes depend on the considered multiplet representation.

This wealth of final states and production modes allows a variety of searches for pair-produced and singly produced VLQs. In many cases, they complement one another and aim to cover the full range of multiplet configurations, masses, and types of VLQs. ATLAS has searched for VLQs in final states with a hadronically decaying Higgs boson appearing together with top and bottom quarks [135, 136], in events

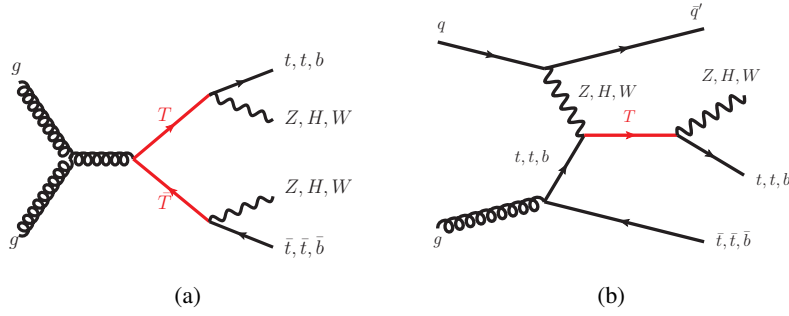


Figure 16: Representative diagrams of (a) pair production and (b) single production of a vector-like  $T$  quark.

Table 2: Production and decay channels explored by the different VLQ searches discussed in this section.

Search	Production mode	Decay channel	Section
Hadronic $T$ search [136]	Single	$T \rightarrow Ht$	6.2.1
Hadronic $B$ search [135]	Single	$B \rightarrow Hb$	6.2.1
Multilepton (single) [137]	Single	$T \rightarrow Zt$	6.2.2
Multilepton (pair) [138]	Pair	$TT \rightarrow ZtVt, BB \rightarrow ZbVb, V = W, Z, H$	6.2.2
High $E_T^{\text{miss}}$ [139]	Pair	$T \rightarrow Vt$ or $B \rightarrow Vb, V = W, Z, H$	6.2.3
Lepton and jets [140]	Single	$T \rightarrow Ht, T \rightarrow Zt$	6.2.4

with multiple leptons [137, 138], in events with large  $E_T^{\text{miss}}$  [139], and in events with a lepton and a large number of jets [140]. The production and decay modes explored by each search discussed in this section are summarized in Table 2.

### 6.2.1 Hadronic searches

Single production of  $T$  and  $B$  quarks is explored in fully hadronic final states, and the two analyses share similar characteristics and challenges. The  $T$  search [136] focuses on the decay channel  $T \rightarrow Ht$ , where the Higgs boson decays into a pair of  $b$ -quarks. The  $B$  search [135] focuses on the decay channel  $B \rightarrow Hb$  and the same Higgs decay is considered. In both cases, the VLQ invariant mass can be reconstructed explicitly by selecting the Higgs boson and the corresponding heavy quark, and it is the search variable used in both analyses. The analyses also share the use of large- $R$  jets to reconstruct and identify the Higgs boson, implementing substructure techniques based on the mass of the jet, the presence and kinematics of  $b$ -tagged variable- $R$  track-jets inside the large- $R$  jet and the  $\tau_{21}$  variable [141], which is a relative measure of whether the jet has a two-body or one-body structure.

The  $B$  analysis uses a four-region variation of the method based on the presence of a forward jet in the event (typical of single VLQ production) and the  $b$ -tagging state of the  $b$ -jet chosen to reconstruct the  $B$  candidate. Correlations are considered by studying events outside the Higgs mass window for the large- $R$  jets chosen as Higgs candidates. Finally, a reweighting method is implemented event-by-event between the control regions used to estimate the background; this allows further correction for kinematic effects produced by correlations between the variables considered in the construction of the ABCD regions.

The  $T$  analysis uses an extension of the ABCD method that brings the number of regions to 81, building a  $9 \times 9$  selection matrix. The different regions correspond to the different tagging states of the two leading large- $R$  jets in the event, i.e. whether these jets are Higgs candidates or not, whether they are top-tagged or not, and whether they contain  $b$ -tagged jets or not. The signal region corresponds to events with one top-tagged jet, one Higgs candidate jet, and at least a total of three  $b$ -tagged jets inside those two jets. The additional regions are used in the background estimation itself, in the normalization of the subdominant  $t\bar{t}$  background, which is estimated from MC samples in the SR, and to evaluate the correlations between the different selection criteria and take them into account in the final background estimation.

The statistical analysis in the two searches is based on the reconstructed invariant mass of the VLQ candidate and finds good agreement between the data and SM prediction in the signal region of each search.

### 6.2.2 Multilepton searches

Events with opposite-sign same-flavour (OSSF) leptons are investigated in searches for pair-produced  $T$  or  $B$  quarks [138] and singly produced  $T$  quarks [137]. In all cases, the relevant decay channel involves a  $Z$  boson decaying into a pair of leptons,  $T \rightarrow Zt$  or  $B \rightarrow Zb$ . Additional leptons can appear in the final state through the leptonic decays of top quarks. Both analyses optimize two search channels independently, one with exactly two OSSF leptons (electrons or muons) and the other with two OSSF leptons and at least one additional lepton. The OSSF lepton pair is used to reconstruct the  $Z$  boson candidate in both channels of both analyses, and it is required to have a mass close to the mass of the  $Z$  boson.

The single-production search defines regions by using the number of forward jets, the number of  $b$ -tagged jets, the number of top-tagged jets,<sup>4</sup> and the number of leptons defining the channel. In the 2-lepton channel, events are assigned to the signal region if they have at least one forward jet, one  $b$ -tagged jet, and one top-tagged jet. Other combinations define control regions to help constrain the major background processes,  $Z$ +jets,  $VV$ , and  $t\bar{t}$  production, which are modelled using MC samples. A kinematic reweighting is used to further constrain the  $Z$ +jets background. In the 3-lepton channel, the signal region is defined by selecting events with at least one  $b$ -tagged jet and at least one forward jet. Additional cuts are applied to the azimuthal angle  $\Delta\phi$  between the reconstructed  $Z$  boson and the non-OSSF lepton or between the  $Z$  boson and the leading  $b$ -tagged jet in the event. Control regions are defined by inverting or removing some of those requirements and selections to help constrain the  $VV$  and  $t\bar{t} + X$  processes (including  $t\bar{t} + V$ ,  $t\bar{t}t\bar{t}$ , and  $t\bar{t}WW$  processes), which produce the dominant backgrounds for this channel. The statistical analysis is performed on the transverse momentum  $p_T(\ell\ell)$  of the OSSF leptons, simultaneously fitting the five CRs and two SRs, and good agreement between the background prediction and data is seen in Figure 17.

The pair-production analysis has many more possible final states than the single-production analysis. One of the VLQs is always expected to decay into a leptonically decaying  $Z$  boson and a heavy quark to provide the OSSF leptons. However, the other VLQ can decay into various bosons:  $W$ ,  $H$ , or  $Z$ . To deal with this type of final state, a multiclass boosted-object tagger (MCBOT) is employed to classify reclustered (RC) jets as  $V$ -tagged,  $H$ -tagged, or top-tagged. This selection aims to take advantage of the large number of jets and consider the possibility of an invisibly decaying  $Z$  boson. Events are also required to have at least one  $b$ -tagged jet. For the two channels, SRs are defined using the number of  $b$ -tagged jets and slightly different definitions of the  $H_T$  variable, which are based on all reconstructed objects relevant to that particular channel. Once the SRs are defined, the MCBOT is used to further classify them according to the tagging status of the RC jet in the event. In total, 19 SRs and 3 CRs are defined and fitted simultaneously

<sup>4</sup> These are jets reclustered with a variable  $R$  parameter value [35] to reconstruct more-boosted or less-boosted top candidates.

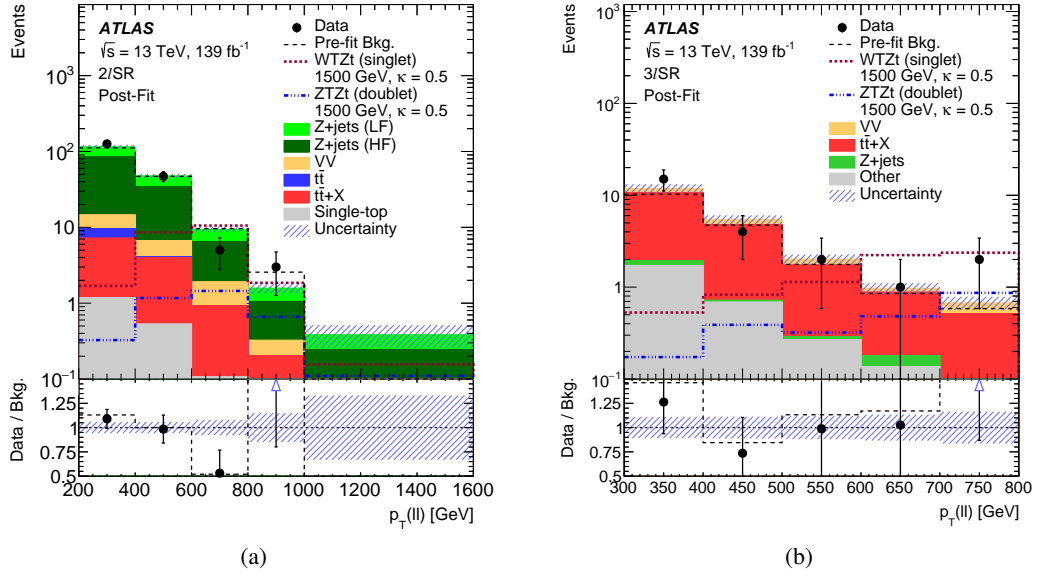


Figure 17: Distributions of  $p_T(\ell\ell)$  in the signal region of the (a) 2-lepton channel and (b) 3-lepton channel of the VLQ search for singly produced  $T$  quarks [137]. The distributions are shown after a background-only fit, with examples of expected signal contributions overlaid.

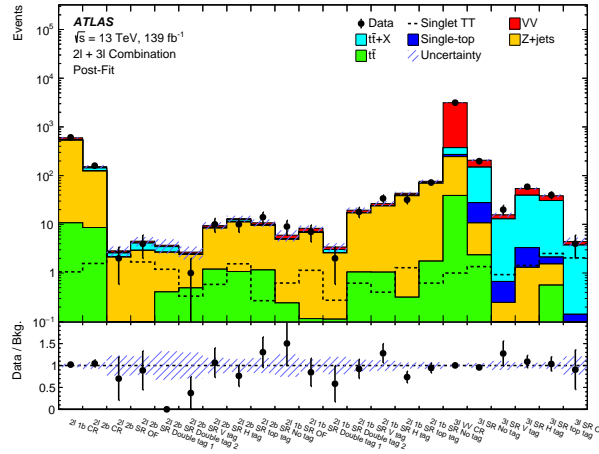


Figure 18: Summary of the data and background yields in all analysis regions from the 2-lepton and 3-lepton channels of the search for pair-produced VLQs [138] after a background-only fit. The expected yields for a benchmark signal are also shown overlaid.

in the statistical analysis, with different variables closely related to the mass or transverse mass of the leptonic VLQ being used in each of them for the final fit. All background processes, dominated by  $Z$ +jets in the 2-lepton channel and  $VV$  and  $t\bar{t} + X$  in the 3-lepton channel, are modelled using MC samples. The background yields in all regions after the background-only fit are shown in Figure 18, and good agreement with data is seen in all signal regions.

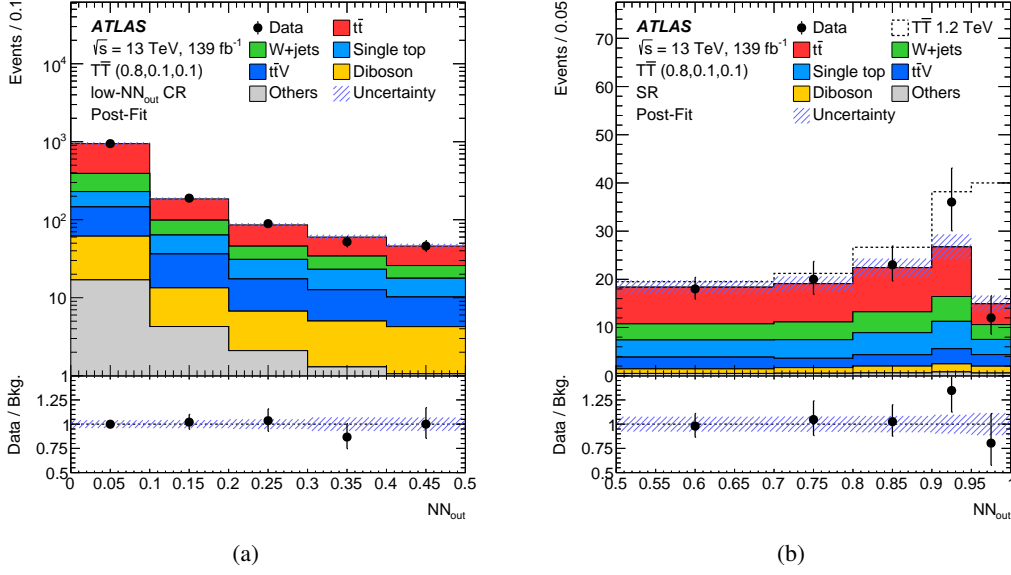


Figure 19: Distributions of the neural network score for (a) one of the control regions and (b) the signal region used in the search for VLQs in events with large  $E_T^{\text{miss}}$  [139]. Distributions are shown after a background-only fit, with a benchmark signal overlaid.

### 6.2.3 Searches in events with large missing transverse momentum

Pair production of VLQs is also investigated in events with a large amount of  $E_T^{\text{miss}}$  [139]. This type of search is particularly sensitive to VLQ decays with a  $Z$  or  $W$  boson in the final state, which can provide a significant amount of  $E_T^{\text{miss}}$  through the presence of neutrinos and are relevant to the search for pair-produced  $B$ ,  $T$ , and  $X$ . Events are required to have  $E_T^{\text{miss}} > 250$  GeV, exactly one lepton (electron or muon) and at least four jets, including at least one  $b$ -tagged jet. Additional requirements on the azimuthal distance between jets and  $E_T^{\text{miss}}$  and on the  $m_T(\ell, E_T^{\text{miss}})$  variable are also imposed. The latter helps to reject  $W$ +jets events, which form one of the major backgrounds in this analysis. Another important background,  $t\bar{t}$ , is reduced by using the  $am_{T2}$  variable. A training region is defined by selecting events with large  $am_{T2}$  and  $m_T(\ell, E_T^{\text{miss}})$  values and one large- $R$  jet. Three additional regions obtained by inverting some of those requirements are used to assist in modelling the  $W$ +jets, single-top, and  $t\bar{t}$  backgrounds. The third region is used to obtain a kinematic event-by-event reweighting of the  $t\bar{t}$  background, applied to correct the MC modelling of this process in the signal region. The first two are used directly in the final fit as control regions. A neural network based on 13 kinematic variables from multiple objects in the event is trained and used to classify events in the training region. High scores define the signal region, while low scores are used as a final control region. The statistical analysis is performed by simultaneously fitting the signal region and three control regions, with all backgrounds modelled using MC samples. The post-fit distributions in the signal region and one of the control regions after a background-only fit are shown in Figure 19 and exemplify the excellent agreement between the data and the expected background.

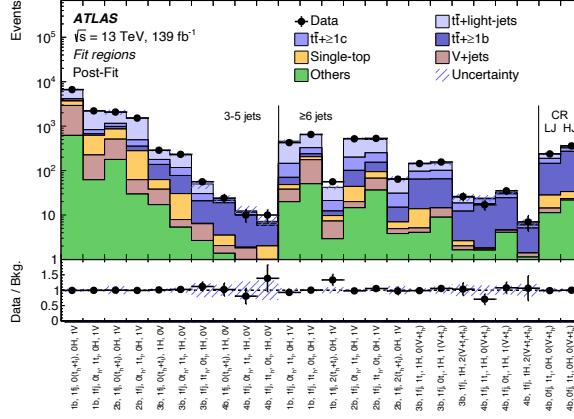


Figure 20: Summary of the data and background yields in all analysis regions used in the search for singly produced  $T$  VLQs in final states with one lepton and multiple jets [140] after a background-only fit.

## 6.2.4 Searches in events with one lepton and multiple jets

Before hadronization, many of the final states that appear in single  $T$  production contain a large number of quarks, top quarks, and  $b$ -quarks, and a heavy boson ( $H$  or  $Z$ ). When the heavy boson decays hadronically (into a pair of  $b$ -tagged jets or other jets) and one of the top quarks decays leptonically, a signature of a single lepton and a large number of jets (from three to six) becomes particularly powerful in selecting and identifying this type of process. To cover the largest possible number of different subprocesses involved in single  $T$  production, a large number of dedicated regions with different jet and hadronically decaying boson multiplicities are investigated [140]. The background from multijet production is suppressed by placing requirements on  $E_T^{\text{miss}}$  and the transverse mass of the lepton and  $E_T^{\text{miss}}$  system. Events must also have at least three jets, with one of them  $b$ -tagged. RC jets are used to identify hadronically decaying boosted top quarks, Higgs bosons, and  $V$  ( $W$  or  $Z$ ) bosons. The mass of each RC jet and its number of subjets are used to tag it as one of the possible hadronic resonances. Top-quark candidates decaying semileptonically are identified by combining the lepton, the  $E_T^{\text{miss}}$ , and one of the  $b$ -tagged jets in the event and imposing kinematic constraints on the combination. A total of 22 signal regions are defined for different multiplicities of jets,  $b$ -tagged jets, leptonically decaying top quarks, top-tagged RC jets, Higgs-tagged RC jets, and  $V$ -tagged RC jets. All of the SRs are also required to have one forward jet. Additional regions without a forward jet are used to help with background modelling in the final fit. All background processes are modelled using MC samples. The multijet background prediction is improved by normalizing it to data in a multijet-enriched region, while a dedicated kinematic reweighting is used to improve the  $t\bar{t}$  and  $W$ +jets modelling, which is known to underestimate the data at high jet multiplicities and/or high  $p_T$ . The statistical analysis in the 22 SRs and 2 CRs uses  $m_{\text{eff}}$ , which shows strong signal discrimination power. Good agreement between the SM prediction and the data in all the fit regions is seen in Figure 20.

## 6.2.5 Limits on VLQ pair production

The two searches looking for pair production of VLQs have complementary sensitivity. Mass limits are set in a two-dimensional plane of the possible branching ratios (BR) of  $T$  and  $B$  decays and are shown in Figure 21. The limits corresponding to the singlet and different doublet hypotheses are shown in each plot.

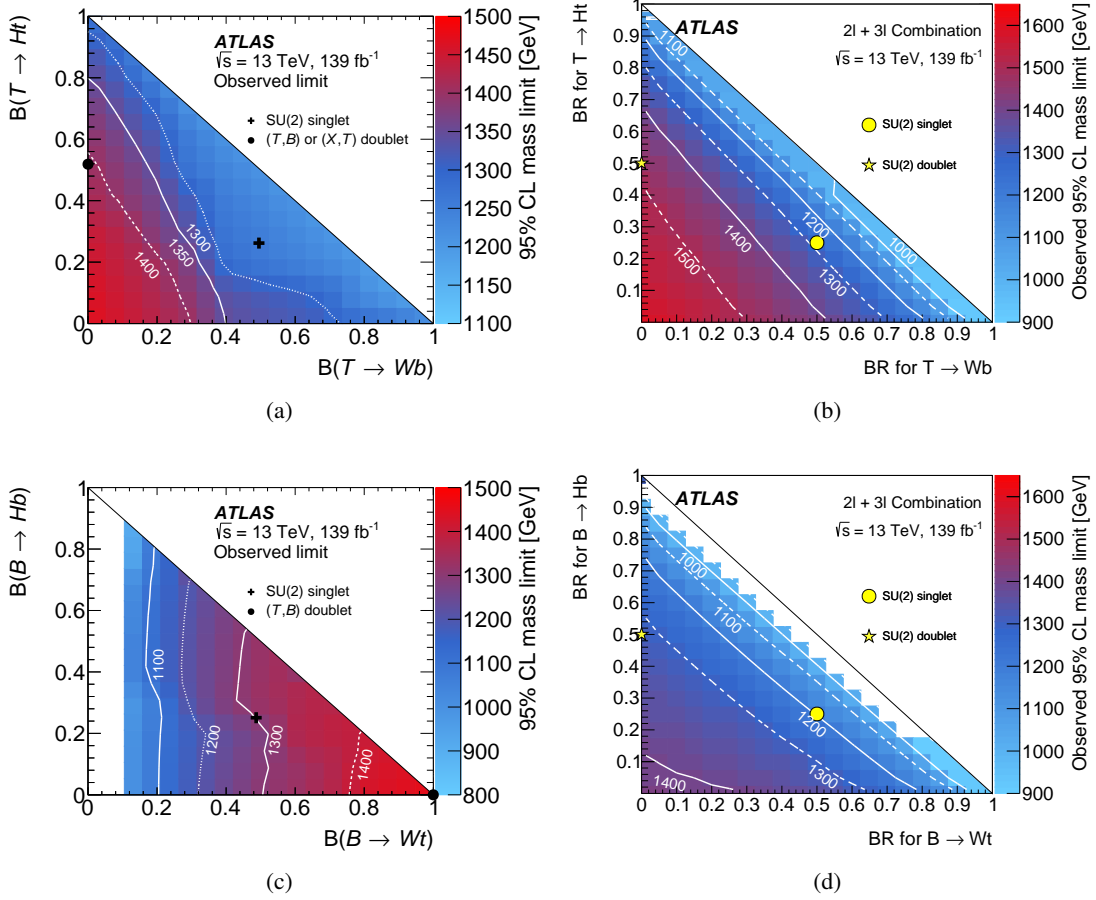


Figure 21: Observed lower limits on the  $T$  and  $B$  masses in the BR plane for pair production of (a,b)  $TT$  and (c,d)  $BB$ . Results from (a,c) the search for VLQs in events with large  $E_T^{\text{miss}}$  [139] and (b,d) the search for pair-produced VLQs in multilepton final states [138] are included. The doublet hypothesis considered in (b,d) is  $(T, B)$ .

For a  $T$  quark, the multilepton search is generally more sensitive, but the  $E_T^{\text{miss}}$ -based search has better sensitivity in the top left corner of the BR plane. They have very similar sensitivities for the singlet and doublet models, excluding masses below about 1.25 TeV and 1.41 TeV, respectively. For a  $B$  quark, the two searches behave very differently and are more sensitive in opposite regions of the BR plane. The  $E_T^{\text{miss}}$ -based search has a higher mass limit in the singlet scenario, excluding masses up to 1.33 TeV. The doublet scenarios in the two searches correspond to different VLQ combinations and thus cannot be compared directly. Masses below  $\sim 1$  TeV are excluded for any BR combination of pair-produced  $B$  and  $T$  quarks.

In addition to these two analyses using the full Run 2 dataset, seven VLQ searches for pair-produced VLQs in a partial Run 2 dataset (recorded between 2015 and 2016) were interpreted together in a single statistical combination [142], which improved on the individual results.

### 6.2.6 Limits on single VLQ production

Limits on single  $T$  production are set for various coupling values as a function of the mass of the VLQ. Limits on the coupling as a function of the  $T$  mass are shown in Figure 22 and Figure 23 for the singlet and  $(T, B)$  or  $(B, Y)$  doublet hypotheses, respectively. Of the three searches, the multilepton analysis has the strongest sensitivity for the full range of masses considered for any multiplet hypothesis. In the semileptonic analysis, the limit for high masses reaches lower coupling values because of a slight deficit of data observed in some signal regions. Only the hadronic  $B$  decay search in ATLAS considers single  $B$  production, and the corresponding limit plots are also shown in Figure 22 and Figure 23. The hadronic  $T$  decay analysis did not consider the doublet hypothesis and, therefore, is not included in Figure 23.



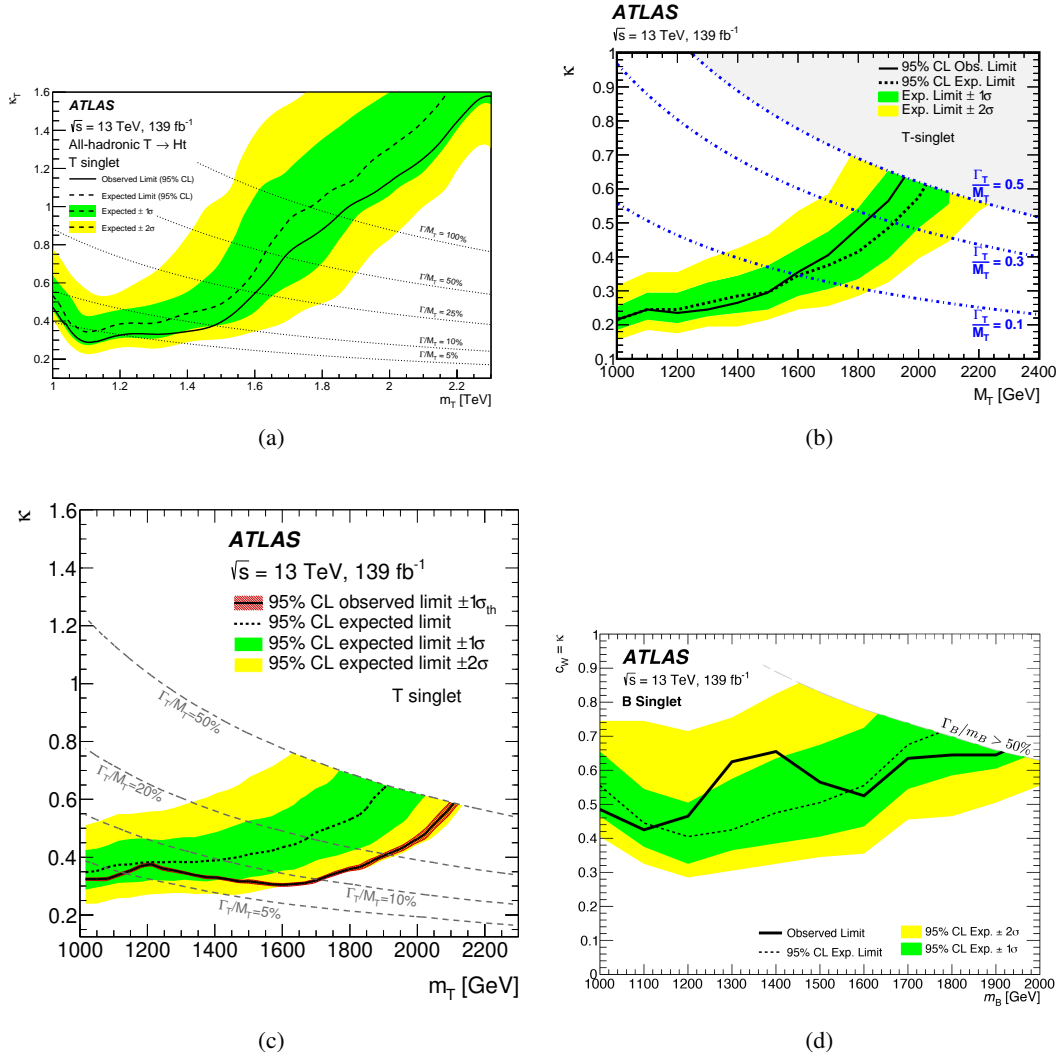


Figure 22: Observed and expected upper limits on (a,b,c) single  $T$  and (d) single  $B$  production as a function of the mass of the VLQ for a singlet hypothesis. Results from searches for (a) singly produced  $T$  in hadronic final states [136], (b) singly produced  $T$  in multilepton final states [137], (c) singly produced  $T$  in final states with one lepton and multiple jets [140] and (d) singly produced  $B$  in hadronic final states [135], are included. The dashed curves represent contours of constant relative VLQ width.

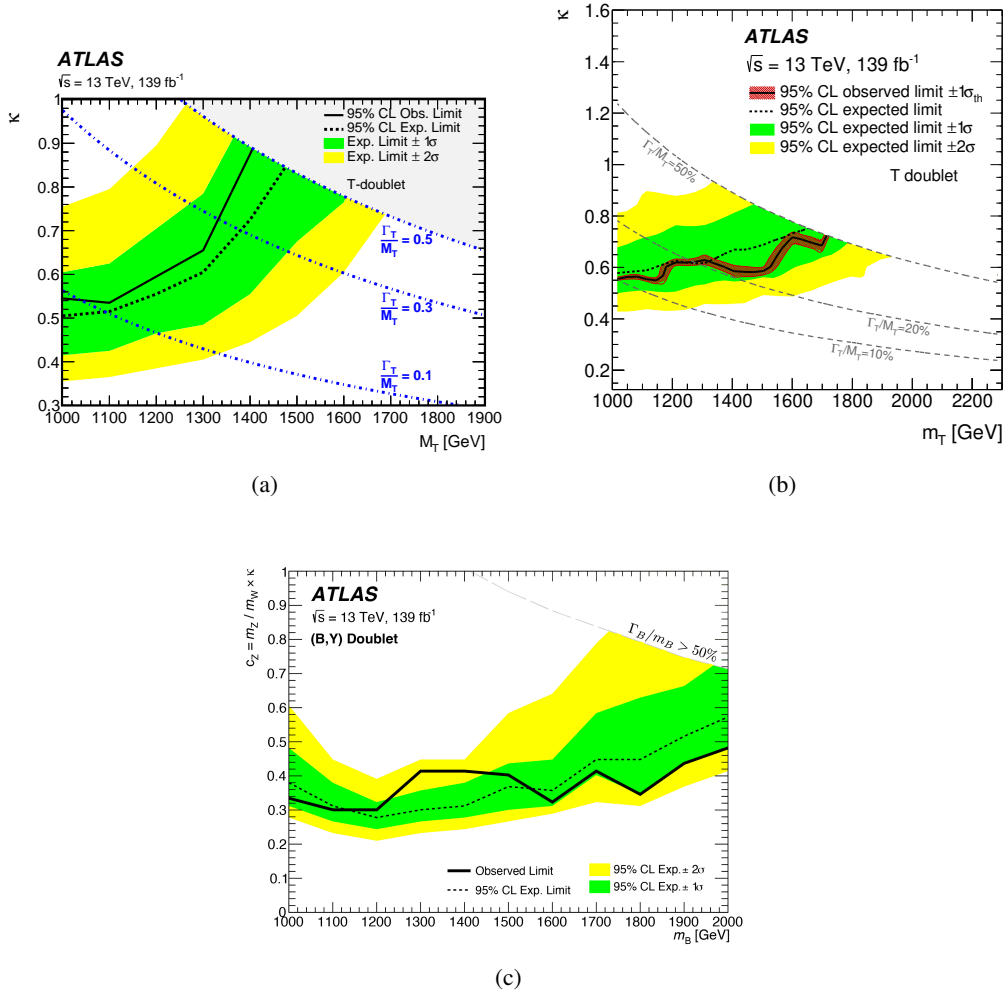


Figure 23: Observed and expected upper limits on (a,b) single  $T$  and (c) single  $B$  production as a function of the mass of the VLQ for a doublet hypothesis. Results from searches for (a) singly produced  $T$  in multilepton final states [137], (b) singly produced  $T$  in final states with one lepton and multiple jets [140] and (c) singly produced  $B$  in hadronic final states [137] are included. The dashed curves represent contours of constant relative VLQ width. The doublet hypothesis considered in (a,b) is  $(T, B)$ .

## 7 Leptoquarks

One striking feature of the SM is the similar structure of the lepton and quark sectors, which, a priori, could have been very different. One possibility that could lie behind the similarity is the presence of a BSM symmetry connecting the two sectors. With this idea in mind, many theories introduce new particles, called leptoquarks (LQs) [113, 143], with both baryon and lepton number. Theories dealing with unification [144], supersymmetric models with R-parity violation [145], and models with composite fermions [146] are some areas that typically consider adding such particles. Having baryon and lepton numbers makes them special, as it confers on them the ability to convert quarks into leptons and vice versa. LQs have fractional charge and are triplets of the strong interaction, with other SM quantum numbers, such as their weak isospin representation or their spin, varying between theories.

Because of their unique properties, they can mediate processes that violate lepton-flavour universality and were proposed as a possible explanation for anomalies observed in  $B$ -meson decays [147–149]. A scalar LQ can also explain the discrepancy between the measured and predicted values of the muon’s anomalous magnetic moment ( $g - 2$ ) [150, 151].

Because they interact strongly, LQs can be pair-produced at the LHC with large cross sections, which explains why this has been the most studied production mode. This production mode is independent of the coupling of the LQ to leptons and quarks but is suppressed for high LQ masses. Single LQ production, in which the LQ coupling to leptons and quarks appears explicitly, becomes more copious than LQ pair production at high LQ mass and coupling values and has also been investigated. Non-resonant LQ production is also possible and has been considered in some searches. Illustrative diagrams of the different modes of LQ production are shown in Figure 24 for a specific choice of LQ coupling and decay chain.

Initially, searches for LQs in ATLAS focused on models in which they would only couple with quarks and leptons of the same generation, with special emphasis on the third-generation LQ that would couple to bottom quarks, top quarks,  $\tau$ -leptons, and  $\nu_\tau$ -neutrinos. However, the possibility of off-diagonal couplings, and therefore cross-generational quark–lepton conversions, was investigated in an attempt to explain the  $B$ -meson and muon  $g - 2$  results [152, 153].

This section starts by discussing the third-generation searches performed by ATLAS in final states with top quarks [154, 155] and bottom quarks [156–159], and finishes by discussing the cross-generational searches with light leptons [160–163] or charm quarks [69] in the final state. Results are discussed in the context of

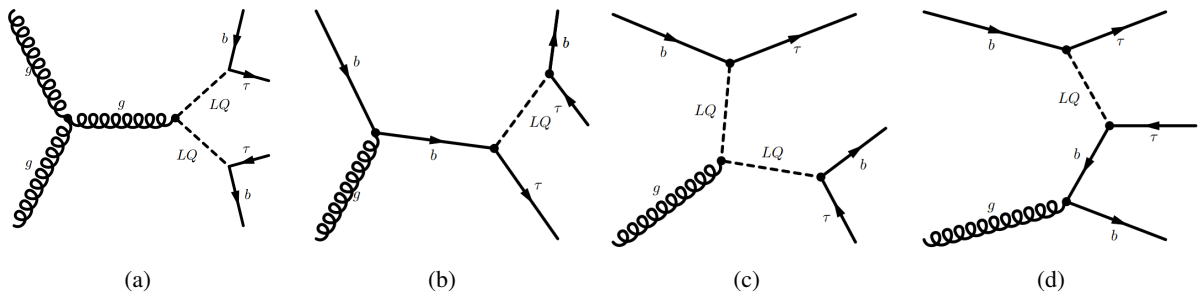


Figure 24: Illustrative Feynman diagrams of (a) LQ pair production, (b,c) single LQ production and (d) non-resonant LQ production.

scalar LQs in this report, but interpretations of vector-like LQs are also included in some of the analyses referenced. The following subsections distinguish between an up-type LQ ( $LQ^u$ , with a charge of  $2/3$ ) and a down-type LQ ( $LQ^d$ , with a charge of  $-1/3$ ).

## 7.1 Searches for LQs with exclusive third-generation couplings

This search type focuses on LQ models in which the LQ couples exclusively or primarily to the third generation of SM fermions ( $LQ_3^{u,d}$  for up-type and down-type LQs respectively). They deal with final states with multiple top quarks, bottom quarks, and  $\tau$ -leptons.

### 7.1.1 Down-type LQs with exclusive third-generation couplings

For scenarios with down-type LQs decaying exclusively into third-generation fermions, two decays are possible:  $t\tau$  and  $b\nu_\tau$ . Both have been investigated in ATLAS in three distinct analyses.

The  $t\tau t\tau$  [154] analysis defines seven orthogonal channels to search for the pair production of LQs, selecting events according to their light-lepton and jet multiplicities, and always requiring the presence of a hadronically decaying  $\tau$ -lepton ( $\tau_{\text{had}}$ ). Additional kinematic variables such as the transverse momentum of the leptons or jets, the missing transverse momentum, and invariant mass combinations among the different objects are used in every channel to separate the SRs from CRs used to help in the modelling of the various SM backgrounds. Additional control regions are built from selections without a reconstructed  $\tau_{\text{had}}$ . Irreducible backgrounds from SM processes are modelled using MC samples, with kinematic reweighting applied to  $t\bar{t}$  processes, one of the major background components. Contributions from fake  $\tau_{\text{had}}$  and non-prompt light leptons are estimated using simulations, with normalization corrections obtained in dedicated regions. In total, 15 CRs and 7 SRs are fitted simultaneously in the statistical analysis, with  $m_{\text{eff}}$  being used as the discriminating variable in the SRs. Figure 25 shows good overall agreement between data and MC simulation.

Two searches have been conducted in ATLAS to explore pair production of LQs decaying in the  $b\nu_\tau$  channel. They both select events with a large amount of  $E_{\text{T}}^{\text{miss}}$  but focus on different final states. One of them [158] focuses on a symmetrical final state in which both LQs decay in the same channel. The final state has two  $b$ -tagged jets in addition to significant  $E_{\text{T}}^{\text{miss}}$ . The other [159] considers the asymmetrical case in which one LQ decays into  $b\nu_\tau$  while the other decays into  $t\tau$ . Compared to the symmetrical search, this search has a final state with one  $\tau$ -lepton and additional jets.

In the symmetrical case, events with large  $E_{\text{T}}^{\text{miss}}$  ( $> 250$  GeV), no light leptons, and between two and four jets are selected to form a signal region (SRA). The leading and subleading jets in the event must be  $b$ -tagged, and no additional  $b$ -tagged jets are allowed. Additional selection criteria are imposed on  $m_{bb}$ ,  $m_{\text{eff}}$  and  $m_{\text{CT}}$ . A second signal region (SRB) has a relaxed requirement on the  $b$ -tagging configuration, in which the leading jet is required not to be  $b$ -tagged. Instead of using the set of kinematic criteria used in SRA, a BDT is employed to define the signal region by using many kinematic variables constructed from the jets in the event and the  $\mathbf{p}_{\text{T}}^{\text{miss}}$ . Two control regions, one associated with each SR, are also defined by selecting events with two opposite-sign same-flavour (OSSF) light leptons to help model the main SM background,  $Z$ +jets. Additional signal regions are defined with different jet and  $b$ -tagged jet criteria, but because they target other BSM particles, they are not discussed here. The statistical analysis relies on a simultaneous fit of the two SRs and process templates provided by MC samples for signal and SM

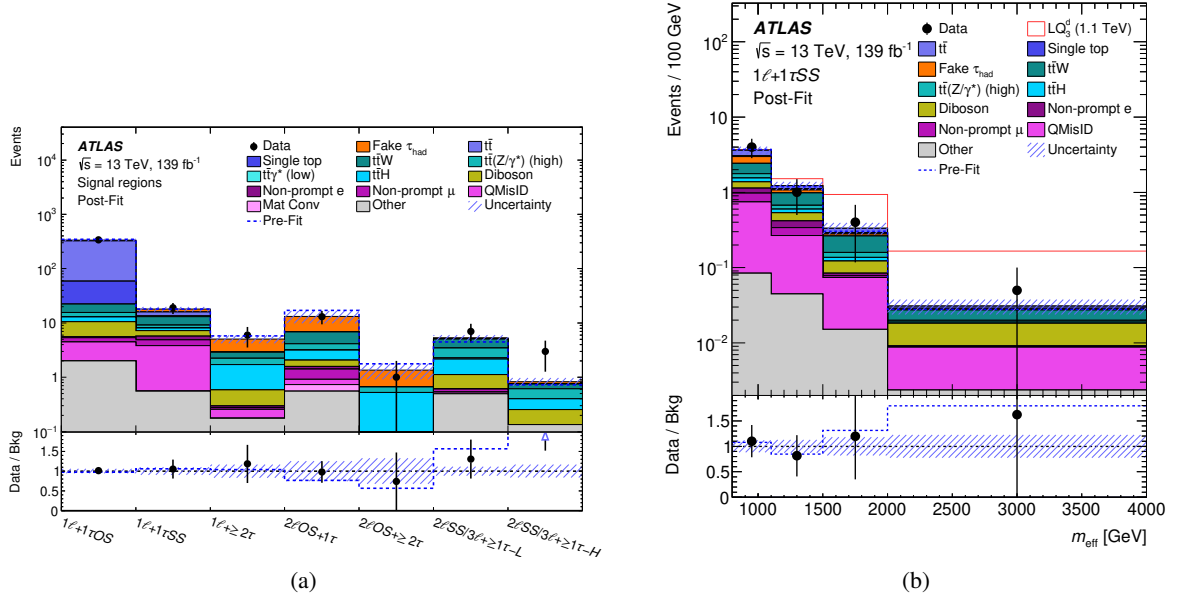


Figure 25: (a) Event yields in all signal regions and (b) the distribution of  $m_{\text{eff}}$  in one of the signal regions used in the search for  $LQLQ \rightarrow t\bar{t}\tau\tau$  [154]. The distributions are shown after a background-only fit.

backgrounds. The fit uses the event yield in the CR, the  $m_{\text{CT}}$  distribution in SRA, and the BDT score in SRB, revealing good agreement between data and background as shown in Figure 26(a).

In the asymmetrical case, a single SR with large  $E_{\text{T}}^{\text{miss}} (> 280 \text{ GeV})$ , at least two  $b$ -tagged jets, no light leptons, and exactly one  $\tau_{\text{had}}$  is used to look for pair production of LQs. Additional requirements are imposed on the  $p_{\text{T}}$  of the  $\tau_{\text{had}}$ , on the scalar sum of the transverse momenta,  $S_{\text{T}}$ , computed from the  $\tau_{\text{had}}$  and the two leading jets, and on  $m_{\text{T}}(X, E_{\text{T}}^{\text{miss}})$  where  $X$  is either one of the two leading jets or the  $\tau$ -lepton. Two CRs which help in modelling some of the important SM backgrounds,  $t\bar{t}$  and single-top production, are defined by inverting or relaxing some of the additional requirements. Two more CRs are defined for events with two  $\tau_{\text{had}}$ . A corresponding di- $\tau$  SR region is defined to target other BSM particles but is not discussed further. The statistical analysis uses the event yield in the CR and the  $p_{\text{T}}$  distribution of the  $\tau$ -lepton in the SR. All signal and background templates are obtained from simulated events. A background-only fit, shown in Figure 26(b), finds good agreement between data and the expected background.

### 7.1.2 Up-type LQs with exclusive third-generation couplings

Two decays, into  $b\tau$  and  $t\nu$ , are allowed for an up-type LQ with exclusive third-generation couplings. Three ATLAS analyses tackle this configuration explicitly, one focusing on pair production of LQs decaying symmetrically in the  $b\tau$  channel [157], another focusing on single production of a LQ decaying the same way [156], and a third focusing on pair production of LQs decaying symmetrically into  $t\nu$  [155]. The asymmetrical search [159] described in the previous section can also be used to search for up-type LQs.

The  $b\tau b\tau$  analysis selects events with either one  $\tau_{\text{had}}$  or two oppositely charged  $\tau_{\text{had}}$ , building two distinct channels. In the single- $\tau$  channel, events must have a light lepton (electron or muon) with charge opposite

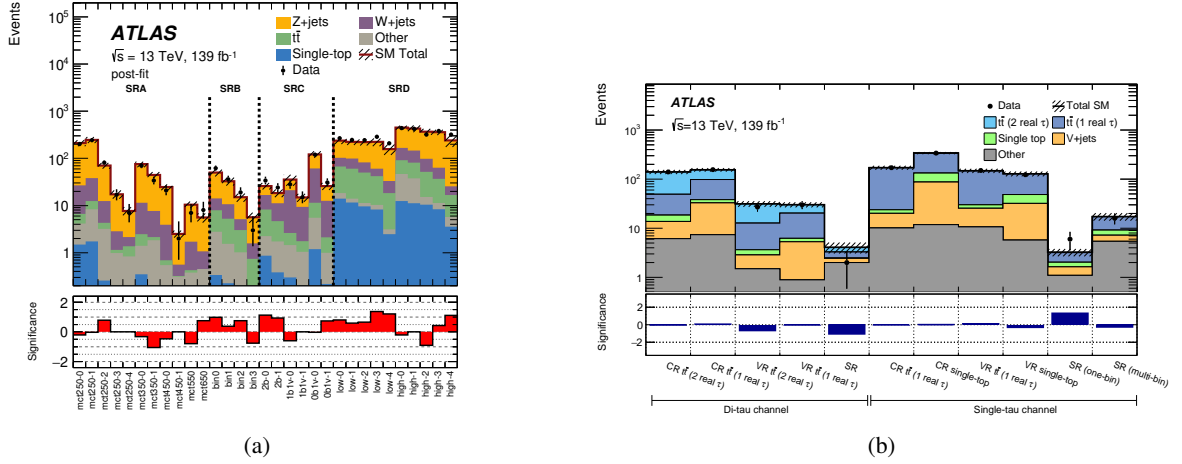


Figure 26: Event yields in (a) all signal regions used in the search for  $LQLQ \rightarrow bb\nu\nu$  [158] and (b) all regions used in the search for  $LQLQ \rightarrow tb\tau\nu$  [159] after a background-only fit. Only (a) SRA and SRB and (b) regions in the single- $\tau$  channel are used while searching for LQ production.

to that of the  $\tau_{\text{had}}$ . Both channels require the presence of at least two jets and one or two  $b$ -tagged jets. An additional requirement is imposed on  $m_{\tau\tau}$ , reconstructed using the MMC technique, to help reduce the  $Z$ +jets background contribution. Finally, requirements on  $S_T$  (the scalar sum of the transverse momenta of the objects in the event) and  $E_T^{\text{miss}}$  are imposed to reduce the contamination from multijet backgrounds. Signal regions are built using a parameterized neural network (PNN), parameterized as a function of the hypothesized LQ's mass. The PNN uses either six or seven variables, depending on the channel, selected from amongst many kinematic, multiplicity, and angular variables. The dominant  $Z$ +jets and  $t\bar{t}$  backgrounds are estimated using MC samples with normalization corrections derived in a  $t\bar{t}$ -rich CR. In the SR, fake- $\tau$  contributions from  $t\bar{t}$  events are estimated from simulated  $t\bar{t}$  events after applying data-driven corrections obtained in a fake-rich CR. A small but non-negligible fake contribution from multijet events is estimated using the fake-factor method. The PNN score is used in the statistical analysis, and the two SRs are fitted simultaneously. Reasonable agreement between data and the SM prediction is obtained after a background-only fit, with a slight deficit of data events observed in the di- $\tau$  channel. The result of the background fit in the di- $\tau$  region is shown in Figure 27.

The  $t\nu\nu$  analysis looks for a pair of LQs in final states with a large amount of  $E_T^{\text{miss}} (> 250 \text{ GeV})$  and a pair of hadronically decaying top quarks. Besides this  $E_T^{\text{miss}}$  requirement, SRs are built using events with exactly zero leptons (electrons, muons, or  $\tau$ -leptons) and at least four jets, two of them  $b$ -tagged. The leading RC jet is also required to have a mass higher than 120 GeV, indicating the presence of a hadronic top-quark decay. Two regions (SRA and SRB) are built according to the value of  $m_{T,\chi^2}$  [52] which makes them sensitive to different mass hypotheses. Additional cuts on variables related to the  $b$ -tagged and RC jets, and their relative positions and kinematic properties, are employed in both regions to increase the sensitivity. Finally, each region is divided into three categories according to the mass of the subleading RC jet. Five CRs built with selections that contain light leptons are used to help in the modelling of the different backgrounds, dominated by  $Z \rightarrow \nu\nu$  production. Additional signal and control regions are defined to look for other BSM particles but are not discussed here. The statistical analysis simultaneously fits the event yields in the six SRs and five CRs. A background-only fit shows good agreement between data and the SM prediction, with a slight excess of data in one of the signal regions, as seen in Figure 27.

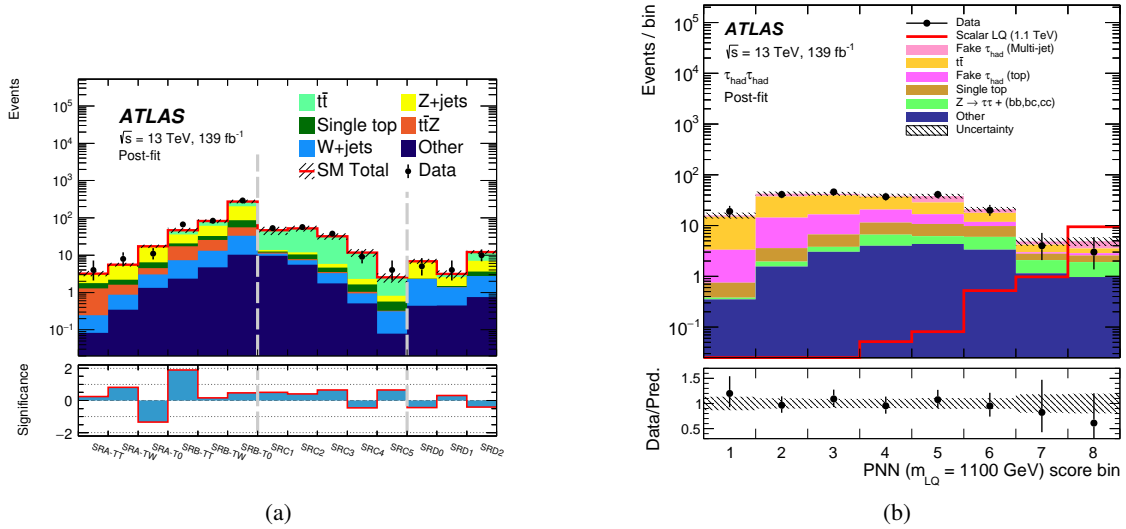


Figure 27: (a) Event yields in all signal regions used in the search for  $LQLQ \rightarrow tt\nu\nu$  [155] and (b) the PNN distribution in the di- $\tau$  signal region used in the search for  $LQLQ \rightarrow bb\tau\tau$  [157] after a background-only fit. (a) Only SRA and SRB are used to search for LQ production.

The single-production analysis proceeds similarly to the pair-production one. It separates events into two channels, one with two  $\tau_{had}$  of opposite charge and the other with one  $\tau_{had}$  and one isolated light lepton (electron or muon) of opposite charge. Both channels define a signal region by requiring at least one  $b$ -tagged jet and imposing additional criteria based on the invariant mass of the visible decay products of the two  $\tau$ -leptons and the angular separation between the light lepton and the  $E_T^{miss}$ . These criteria aim to reduce the  $Z \rightarrow \tau\tau$  and  $t\bar{t}$  backgrounds. Each signal region is divided into two  $p_T$  ranges,  $p_T < 200$  GeV and  $p_T > 200$  GeV, making four signal regions. In the single- $\tau$  channel, the  $t\bar{t}$  and single-top backgrounds are modelled using MC samples with a data-driven correction derived in a dedicated CR. In the SR, fake- $\tau$  contributions from top-quark processes are estimated similarly to the pair-production analysis, using a region rich in fakes. A final contribution from multijet events faking  $\tau$ -leptons is estimated using a data-driven fake factor. In the di- $\tau$  channel, defining a top-quark-process-rich CR close to the SR, as is done in the single- $\tau$  channel, is very complex, and the modelling is corrected using a kinematic reweighting based on  $S_T$ , which is computed from the two  $\tau_{had}$  and the leading- $p_T$   $b$ -jet. Background from  $Z \rightarrow \tau\tau$  is estimated from MC simulations, with a scale factor obtained from a CR with only one  $\tau_{had}$ . Background from multijet events is estimated using a data-driven fake-factor method. The statistical analysis employs the  $S_T$  distributions in the four signal regions. Reasonable agreement is found between data and the SM background, with a minor excess of data observed in the high- $p_T$  signal region for high  $S_T$ .

### 7.1.3 Limits on LQs with exclusive third-generation couplings

In the absence of significant excesses in data, limits are obtained for the pair production of scalar leptoquarks as a function of the mass of the LQ for different values of the BR to  $b\tau$  or  $t\tau$  for down-type or up-type leptoquarks respectively. Two-dimensional limits on the production of up-type and down-type scalar leptoquarks as a function of the mass of the LQ and its BR are shown in Figure 28. In addition to the



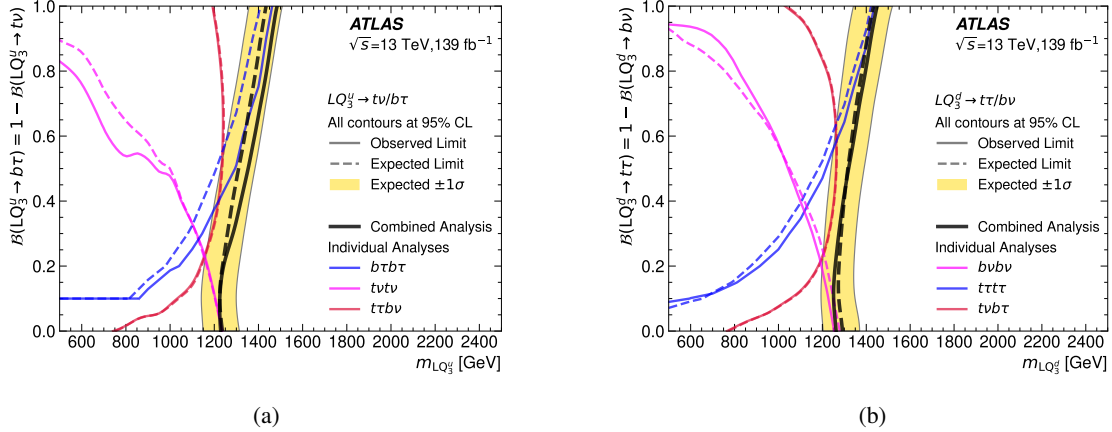


Figure 28: Two-dimensional limits (a) on the production of up-type scalar leptoquarks with exclusive third-generation couplings as a function of the mass of the LQ and the BR to  $b\tau$  from the search for (blue)  $LQLQ \rightarrow b\tau\tau$  [157], (red)  $LQLQ \rightarrow b\tau\nu$  [159], (pink)  $LQ \rightarrow \tau\nu\nu$  [155] and (black) their statistical combination [164] and (b) on the production of down-type scalar leptoquarks with exclusive third-generation couplings as a function of the mass of the LQ and the BR to  $\tau\nu$  from the search for (blue)  $LQLQ \rightarrow \tau\tau\tau$  [154], (red)  $LQLQ \rightarrow \tau\tau\nu$  [159], (pink)  $LQLQ \rightarrow \nu\nu\nu$  [158] and (black) their statistical combination.

limits obtained in the individual searches, the result obtained after a statistical combination [164] of those searches is also shown in all cases. Two of the searches described in this section [157, 159] also include interpretations regarding the pair production of vector-type LQs. Lower limits on the mass are between 200 and 400 GeV higher than the corresponding mass limits for scalar LQs in the same BR scenario. Searches with visible decays in the final state are more sensitive to higher values of the BR, while searches with neutrinos in the final state become important for lower values.

The analysis focusing on singly produced LQs [156] sets limits on different models of vector-like LQs. Despite its focus on single production, it considers the three possible production modes in its interpretation: non-resonant, single, and pair production. In the Yang–Mills scenario, the observed lower limits on the LQ mass are between 1.58 TeV and 2.05 TeV, depending on the coupling. The lower limits in the minimal-coupling scenario are between 1.35 TeV and 1.99 TeV. Finally, the lower limits for a scalar LQ scenario with charge  $(4/3)e$  are between 1.28 TeV and 1.53 TeV. Figure 29 summarizes those limits.

## 7.2 Searches for LQs with cross-generational couplings

These searches explore the possibility of an LQ mediating an interaction that connects quarks and leptons from different generations ( $LQ_{\text{mix}}^{u,d}$  for up-type and down-type LQ, respectively). Most deal with final states with multiple light leptons (electrons or muons) and multiple bottom or top quarks. The other cross-generational possibility (light quarks and  $\tau$ -leptons) is also investigated in one of the searches described. These cross-generational couplings are particularly relevant in models attempting to explain  $B$ -meson and muon  $g - 2$  results. Electron and muon selections are considered independently, duplicating the SRs and CRs for use in separate statistical analyses.

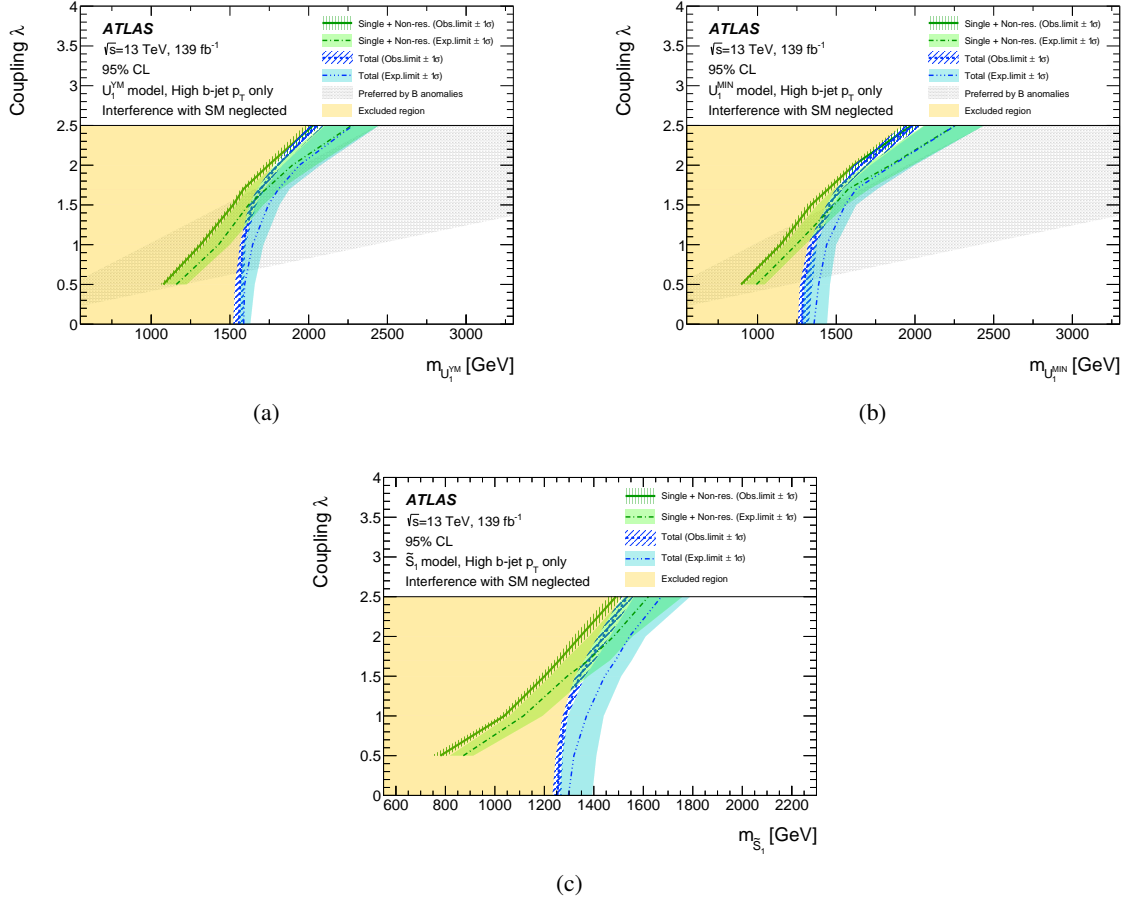


Figure 29: Two-dimensional limits for single plus non-resonant production of (a) vector-like LQs in the Yang–Mills scenario, (b) vector-like LQs in the minimal-coupling scenario and (c) scalar LQs. Although the search [156] focuses on singly produced LQs, its interpretation includes pair production in the ‘Total’ limits.

### 7.2.1 Up-type LQs with cross-generational couplings

Two searches for pair-produced up-type LQs with cross-generational couplings have been performed in ATLAS. One is aimed at final states with exactly two light leptons [163] and the other is aimed at final states with one light lepton [161].

For the two-lepton analysis, events with exactly two OSSF light leptons (electrons or muons) and at least two jets are selected. Additional requirements on the invariant mass and  $p_T$  of the dilepton system suppress background from Drell–Yan and  $Z$  boson production. LQ candidates are identified from the different possible pairs of lepton+jet by choosing the two pairs closest in  $m_{\ell j}$ . The maximum and minimum  $m_{\ell j}$  in the event is used to construct the  $m^{\text{asym}}$  variable, which helps to reduce the SM background further. Events with low  $m^{\text{asym}}$  form a single signal region, while the rest constitute a sideband region (SB) that is used as a CR in the statistical analysis. A second CR is defined to help in the modelling of the  $t\bar{t}$  background by selecting events with two opposite-sign opposite-flavour leptons. Two independent statistical analyses are defined, one targeting  $LQ \rightarrow b\ell$  decays and the other targeting  $LQ \rightarrow c\ell$  decays. For the former decay,

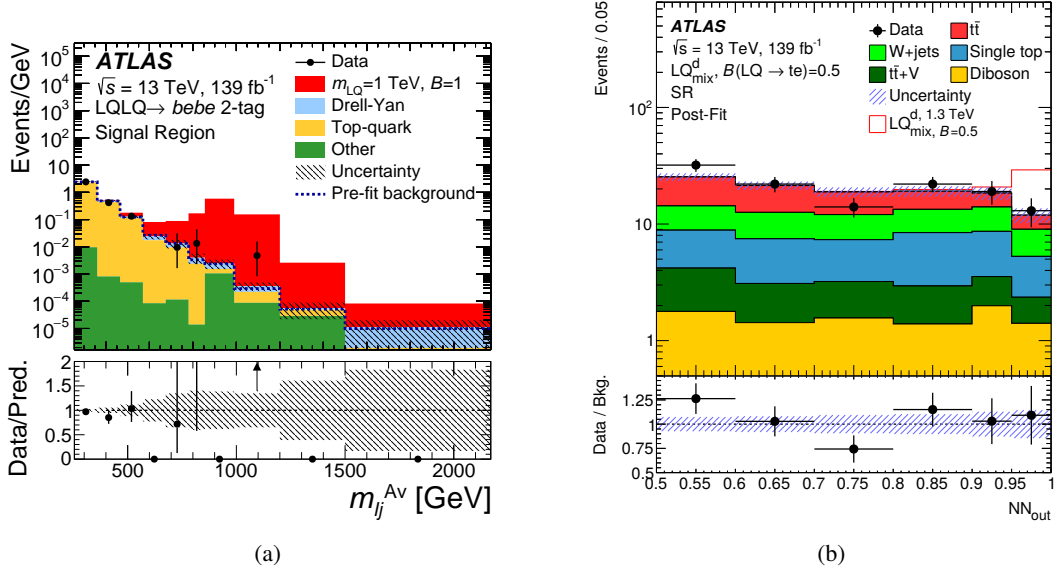


Figure 30: (a) Average invariant mass of the lepton+jet system in one of the SRs from the search for up-type LQs in final states with two light leptons [163] and (b) NN score in the SR from the search for LQs in final states with one light lepton [161] after a background-only fit to data.

the SR and SB are split into three subregions according to the number of  $b$ -tagged jets in the event (zero, one, or at least two). For the latter decay, events in the SR and SB are separated into those with zero tags, at least one  $c$ -tag, and at least one  $b$ -tag. Events with a  $b$ -tagged jet and a  $c$ -tagged jet are placed in the  $c$ -tagged category. Both statistical analyses use the distribution of the average lepton+jet invariant mass of the two LQ candidates in the event, and all SM and signal processes are modelled using MC samples. The data and MC simulation agree well, as shown in Figure 30(a) for one of the electron selection's SRs.

In the one-lepton analysis, events with exactly one lepton (electron or muon), a significant amount of  $E_T^{\text{miss}}$ , and at least four jets are selected. This very general selection can capture events from a variety of up- and down-type LQ decay modes ( $LQ \rightarrow t\nu$ ,  $LQ \rightarrow b\ell$ ,  $LQ \rightarrow t\ell$  and  $LQ \rightarrow b\nu$ ). Events with at least one  $b$ -tagged jet, large  $m_T(\ell, E_T^{\text{miss}})$ , and high  $am_{T2}$  are assigned to a training region. In this region, a neural network (NN) is trained to separate signal and background events, using 15 input variables related to the objects in the event, including the lepton flavour. An SR is defined using the events with a high NN score, while the lower score region is kept as a CR. Two additional CRs are defined to help in modelling the single-top and  $W$ +jets backgrounds with selections based on the presence of two  $b$ -tagged jets and lower  $m_T(\ell, E_T^{\text{miss}})$  respectively. A kinematic reweighting of the MC prediction of the  $t\bar{t}$  background is implemented before the statistical analysis, with corrections obtained in a  $t\bar{t}$ -rich region defined using  $am_{T2}$ . The statistical analysis uses the distribution of the NN score in the SR and the overall event yield in each CR, with all signal and background processes modelled using MC samples. The data and SM prediction agree well after a background-only fit, as shown in Figure 30(b) for the electron selection's SR.

## 7.2.2 Down-type LQs with cross-generational couplings

Three ATLAS searches consider the scenario of a down-type LQ with cross-generation couplings and are defined according to the number of light leptons present in the final state. The one-lepton search [161] is described in Section 7.2.1, as the same search is also used for up-type scenarios. A separate two-lepton search is, however, introduced [162] to take into account the presence of top quarks, and a recent multilepton analysis [160] investigates events with two, three or four light leptons in the final state arising from the pair production of LQs and the  $LQ \rightarrow t\ell$  decay channel.

The dilepton analysis builds a single SR with events containing exactly two OSSF light leptons, at least two large- $R$  jets, and large  $m_{\ell\ell}$ , which is used to suppress the background from  $Z$  boson production. A CR defined to help in the modelling of  $Z$ +jets production is built with events having lower  $m_{\ell\ell}$  values. A second control region with OS different-flavour pairs of leptons is built to help model the  $t\bar{t}$  background. A BDT is used in the SR to further separate signal and background, with its input including variables related to the substructure and kinematics of the large- $R$  jets. The BDT is parameterized using the masses of the different signal hypotheses, which are included in the training. The BDT score in the SR and the overall number of events in each CR are used in the statistical analysis, with all signal and background templates modelled using MC samples. A background-only fit to data, shown in Figure 31(a) for all fitted regions, reveals good agreement between data and MC simulation.

The multilepton analysis is divided into three distinct channels, defined by the lepton multiplicity in each event: two same-sign light leptons ( $2\ell$ SS), three light leptons ( $3\ell$ ), or at least four leptons ( $4\ell$ ). Only the  $3\ell$  and  $4\ell$  channels contain signal regions, while the  $2\ell$  channel is used entirely to define CRs to help in modelling the  $t\bar{t}$  and single-top backgrounds. Additional CRs are defined in the  $3\ell$  channel to help model other SM backgrounds, such as  $t\bar{t} + Z$  or diboson production. In the  $3\ell$  channel, events are classified as being in the signal region if they have at least two jets, at least one  $b$ -tagged jet, and a pair of opposite-sign same-flavour leptons that have a mass far from the  $Z$  boson mass window, which helps to suppress SM background containing a  $Z$  boson. Events are also required to have a large ( $> 200$  GeV) invariant mass  $m_{\ell\ell}^{\min}$ , which corresponds to the smallest invariant mass among of all two-lepton combinations and has the ability to separate background and signal processes very efficiently. A procedure to identify electrons with incorrect charge assignment that originate from internal photon conversions or photon conversions in matter is implemented through a BDT discriminant. Electrons in the signal region are required to pass a conversion veto, while events with electrons not passing the veto are assigned to one of two additional CRs. The SR is split in two, according to the flavour of the OSSF pair of leptons. In the  $4\ell$  channel, events are classified following criteria very similar to those in the  $3\ell$  channel, except for the conversion veto, which is not applied. The SR is split in two, according to the lepton flavour with higher multiplicity. For events with two electrons and two muons, the leading lepton determines the SR. Two independent statistical analyses are defined, one with only the electron SRs and one with only the muon SRs. All considered backgrounds and signals, except that from electrons with misassigned charge, are estimated using MC samples. The predicted diboson, non-prompt-lepton, and  $t\bar{t}$  backgrounds from simulation are improved using data-driven corrections obtained from dedicated CRs. The estimated background from electrons with misassigned charge is fully data-driven. The statistical analyses use the  $m_{\text{eff}}$  distribution in all SRs, in the  $3\ell$  CR, and in one of the CRs of the  $2\ell$  channel. In the rest of the CRs, the overall number of events is used. The data and background prediction agree reasonably well in all SRs, with small data excesses in the electron SRs. This is shown in Figure 31(b) for one of those regions.

The only ATLAS analysis considering cross-generational couplings without light leptons focuses on LQs decaying into a  $\tau$ -lepton and a  $c$ -quark [69]. Events are selected for a SR if they have two reconstructed

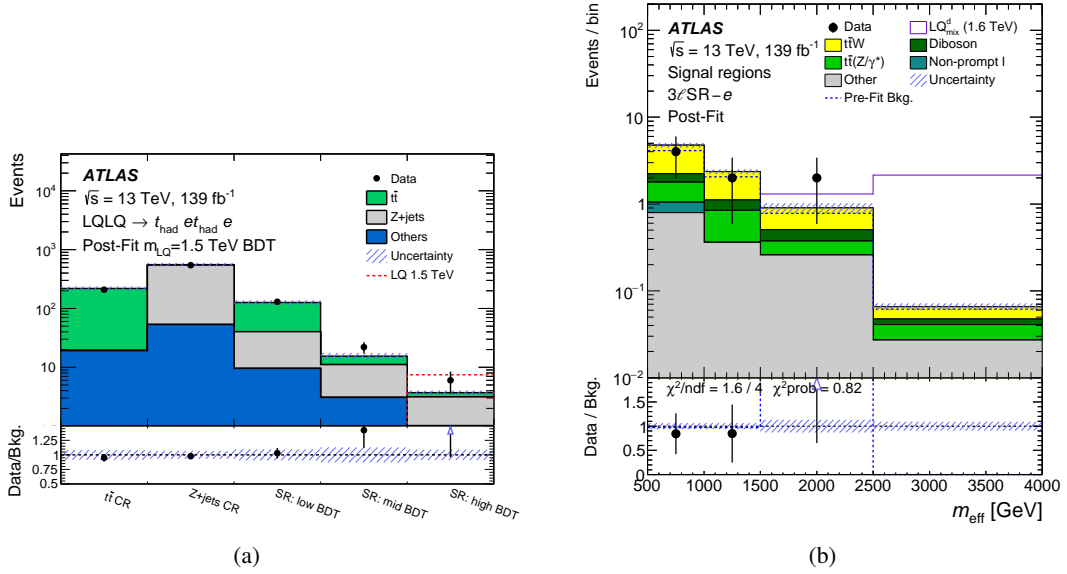


Figure 31: (a) Distribution of the event yields in all fitted regions of the electron selection used in the search for down-type LQs in final states with two light leptons [162] and (b) the effective mass in one of the SRs used in the search for down-type LQs in multilepton final states [160] after a background-only fit to data.

hadronically decaying  $\tau$ -leptons and at least two reconstructed jets. Events with any light leptons are vetoed. The two  $\tau_{\text{had}}$  are required to be well separated and have opposite charges. To suppress the  $Z \rightarrow \tau\tau$  background,  $m_{\tau\tau}^{\text{col}}$  is required to be larger than 110 GeV. The visible momentum fraction for the two  $\tau$  candidates, i.e. the ratio of the visible  $p_T$  to the estimated total  $p_T$  of their decay products, is used to reduce the background from fake- $\tau$  sources. Two CRs are defined and used in the statistical analysis: a CR defined for lower values of  $m_{\tau\tau}^{\text{col}}$  to help model the  $Z \rightarrow \tau\tau$  background and another one using a single- $\tau$  selection in order to improve the modelling of background from single-top and  $t\bar{t}$  production. The statistical analysis uses the  $S_T$  distributions in the SR and the two CRs with all signal and background processes modelled using MC samples, except for the fake background due to jets misidentified as  $\tau_{\text{had}}$ , which is estimated using a fake-factor method. The data is in good agreement with the SM prediction in the SR after a background-only fit.

### 7.2.3 Limits on LQs with cross-generational couplings

In the absence of any significant excess in data, limits are obtained for the pair production of scalar leptoquarks with cross-generational couplings as a function of the mass of the LQ for different values of the branching ratio to  $b\ell$  or  $t\ell$  for down-type or up-type leptoquarks respectively. Two-dimensional limits on the production of up-type and down-type scalar leptoquarks as a function of the mass of the LQ and its BR are shown in Figure 32. In addition to the limits obtained in the individual searches, the result obtained after a statistical combination [164] of those searches is also shown in all cases. Results are shown separately for muon and electron final states. Searches with fully visible final states reach higher in mass but lose sensitivity rapidly as the BR approaches zero. Searches that consider semi-invisible final states are less sensitive but obtain more consistent limits as a function of the BR.

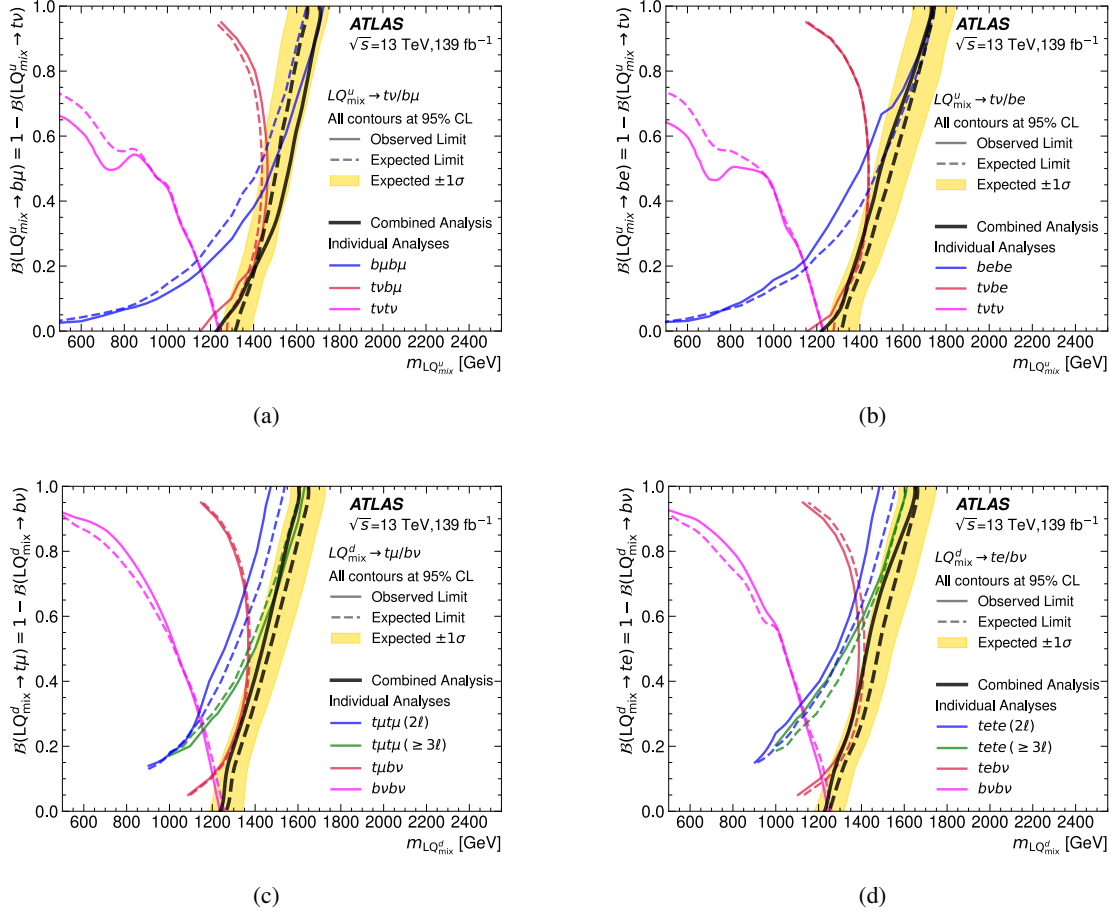


Figure 32: Two-dimensional limits (a,b) on the production of up-type scalar leptoquarks with cross-generational couplings as a function of the mass of the LQ and the BR to  $b\ell$  from the search of up-type LQs in final states with (blue) two leptons [163], (red) only one lepton [165], (pink) no leptons [158] and (black) their statistical combination [164], and (c,d) on the production of down-type scalar leptoquarks with cross-generational couplings as a function of the mass of the LQ and the BR to  $t\ell$  from the search of down-type leptoquarks in final states with (blue) two leptons [162], (green) multiple leptons [166], (red) only one lepton [165], (pink) no leptons [158] and (black) their statistical combination [164]. Electron and muon final states are considered separately.

The  $\tau c$  analysis sets limits on the pair-production of LQs that decay exclusively into a  $\tau$ -lepton and  $c$ -quark as a function of the LQ mass. LQs with masses below 1.3 TeV are excluded for the model considered.

## 8 Charged-lepton flavour violation

As discussed in Section 5, neutrinos oscillate, indicating that lepton flavour violation (LFV) does occur in nature. However, no LFV has ever been seen for processes involving charged leptons, even though no fundamental principles forbid it. Charged-lepton flavour transitions mediated by neutrino oscillations should occur, but their predicted rate is negligibly small in the SM (e.g.  $\mathcal{B}(Z \rightarrow e\mu) < 4 \times 10^{-60}$ ).

## 8.1 Lepton flavour violation in Z boson decay

In some BSM theories, LFV rates can be significantly enhanced by interactions involving new particles such as heavy neutrinos [167]. It is therefore interesting, given the abundance of Z bosons produced at the LHC, to look for LFV decays of the Z boson as a probe for new physics, as was done in the  $Z \rightarrow e\mu$  channel [168] and the  $Z \rightarrow e\tau$  and  $Z \rightarrow \mu\tau$  channels, with the  $\tau$ -lepton decaying leptonically [169] or hadronically [170]. The limits obtained in these channels are summarized in Table 3.

In the  $e\mu$  final state [168], the invariant mass of the Z boson candidate can be reconstructed fully from the visible leptons: the search can thus look for a narrow signal peak in the invariant mass distribution of the oppositely charged leptons, restricted to the range  $70 < m_{e\mu} < 110$  GeV. The main background comes from leptonic decays of  $\tau$ -leptons in the  $Z \rightarrow \tau\tau$  process, misidentification of a muon as an electron in  $Z \rightarrow \mu\mu$  events, or dileptonic decays in  $t\bar{t}$  or diboson production. While the  $t\bar{t}$  background is reduced by rejecting events with a  $b$ -tagged jet, jets with  $p_T > 60$  GeV, or  $E_T^{\text{miss}} > 50$  GeV, the main background reduction strategy is to use a BDT to select events in the signal region. This BDT is based on the  $p_T$  of the leading jet (when there is one), the  $E_T^{\text{miss}}$ , and the transverse momentum of the electron–muon system,  $p_T^{e\mu}$ . Control regions with same-flavour or same-sign lepton pairs are also used to help constrain some of the background contributions. The resulting invariant mass distribution in the SR is shown in Figure 33(a), where the data is seen to agree well with the background predictions. A binned fit of this distribution gives an  $e\mu$  branching ratio value that is consistent with zero within uncertainties, the systematic uncertainties being dominated by the statistical uncertainty of the simulated  $Z \rightarrow \tau\tau$  and  $Z \rightarrow \mu\mu$  processes.

In the  $\ell\tau_{\text{had}}$  channel [170], where  $\ell = e, \mu$  and the  $\tau_{\text{had}}$  can be either one-pronged (1P) or three-pronged (3P), the  $\ell$  and  $\tau_{\text{had}}$  are required to have opposite electric charges. The value of  $m_T(\tau_{\text{had-vis}}, E_T^{\text{miss}})$  is required to be less than 35 GeV to remove  $Z \rightarrow \tau\tau$  and  $W$ +jets backgrounds,  $m_{\ell\tau_{\text{had-vis}}}$  must be above 60 GeV to be compatible with a Z boson decay, and no  $b$ -tagged jets must be found in the events to reject

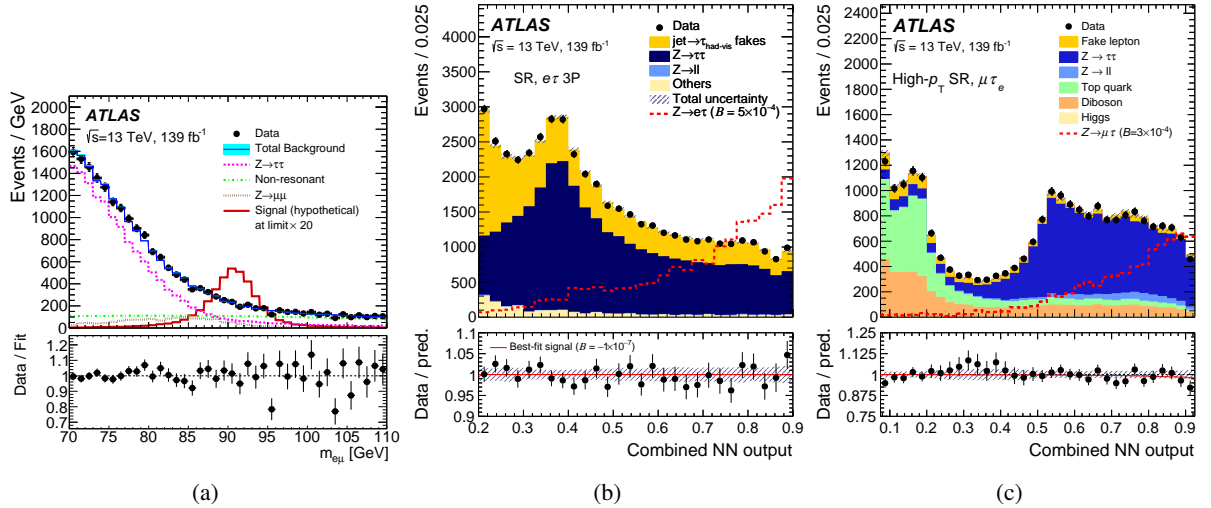


Figure 33: Observed distribution of the final discriminating variables compared to the expected background and example LFV Z signals: (a) the  $e\mu$  invariant mass in the  $Z \rightarrow e\mu$  search [168], and the combined NN score in the (b)  $e\tau(3P)$  SR of the  $Z \rightarrow \ell\tau_{\text{had}}$  search [170] and in the (c)  $\mu\tau_e$  SR of the  $Z \rightarrow \ell\tau_{\ell'}$  search [169].



Table 3: 95% CL upper limits on the LFV branching ratio of the  $Z$  boson, in the various  $\ell\ell'$  channels.

Channel	Upper limit on $\mathcal{B}(Z \rightarrow \ell\ell')$
$e\mu$	$2.62 \times 10^{-7}$
$e\tau$ ( $\tau_{\text{had}}$ and $\tau_{\ell'}$ channels combined)	$5.0 \times 10^{-6}$
$\mu\tau$ ( $\tau_{\text{had}}$ and $\tau_{\ell'}$ channels combined)	$6.5 \times 10^{-6}$

top-quark-related backgrounds. After these selections, three NN classifiers for each of the four channels ( $(\ell = e, \mu) \times (\tau_{\text{had}} = 1\text{P}, 3\text{P})$ ) are used to discriminate further against  $W$ +jets,  $Z \rightarrow \tau\tau$  and  $Z \rightarrow \ell\ell$  background processes, respectively. They use low-level inputs such as  $\ell$  and  $\tau_{\text{had-vis}}$  kinematic variables and the  $E_{\text{T}}^{\text{miss}}$ , but also higher-level inputs which are properties of the  $\ell - \tau_{\text{had-vis}} - E_{\text{T}}^{\text{miss}}$  system, such as  $m_{\ell\tau}^{\text{col}}$ . To estimate the remaining  $Z$ +jets background in the SR, two CRs are used: one for the  $Z \rightarrow \tau\tau$  background (built by reversing the  $m_{\text{T}}$  and  $m_{\ell\tau_{\text{had-vis}}}$  requirements and requiring  $m_{\ell\tau}^{\text{col}}$  to be compatible with the  $Z$  boson mass), and one for the  $Z \rightarrow \ell\ell$  background (built by reversing the corresponding NN output requirement). A fake-factor method is used to estimate the remaining background in which a  $\tau_{\text{had}}$  is falsely identified. The distribution of the final discriminating variable in the  $e\tau(3\text{P})$  SR, the combined NN score, is shown in Figure 33(b) along with an example expected signal. Since the data does not deviate significantly from the expected background in the SR, limits are set on the LFV  $Z$  boson branching ratios, combining them with the Run 1 results [171].

These results can be improved significantly by also examining the  $\ell\tau_{\ell'}$  channel [169], in which the leptonic  $\tau_{\ell'} \rightarrow \ell' + 2\nu$  decay is considered instead. In this search, the two light leptons  $\ell$  and  $\ell'$  are required to have different flavours and opposite electric charges and no  $\tau_{\text{had}}$  candidate must be found, in order to remain orthogonal to the  $\ell\tau_{\text{had}}$  channel. As in the hadronic channel, a  $b$ -jet veto is imposed, and similar variables, based on the leading and subleading leptons ( $\ell_0$  and  $\ell_1$ ), are used to reject backgrounds:  $m_{\text{T}}(\ell_1, E_{\text{T}}^{\text{miss}}) < 35$  GeV and  $m_{\ell_0\ell_1} > 40$  GeV. Furthermore,  $|\Delta\phi(\ell_0, E_{\text{T}}^{\text{miss}})| > 1$  is required and, in the  $\mu\tau_e$  channel, the electron  $p_{\text{T}}$  reconstructed from its track must be compatible with the transverse energy reconstructed from its cluster, i.e.  $p_{\text{T}}^{\text{track}}/E_{\text{T}}^{\text{cluster}} < 1.1$ , to reject muons faking electrons. The  $m_{\ell\tau}^{\text{col}}$  variable is also used here, built with the same collinear assumptions for the  $2\nu$  system as made for the single  $\nu$  in the hadronic channel. The main background comes from dileptonic  $Z \rightarrow \tau\tau \rightarrow \ell\ell' + 4\nu$ , with some contribution from  $t\bar{t}$  and diboson production. Three NN classifiers are built to discriminate against these, and their combined score<sup>5</sup> is used to select the events in the SR. A  $Z \rightarrow \tau\tau$  CR is built by reversing its corresponding NN score, and a fake-factor method is used to estimate misidentified-lepton background. The combined NN score used as the final discriminant in the  $\mu\tau_e$  channel is shown in Figure 33(c), where it is compared with the predicted background and an LFV signal. Since no excess in data is seen in this search, limits are set on the  $Z$  LFV branching ratios, combining them with the hadronic channel limits.

## 8.2 Lepton flavour violation in the decay of a heavy $Z'$

A new gauge boson  $Z'$ , as introduced in Section 4, could also have LFV decays. The three final states  $e\mu$ ,  $e\tau_{\text{had}}$  and  $\mu\tau_{\text{had}}$  were therefore probed at high mass in a search for such a signal [172], by requiring that the invariant mass of different-flavour, opposite-sign leptons be above 600 GeV and that these leptons be back-to-back in the transverse plane. Since the  $\tau_{\text{had}}$  in this search are more boosted than the ones in

<sup>5</sup> The combined score is computed as  $1 - \sqrt{(1/3)\sum_{i=1}^3 (1 - \text{NN}_i)^2}$ , where  $\text{NN}_i$  are the individual scores.

the  $Z$  boson LFV search discussed in the previous section, the collinear approximation used to assign a four-momentum to the neutrino from the  $\tau$  decay is even more justified here and is used to reconstruct the invariant mass, significantly improving its resolution.

The irreducible background in each channel is dominated by  $t\bar{t}$  and  $WW$  production. In the SR, the  $t\bar{t}$  background is reduced by rejecting events with  $b$ -tagged jets, a criterion which is reversed to build a CR for this background. A  $WW$  CR is built by reversing the  $\Delta\phi(\ell, \ell')$  selection in the  $e\mu$  channel. In the channels involving  $\tau_{\text{had}}$ , such  $WW$  CRs would suffer from too large a contamination from fake leptons and are not used. Instead, the correction factor  $k$  that needs to be applied to the  $WW$  simulation in a given  $\tau_{\text{had}}$  channel is extrapolated from the one obtained in the  $e\mu$  channel, by multiplying it by the ratio of the correction factors obtained in the  $t\bar{t}$  CRs:  $k_{WW}^{e(\mu)\tau_{\text{had}}} = k_{WW}^{e\mu} \times k_{t\bar{t}}^{e(\mu)\tau_{\text{had}}} / k_{t\bar{t}}^{e\mu}$ , this extrapolation being applicable due to lepton-flavour universality. The reducible fake-lepton backgrounds are estimated using either a matrix method in the  $e\mu$  channel or dedicated CRs enriched in  $W$ +jets events in the  $e\tau_{\text{had}}$  and  $\mu\tau_{\text{had}}$  channels.

In each of the three channels, the total uncertainty is dominated by the statistical precision, and a binned profile-likelihood fits is performed on  $m_{\ell\ell'}$ . Since the data agree with the expected background, limits are set on the  $Z'$  mass, assuming an SSM benchmark augmented with one non-zero LFV  $\ell\ell'$  coupling at a time, which is taken to be the same as the corresponding  $\ell\ell$  coupling. The observed (expected) lower limits placed on  $m_{Z'}$  are 5.0 (4.8), 4.0 (4.3) and 3.9 (4.2) TeV for decay into  $e\mu$ ,  $e\tau$ , and  $\mu\tau$ , respectively.

## 9 Hidden sectors leading to long-lived neutral particles

In models with a hidden (or *dark*) sector, new particles which are neutral under the SM gauge groups are introduced; these particles can potentially interact between themselves via new interactions in which the SM particles are neutral. The SM and dark particles thus exist in parallel and can only communicate through a mediator (or *portal*): this mediator can, for example, be the SM Higgs boson or a new scalar, pseudoscalar, vector or axial-vector particle carrying a double SM–dark charge (i.e. a *bi-fundamental* mediator) or mixing with a SM particle with small probability. These models can often offer candidates to explain the nature of dark matter, which is the focus of Section 10. The present section instead focuses on hidden sectors for which the very small coupling to the SM through the portal of interest leads to neutral long-lived particles (LLPs) which decay at some point in the detector. This leads to very distinctive signatures which are sometimes more akin to detector noise or beam-induced background than to SM processes from the  $pp$  collisions. Decays of the Higgs boson into such LLPs are predicted in multiple BSM theories, such as some models with neutral naturalness [173, 174]. Here, neutral LLPs produced through a Higgs or Higgs-like portal are the subject of four different searches: for dark-photon jets [175, 176], for a long-lived pseudoscalar via displaced decay vertices in the inner detector [177], and for a long-lived scalar via displaced jets in the calorimeter [178] or in the muon spectrometer [179].

### 9.1 Search for dark-photon jets

The long-lived particle can be a light dark photon ( $\gamma_d$ ) which would have a small but non-zero value of the parameter  $\epsilon$  for mixing with the SM photon. It would therefore decay into leptons and light quarks with branching ratios and a lifetime determined by its mass and  $\epsilon$ . They would be pair-produced through a Higgs boson decay, either directly as in the Hidden Abelian Higgs Model (HAHM) [180], or through a more complex chain involving other dark-sector particles as in the Falkowski–Ruderman–Volansky–Zupan

(FRVZ) model [181, 182] (see Figure 34(a)). Due to their small mass, dark photons would be highly boosted: their decays would be seen as jet-like structures composed of a collimated group of fermions, called dark-photon jets. Three Higgs boson production modes are considered and combined: gluon–gluon fusion (ggF) and  $WH$  [175], and VBF [176].

If the displaced  $\gamma_d$  decays into a pair of muons, it can be seen as a muonic dark-photon jet ( $\mu$ DPJ), i.e. collimated stand-alone muon spectrometer (MS) tracks which are not matched to a prompt muon and are not close to a jet. Cosmic-ray muons in time coincidence with a  $pp$  collision can be an important source of background for  $\mu$ DPJs: a DNN is trained to discriminate between simulated signal and a cosmic-ray-enriched dataset collected during empty bunch crossings, using as inputs the MS track position, direction and timing. A displaced  $\gamma_d$  decaying into electrons or quarks can be seen, for an appropriate range of lifetimes, as a calorimeter DPJ (caloDPJ), i.e. a jet with an unusually low EMF, the fraction of its total energy that is deposited in the EM calorimeter. To select caloDPJs efficiently, the cleaning selections which are usually applied to jets are relaxed, e.g. by removing the usual JVT or EMF criteria. Other selections are applied, such as a timing requirement to remove cosmic-ray muons or beam-induced background (BIB). Multijet events can also mimic caloDPJs: a ‘QCD’ NN is therefore trained on MC signal and background events, using as inputs the shape of the calorimeter energy deposits associated with the jet. These inputs are also used to train another NN against a BIB-enriched dataset, collected with a dedicated trigger.

Events without leptons are then selected for the ggF [175] and VBF [176] categories, while events with one lepton are used for the  $WH$  category [175]. In the ggF and VBF SRs, dedicated  $\mu$ DPJ triggers are used in combination with  $E_T^{\text{miss}}$  (VBF) or low-EMF (ggF) triggers, while lepton triggers are used for  $WH$ . In the ggF SRs, two DPJs are required. Besides the use of the NNs mentioned above, selections are made on the azimuthal separation  $\Delta\phi_{\text{DPJs}}$  of the DPJs and their timing, and they are required to be ID-isolated: the scalar sum of the  $p_T$  ( $\Sigma p_T$ ) of all inner-detector (ID) tracks found close to the DPJ direction must be small. In the  $WH$  SRs, the events are required to have at least a minimum amount of  $E_T^{\text{miss}}$  and  $m_T$ , and no  $b$ -tagged jet. Events are further separated into those having only one caloDPJ (in which case the  $m_T$  requirement is increased to reduce the  $W$ +jets background), two or more caloDPJs, or a mix of caloDPJ and  $\mu$ DPJ. Besides the use of the QCD NN, timing, low-JVT and low-width selections on the caloDPJ, an upper limit is placed on the minimum  $\Delta\phi(\text{DPJ}, E_T^{\text{miss}})$  value. In the VBF SRs, the special production topology is selected by requiring a pair of highly energetic jets separated by a significant gap in  $\eta$ , resulting in a large value of  $m_{\text{jj}}$ , besides requiring some  $E_T^{\text{miss}}$  and vetoing on the presence of leptons or  $b$ -tagged jets. This reduces the SM background relative to the other channels, allowing selected events to have a minimum of only one DPJ, which must be ID-isolated and central, and either be neutral (for a  $\mu$ DPJ) or have a good NN score (for a caloDPJ).

For each SR, an ABCD method is used to estimate the background. Possible signal leakage from the SR into the other three regions is accounted for by a simultaneous fit of the signal and background in all regions. In the ggF SRs, the planes are formed by the larger  $\Sigma p_T$  value of the two DPJs, and either  $\Delta\phi_{\text{DPJs}}$  or the QCD NN score, the latter also being used for the caloDPJ VBF search. In the  $WH$  SRs, they are based on  $\min \Delta\phi(\text{DPJ}, E_T^{\text{miss}})$  and the minimum QCD NN score. For the VBF  $\mu$ DPJ search, the ABCD plane uses the charge of the  $\mu$ DPJ versus its ID isolation.

In all SRs, the data are compatible with the expected background within statistically dominated uncertainties. Limits on the FRVZ model obtained by combining the ggF,  $WH$  and VBF categories are shown in Figure 34(b) in the  $\epsilon$  versus  $m_{\gamma_d}$  plane for various  $H \rightarrow 2\gamma_d$  branching ratios: for  $m_{\gamma_d} < 2m_\mu$ , the sensitivity drops because  $\mu$ DPJs do not contribute anymore, while above this range the structures seen in the displayed limits depend on the  $\gamma_d$  branching ratios, as decays into QCD resonances significantly alter the sensitivity. The figure also shows the complementarity of that search to a previous Run 1 ATLAS

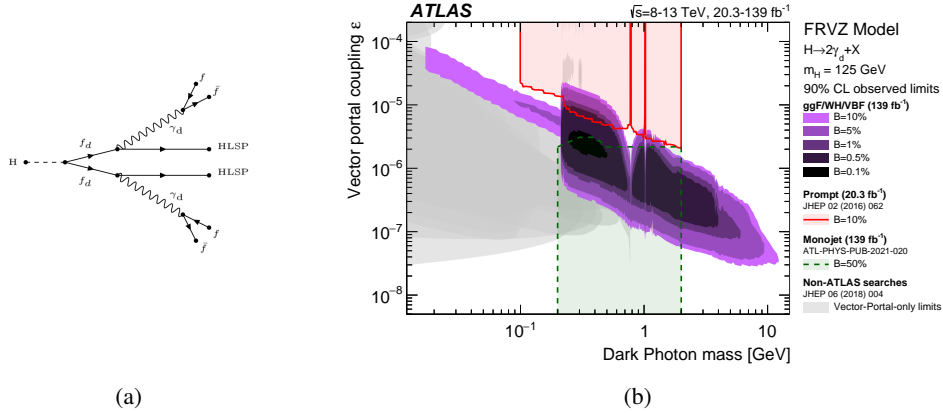


Figure 34: (a) Example of dark-photon production and decay in the FRVZ model, where  $f_d$  are dark-sector fermions and HLSP is the hidden lightest stable particle. (b) Exclusion at 90% CL in the plane of the kinetic mixing parameter  $\epsilon$  versus the  $\gamma_d$  mass for different values of the  $H \rightarrow 2\gamma_d$  branching ratio obtained in the search for dark-photon jets [175, 176] in the context of the FRVZ model, compared to other exclusions (see the text).

search for prompt dark photons [183], which was able to exclude larger couplings, and also to the jet+ $E_T^{\text{miss}}$  analysis that is discussed in Section 10.1.1, which is able to rule out lower couplings at intermediate masses for a large branching ratio, and to non-ATLAS searches [184] which exclude lower masses/couplings when some assumptions are made about the interactions.

## 9.2 Searches for long-lived scalars or pseudoscalars in the decay of a Higgs-like boson

### 9.2.1 Looking for decays in the inner detector

This search [177] focuses on a simplified model in which two new long-lived pseudoscalars  $a$  are produced in the decay of the Higgs boson and then decay via the  $a \rightarrow b\bar{b}$  mode<sup>6</sup> within the inner-detector volume, leading to DVs. In this model, the proper lifetime and mass of  $a$  are free parameters. The  $Z(\rightarrow \ell\ell)H$  production channel is investigated because the two leptons offer a highly efficient trigger and selection strategy. Searches for prompt  $a$  decays were also pursued, using a partial Run 2 dataset, and are reviewed in another report.

Standard and LRT tracks (see Section 5.1) are used to reconstruct the DVs. Tracks which are too loosely associated with the DVs are removed and some quality requirements are applied to the DVs: they must be within the inner tracker but not within known detector material, have a good  $\chi^2/n_{\text{dof}}$  vertex fit, have at least three tracks including at least one with transverse impact parameter  $|d_0| > 3$  mm, and be within  $\Delta R = 0.6$  of one of the four leading jets. Vertices due to random track crossings are suppressed by requiring  $m/\Delta R_{\text{max}} > 3$  GeV, where  $m$  is the vertex mass and  $\Delta R_{\text{max}}$  is the maximal angular separation found between any given track and the combined momentum of the remaining vertex constituents when removing this track.

<sup>6</sup> This decay should be dominant when kinematically accessible if  $a$  mixes with the Higgs boson and inherits its Yukawa couplings.

Events are selected by requiring two OS same-flavour leptons with an invariant mass compatible with the  $Z$  boson, at least two jets, and at least two DVs matched to different jets. Furthermore, one of these two jets must have low track activity: the ratio of the  $p_T$  of all its geometrically-matched prompt tracks to its total  $p_T$  must be low, and it must be mostly geometrically matched to tracks which have a low probability of being compatible with any  $pp$  collision PV candidate  $i$ , based on a measurement of  $p_T^{\text{jet trk} \in i} / p_T^{\text{all jet trk}}$ . A CR is defined by reversing the DV multiplicity requirement; it is used to compute a probability for a jet to be matched to a DV, as a function of the jet kinematics and properties, and this probability is used to estimate the number of background events in the SR, which is predicted to be  $1.30 \pm 0.08$  (stat.)  $\pm 0.27$  (syst.). Zero events are observed in the SR, and limits on the branching ratio of  $H \rightarrow aa \rightarrow b\bar{b}b\bar{b}$  are set as a function of the proper lifetime of  $a$  for various  $a$  mass scenarios, as shown in Figure 35(a).

## 9.2.2 Looking for decays in the calorimeters

Searches are also conducted for a hidden sector which is connected to the SM via a heavy scalar boson  $\Phi$  which decays into two long-lived scalar particles  $s$ . While  $\Phi$  can be the Higgs boson, the search also considers  $\Phi$  masses ranging from 60 GeV to 1 TeV and  $s$  masses from 5 to 475 GeV, with  $s$  decaying into SM fermions. In this model the couplings of  $s$  to SM fermions are determined by the Higgs boson's Yukawa couplings through mixing, so  $s$  decays preferentially into the heaviest SM fermion pair which is kinematically accessible, thus usually favouring hadronic decays. The signal models considered assume gluon–gluon fusion (ggF) production of  $\Phi$ .

A search for  $\Phi \rightarrow ss$  with  $s$  decaying mainly in the calorimeters is performed [178], each  $s$  being reconstructed as a jet which is narrow, trackless and has a low EMF value, a signature which is similar to that of the calorimetric dark-photon jets (caloDPJs) previously discussed in Section 9.1. Two SRs labelled low- $E_T$  or high- $E_T$  are designed, targeting a value of  $m_\Phi$  below or above 200 GeV, respectively.

The events are selected using a low-EMF jet trigger and are required to have at least two jets after applying, like in the dark photon ( $\gamma_d$ ) search, a modified cleaning algorithm where, in this case, the jet EMF requirement is removed. Furthermore, the jets must be trackless, ensured by requiring  $\Sigma \Delta R_{\min}(\text{jet}, \text{tracks}) > 0.5$ , where the sum runs over selected jets which have  $p_T > 50$  GeV and  $\Delta R_{\min}(\text{jet}, \text{tracks})$  is the angular distance between the jet and the closest PV-associated track with  $p_T > 2$  GeV.

These jets are then tagged using two complex NNs (low- $E_T$  or high- $E_T$ ) which are trained using three samples: a sample of MC signal events (low- $E_T$  or high- $E_T$ ), a sample of SM multijet events taken from a dataset of events passing a jet trigger but failing the low-EMF trigger, and a BIB sample, collected with a dedicated trigger. The inputs to these per-jet NNs are low-level jet information concerning the jet-associated tracks, calorimeter-energy topological clusters, muon-spectrometer track segments, and general kinematics; each NN outputs three scores to classify these jets as either signal-like, multijet-like or BIB-like.

At event level, a BDT is then trained to further discriminate between BIB and signal events, separately for the low- $E_T$  and high- $E_T$  cases, using as input variables not only the per-jet NN scores but also event-level kinematics such as the angular distance between the signal jet candidates, or  $H_T^{\text{miss}}/H_T$  where  $H_T^{\text{miss}}$  is the magnitude of the vectorial sum of the jet  $p_T$  while  $H_T$  is the scalar sum of the jet  $p_T$ . A selection on the BDT output is then made along with other selections, including one on the jet timing, to further suppress the BIB and ensure that the only significant remaining background consists of multijet events. Once this is done, the low- $E_T$  and high- $E_T$  SRs are defined by final selections on  $H_T^{\text{miss}}/H_T$ , the EMF of the signal jets, their  $p_T$ , and the product of the two highest per-jet NN signal scores.

An ABCD method is used to estimate the background, using  $\Delta R_{\min}(\text{jet, tracks})$  and the low- $E_T$  or high- $E_T$  BDT event score as the uncorrelated variables. After the fit to the four regions, the 22 (23) observed data events in the low- $E_T$  (high- $E_T$ ) SR agree well with the  $18.8 \pm 3.5$  ( $20.6 \pm 4.0$ ) estimated background events. Limits are then placed on the cross section times branching ratio of the mediator's decay  $\Phi \rightarrow ss$  as a function of the  $s$  lifetime for various masses of  $\Phi$  and  $s$ , an example of which is shown in Figure 35(b) for the case in which  $\Phi$  has a mass of 60 GeV.

### 9.2.3 Looking for decays in the muon spectrometer

A search was also performed to look for  $s$  decaying in the muon spectrometer [179]. These decays would be seen as DVs in the MS. A dedicated algorithm is used to reconstruct the MS DVs [185]. In the MS, MDT chambers consist of two sets (called multilayers) of three or four layers of drift tubes. Hits in the multilayers can form track segments, and segments coming from the two multilayers can form tracklets. Displaced vertices are formed from clusters of three tracklets in the barrel, or four in the endcaps.

After passing a dedicated MS-based trigger, events are selected by requiring at least one MS DV which must be geometrically matched to the MS cluster found by the trigger. If two trigger MS clusters are found, two MS DVs must be matched. Requirements are also made on the position in  $\eta$  and the transverse decay radius  $L_{xy}$  of the DV in order to reduce the background, which is dominated by *punch-through* jets, i.e. jets which are not fully contained in the calorimeter volume and create tracks in the MS. Since signal events are expected to have many more hits than a reconstructed MS DV in a background event, the number of hits found in the MDT and the RPC or TGC in a cone around the DV must be high. To reduce the background, the DVs are also required to be isolated from any significant activity in the ID, and from any large-EMF jets. In the SR, at least two isolated DVs must be found, well separated in  $\Delta R$ .

The remaining background is estimated in a data-driven way. This background is dominated by events in which there are two isolated DVs, but only one MS cluster found by the trigger. These events are estimated by counting the number of events in a CR in which there is only one isolated DV and it is matched to the only MS cluster, and weighting them by the probability to find another, unassociated DV which is unmatched to any MS cluster. This probability is measured in a dataset selected with a zero-bias trigger, by dividing the total number of unmatched DVs by the total number of events. Background events in which there are two DVs matched to two MS clusters are also estimated in a data-driven way, but give a much smaller contribution. In the SR, the expected background is  $0.32 \pm 0.05$  events and zero events are observed. Limits are set in the same planes as for the calorimeter-based search, as shown in Figure 35(b). The MS search excludes smaller branching ratios than the calorimeter-based search, but the calorimeter-based search probes lower lifetimes, as expected.



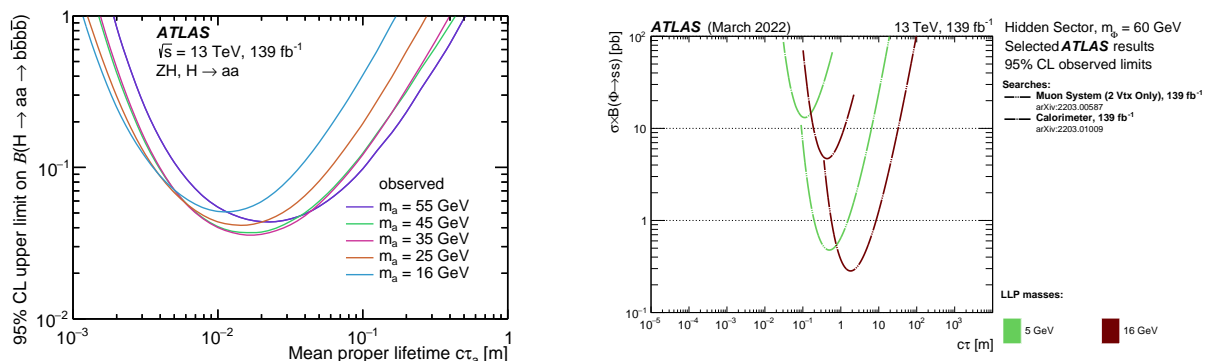


Figure 35: (a) Upper limit on the branching ratio of  $H \rightarrow aa \rightarrow b\bar{b}b\bar{b}$  obtained as a function of the proper lifetime of  $a$  for various mass hypotheses in the displaced vertex analysis [177]. (b) Observed upper limit on the cross section times branching ratio of the mediator’s decay  $\Phi \rightarrow ss$  as a function of the  $s$  lifetime for a  $\Phi$  mass of 60 GeV and two  $s$  masses as obtained by looking for decays in the calorimeters [178] and the muon spectrometer [179]. For clarity, parts of the exclusion curves outside the most sensitive region are omitted.

## 10 Dark-matter candidates

The nature of dark matter (DM), whose existence is supported by a variety of astrophysical and cosmological measurements [186–193], remains one of the biggest puzzles in modern physics. Should DM be a particle interacting weakly with SM particles, it could be possible to detect it in various ways: directly, via elastic scattering of the local DM by nuclei or electrons in a low-background detector [194–209]; indirectly, by the detection of their annihilation or decay products in the universe [210–218]; or by producing them at colliders, which is the way explored here.

Weakly interacting massive particles (WIMPs), often denoted by  $\chi$ , are a class of DM candidates of particular interest for the ATLAS experiment. With a DM particle mass close to the electroweak scale and an interaction strength with SM particles of the order of the weak interaction’s strength, they could be readily pair-produced at the LHC. They are also cosmologically interesting as indicated by the so-called WIMP miracle [219]: with these mass and coupling scales, the right relic density can easily be achieved via a freeze-out mechanism in the early universe.

Once pair-produced in proton–proton collisions the WIMPs, since they interact only weakly and are stable, would only be detectable through the presence of missing transverse momentum: thus, to be detected, some visible particles must also be produced in the interaction in order to measure this  $p_T$  imbalance. These visible particles can come from a chain of decays ending in the WIMP particles, such as in R-parity-conserving supersymmetric scenarios [130, 220–222], or from initial-state radiation (ISR) in a simplified model of DM pair production, to name but two examples.

This section focuses on searches guided by simplified models of DM, produced through a vector, axial-vector, pseudoscalar or Higgs portal, largely following the work of the DM Forum/LHC DM Working Group [223–226]. The constraints placed on these models by some of the DM searches introduced here are also compared with those from direct-detection experiments. A more exotic model, in which DM is a composite stable particle of a strongly interacting hidden sector is also discussed. A stable WIMP which can be a DM candidate often features in supersymmetric models that conserve R-parity; a thorough review of ATLAS searches for supersymmetry can be found elsewhere [227].



## 10.1 Vector or axial-vector portal

In order to search for DM at the LHC, some interactions between DM particles and SM particles must be assumed. Here, the focus is on a simplified model in which the DM candidate is a Dirac fermion and the DM–SM interactions are due to a new U(1) symmetry under which they are charged. Five free parameters are considered: the mass of the new vector ( $Z'_V$ ) or axial-vector ( $Z'_A$ ) mediator,  $m'_Z$ , the mass of the DM candidate,  $m_\chi$ , and the coupling of the  $Z'$  to the quarks,  $g_q$ , to the DM candidate,  $g_\chi$ , and to the charged and neutral leptons  $g_\ell$ , where the couplings  $g_q$  and  $g_\ell$  are assumed to be universal in flavour. The width of the mediator is taken to be the minimum width allowed given the couplings and masses.

The searches looking for such V/A-mediated DM pair production then rely on the presence of an ISR gluon [228], photon [229], or  $Z$  boson [230], as shown in Figure 36(a). While the first two searches are presented in this section, the  $Z$  boson one is instead discussed in Section 10.3.3, as its impact in the Higgs-portal model is more important than in this ISR-based model. Since  $g_q$  must be non-zero for the LHC to produce DM, and because  $g_\ell$  could also be non-zero, the resonant searches (see Figure 36(b)) presented in Section 4 also put interesting constraints on these models, as shown in Section 10.1.3.

### 10.1.1 The jet+ $E_T^{\text{miss}}$ analysis

Since gluon emission dominates ISR production, the jet+ $E_T^{\text{miss}}$  search [228] has a very broad range of applicability which also probes other DM models such as the one in the invisible-Higgs search (see Section 10.3), or exotic models related to gravity (see Section 12), amongst others. The analysis, based on a  $E_T^{\text{miss}}$  trigger, requires the presence of at least one high- $p_T$  small- $R$  jet along with a large value of  $E_T^{\text{miss}}$ . Although this analysis is often dubbed ‘mono-jet’, this is not a faithful description as the selection does allow up to three additional jets to allow for extra radiation, and to reduce the associated modelling systematic uncertainties. The selected jets are required to be well separated from the  $E_T^{\text{miss}}$  direction to reduce the background due to mismeasured multijet events, with a larger separation required in events with the least  $E_T^{\text{miss}}$ , which are more problematic. Finally, events are vetoed if they contain identified electrons, photons, muons or  $\tau$ -leptons. To increase the sensitivity, the SR is binned in  $E_T^{\text{miss}}$ .

The main SM background comes from  $Z(\rightarrow \nu\nu)$ +jets, along with a significant contribution of  $W(\rightarrow \ell\nu)$ +jets events in which the lepton is not identified. Much smaller contributions come from  $Z(\rightarrow \ell\ell)$ +jets, top-related and diboson processes; the multijet and non-collision backgrounds are determined in a fully data-driven way, but are found to contribute at a level of at most 1.2% in the lowest  $E_T^{\text{miss}}$  bin. Five CRs are built by reversing the lepton veto, requiring exactly one electron or muon with an  $m_T$  value compatible with a  $W$  boson, for the two  $W(\rightarrow \ell\nu)$ +jets CRs and the combined  $t\bar{t}$  CR, or exactly two electrons or muons with an  $m_{\ell\ell}$  value compatible with the  $Z$  boson for the  $Z(\rightarrow \ell\ell)$ +jets CRs. By either vetoing or requiring events with a  $b$ -tagged jet, the  $W(\rightarrow \ell\nu)$ +jets CRs are separated from the  $t\bar{t}$  CR. Further selections based on the  $E_T^{\text{miss}}$  and jets are applied in the  $1e$  CRs to suppress the multijet background. Finally, the  $E_T^{\text{miss}}$  distribution of these backgrounds in the SR, arising from neutrinos or unidentified charged leptons, is mimicked by computing an  $E_T^{\text{miss}}$  proxy ( $p_T^{\text{recoil}}$ ), effectively treating the charged leptons as invisible.

Instead of using the  $Z$ +jets and  $W$ +jets CRs separately to constrain their respective backgrounds, the uncertainties are reduced by using the four  $W$  and  $Z$  CRs simultaneously to constrain the main  $Z(\rightarrow \nu\nu)$ +jets background. This is made possible by a careful study of the correlations between the QCD corrections to the  $Z$ +jets and  $W$ +jets processes, with dedicated high-order QCD and electroweak parton-level predictions [231] provided separately for  $W$ +jets,  $Z(\rightarrow \ell\ell)$ +jets and  $Z(\rightarrow \nu\nu)$ +jets as a function of the vector boson’s

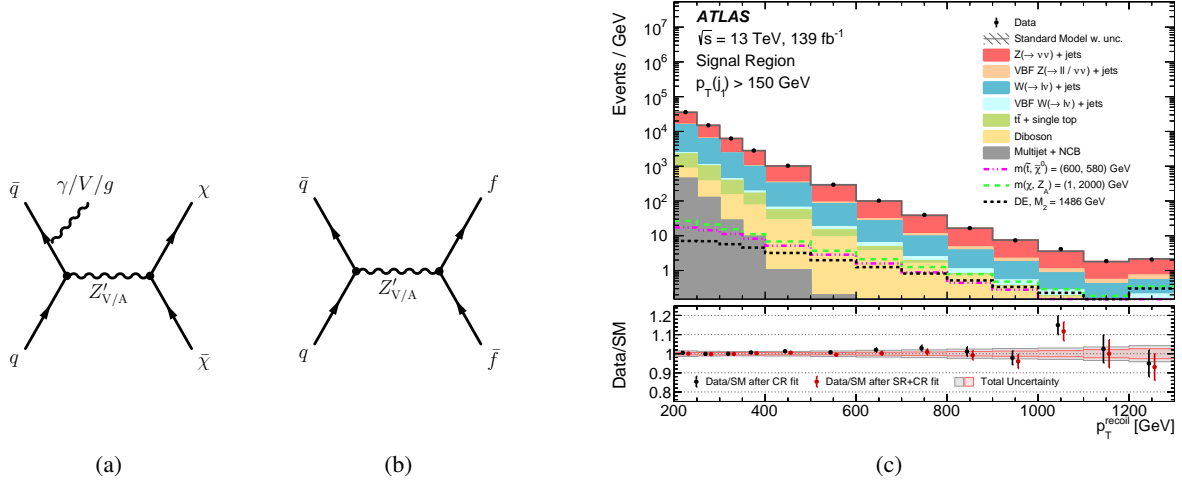


Figure 36: Production, through a V/A portal in the  $s$ -channel, of (a) a DM pair along with ISR or (b) a fermion pair, and (c) measured distribution of  $p_T^{\text{recoil}}$  in the SR of the jet+ $E_T^{\text{miss}}$  search [228] compared to the expected background and some exotic-model signals (including an A-portal DM model with  $(g_q, g_\chi, g_\ell) = (0.25, 1, 0)$ ).

$p_T$ . These are used to reweight the SHERPA 2.21  $Z$ +jets and  $W$ +jets MC event samples, leading to a good description of their respective and relative  $p_T^{\text{recoil}}$  distributions. Because of this, the simultaneous binned-likelihood fit of the five CRs needs only three background normalization factors to adjust the MC-based expectations to the data across all bins: a common one for the  $W$ +jets and  $Z$ +jets backgrounds, one for the  $t\bar{t}$  background and one for the single-top background. This advanced background estimation method leads to much reduced systematic uncertainties, at the level of 1.5%–4.2%, depending on the bin. The dominant remaining uncertainties, besides those in the  $V$ +jets predictions, are those related to the electron, muon and jet identification and reconstruction efficiencies. The resulting  $p_T^{\text{recoil}}$  distribution in the SR after a simultaneous fit to all regions is shown in Figure 36(c). Good overall agreement between the data and the background prediction is obtained, so limits can be set, as is shown in Section 10.1.3.

### 10.1.2 The $\gamma+E_T^{\text{miss}}$ analysis

This analysis [229] looks for a final state in which there is a well-identified high- $p_T$  photon, on which the trigger is based, and a large and significant amount of  $E_T^{\text{miss}}$  in a direction well separated from the photon (and an eventual extra jet). The photon must loosely point back to the PV to suppress the non-collision background, and a veto on leptons ( $e, \mu, \tau$ ) is imposed. The SR is binned in  $E_T^{\text{miss}}$  to improve the sensitivity. The main backgrounds stem from a  $Z(\rightarrow \nu\nu)$  boson, or a  $W(\rightarrow \ell\nu)$  boson where the lepton is missed, produced in association with a photon. Smaller contributions are also expected from  $\gamma$ +jet events, especially in the lower  $E_T^{\text{miss}}$  bin, and from electrons or jets falsely identified as photons. While the fake-photon backgrounds are estimated in a fully data-driven way,  $V\gamma$  CRs are constructed by inverting the lepton veto, and a  $\gamma$ +jet CR is defined mainly by reversing the  $E_T^{\text{miss}}$  requirement. Good agreement between data and the expected background is seen in the SR, within uncertainties dominated by the statistical precision.

### 10.1.3 Complementarity of ATLAS searches

The results of the  $X+E_T^{\text{miss}}$  and resonant searches are complementary for the V/A mediators [232], as can be seen in Figure 37, which shows the observed limits obtained for the individual analyses in the  $m_\chi$  versus  $m'_{Z'}$  plane for four benchmarks as recommended in Ref. [225]. The first two benchmarks are for an A mediator which is either leptophobic,  $(g_q, g_\chi, g_\ell) = (0.25, 1, 0)$ , or has a small lepton coupling,  $(g_q, g_\chi, g_\ell) = (0.1, 1, 0.1)$ , while the two last benchmarks are for a V mediator which is leptophobic,  $(g_q, g_\chi, g_\ell) = (0.25, 1, 0)$ , or has a much smaller coupling to leptons,  $(g_q, g_\chi, g_\ell) = (0.1, 1, 0.01)$ . The lepton-coupling scenarios differ between the A and the V models, because in the case of a pure vector, the lepton coupling can be much smaller than the quark coupling, if for example the mediator couples to quarks and DM at tree level but couples to leptons at loop-level through mixing with SM gauge bosons.

For sufficiently large couplings of the  $Z'$  to quarks or to leptons, the resonant searches are able to exclude the parameter space up to mediator masses of around 3.6 TeV, as the branching ratio of the  $Z'$  to visible states dominates the sensitivity. When these couplings are lowered while maintaining a relatively large DM coupling, the region excluded by constraints from resonant searches starts to shrink, mainly covering the parameter space for which the mediator cannot decay on-shell into DM, thus making the visible final state much more likely. For the  $Z' \rightarrow qq$  scenarios, the lowest mediator masses are excluded by previous dijet resonant searches performed on a partial Run 2 dataset; they avoided the jet trigger threshold of the high-mass dijet resonance search by either doing the analysis at trigger level [233] or requiring the presence of an additional ISR object in order to satisfy the trigger [234, 235]. Conversely, the  $X+E_T^{\text{miss}}$  searches cover the region where the on-shell decay into DM is possible, and in that case are also able to cover very low mediator masses, which is difficult for the resonant searches because of triggering limitations. However, the  $X+E_T^{\text{miss}}$  searches also depend on the value of  $g_q$ , as can be seen by comparing the different coupling scenarios, because the production cross section of the  $Z'$  depends on that coupling.

## 10.2 Vector portal with a dark Higgs boson

The simplified model described in the previous section can be extended with a dark Higgs boson  $s$  to generate the DM mass through Yukawa interactions [237]. If  $m_s < m_\chi$ , a new annihilation channel into SM particles can open, relaxing the relic density constraints shown in the previous section. In this two-mediator model [238], a Majorana DM candidate is considered and there are two additional dark-Higgs free parameters:  $m_s$  and the mixing angle with the SM Higgs boson,  $\theta$ . This model can lead to an  $s+E_T^{\text{miss}}$  final state with  $s \rightarrow WW/ZZ$  at high enough  $m_s$ , as shown in Figure 38(a). The signal models considered assume  $m_\chi = 200$  GeV (to forbid the  $s \rightarrow \chi\chi$  decay for the  $m_s$  considered), along with  $\sin\theta = 0.01$ ,  $g_\chi = 1.0$  and  $g_q = 0.25$ . While the  $g_q$  and  $g_\chi$  values used here are excluded by the resonant  $Z'$  searches in the simplified model shown in the last section, this does not lessen the interest of looking for the unique  $s+E_T^{\text{miss}}$  signature of this more complete model, as the couplings can be varied to relax the constraints.

Two final states are explored: a fully hadronic  $WW/ZZ$  final state [239], not described further here, and a more sensitive semileptonic  $WW$  final state [240]. In both analyses, boosted dark-Higgs decays can lead to multi-prong large- $R$  jets. A track-assisted reclustering (TAR) is used [241], in which the resolution of the reclustered jet substructure variables is improved by using information from ID tracks which are matched to the small- $R$  jet constituents.

In the semileptonic channel, events must have exactly one lepton with a large value of  $m_T(\ell, E_T^{\text{miss}})$ , a large and significant amount of  $E_T^{\text{miss}}$  and no  $b$ -tagged jets, to suppress the  $t\bar{t}$  background. A  $W$  boson

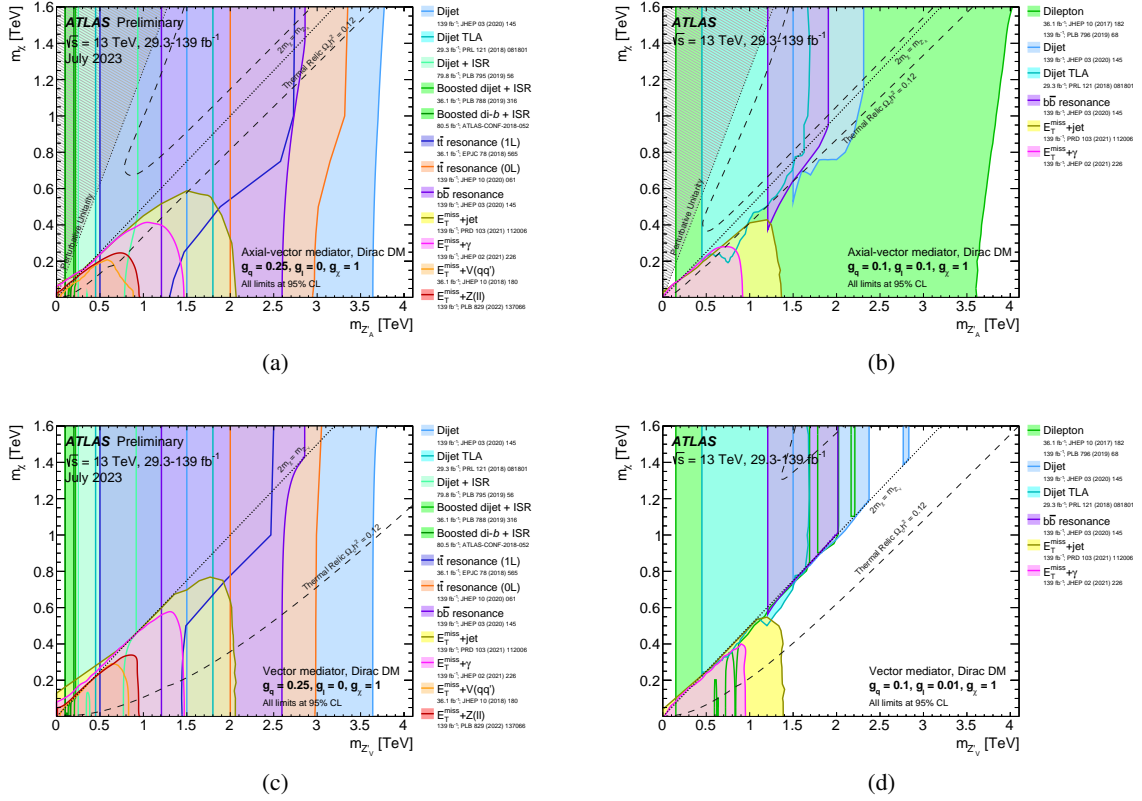


Figure 37: Regions in the  $m_\chi$  versus  $m'_Z$  plane that are excluded at 95% CL by resonant and  $X+E_T^{\text{miss}}$  searches, for the four coupling scenarios described in the text. Dashed curves labelled ‘thermal relic’ correspond to parameters consistent with a DM density of  $\Omega h^2 = 0.12$  as computed in MadDM [225, 236] when assuming a standard thermal history. (c) For the parameter space above the line, or (a,b,d) in between these lines,  $\Omega h^2 < 0.12$ . The dotted line indicates the kinematic threshold where the mediator can decay on-shell into DM.

candidate must then be found with a mass compatible with that boson, and which must not be too far away from the lepton. In the merged SR, this candidate is given by a two-pronged TAR jet, and in the resolved SR, by a high- $p_T$  system of two small- $R$  jets. The discriminating variable in both SRs is the minimum possible reconstructed mass of the dark-Higgs boson candidate, assuming that the charged lepton is massless. Dedicated CRs are used to estimate the dominant  $W$ +jets and subdominant  $t\bar{t}$  backgrounds, built by reversing the lepton- $W$  angular separation requirement or the  $b$ -tagging veto.

As no significant excess above the expected background is found, limits are set on the model parameters in the two analyses, as shown in Figure 38(b); the semileptonic channel sets the most stringent limits.

### 10.3 Higgs portal

Another interesting avenue to explore is whether the Higgs boson, the last piece of the SM discovered by the ATLAS and CMS Collaborations in 2012 [242, 243], can act as a portal between DM and the SM via either Yukawa-type couplings or other mechanisms [244–257]. An exciting signature of this type of interaction would be the decay of the Higgs boson into a pair of DM particles, if kinematically allowed,

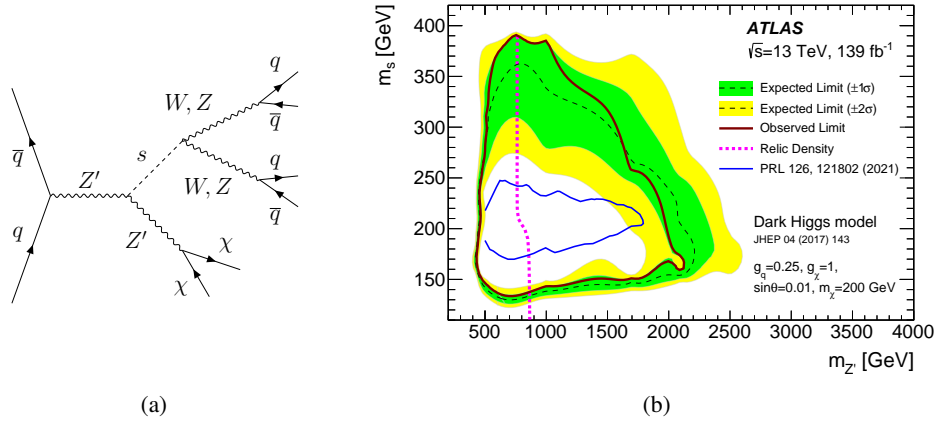


Figure 38: (a) Production of a  $WW/ZZ + E_T^{\text{miss}}$  final state in the two-mediator model comprising a  $Z'$  and a dark Higgs  $s$ , and (b) corresponding exclusion contours set by (red line) the semileptonic [240] and (blue line) fully hadronic [239] channels. In (b), the  $m'_Z$  values above the dashed relic density line correspond to a DM overabundance.

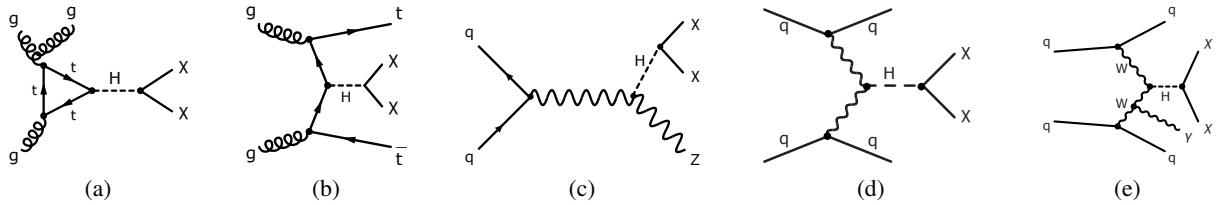


Figure 39: The various diagrams leading to final states which are probed in the search for a DM Higgs portal: (a) ggF with an ISR gluon, (b)  $t\bar{t}$  associated production, (c)  $Z$ -associated production, (d) VBF, and (e) VBF with a photon.

leading to an *invisible* Higgs decay. As long as there is a visible final-state object, this invisible Higgs decay can be searched for in various Higgs boson production modes: VBF, associated production with a weak boson ( $VH$ ) or a  $t\bar{t}$  pair ( $t\bar{t}H$ ), or even ggF if one relies on ISR, as shown in Figure 39. This section covers these various searches, in increasing order of expected sensitivity, and their combination.

All of the presented results assume that the Higgs boson production cross section is the one predicted by the SM [258–264] and that the Higgs boson mass is 125 GeV. The invisible Higgs decay is mimicked by using the SM  $H \rightarrow Z^*Z \rightarrow 4\nu$  process (which has a 0.1% branching ratio in the SM).

### 10.3.1 Gluon–gluon fusion

As ggF is the main Higgs boson production channel at the LHC, it would seem natural to start an invisible-Higgs search with this channel. However, as in the V/A simplified model, this search must rely on an ISR jet against which the Higgs boson decay products recoil as shown in Figure 39(a), leading to the jet+ $E_T^{\text{miss}}$  final state [228] already discussed in Section 10.1.1. This analysis places a 95% CL observed (expected) upper limit of 0.34 (0.39 $^{+0.16}_{-0.11}$ ) on the branching ratio for an invisibly decaying Higgs boson, where the sensitivity is mainly driven by the lower  $E_T^{\text{miss}}$  region.

### 10.3.2 Production in association with a $t\bar{t}$ pair

In order to fully exploit the data, even the  $t\bar{t}H$  production mode can be used; in spite of having the smallest production cross section, it competes favourably with ggF production when combining [165] the various final states from the two top decays, which can contain zero [155], one [265] or two [266] leptons. It can also be used in searches motivated by other DM models, as shown in Section 10.4.

The 0-lepton search is described in Section 7 as it is also used as a leptoquark search. However, the DM search combination [165] extends it with three additional SRs which are able to improve the acceptance for events with lower  $E_T^{\text{miss}}$  or lower-momentum objects by relying on a combination of  $E_T^{\text{miss}}$  and  $b$ -tagged jet triggers. This improves the expected sensitivity to invisible Higgs decay by 12%. The combined observed (expected) upper limit on the Higgs-to-invisible branching ratio is 0.95 ( $0.52^{+0.23}_{-0.16}$ ).

In the 1-lepton channel [265], events must have one electron or muon, at least four small- $R$  jets, of which two must be  $b$ -tagged, sizeable and significant  $E_T^{\text{miss}}$ , and large  $m_T(\ell, E_T^{\text{miss}})$ . An algorithm based on a variable jet radius is used to catch both the highly boosted and less boosted hadronically decaying top-quark candidates. In order to remove background coming from dileptonic  $t\bar{t}$  decays in which one lepton is not reconstructed, a variable called *topness* [267] is used, based on top quark and  $W$  boson mass constraints and considering an invisible lepton candidate. The SR is split into four bins in  $\Delta\phi(\mathbf{p}_T^{\text{miss}}, \ell)$  and the dominant dileptonic  $t\bar{t}$  and  $t\bar{t} + Z$  backgrounds are estimated through dedicated CRs, built by either reversing the topness requirement, or requiring more leptons. This search is expected to be less sensitive than the 0-lepton channel, but its observed limit is found to be slightly more stringent: at 95% CL, the observed (expected) upper limit on the branching ratio is 0.74 ( $0.80^{+0.40}_{-0.26}$ ).

The most sensitive  $t\bar{t}H$  channel is the 2-lepton one [266], which requires two opposite-sign leptons (electrons or muons) along with at least one  $b$ -tagged jet and a significant amount of  $E_T^{\text{miss}}$ . Furthermore, the azimuthal angle  $\Delta\phi_{\text{boost}}(\mathbf{p}_T^{\text{miss}}, \mathbf{p}_T^{\text{boost}})$  must be smaller than 1.5, where  $\mathbf{p}_T^{\text{boost}}$  is defined as the vectorial sum of the  $\mathbf{p}_T^{\text{miss}}$  and the  $p_T$  of the leptons. The events are then separated depending on whether they contain same-flavour leptons (incompatible with the  $Z$  boson mass), or different-flavour leptons. The discriminating variable, in which the SR is binned, is  $m_{T2}$ . The main backgrounds after all requirements,  $t\bar{t}$  and  $t\bar{t} + Z$  events, are estimated using dedicated CRs, based on  $e\mu$  events at lower values of  $m_{T2}$  or on the presence of three leptons, respectively. The data agree well with the background expectations, as shown in Figure 40(a): the observed (expected) upper limit on the Higgs-to-invisible branching ratio is 0.36 ( $0.40^{+0.18}_{-0.12}$ ) at 95% CL.

Combining the three  $t\bar{t}H$  channels increases the sensitivity further: the combined expected limit is  $0.30^{+0.13}_{-0.09}$ , with an overall uncertainty dominated by the statistical precision of the data. The observed value of 0.38 agrees well with the expected limit.

### 10.3.3 Production in association with a $Z$ boson

The  $Z(\rightarrow \ell\ell)H$  channel puts even more stringent constraints on the Higgs-to-invisible branching ratio [230]: the leptonic trigger allows the analysis to probe  $E_T^{\text{miss}}$  values which are not as high as in the jet+ $E_T^{\text{miss}}$  analysis, thus increasing the sensitivity of the search to this particular signal, and the larger production cross section and relatively clean final state provide better sensitivity than the  $t\bar{t}H$  channel. This analysis is also sensitive to other DM signals (see Sections 10.1 and 10.4).



Events are selected by requiring exactly two opposite-sign electrons or muons with an invariant mass compatible with a  $Z$  boson. Since the leptons should recoil against an invisible Higgs boson, their angular separation should not be too large, and the events should have a large and significant  $E_T^{\text{miss}}$ . In order to increase the sensitivity further, the SR uses a BDT which is based on eight kinematic variables. After this selection, the dominant background comes from the  $ZZ$  process, followed by  $WZ$ ,  $Z$ +jets and smaller non-resonant backgrounds ( $WW$ ,  $t\bar{t}$ , single-top and  $Z \rightarrow \tau\tau$ ). Three CRs are used: an  $e\mu$  CR to constrain the non-resonant backgrounds, a  $4\ell$  CR to estimate the  $ZZ$  contribution, and a  $3\ell$  CR to estimate the  $WZ$  background. The  $Z$ +jets contribution is taken from MC simulation, but verified in a validation region reversing the requirement on  $S_{E_T^{\text{miss}}}$ . The resulting BDT output distribution is shown in Figure 40(b).

The best-fit Higgs-to-invisible branching ratio is found to be  $(0.3 \pm 9.0)\%$  where the uncertainty is dominated by the  $ZZ$  modelling uncertainties and the jets/ $E_T^{\text{miss}}$ -related experimental uncertainties. The observed 95% CL upper limit of 0.19 set on the branching ratio coincides with the expected limit.

### 10.3.4 Vector-boson fusion

The most sensitive channel in the search for a DM Higgs portal is VBF production [268], leading to a VBF jets+ $E_T^{\text{miss}}$  final state. While this final state differs from the ggF jet+ $E_T^{\text{miss}}$  one by the VBF characteristics of the jets, many of the analysis techniques for the two analyses are similar. After requiring a large  $E_T^{\text{miss}}$  value and imposing a veto on leptons and photons, the analysis exploits the VBF signature. In this topology, the two leading jets are usually in opposite hemispheres of the detector,  $\eta^{j1} \cdot \eta^{j2} < 0$ , and are more forward, leading to a large separation in pseudorapidity and a large invariant mass. Unlike the jets in a multijet background event, which are likely to be back-to-back, the expected signal jets must balance the significant  $p_T$  of the Higgs boson, leading to a smaller azimuthal separation. As in the jet+ $E_T^{\text{miss}}$  analysis, extra jets are allowed in the SR to increase the acceptance and reduce the associated modelling systematic uncertainties. However, given the absence of colour connection between the two VBF quarks, the VBF process has less hadronic activity in the *central* rapidity region between the two leading jets. Furthermore, the dijet invariant mass constructed from a jet radiated by a VBF quark and one of the two leading jets should be small relative to the invariant mass of the two leading jets. Consequently, up to two extra jets are allowed, but only if they are compatible with the VBF process, i.e. by requiring both their centrality as defined in Ref. [269] and their dijet invariant mass to be small. Further suppression of the multijet background is achieved by requiring the  $p_T$  of the jet system (including jets tagged as pile-up jets by the JVT algorithm) to be large. The  $E_T^{\text{miss}}$  soft term is also required to be small to remove  $W(\rightarrow \mu\nu)$ +jets events in which the muon is not identified but is still seen as a high- $p_T$  track in the inner detector. Finally, a veto on the presence of more than one  $b$ -tagged jet is imposed to ensure orthogonality with the  $t\bar{t}H$  search described above. This rejects very few events, as the VBF jets are mostly forward and hence outside the inner-detector acceptance which is used in  $b$ -tagging.

In order to increase the sensitivity, the SR is subdivided into 16 different regions, according to the  $E_T^{\text{miss}}$ , number of jets, dijet invariant mass, and azimuthal angle between the two leading jets. As in the jet+ $E_T^{\text{miss}}$  analysis, the main backgrounds are  $Z(\rightarrow \nu\nu)$ +jets and  $W(\rightarrow \ell\nu)$ +jets, and the same strategy is used to evaluate them: 1- and 2-lepton CRs are built, and dedicated NLO theoretical calculations [270] performed in the relevant phase space are used to fix the  $Z/W$  ratio, reducing the statistical uncertainties in the determination of the dominant  $Z(\rightarrow \nu\nu)$ +jets background by using all leptonic CRs simultaneously to constrain it. The smaller multijet background is determined in a fully data-driven way, using two independent methods because it can come either from jet mismeasurements or from a pile-up jet being wrongly identified as a VBF jet. Although a smaller component than the  $V$ +jets background, unlike in



the ggF analysis, the multijet background is not found to be negligible in all SR bins, as can be seen in Figure 40(c), representing from 0.4% up to almost 14% of the total background.

Since no significant excess is seen, an upper limit of 0.145 is set on the branching ratio of invisible Higgs boson decays, in agreement with the expected limit of  $0.103^{+0.041}_{-0.028}$ , where the main uncertainties are related to the data statistics, the multijet background estimate, lepton identification, and the jet energy resolution.

### VBF jets+ $E_T^{\text{miss}}$ + $\gamma$

The VBF production mode is further exploited, by requiring the presence of an additional photon [271], as depicted in Figure 39(e) – the photon veto in the VBF jets+ $E_T^{\text{miss}}$  analysis makes these channels orthogonal. Considerations similar to those described above are used to select events with a large  $E_T^{\text{miss}}$ , VBF jets and no leptons. Specific requirements are then made on the photon. Since it is usually radiated from one of the scattering  $W$  bosons, it is expected to be produced within the rapidity gap of the VBF jets, not be too energetic (to remove  $\gamma$ +jets background events), be well separated from the  $E_T^{\text{miss}}$ , and have a trajectory that, when extrapolated to the beamline, is loosely compatible with the PV (to remove non-collision background). Finally, a dense neural network is trained using the most significant kinematic features, and four bins in its output score form the SR. The main  $Z\gamma$ +jets and  $W\gamma$ +jets backgrounds are estimated using CRs, built by reversing the photon centrality requirement or by requiring one lepton in the final state, respectively.

The observed limit set by this analysis on the branching ratio of invisible Higgs boson decays is 0.37, in line with the expected value of  $0.34^{+0.15}_{-0.10}$ , where the uncertainty is dominated by the data statistics.

### 10.3.5 Combination of all channels

A summary of the upper limits obtained in the channels described above is shown in Figure 40(d), along with a combination of these results alone and with the previous Run 1 results [272]. The Run 2 combination gives an observed (expected) upper value of 0.113 ( $0.080^{+0.031}_{-0.022}$ ), an improvement of 22% on the sensitivity of the most sensitive VBF jets+ $E_T^{\text{miss}}$  channel. In combination with the Run 1 results, the expected sensitivity is further improved by 4%, with an upper limit at 0.107 ( $0.077^{+0.030}_{-0.022}$ ). In the Run 2 combination, the leading systematic uncertainties are related to the  $W/Z$ +jets modelling uncertainties; without any systematic uncertainties, the upper limit would improve by 50%.

## 10.4 Pseudoscalar portal

Another possibility for a DM mediator would be the addition of a pseudoscalar portal. As  $t$ -channel interactions via a pseudoscalar would be suppressed in the non-relativistic limit, the sensitivity of direct-detection experiments in this case would be very low, so it is especially important to consider this portal at the LHC because it could offer a unique opportunity for detection.

The model considered here is the 2HDM+ $a$  model suggested by the LHC DM Working Group [226], which is the simplest gauge-invariant and renormalizable ultraviolet completion of the simplified pseudoscalar model initially recommended by the LHC DM Forum [223], which only contained the DM candidate and the mediator. This model is a type-II two-Higgs-doublet (2HDM) model [273] to which an additional pseudoscalar  $a$  and a fermionic DM candidate  $\chi$  are added. After electroweak symmetry breaking, the 2HDM contains five Higgs bosons: a lighter CP-even boson,  $h$ , a heavier CP-even boson,  $H$ , a CP-odd boson,  $A$ , and two charged bosons,  $H^\pm$ . While the phenomenology of the model would be determined by 14 free parameters, some benchmark choices are made in order to match  $h$  with the observed SM

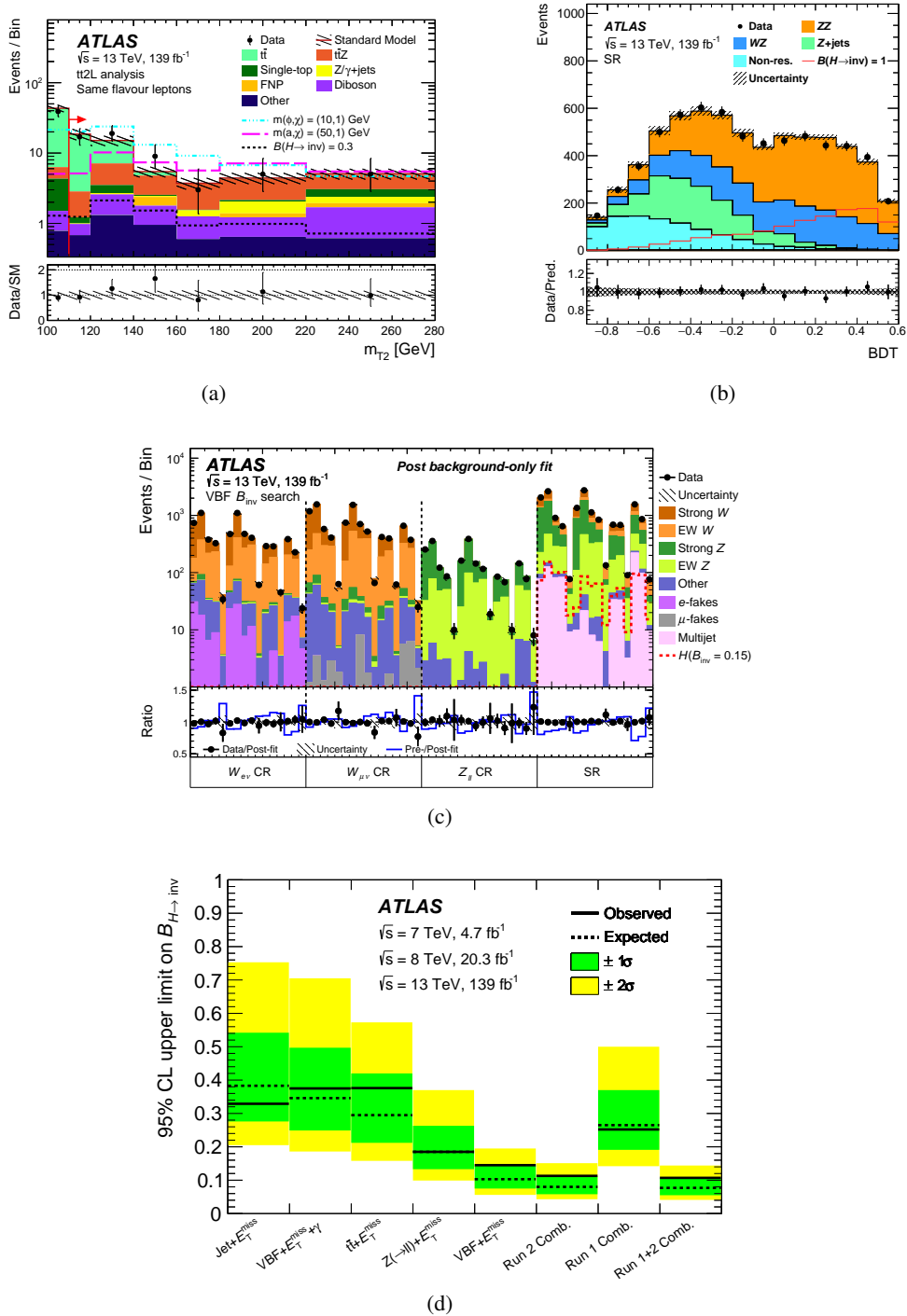


Figure 40: Measured distributions of (a)  $m_{T2}$  in the 2-lepton  $t\bar{t}H$  SR [266] where the SR requirement is shown by the red arrow, (b) the BDT output distribution in the  $Z+E_T^{\text{miss}}$  SR [230] and (c) the yields in each of the CR and SR bins of the VBF jets+ $E_T^{\text{miss}}$  analysis [268], compared to the estimated background and an invisible-Higgs-decay signal with a (a) 30%, (b) 100% or (c) 15% branching ratio. The observed and expected 95% CL upper limits (d) on the Higgs-to-invisible branching ratio for the individual Run 2 analyses, along with the combination of these results alone and with the previous Run 1 results [272].

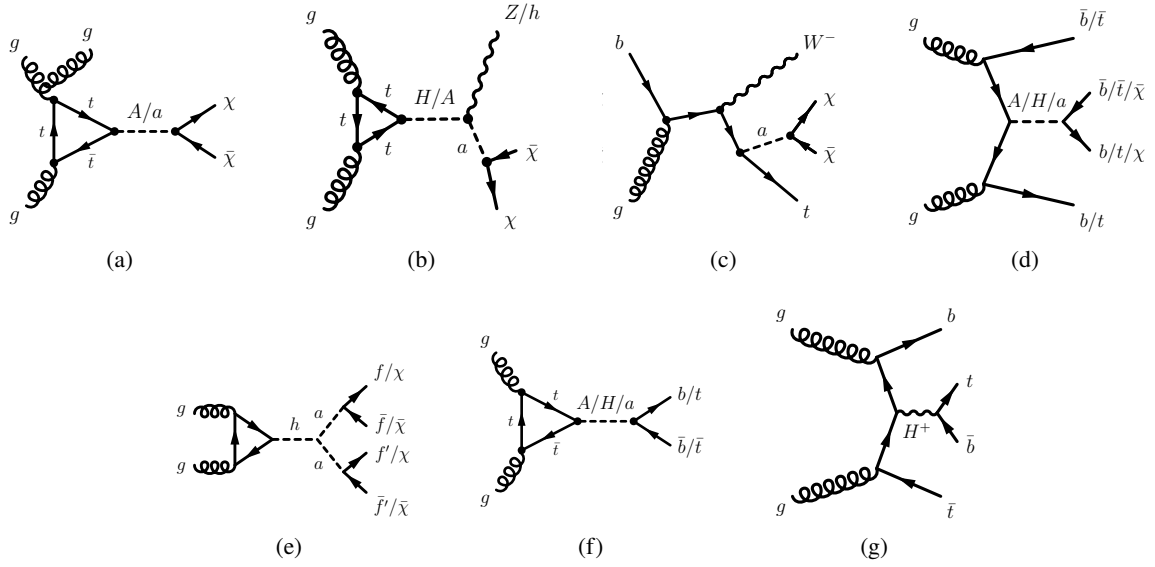


Figure 41: Examples of Feynman diagrams leading to various final states expected in the 2HDM+a model: (a)  $\text{jet}+E_{\text{T}}^{\text{miss}}$ , (b)  $Z+E_{\text{T}}^{\text{miss}}$  and  $h+E_{\text{T}}^{\text{miss}}$  resonant production, (c)  $Wt+E_{\text{T}}^{\text{miss}}$ , (d)  $tttt/ttbb/bbbb/tt+E_{\text{T}}^{\text{miss}}/bb+E_{\text{T}}^{\text{miss}}$  final states through associated  $A/H/a$  production, (e) decay of a SM Higgs boson into a pair of  $a$ -bosons that subsequently decay into fermions or DM, (f) resonant  $tt$  or  $bb$  production, and (g)  $tbH^{\pm}(tb)$  production.

Higgs boson, to ensure the stability of the Higgs potential, or to evade electroweak precision measurement constraints. In the end, the benchmarks are defined by five parameters: the mass of the heavy Higgs bosons, which are taken to be degenerate,  $m_A = m_H = m_{H^{\pm}}$ ; the mass of the pseudoscalar mediator,  $m_a$ ; the mass of the DM particle,  $m_{\chi}$ ; the mixing angle  $\theta$  between the two CP-odd states  $a$  and  $A$ ; and the ratio of the vacuum expectation values of the two Higgs doublets,  $\tan\beta$ .

This model leads to a large number of final states which can be probed. Some examples of their production modes are shown in Figure 41. The following final states were explored in Run 2, and some are introduced in previous sections: the ubiquitous  $\text{jet}+E_{\text{T}}^{\text{miss}}$  (see Section 10.3.1),  $Z+E_{\text{T}}^{\text{miss}}$  (see Section 10.3.3),  $h+E_{\text{T}}^{\text{miss}}$  [274–276],  $Wt+E_{\text{T}}^{\text{miss}}$  [277, 278],  $tt+E_{\text{T}}^{\text{miss}}$  (see Section 10.3.2),  $tbtb$  [279],  $bbbb$ ,  $tttt$ ,  $bb$  and  $tt$  (see Section 4). A statistical combination of some of these has also been performed [280]. In this section, the searches not already discussed in the context of other models are introduced, and their complementarity in covering the model parameter space is discussed. Since the  $tbH^{\pm}(tb)$  search [279] does not specifically target this model, but in general the production of a charged Higgs boson in association with a top quark and bottom quark, as shown in Figure 41(g), it is reviewed in another report discussing extended Higgs sectors but not here.

#### 10.4.1 The $h+E_{\text{T}}^{\text{miss}}$ searches

The 2HDM+a model provides mechanisms in which the  $h+E_{\text{T}}^{\text{miss}}$  signature could be produced resonantly (see Figure 41(b)), making this final state a particularly sensitive probe for this model, unlike those in which the visible object comes from ISR. Three  $h+E_{\text{T}}^{\text{miss}}$  channels with different Higgs boson decays have been

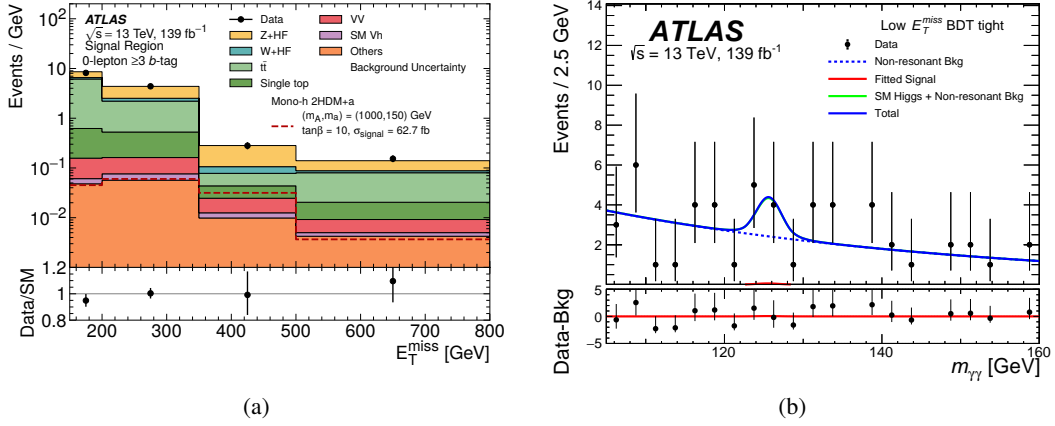


Figure 42: (a) The measured  $E_T^{\text{miss}}$  distribution in the 3- $b$ -tagged resolved and merged SRs of the  $h(bb)+E_T^{\text{miss}}$  search [274] and (b) the measured  $m_{\gamma\gamma}$  distribution in the BDT tight signal regions with low  $E_T^{\text{miss}}$  used in the  $h(\gamma\gamma)+E_T^{\text{miss}}$  search [275], compared to expected background and an example 2HDM+ $a$  signal.

explored, the most sensitive one being the  $h(bb)+E_T^{\text{miss}}$  channel [274], followed by the  $h(\gamma\gamma)+E_T^{\text{miss}}$  [275] and  $h(\tau\tau)+E_T^{\text{miss}}$  [276] channels. The two most sensitive ones are discussed below.

### The $h(bb)+E_T^{\text{miss}}$ channel

Two regions are defined in this search, based on an  $E_T^{\text{miss}}$  trigger, depending on the expected boost of the Higgs boson: a resolved region, defined at lower  $E_T^{\text{miss}}$  values, and a merged region, at higher values. A lepton ( $e, \mu, \tau$ ) veto is imposed and a minimum angular separation between the  $E_T^{\text{miss}}$  and the  $p_T$  of each of the three leading jets is required in both SRs. The reconstructed Higgs boson mass  $m_h$  is corrected for nearby muons to improve its accuracy when  $b$ -hadrons decay semileptonically. For better sensitivity, both SRs are binned in  $E_T^{\text{miss}}$ , in the number of  $b$ -tagged jets (two or at least three), and in  $m_h$ .

In the resolved SR, the Higgs boson candidate is reconstructed from the two  $b$ -tagged small- $R$  jets with the highest  $p_T$ . It must have a mass loosely compatible with the Higgs boson and a large  $p_T$ . To remove the multijet background, the  $E_T^{\text{miss}}$  must be significant. The dominant semileptonic  $t\bar{t}$  background is suppressed by using  $m_T(b, E_T^{\text{miss}})$  built from each  $b$ -tagged jet. Because this background enters the SR when the lepton is missed, the leptonically decaying  $W$  boson would be seen as  $E_T^{\text{miss}}$ , and this transverse mass would have an endpoint at the top-quark mass, while the signal could have higher values. Furthermore, as the signal usually contains fewer jets than the background, up to four (five) jets are allowed when there are two (at least three)  $b$ -tagged jets. In the merged SR, at least one large- $R$  jet is required. In order to identify the  $b$ -tagged subjets coming from the Higgs decay, even in highly boosted scenarios, variable- $R$  track-jets are used. [35]. A Higgs boson candidate is identified as the large- $R$  jet if its two leading associated track-subjets are  $b$ -tagged, and if its muon-corrected mass falls in a range loosely compatible with the Higgs boson.

After these selections, the main backgrounds, the  $t\bar{t}$  and  $W/Z$  + heavy-flavour (HF) processes, are estimated using 1-muon and 2-lepton CRs. In Figure 42(a), the resulting yields measured in data as a function of  $E_T^{\text{miss}}$  are compared with the background expectations in the 3- $b$ -tagged SRs. Good agreement is observed in all SRs within the uncertainties, which are dominated by statistical uncertainties in the merged regions and by systematic uncertainties in the resolved regions, the latter being mostly affected by the modelling of the  $t\bar{t}$  background, the uncertainties in the jet calibration, and the limited MC sample size.

### The $h(\gamma\gamma)+E_T^{\text{miss}}$ channel

In this channel [275], the trigger is based on the photon pair. The  $E_T^{\text{miss}}$  requirement can thus be lower than in the  $h(bb)$  channel, covering the parameter space in which a less-boosted Higgs boson is expected. The  $m_{\gamma\gamma}$  value must be loosely compatible with the Higgs boson, and each photon must have a sizeable  $p_T/m_{\gamma\gamma}$ . A lepton ( $e, \mu$ ) veto is applied. Given the low ID activity expected, the PV might not be well selected; to avoid these cases, selected events must not have an  $E_T^{\text{miss}}$  value which changes significantly if computed with an alternative NN-based PV algorithm [281]. Four SRs are built: at low and high  $E_T^{\text{miss}}$ , and with looser or tighter purity given by the score of a BDT (which uses  $S_{E_T^{\text{miss}}}$  and the diphoton  $p_T$  as inputs). A functional form is fitted in each SR: for the signal and the SM Higgs boson background, a double-sided Crystal Ball function is used, while the non-resonant background is modelled by an exponential function of the type  $e^{am_{\gamma\gamma}}$ , as shown in Figure 42(b) in the low- $E_T^{\text{miss}}$ , BDT tight SR. No significant excess is seen in any of the SRs for any of the signals considered.

### 10.4.2 The $Wt+E_T^{\text{miss}}$ searches

The rich phenomenology of the 2HDM+ $a$  model also includes the production of a  $Wt+E_T^{\text{miss}}$  final state, which can be produced when an initial  $b$ -quark radiates either a  $W$  boson (as shown in Figure 41(c)) or a charged Higgs boson which subsequently decays as  $H^- \rightarrow aW^-$ . Depending on the decay mode of the top quark and the  $W$  boson, this can lead to final states containing zero, one or two leptons, all of which have been explored [277, 278].

In the 0-lepton channel [278], at least four jets are required, exactly one of which must be  $b$ -tagged and another being a large- $R$  jet tagged as a  $W$  boson. Since the boosted  $W$  boson is assumed to come from the  $H^-$  decay, the  $W$ -tagged jet and the  $b$ -tagged jet must not, when combined, be compatible with a top-quark decay in mass. A large and significant value of  $E_T^{\text{miss}}$  is required, which must be well separated from the selected jets. A large value of  $m_T(b, E_T^{\text{miss}})$  is also required in order to remove the semileptonic  $t\bar{t}$  background in which the  $E_T^{\text{miss}}$  comes from a missed  $W$  boson. The SR is binned in  $E_T^{\text{miss}}$  to improve the sensitivity. After these selections, the main backgrounds come from  $V$ +jets and semileptonic  $t\bar{t}$  events.

The 1-lepton channel [278] requires the presence of at least two jets, and the requirements placed on the  $b$ -tagged jet,  $E_T^{\text{miss}}$ ,  $S_{E_T^{\text{miss}}}$  and  $\Delta\phi(E_T^{\text{miss}}, \text{jet})$  are similar to those in the 0-lepton channel. The leptonically decaying  $W$  boson can come from the decay of either the top quark or the  $H^-$  in the signal, each case being the target of a different SR ( $\text{SR}^{\text{lep.top}}$  and  $\text{SR}^{\text{had.top}}$ ). In  $\text{SR}^{\text{lep.top}}$ , the hadronically decaying  $W$  boson can be boosted, so the presence of a  $W$ -tagged large- $R$  jet is required. In  $\text{SR}^{\text{had.top}}$ , at least three jets are required. In both SRs, a large value of  $m_T(\ell, E_T^{\text{miss}})$  (compatible with the top-quark mass in  $\text{SR}^{\text{lep.top}}$  but not in  $\text{SR}^{\text{had.top}}$ ) is required, as well as an  $am_{T2}$  value above the top-quark mass. Finally, the two SRs are kept orthogonal by requiring a lower value ( $\text{SR}^{\text{had.top}}$ ) or higher value ( $\text{SR}^{\text{lep.top}}$ ) of the invariant mass of the leading  $b$ -tagged jet and the highest- $p_T$  jet which is not  $b$ -tagged. While the low number of events expected in  $\text{SR}^{\text{lep.top}}$  does not allow it to be subdivided further, five bins in  $E_T^{\text{miss}}$  are used in  $\text{SR}^{\text{had.top}}$ . In these SRs, the main backgrounds are dileptonic  $t\bar{t}$  and either  $t\bar{t}Z$  (in  $\text{SR}^{\text{lep.top}}$ ) or  $W$ +jets (in  $\text{SR}^{\text{had.top}}$ ).

In the 2-lepton channel [277], the events must contain OS leptons that are incompatible with the  $Z$  boson mass (if they are of the same flavour), at least one jet (well separated from the  $E_T^{\text{miss}}$ ), including at least one  $b$ -tagged jet. The dileptonic  $t\bar{t}$  and  $t\bar{t}V$  backgrounds are reduced by three mass requirements. The first requires a large value of  $m_{T2}$ . The second imposes an upper bound on the minimum invariant mass found by combining the highest- $p_T$   $b$ -tagged jet with each of the leptons. The last one is constructed by assembling the two leptons ( $\ell_{1,2}$ ) with the two jets with the highest  $b$ -tagging score ( $j_{1,2}$ ) in all lepton-jet combinations.

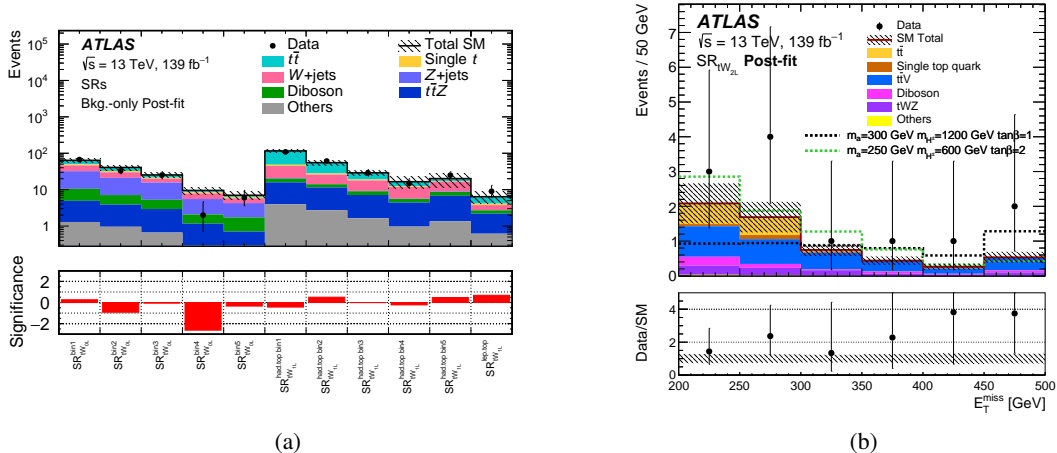


Figure 43: (a) Number of events found in each of the 0- and 1-lepton channel SRs [278] and (b)  $E_T^{\text{miss}}$  distribution in the 2-lepton SR [278] of the  $Wt+E_T^{\text{miss}}$  search compared to the SM background expectation. In (b), examples of signal distributions are also shown.

Assuming they come from top-quark decays, requiring  $m_{b\ell}^t = \min(\max(m_{\ell_1 j_1}, m_{\ell_2 j_2}), \max(m_{\ell_1 j_2}, m_{\ell_2 j_1}))$  to be above 150 GeV suppresses these backgrounds. The main SM background contributions in this SR are  $t\bar{t}$ ,  $t\bar{t}Z$  and  $tWZ$  processes, followed by diboson events.

In all these channels, dedicated CRs are used to constrain the main backgrounds. In the 0-lepton channel, 1- and 2-lepton CRs are defined to constrain the  $t\bar{t}$  and  $W$ +jets backgrounds. In the 1-lepton channel, the  $t\bar{t}$  CR is built by reversing the requirement on  $am_{T2}$  and the veto on a second  $b$ -tagged jet. In the 2-lepton channel, it is built by reversing the  $m_{T2}$  and  $m_{b\ell}^t$  requirements. In both the 1- and the 2-lepton channels, a 3-lepton 3-jet CR is used to constrain the  $t\bar{t}Z$  background. In the 2-lepton channel, a 3-lepton  $WZ$  CR is also built, with a lower jet multiplicity.

The event yields in all SRs of the three analysis channels are shown in Figure 43. Reasonable agreement is found in all SRs, the discrepancy seen in the 2-lepton channel being lower than  $2\sigma$ .

### 10.4.3 Exclusions in the 2HDM+ $a$ parameter space

A statistical combination of the most sensitive channels,  $h(bb)+E_T^{\text{miss}}$ ,  $Z(\rightarrow \ell\ell)+E_T^{\text{miss}}$  and  $tH^\pm(tb)$ , was performed in Ref. [280], which provides an extensive set of exclusion limits. The constraints are evaluated for some representative benchmark scenarios, in which only one or two of the five free parameters introduced in Section 10.4 are varied at a time, as shown for some examples in Figure 44, thus showing some of the complementarity of the searches introduced above. The value of  $m_\chi$ , while having a strong effect on cosmological parameters such as the relic density, has only a limited impact on the collider searches for  $m_\chi < m_a/2$  and is thus not varied in the figures shown here.

In the  $(m_a, m_A)$  plane shown in Figure 44(a), the pseudoscalar hierarchy is explored, with  $\tan\beta = 1.0$  (favouring couplings to up-type quarks) and  $\sin\theta = 0.35$  (giving small  $A$ - $a$  mixing). The exclusion is dominated at lower  $m_a$  by the  $h(bb)+E_T^{\text{miss}}$  and  $Z(\rightarrow \ell\ell)+E_T^{\text{miss}}$  channels, due to the resonant nature



of the production mechanism. The  $Z(\rightarrow \ell\ell)+E_T^{\text{miss}}$  channel is able to probe lower  $m_A$  values because a lower  $E_T^{\text{miss}}$  is expected there, and the  $h(bb)+E_T^{\text{miss}}$  analysis is based on an  $E_T^{\text{miss}}$  trigger. Conversely, the  $h(bb)+E_T^{\text{miss}}$  channel is more sensitive at higher values of  $m_A$  because of a specific increase in the non-resonant  $a^* \rightarrow ah$  production cross section there. At higher values of  $m_a$ , the  $tbH^\pm(tb)$  channel dominates; as a direct search for charged Higgs production, it is relatively insensitive to the value of  $m_a$ .

In the  $(\tan\beta, m_A)$  plane shown in Figure 44(b), a value  $m_a = 250$  GeV is chosen to suppress  $a \rightarrow t\bar{t}$  and thus favour  $a \rightarrow \chi\chi$ . The exclusion is mainly driven by the  $Z(\rightarrow \ell\ell)+E_T^{\text{miss}}$  analysis, except at larger values of  $m_A$  as explained above, where the  $h(bb)+E_T^{\text{miss}}$  channel can dominate. The sensitivity of the  $tbH^\pm(tb)$  and  $tttt$  channels is seen to increase at low  $m_A$ , for which the heavy-Higgs production cross section is larger, and at low  $\tan\beta$ , as it favours third-generation couplings.

Finally, the exclusion as a function of  $\sin\theta$  is shown in Figure 44(c), which highlights the interplay between invisible and visible mediator decays due to the direct dependence of the couplings  $g_{Aha}$ ,  $g_{HZa}$  and  $g_{at\bar{t}}$  on  $\sin\theta$ : the higher values of  $\sin\theta$  are covered by the  $Z(\rightarrow \ell\ell)+E_T^{\text{miss}}$  analysis, but its sensitivity at lower  $\sin\theta$  falls quickly and the  $tbH^\pm(tb)$  analysis becomes dominant. Although less sensitive than the  $Z(\rightarrow \ell\ell)+E_T^{\text{miss}}$  analysis, the  $Wt+E_T^{\text{miss}}$  channel's sensitivity becomes comparable to that of  $h(bb)+E_T^{\text{miss}}$  at high  $\sin\theta$  values, but the observed limit is weaker due to the small excess seen in the 2-lepton channel.

## 10.5 Comparison with direct-detection experiments

While the pseudoscalar portal discussed above would evade direct detection, the limits obtained in the V/A and Higgs portal models can, with some assumptions, be translated into limits on the WIMP–nucleon scattering cross section and thus compared with limits obtained by DM direct-detection experiments. As described in Ref. [224], this translation can be made in the V/A simplified model once the couplings introduced in Section 10.1 are fixed (to  $(g_g, g_\chi, g_\ell) = (0.25, 1, 0)$  here). A Higgs or vector mediator would lead to spin-independent scattering, while an axial-vector mediator would lead to spin-dependent scattering. For a DM Higgs portal, an effective-field theory framework is used [249], where the scale of new physics is well above the Higgs boson mass, and the DM particle is either a scalar or vector boson or a Majorana fermion. For a vector DM candidate, some ultraviolet-complete models in which it is the gauge field of a new  $U(1)'$  group are also considered [282–284]. In these models a dark Higgs boson, with mass  $m_2$  and mixing angle  $\alpha$  with the SM Higgs boson, is introduced to generate the DM candidate's mass.

The limits obtained are shown in Figure 45, where one can see the complementarity of the approaches. The collider searches presented here are particularly helpful in covering the low-mass region of the parameter space, which is kinematically easily accessible at the LHC but very difficult to probe in direct-detection experiments because of the very low induced recoil energies. The invisible-Higgs search can even probe below the *neutrino fog* limit, the parameter space in which the neutrino background becomes dominant for direct-detection searches, but it becomes irrelevant for DM masses above  $m_H/2$ , where the Higgs boson would not decay invisibly. The spin-dependent interaction, which the direct-detection experiments constrain much less than the spin-independent one, is probed very effectively by the collider searches.



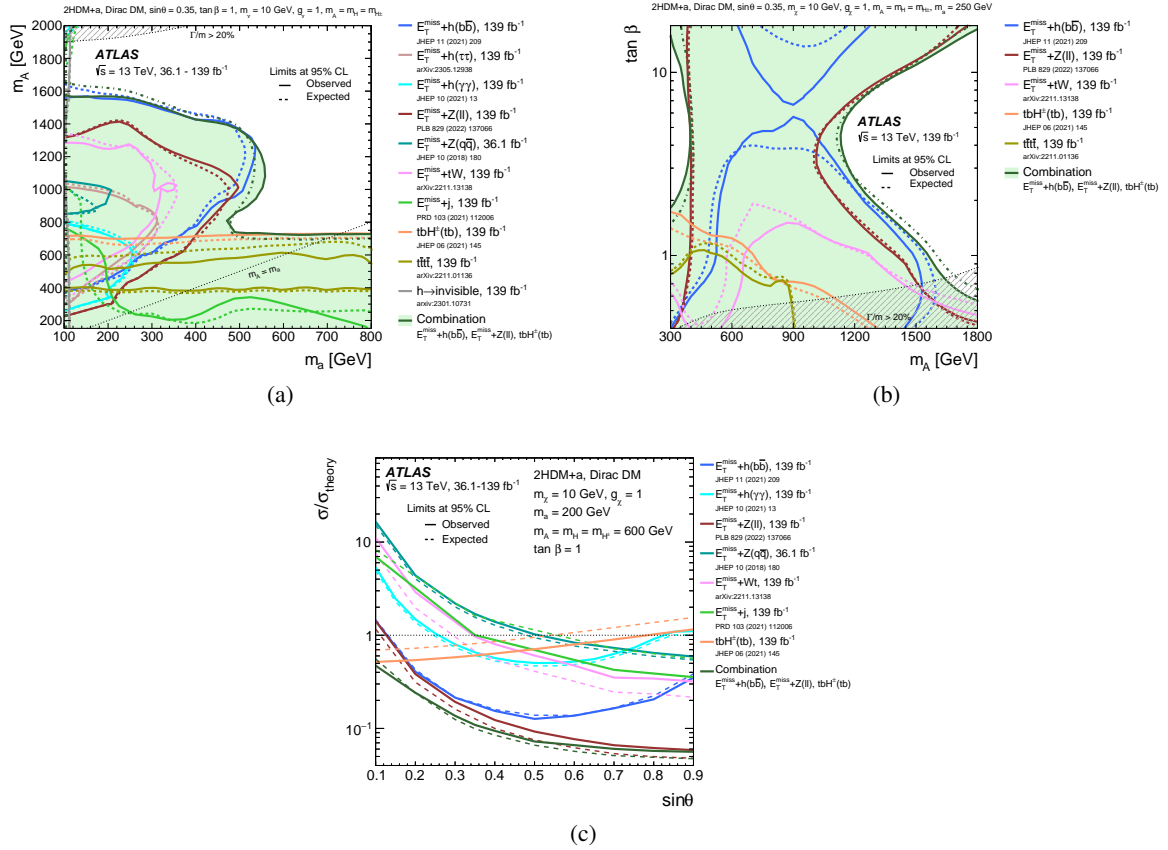


Figure 44: Observed (solid lines) and expected (dashed lines) exclusion limits [280] (a) in the  $(m_a, m_A)$  plane with  $\sin\theta = 0.35$ ,  $\tan\beta = 1$ ,  $m_\chi = 10$  GeV and  $g_\chi = 1$ , (b) in the  $(m_A, \tan\beta)$  plane for  $\sin\theta = 0.35$ ,  $m_a = 250$  GeV,  $m_\chi = 10$  GeV and  $g_\chi = 1$ , and (c) as a function of  $\sin\theta$  for  $\tan\beta = 1$ ,  $m_a = 200$  GeV,  $m_\chi = 10$  GeV,  $g_\chi = 1$  and  $m_A = 600$  GeV.

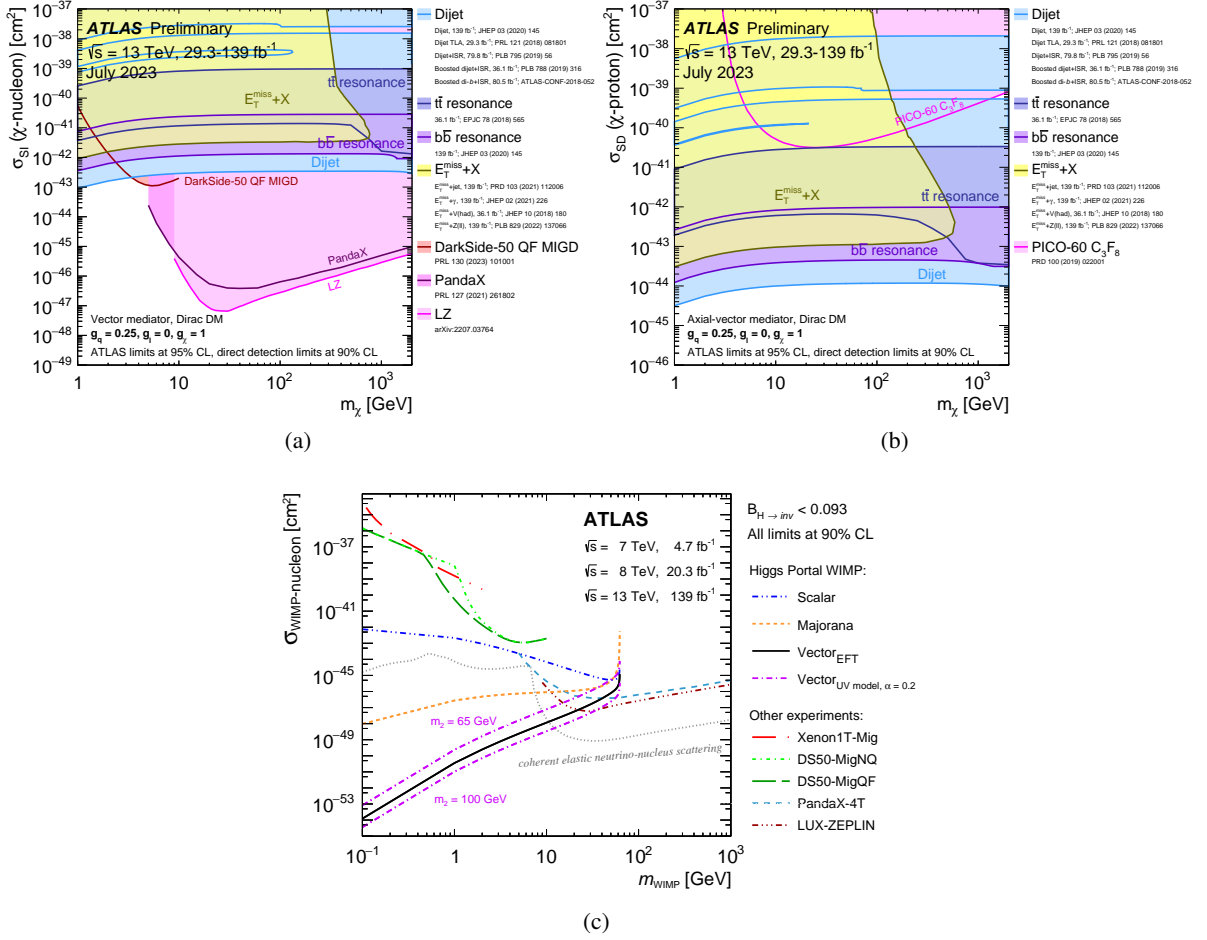


Figure 45: Comparison of the limits obtained (a,b) at 95% CL by the resonant and  $X+E_T^{\text{miss}}$  searches in the V/A model or (c) at 90% CL from the invisible-Higgs searches [272] with the limits obtained by direct-detection experiments in the plane of (a,c) the spin-independent  $\chi$ -nucleon scattering cross section versus  $m_\chi$  or (b) the spin-dependent  $\chi$ -proton scattering cross section versus  $m_\chi$  for different model assumptions. In (c), besides the direct-detection limits [195, 203, 285, 286], the coherent elastic neutrino-nucleus scattering *neutrino fog* expected for a germanium target [287, 288] is also shown.

## 10.6 Strongly coupled hidden sector

If there is a strongly coupled dark sector, its matter fields (the *dark quarks*) produced from SM particles through a mediator could hadronize into dark hadrons [289–292]. Depending on the parameters of the models, some dark mesons would be stable (and be DM candidates) while some would decay back into SM particles. Two searches for such dark sectors are presented here: one in which there is a bi-fundamental mediator  $\Phi$  which couples SM quarks to dark quarks via the  $t$ -channel [293], and one in which the mediator is a  $Z'$  boson, producing the dark quarks in the  $s$ -channel [294].

In the  $t$ -channel production search [293], two jets would be produced in a non-resonant way; since they are composed of SM particles and invisible dark hadrons, they are known as semi-visible jets [295]. Some  $E_T^{\text{miss}}$  is thus expected and could even point in the direction of a jet, a possibility which is usually excluded by azimuthal separation requirements in other LHC DM searches. The dark QCD parameters of the signal samples are fixed in accord with Refs. [295, 296], with the  $\Phi q q_d$  coupling,  $\lambda$ , set to 1. The free parameters considered are thus the branching ratio for decay of unstable dark mesons into stable dark mesons,  $R_{\text{inv}}$ , and the mediator mass,  $m_\Phi$ . Since the analysis targets high mediator masses, and mismeasured jets from the multijet background need to be suppressed, the analysis selects events with  $E_T^{\text{miss}}$  and  $H_T$  values above 600 GeV. The events must contain at least two jets, with one being  $\Delta\phi < 2.0$  away from the  $E_T^{\text{miss}}$  direction, and no lepton. Taking  $j_1$  and  $j_2$  to be the closest and farthest jets in azimuth from the  $E_T^{\text{miss}}$  direction, their  $p_T$  balance,  $p_T^{\text{bal}} = |\vec{p}_T(j_1) - \vec{p}_T(j_2)| / (p_T(j_1) + p_T(j_2))$ , and their azimuthal separation are two largely uncorrelated discriminating variables, which are binned to form nine SRs. The main  $W/Z$ +jets and semileptonic  $t\bar{t}$  backgrounds are constrained using three muon CRs: one with two OS muons, and two with one muon and no or one  $b$ -tagged jet. The small multijet background is normalized in a CR at lower  $E_T^{\text{miss}}$  and high azimuthal separation. The event yield in the SRs agrees well with the background expectations, so limits are drawn in the  $(m_\Phi, R_{\text{inv}})$  plane, as shown in Figure 46(a), excluding the region up to  $m_\Phi = 2.7$  TeV. At large values of  $R_{\text{inv}}$ , for which a jet could simply disappear, the jet+ $E_T^{\text{miss}}$  analysis introduced in Section 10.3.1 complements this analysis, excluding higher  $m_\Phi$  values.

In the  $s$ -channel production search [294], the dark mesons are assumed to decay promptly into SM particles and the fraction of invisible components is assumed to be negligible, following the benchmark models from Ref. [297] (for which the lightest dark baryons could still be DM candidates). Due to the double hadronization process (first in the dark sector and then in the SM), the dark jets considered are typically wider than the SM QCD jets and, for the dark-sector models considered, have a higher associated charged-particle multiplicity due to the multiplicity of dark mesons produced in the dark shower and their decays. The analysis thus selects events containing two high- $p_T$  large- $R$  jets with high track multiplicity, and looks for a resonant excess in  $m_{JJ}$ . The smooth  $m_{JJ}$  shape of the dominant SM QCD multijet background is determined in a data-driven way. Since no significant excess is seen, limits are placed on the cross section times branching ratio for the production of dark quarks through a  $Z'$  mediator as a function of the  $Z'$  mass, as shown for one benchmark in Figure 46(b). In this figure, the limits are compared with theory predictions for given values of  $g_q$  and  $g_{q_d}$ , the couplings of the  $Z'$  to SM quarks and to dark quarks, respectively. For the values chosen,  $g_q = 0.05$  and  $g_{q_d} = 0.2$ , this analysis is able to exclude  $Z'$  masses up to 3.0 TeV for this model, while the  $Z' \rightarrow qq$  dijet resonance search constraints [64] are evaded due to the small  $g_q$  value.

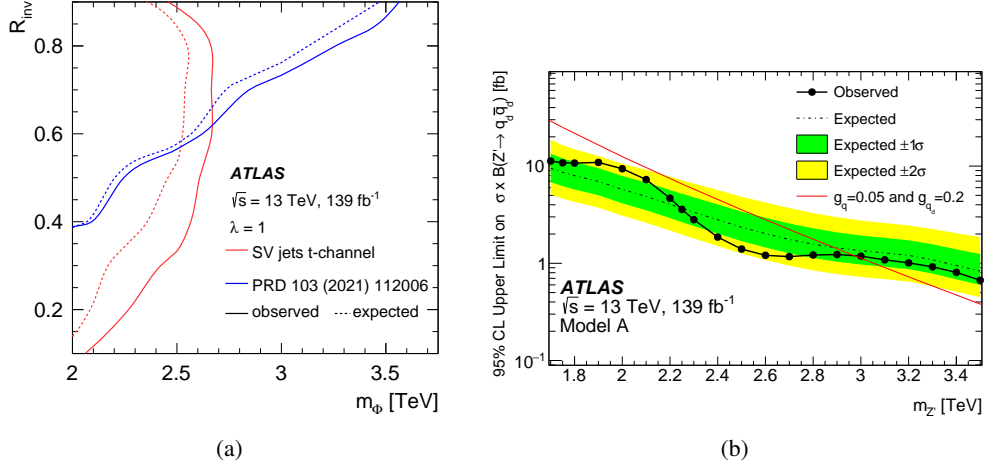


Figure 46: (a) Limits in the  $(m_\phi, R_{\text{inv}})$  plane obtained in the  $t$ -channel search for semi-visible (SV) jets [293] and in the  $\text{jet}+E_{\text{T}}^{\text{miss}}$  search. (b) Limits set on the cross section times branching ratio for the production of dark quarks through a  $Z'$  mediator as a function of the  $Z'$  mass for one of the benchmark considered in the  $s$ -channel search [294], compared to a theory prediction.

## 11 Long-lived multi-charged or highly ionizing particles

Long-lived particles need not be neutral like the ones discussed in the last two sections. Indeed, various BSM theories predict the existence of particles with more than one unit of electric charge.

They can have relatively low charge multiplicity  $|z|$ , being known as multi-charged particles (MCPs), such as the two doubly charged fermions predicted by the almost-commutative model [298], the stable multi-charged technibaryons predicted in the walking technicolour model [299], or the long-lived doubly charged Higgs bosons predicted in the left–right symmetric model [300]. In this case, they would behave like higher-mass, more ionizing muons in the detector.

They can also have very high charge multiplicity, being known as highly ionizing particles (HIPs), such as strange matter [301] and Q-balls [302]. Dirac magnetic monopoles [303] are also classified as HIPs; they have a magnetic charge  $Ne/2\alpha \approx 68.5Ne$  (where  $N$  is an integer,  $e$  is the electron charge and  $\alpha \approx 1/137$  is the fine-structure constant), and an  $N = 1$  Dirac monopole would have an energy loss in the detectors comparable to that of an ion of electric charge  $|z| = 68.5$ .

Searches for these two signatures were conducted as described below, with the MCP search targeting the range  $2 < |z| < 7$  [304] and the HIP search covering  $20 < |z| < 100$  [305]. In both cases, Drell–Yan (DY) and photon-fusion (PF) pair-production processes are considered, following the model described in Ref. [306].

As mentioned above, the MCPs would look like heavy muons with a higher specific energy loss  $dE/dx$  in the pixel, TRT and MDT subdetectors. Since the muon trigger is only sensitive to particles with  $\beta = v/c > 0.65$ , due to built-in timing restrictions, two other triggers are also used: the calorimeter-based  $E_{\text{T}}^{\text{miss}}$  trigger, which relies on the presence of ISR in the signal events, and a late-muon trigger which fires in events which have a jet in the current bunch-crossing and a muon in the next one. The events are then selected by requiring the presence of a central ID–MS combined muon, which must be well isolated

from other tracks found in the silicon detectors. This isolation criterion is useful for removing events in which the large ionization loss would be due to multiple particle crossings instead of a unique MCP. Four variables are then used to build the signal regions: the  $dE/dx$  significance,  $S(dE/dx)$ , in each of the three subdetectors, and  $f^{\text{HT}}$ , the number of high-threshold (HT) hits<sup>7</sup> divided by the number of low-threshold hits on the track as measured in the TRT. The  $S(dE/dx)$  variables are defined as the difference between the observed signal and the average value expected for a relativistic muon, divided by its root-mean-square width, where the expected values are measured in a  $Z \rightarrow \mu\mu$  control region. A SR is defined for  $z = 2$ , requiring  $S(\text{pixel } dE/dx) > 13$ ,  $S(\text{TRT } dE/dx) > 2$  and  $S(\text{MDT } dE/dx) > 4$ . Since the pixel  $dE/dx$  measurement saturates for higher  $z$  values, and the corresponding hits are not recorded, this variable is not used in the SR defined to target  $z > 2$ , which instead requires  $f^{\text{HT}} > 0.7$  and  $S(\text{MDT } dE/dx) > 7$ . In both regions, the background is estimated in a data-driven way using an ABCD method. In the  $z = 2$  SR, the ABCD regions are defined in the TRT versus MDT  $dE/dx$  plane, while in the  $z > 2$  SR,  $f^{\text{HT}}$  and  $S(\text{MDT } dE/dx)$  are used instead. This results in an expected background of  $1.6 \pm 0.4$  (stat.)  $\pm 0.5$  (syst.) events in the  $z = 2$  SR, where 4 events are observed, and of  $0.034 \pm 0.002$  (stat.)  $\pm 0.004$  (syst.) events in the  $z > 2$  SR, where no events are observed.

At higher electric charge multiplicity, a HIP passing through the TRT would not only produce a HT hit in a given straw but also produce other HT hits in neighbouring straws via the many  $\delta$ -rays it generates. Furthermore, because a HIP is too heavy to produce a shower in the EM calorimeter, its energy deposit in this detector would remain narrow even though it is likely to be stopped there. The event selection for such events starts with a custom HIP trigger based on these properties. The usual tracking algorithms are not used in this search since they can be confused by the multiple  $\delta$ -rays, and because magnetic monopoles, which are one of the signals targeted in this search, would bend in the  $r$ - $z$  (and not the usual  $r$ - $\phi$ ) plane. Instead, HIP reconstruction proceeds in three steps: it starts with an EM cluster which defines a  $\phi$  direction near which TRT hits are counted; this direction is refined to align with the richest HT-hits region; and then this new  $\phi$  direction is used as the centre of an 8-mm-wide rectangular road in the barrel (or a 12 mrad  $r$ - $\phi$  wedge in the endcap), which should capture the energy deposited while not including too many pile-up hits. As in the MCP case, the fraction of HT hits  $f^{\text{HT}}$  found in the road (or wedge) is used as a discriminating variable. Another powerful variable in this search is  $w$ , which is the average of the three fractions of EM cluster energy found in the  $N$  most energetic cells of the presampler ( $N = 2$ ) and the first ( $N = 4$ ) and second ( $N = 5$ ) layers of the EM calorimeter, where the energy in each of these layers must exceed some minimum value. The SR is defined by requiring  $f^{\text{HT}} \geq 0.77$  and  $w \geq 0.93$ . These two variables also form the ABCD plane that is used to estimate the background. After these selections,  $0.15 \pm 0.04$  (stat.)  $\pm 0.05$  (syst.) background events are expected in the SR, and no events are observed.

Both the MCP and HIP searches allow limits to be placed in the plane of the production cross section versus the electric charge, as shown for the Drell–Yan production mode in Figure 47. Similar limits are obtained for the PF production mode. The HIP search is also interpreted in terms of magnetic monopoles: for example, for an  $N = 1$  spin-0 magnetic monopole, the search excludes masses up to 2.1 TeV (3.4 TeV) in the DY (PF) production mode.

---

<sup>7</sup> The HT is designed to discriminate between energy depositions from transition-radiation photons and the energy loss by minimum-ionizing particles.

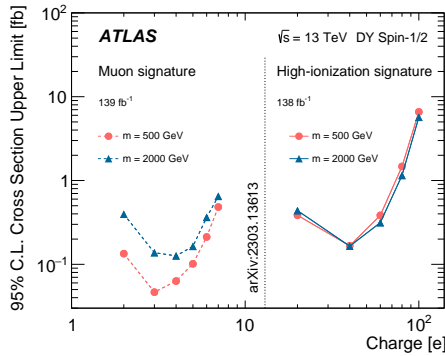


Figure 47: Observed exclusion limit on the cross section versus electric charge multiplicity as seen in the MCP (muon signature) and HIP (high-ionization signature) searches [304, 305], for DY production. The models with 500 GeV masses are strongly excluded, given that a DY production cross section ( $\sigma_{\text{DY}}$ ) of at least a few fb is expected for the lowest charge considered and grows with the charge. At 2 TeV, none of the MCP models are excluded because  $\sigma_{\text{DY}} \leq O(0.01)$  fb is expected over the charge range considered, while for HIPs, the limits obtained between  $40e$  and  $80e$  are lower than the expected  $\sigma_{\text{DY}}$ .

## 12 Extra dimensions, gravitons and quantum black holes

The ATLAS experiment is also able to explore scenarios trying to bridge the gap between particle physics and gravity. Multiple BSM theories seek to explain the weakness of gravity relative to the other known fundamental interactions, sometimes using extra dimensions (EDs) to solve this puzzle [307, 308]. If our four dimensions exist on a sheet in a higher-dimensional space, and if gravitons, the hypothetical spin-2 mediators of gravity, are able to propagate across these EDs, then gravity could appear weaker than it actually is.

### 12.1 Gravitons in the ADD and RS scenarios

The Arkani-Hamed, Dimopoulos and Dvali (ADD) model comprises  $n$  large extra dimensions of size  $R$  [307] which transforms the fundamental scale  $M_D$  of the  $4+n$ -dimensional theory into the Planck scale via  $M_{\text{Planck}}^2 \sim M_D^{2+n} R^n$ . The compactification of the EDs results in a Kaluza–Klein (KK) tower of massive graviton modes with a mass splitting that is inversely proportional to  $R$ . Since large EDs are postulated, the observable graviton states appear as a continuum. If produced in the  $pp$  collisions, the KK graviton ( $G_{\text{KK}}$ ) escapes into the EDs, and the searches must rely, as in the DM searches discussed in Section 10, on the production of a visible object, such as an ISR jet or photon. The jet+ $E_{\text{T}}^{\text{miss}}$  analysis (see Section 10.3.1) has looked for such KK gravitons, setting limits on  $M_D$  at the multi-TeV level for  $n$  values from 2 to 6,<sup>8</sup> as can be seen in Figure 48(a). The photon+ $E_{\text{T}}^{\text{miss}}$  search for this signal was also pursued, with early Run 2 data, but proved less sensitive [309].

KK gravitons can also be obtained in a Randall–Sundrum (RS) model of EDs [308]. In the original version of the RS model, here called RS1, a five-dimensional anti-de Sitter spacetime is postulated, in which SM particles and gravity are localized on two different branes. Since the fifth (extra) dimension is warped,

<sup>8</sup> The  $n = 1$  case is already largely ruled out by gravitational measurements, as the corresponding  $R$  to have  $M_D$  at the TeV scale would be larger than the Earth–Sun distance, while for  $n = 2$ , it is already at the mm scale.

the strength of gravity appears exponentially suppressed by the warp factor on the SM brane. In the bulk version of the RS model, only the Higgs boson is fixed on the TeV brane, while the other SM fields are allowed to propagate in the bulk of the ED. The SM particles are the zero-modes of these five-dimensional fields, and their mass hierarchies can be explained by localizing the heavy-fermion fields nearer the TeV brane, and the lighter ones, nearer the Planck brane. Since the  $G_{\text{KK}}$  are localized near the TeV brane, their couplings to light fermions are suppressed, contrary to the RS1 scenario. The signal samples in the search for RS KK gravitons, which can be seen as well-separated narrow resonances, are produced for given choices of  $k/M_{\text{Planck}}$ , where  $k$  is the curvature parameter.

The RS KK graviton can decay into gluons or quarks [310] and the dijet resonance analysis (see Section 3.1) is therefore sensitive to part of the parameter space. The model considered is one of a RS1 KK graviton decaying into  $b$ -quarks with  $k/M_{\text{Planck}} = 0.2$ . The limit set on the lightest graviton’s mass ( $m_{G_{\text{KK}}}$ ) in this model, obtained by using the  $b$ -tagged SR of the dijet analysis, is given in Table 4. A search was also performed in the semileptonic  $t\bar{t}$  final state with a partial Run 2 dataset [311]: its interpretation in terms of bulk RS gravitons gives weaker limits than those reported below, as shown in Table 4. It was also interpreted in terms of a search for the first mode of the bulk RS KK gluon, excluding masses below 3.8 TeV for a 15% resonance width. The dilepton resonance search introduced in Section 4.1.1, although not giving a mass limit for these specific models, provides auxiliary material for reinterpreting the obtained generic limits in terms of spin-2 resonances.

RS1 KK gravitons can also decay into photons, and a search for a high-mass  $\gamma\gamma$  resonance [312] was performed for signals with  $k/M_{\text{Planck}} \leq 0.1$ . In this analysis, two tight and isolated photons are required, with  $m_{\gamma\gamma} > 150$  GeV, and with the leading (subleading) photon having  $p_{\text{T}} > 0.3$  (0.25)  $m_{\gamma\gamma}$ . Templates of the  $m_{\gamma\gamma}$  distributions are obtained by fitting a functional form to the distributions obtained either from MC simulation (for the non-resonant  $\gamma\gamma$  background) or from a CR reversing some of the photon identification selection (for the  $\gamma$ +jet background). The relative amount of each background is determined using two-dimensional sidebands around the signal region for each photon. These sidebands are built by relaxing the photon isolation and identification criteria, and the  $\gamma\gamma$  purity in the SR is found to be around 97% above 400 GeV. Since no resonant excess is seen above this background in data, a limit is set on  $m_{G_{\text{KK}}}$ , as shown in Table 4.

A pair of Higgs bosons can also result from the bulk RS  $G_{\text{KK}}$  decay; such an interpretation was given in the resonant  $HH \rightarrow bbbb$  search [313], which uses a resolved SR and a boosted SR to probe lower or higher  $m_{G_{\text{KK}}}$ . In the resolved channel, four  $b$ -tagged jets are required and their pairing into two Higgs boson candidates  $H_1$  and  $H_2$  is decided by using a BDT. In the boosted SR, two high- $p_{\text{T}}$  large- $R$  jets form the candidates, with two to four associated  $b$ -tagged track-jets. To reject the multijet background,  $H_1$  and  $H_2$  must not be too far apart in  $\eta$ , and in the resolved SR the  $t\bar{t}$  background is suppressed with a top-quark veto, which is based on attempts to reconstruct top quarks from the jets at hand. The SR in both regimes is then defined as an enclosed space in the  $(m_{H_1}, m_{H_2})$  plane around the expected reconstructed Higgs boson masses, with an annulus around it defining a CR which is used in the dominant multijet background’s estimation. In the resolved SR, the background is estimated from data in a 2- $b$ -tagged region, whose shape is corrected using event kinematic knowledge obtained from the annular CR with a neural network. In the boosted regime, events in regions with a lower number of  $b$ -tagged track-jets are used in conjunction with the annular CR in a simultaneous fit. The di-Higgs mass is the final discriminant and, in the resolved SR, it is corrected for better accuracy by rescaling the reconstructed  $H_1$  and  $H_2$  masses to 125 GeV. Since no significant excess is seen, the two channels are combined to provide a limit on  $m_{G_{\text{KK}}}$ , listed in Table 4.

Finally, diboson resonance searches, which are discussed as  $W'$  and  $Z'$  searches in Section 4, are also sensitive to scenarios with bulk RS KK gravitons, as summarized in Ref. [314]. A comparison of the



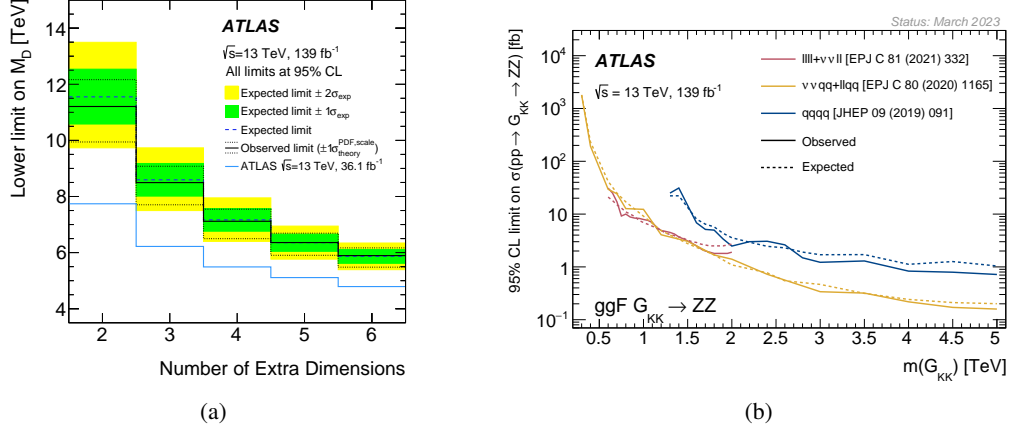


Figure 48: Observed exclusion limit on (a) the fundamental scale  $M_D$  versus the number of extra dimensions in the ADD model, obtained by the  $jet+E_T^{miss}$  analysis [228], and on (b) the cross section times branching ratio versus the mass of the graviton in a bulk RS model, obtained in the  $ZZ$  resonance searches [314].

Table 4: 95% CL lower limits on the lightest KK graviton mass obtained in various analyses for various RS scenarios.

Analysis final state	Model	$k/M_{\text{Planck}}$	Excluded mass range for $m_{G_{KK}}$ [TeV]
$bb$	RS1	0.2	$< 2.8$
$\gamma\gamma$	RS1	0.1	$< 4.5$
Semileptonic $t\bar{t}$ (36.1 fb $^{-1}$ )	bulk RS	1.0	0.45–0.65
$HH \rightarrow bbbb$	bulk RS	1.0	0.298–1.46
$WW/ZZ \rightarrow qqqq$	bulk RS	1.0	1.3–1.8
$WW \rightarrow \ell\nu qq + ZZ \rightarrow \ell\ell qq$			
ggF production	bulk RS	1.0	$< 2.0$
VBF production	bulk RS	1.0	$< 0.76$
$ZZ \rightarrow \ell\ell\ell\ell + ZZ \rightarrow \ell\ell\nu\nu$	bulk RS	1.0	$< 1.83$

limits on the production cross section in the three  $ZZ$  channels (fully hadronic, semileptonic and fully leptonic) is shown in Figure 48(b), while the limits on  $m_{G_{KK}}$  obtained by the various analyses for a value of  $k/M_{\text{Planck}} = 1.0$  are summarized in Table 4. While most of the analyses focus on ggF production, the semileptonic  $WW/ZZ$  search also probes VBF production of the graviton, which is also interesting given the light-fermion suppression of the bulk RS  $G_{KK}$  couplings.

## 12.2 Gravitons in the clockwork gravity model

The continuum clockwork gravity model [315, 316], which has a five-dimensional spacetime metric, is also related to the gravity/weak-scale hierarchy problem. It predicts a narrowly-spaced spectrum of KK gravitons which can appear as a long-range semi-periodic structure in the invariant mass distribution: near the onset of the graviton spectrum, which is governed by a mass parameter  $k_{CW}$ , the mass splittings are generally of the order of a few percent and can be resolved in a  $\gamma\gamma$  or  $ee$  search, while the splitting decreases and becomes unresolvable for higher graviton modes. The cross section is determined by  $M_5$ , the

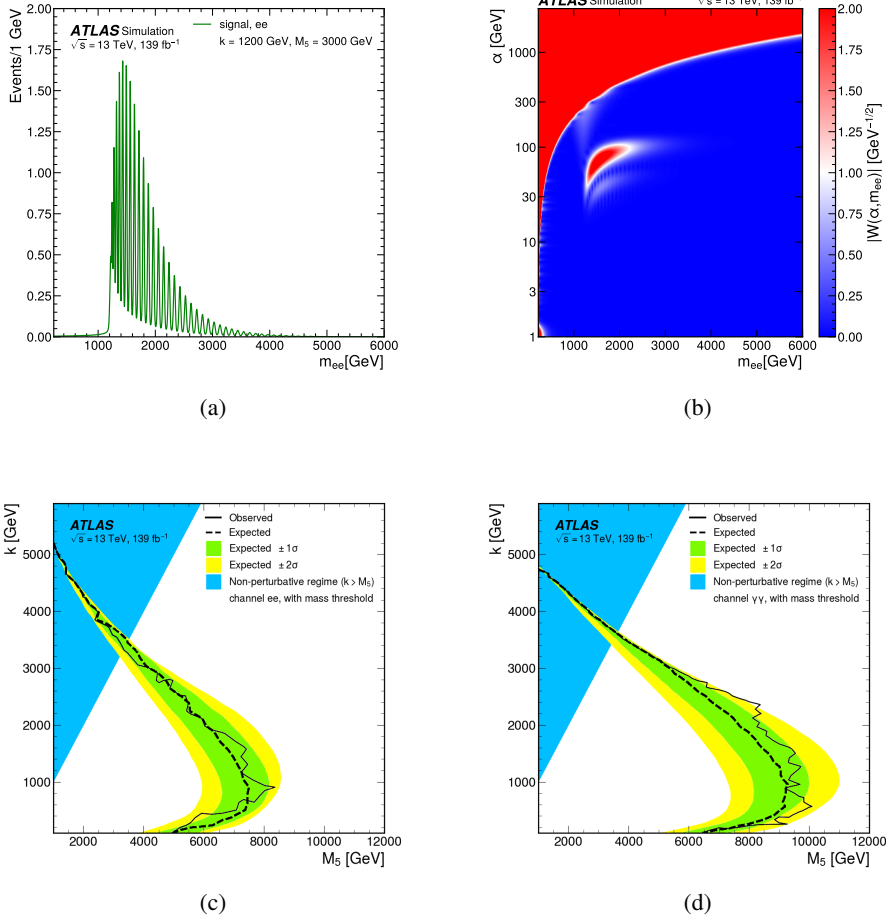


Figure 49: Example, in the  $ee$  channel of the clockwork analysis [317] and for  $k_{CW} = 1200$  GeV (here called  $k$ ) and  $M_5 = 3000$  TeV, of (a) a signal invariant mass distribution and (b) a simulated signal-plus-background scalogram in which  $\alpha$  is inversely proportional to the frequency and  $W$  is the amplitude coefficient. The limits in the  $k_{CW}$  versus  $M_5$  plane is shown for (c) the  $ee$  channel and (d) the  $\gamma\gamma$  channel.

five-dimensional reduced Planck mass. A search for this periodic spectrum of resonances was performed in the  $ee$  channel [317], using the invariant mass spectrum from the  $Z' \rightarrow \ell\ell$  search discussed in Section 4.1, and in the diphoton channel, using the spectrum from the search described in the previous section. In both cases, a functional form is fitted to the data to estimate the background. The signals are modelled using analytic invariant-mass templates including detector resolution effects, an example of which can be seen in Figure 49(a). Continuous wavelet transforms (using a Morlet wavelet definition [318]) are used to analyse the mass spectra in the frequency domain, transforming these spectra into images (called scalograms) displaying the wavelet amplitude in the frequency versus invariant mass plane. In these scalograms, a signal would appear as a region of high amplitude localized in frequency and mass above a more continuous background, as shown in Figure 49(b). In order to analyse these images in terms of the clockwork model, a NN classifier is used. No significant excess is seen and limits are set, as shown in Figures 49(c) and 49(d).

### 12.3 Quantum black holes

In the ADD and the RS models, quantum black holes (QBH) could potentially be produced at the LHC [319, 320] when the energy is above the fundamental Planck scale  $M_D$ . Unlike semi-classical black holes, which decay due to Hawking radiation into multiparticle final states, QBHs with masses near  $M_D$  decay into two-particle final states [321]. The dijet search can therefore also be used in this case. Signal events were generated for the ADD case with BLACKMAX [322] for  $n = 6$  and various  $M_D$  values, and the results of the dijet search in its inclusive signal region were reinterpreted to obtain limits on the cross section as a function of the QBH mass,  $m_{\text{QBH}}$ .

The search for QBHs can also be performed in final states that violate SM global symmetries: this is done by looking for a resonance in the  $eq$  and  $\mu q$  final states [323]. In this search, QBH 3.0 [324] is used in conjunction with PYTHIA 8 to generate events in the ADD (with  $n = 6$ ) and RS1 scenarios. The events are selected by requiring the presence of exactly one high- $p_T$  jet and one high- $p_T$  lepton with  $m_{\ell j} > 2$  TeV.<sup>9</sup> The main background comes from  $W$ +jets events, with some smaller contributions from  $t\bar{t}$  and  $Z$ +jets events. These are estimated using CRs at lower  $m_{\ell j}$ , requiring or not requiring the presence of  $b$ -tagged jets,  $E_T^{\text{miss}}$ , or an extra lepton. In the electron channel, the fake-lepton background contribution is estimated via a matrix method. The main uncertainties in the background estimation come from uncertainties in the jet energy resolution and lepton modelling. The data agree with background-only expectations, and the limits from the electron and muon channels, yielding very similar sensitivities, are combined.

For the ADD model, the dijet search places a lower limit on  $m_{\text{QBH}}$  at 9.4 TeV, while the limit set by the  $e/\mu$ +jet search is 9.2 TeV. The  $e/\mu$ +jet analysis is also interpreted in terms of an RS1 model, resulting in a limit of  $m_{\text{QBH}} > 6.8$  TeV.

## 13 Summary and conclusions

The Run 2 data have offered an unprecedented opportunity to search for answers to many of the fundamental questions still open today in high-energy physics. While no significant excess of events in data has been seen, the rich harvest of results has redefined the possible paths for physics beyond the Standard Model, putting more stringent constraints on the scales and couplings of new states as shown in this report and also summarized in Ref. [325]. A comparison of limits obtained by analyses presented in this report with those obtained in similar analyses performed with the Run 1 dataset is presented in Table 5, showing the evolution of the constraints.

While the increases in integrated luminosity and centre-of-mass energy have both greatly contributed to the improvement in the limits, new or improved techniques for object identification, such as the large-radius tracking used in some long-lived-particle searches, new theoretical computations, such as the NLO  $Z/W$ +jets dedicated computations used in the jet+ $E_T^{\text{miss}}$  and vector-boson-fusion jets+ $E_T^{\text{miss}}$  analyses, and better analysis techniques, relying for example on machine learning, have all played their part in beating the simple scaling of the Run 1 results in many cases. But the improvements have not stopped there either – the Run 2 analyses have also pushed back the frontiers by looking for new final states, such as semi-visible jets or clockwork gravitons, which could have passed through the net cast by the Collaboration in Run 1.

---

<sup>9</sup> Given that the signal is generated at LO, vetoing additional jet activity affects the signal acceptance in a way that can be corrected for by studying the veto effect in NLO  $V$ +jets events.

Table 5: Comparison between some 95% CL lower limits obtained by Run 2 analyses presented in the indicated sections of this report and the limits obtained in similar analyses with the Run 1 dataset.

Model and final state	Section	Excluded Range	
		Run 1	Run 2
$q^*$ in a dijet resonance	3.1	$m < 4.06$ TeV [326]	$m < 6.7$ TeV
$Z'_{\text{SSM}}$ in a dilepton resonance	4.1.1	$m < 2.90$ TeV [327]	$m < 5.1$ TeV
Type-III seesaw heavy leptons in $\ell\ell\nu\nu qq$	5.3	$m < 335$ GeV [328]	$m < 790$ GeV
VLQ $T$ (Singlet, $2\ell + 3\ell$ )	6.2	$m < 0.66$ TeV [329]	$m < 1.27$ TeV
Scalar $LQ_3^u$ ( $LQLQ \rightarrow tvtv$ )	7	$m < 640$ GeV [330]	$m < 1240$ GeV
LFV $Z \rightarrow e\mu$	8.1	$\mathcal{B} < 7.5 \times 10^{-7}$ [331]	$\mathcal{B} < 2.62 \times 10^{-7}$
FRVZ $\gamma_d$ in $H \rightarrow 2\gamma_d + X$ with $\mathcal{B}(H \rightarrow 2\gamma_d) = 10\%$ and $m_{\gamma_d} = 0.4$ GeV	9.1	$15 < c\tau < 260$ mm [332]	$0.42 < c\tau < 1001$ mm
$H \rightarrow$ invisible combination	10.3	$\mathcal{B} < 0.252$ [333]	$\mathcal{B} < 0.113$
Multi-charged particle with $ z  = 2$	11	$m < 660$ GeV [334]	$m < 1060$ GeV
ADD with $n = 6$ in jet+ $E_T^{\text{miss}}$	12.1	$M_D < 3.06$ TeV [335]	$M_D < 5.9$ TeV

With Run 3 now well underway, this strategy will be pursued further. While the increase in centre-of-mass energy from 13 to 13.6 TeV might seem modest compared to the 8 to 13 TeV jump from Run 1 to Run 2, it translates to a production cross-section increase which is not negligible for high-mass states. This, coupled with the increased global data sample, upgrades to the detector (notably trigger-related ones) and the relentless performance and analysis improvement efforts, will further boost the sensitivity of the searches. Run 3 will be followed by the HL-LHC phase, which will increase the data sample tenfold with a further upgraded detector, allowing even more uncharted parameter space to be probed. The voyage of exploration is far from over!

## Acknowledgements

We thank CERN for the very successful operation of the LHC and its injectors, as well as the support staff at CERN and at our institutions worldwide without whom ATLAS could not be operated efficiently.

The crucial computing support from all WLCG partners is acknowledged gratefully, in particular from CERN, the ATLAS Tier-1 facilities at TRIUMF/SFU (Canada), NDGF (Denmark, Norway, Sweden), CC-IN2P3 (France), KIT/GridKA (Germany), INFN-CNAF (Italy), NL-T1 (Netherlands), PIC (Spain), RAL (UK) and BNL (USA), the Tier-2 facilities worldwide and large non-WLCG resource providers. Major contributors of computing resources are listed in Ref. [336].

We gratefully acknowledge the support of ANPCyT, Argentina; YerPhI, Armenia; ARC, Australia; BMWFW and FWF, Austria; ANAS, Azerbaijan; CNPq and FAPESP, Brazil; NSERC, NRC and CFI, Canada; CERN; ANID, Chile; CAS, MOST and NSFC, China; Minciencias, Colombia; MEYS CR, Czech Republic; DNRF and DNSRC, Denmark; IN2P3-CNRS and CEA-DRF/IRFU, France; SRNSFG, Georgia; BMBF, HGF and

MPG, Germany; GSRI, Greece; RGC and Hong Kong SAR, China; ISF and Benoziyo Center, Israel; INFN, Italy; MEXT and JSPS, Japan; CNRST, Morocco; NWO, Netherlands; RCN, Norway; MEiN, Poland; FCT, Portugal; MNE/IFA, Romania; MESTD, Serbia; MSSR, Slovakia; ARRS and MIZŠ, Slovenia; DSI/NRF, South Africa; MICINN, Spain; SRC and Wallenberg Foundation, Sweden; SERI, SNSF and Cantons of Bern and Geneva, Switzerland; MOST, Taipei; TENMAK, Türkiye; STFC, United Kingdom; DOE and NSF, United States of America.

Individual groups and members have received support from BCKDF, CANARIE, CRC and DRAC, Canada; PRIMUS 21/SCI/017 and UNCE SCI/013, Czech Republic; COST, ERC, ERDF, Horizon 2020, ICSC-NextGenerationEU and Marie Skłodowska-Curie Actions, European Union; Investissements d’Avenir Labex, Investissements d’Avenir Idex and ANR, France; DFG and AvH Foundation, Germany; Herakleitos, Thales and Aristeia programmes co-financed by EU-ESF and the Greek NSRF, Greece; BSF-NSF and MINERVA, Israel; Norwegian Financial Mechanism 2014-2021, Norway; NCN and NAWA, Poland; La Caixa Banking Foundation, CERCA Programme Generalitat de Catalunya and PROMETEO and GenT Programmes Generalitat Valenciana, Spain; Göran Gustafssons Stiftelse, Sweden; The Royal Society and Leverhulme Trust, United Kingdom.

In addition, individual members wish to acknowledge support from CERN: European Organization for Nuclear Research (CERN PJAS); Chile: Agencia Nacional de Investigación y Desarrollo (FONDECYT 1190886, FONDECYT 1210400, FONDECYT 1230987); China: National Natural Science Foundation of China (NSFC - 12175119, NSFC 12275265); European Union: European Research Council (ERC - 948254, ERC 101089007), Horizon 2020 Framework Programme (MUCCA - CHIST-ERA-19-XAI-00), Italian Center for High Performance Computing, Big Data and Quantum Computing (ICSC, NextGenerationEU); France: Agence Nationale de la Recherche (ANR-20-CE31-0013, ANR-21-CE31-0022), Investissements d’Avenir Labex (ANR-11-LABX-0012); Germany: Baden-Württemberg Stiftung (BW Stiftung-Postdoc Eliteprogramme), Deutsche Forschungsgemeinschaft (DFG - 469666862, DFG - CR 312/5-2); Italy: Istituto Nazionale di Fisica Nucleare (ICSC, NextGenerationEU); Japan: Japan Society for the Promotion of Science (JSPS KAKENHI 22H01227, JSPS KAKENHI 22KK0227, JSPS KAKENHI JP21H05085, JSPS KAKENHI JP22H04944); Netherlands: Netherlands Organisation for Scientific Research (NWO Veni 2020 - VI.Veni.202.179); Norway: Research Council of Norway (RCN-314472); Poland: Polish National Agency for Academic Exchange (PPN/PPO/2020/1/00002/U/00001), Polish National Science Centre (NCN 2021/42/E/ST2/00350, NCN OPUS nr 2022/47/B/ST2/03059, NCN UMO-2019/34/E/ST2/00393, UMO-2020/37/B/ST2/01043, UMO-2022/47/O/ST2/00148); Slovenia: Slovenian Research Agency (ARIS grant J1-3010); Spain: BBVA Foundation (LEO22-1-603), Generalitat Valenciana (Artemisa, FEDER, IDIFEDER/2018/048), Ministry of Science and Innovation (RYC2019-028510-I, RYC2020-030254-I), PROMETEO and GenT Programmes Generalitat Valenciana (CIDEAGENT/2019/023, CIDEAGENT/2019/027); Sweden: Swedish Research Council (VR 2022-03845), Knut and Alice Wallenberg Foundation (KAW 2022.0358); Switzerland: Swiss National Science Foundation (SNSF - PCEFP2\_194658); United Kingdom: Leverhulme Trust (Leverhulme Trust RPG-2020-004); United States of America: Neubauer Family Foundation.

## References

- [1] L. Evans and P. Bryant, *LHC Machine*, [JINST 3 \(2008\) S08001](#).
- [2] ATLAS Collaboration, *The ATLAS Experiment at the CERN Large Hadron Collider*, [JINST 3 \(2008\) S08003](#).

- [3] ATLAS Collaboration, *ATLAS Insertable B-Layer: Technical Design Report*, ATLAS-TDR-19; CERN-LHCC-2010-013, 2010, URL: <https://cds.cern.ch/record/1291633>, Addendum: ATLAS-TDR-19-ADD-1; CERN-LHCC-2012-009, 2012, URL: <https://cds.cern.ch/record/1451888>.
- [4] B. Abbott et al., *Production and integration of the ATLAS Insertable B-Layer*, *JINST* **13** (2018) T05008, arXiv: [1803.00844](https://arxiv.org/abs/1803.00844) [[physics.ins-det](#)].
- [5] ATLAS Collaboration, *Performance of the ATLAS trigger system in 2015*, *Eur. Phys. J. C* **77** (2017) 317, arXiv: [1611.09661](https://arxiv.org/abs/1611.09661) [[hep-ex](#)].
- [6] ATLAS Collaboration, *The ATLAS Collaboration Software and Firmware*, ATL-SOFT-PUB-2021-001, 2021, URL: <https://cds.cern.ch/record/2767187>.
- [7] ATLAS Collaboration, *Luminosity determination in pp collisions at  $\sqrt{s} = 13$  TeV using the ATLAS detector at the LHC*, *Eur. Phys. J. C* **83** (2023) 982, arXiv: [2212.09379](https://arxiv.org/abs/2212.09379) [[hep-ex](#)].
- [8] ATLAS Collaboration, *Luminosity determination in pp collisions at  $\sqrt{s} = 13$  TeV using the ATLAS detector at the LHC*, ATLAS-CONF-2019-021, 2019, URL: <https://cds.cern.ch/record/2677054>.
- [9] ATLAS Collaboration, *The performance of the jet trigger for the ATLAS detector during 2011 data taking*, *Eur. Phys. J. C* **76** (2016) 526, arXiv: [1606.07759](https://arxiv.org/abs/1606.07759) [[hep-ex](#)].
- [10] ATLAS Collaboration, *Performance of electron and photon triggers in ATLAS during LHC Run 2*, *Eur. Phys. J. C* **80** (2020) 47, arXiv: [1909.00761](https://arxiv.org/abs/1909.00761) [[hep-ex](#)].
- [11] ATLAS Collaboration, *Performance of the ATLAS muon triggers in Run 2*, *JINST* **15** (2020) P09015, arXiv: [2004.13447](https://arxiv.org/abs/2004.13447) [[physics.ins-det](#)].
- [12] ATLAS Collaboration, *Performance of the missing transverse momentum triggers for the ATLAS detector during Run-2 data taking*, *JHEP* **08** (2020) 080, arXiv: [2005.09554](https://arxiv.org/abs/2005.09554) [[hep-ex](#)].
- [13] T. Sjöstrand, S. Mrenna and P. Skands, *A brief introduction to PYTHIA 8.1*, *Comput. Phys. Commun.* **178** (2008) 852, arXiv: [0710.3820](https://arxiv.org/abs/0710.3820) [[hep-ph](#)].
- [14] T. Sjöstrand et al., *An introduction to PYTHIA 8.2*, *Comput. Phys. Commun.* **191** (2015) 159, arXiv: [1410.3012](https://arxiv.org/abs/1410.3012) [[hep-ph](#)].
- [15] J. Alwall et al., *The automated computation of tree-level and next-to-leading order differential cross sections, and their matching to parton shower simulations*, *JHEP* **07** (2014) 079, arXiv: [1405.0301](https://arxiv.org/abs/1405.0301) [[hep-ph](#)].
- [16] P. Nason, *A new method for combining NLO QCD with shower Monte Carlo algorithms*, *JHEP* **11** (2004) 040, arXiv: [hep-ph/0409146](https://arxiv.org/abs/hep-ph/0409146).
- [17] S. Frixione, P. Nason and C. Oleari, *Matching NLO QCD computations with parton shower simulations: the POWHEG method*, *JHEP* **11** (2007) 070, arXiv: [0709.2092](https://arxiv.org/abs/0709.2092) [[hep-ph](#)].
- [18] S. Alioli, P. Nason, C. Oleari and E. Re, *A general framework for implementing NLO calculations in shower Monte Carlo programs: the POWHEG BOX*, *JHEP* **06** (2010) 043, arXiv: [1002.2581](https://arxiv.org/abs/1002.2581) [[hep-ph](#)].
- [19] D. J. Lange, *The EvtGen particle decay simulation package*, *Nucl. Instrum. Meth. A* **462** (2001) 152.



- [20] E. Bothmann et al., *Event generation with Sherpa 2.2*, *SciPost Phys.* **7** (2019) 034, arXiv: [1905.09127 \[hep-ph\]](#).
- [21] A. D. Martin, W. J. Stirling, R. S. Thorne and G. Watt, *Parton distributions for the LHC*, *Eur. Phys. J. C* **63** (2009) 189, arXiv: [0901.0002 \[hep-ph\]](#).
- [22] ATLAS Collaboration, *The Pythia 8 A3 tune description of ATLAS minimum bias and inelastic measurements incorporating the Donnachie–Landshoff diffractive model*, ATL-PHYS-PUB-2016-017, 2016, URL: <https://cds.cern.ch/record/2206965>.
- [23] ATLAS Collaboration, *The ATLAS Simulation Infrastructure*, *Eur. Phys. J. C* **70** (2010) 823, arXiv: [1005.4568 \[physics.ins-det\]](#).
- [24] S. Agostinelli et al., *GEANT4 – a simulation toolkit*, *Nucl. Instrum. Meth. A* **506** (2003) 250.
- [25] ATLAS Collaboration, *The simulation principle and performance of the ATLAS fast calorimeter simulation FastCaloSim*, ATL-PHYS-PUB-2010-013, 2010, URL: <https://cds.cern.ch/record/1300517>.
- [26] ATLAS Collaboration, *Early Inner Detector Tracking Performance in the 2015 Data at  $\sqrt{s} = 13$  TeV*, ATL-PHYS-PUB-2015-051, 2015, URL: <https://cds.cern.ch/record/2110140>.
- [27] ATLAS Collaboration, *Performance of the ATLAS track reconstruction algorithms in dense environments in LHC Run 2*, *Eur. Phys. J. C* **77** (2017) 673, arXiv: [1704.07983 \[hep-ex\]](#).
- [28] ATLAS Collaboration, *Performance of the reconstruction of large impact parameter tracks in the inner detector of ATLAS*, ATL-PHYS-PUB-2017-014, 2017, URL: <https://cds.cern.ch/record/2275635>.
- [29] ATLAS Collaboration, *Vertex Reconstruction Performance of the ATLAS Detector at  $\sqrt{s} = 13$  TeV*, ATL-PHYS-PUB-2015-026, 2015, URL: <https://cds.cern.ch/record/2037717>.
- [30] ATLAS Collaboration, *Topological cell clustering in the ATLAS calorimeters and its performance in LHC Run 1*, *Eur. Phys. J. C* **77** (2017) 490, arXiv: [1603.02934 \[hep-ex\]](#).
- [31] ATLAS Collaboration, *Jet reconstruction and performance using particle flow with the ATLAS Detector*, *Eur. Phys. J. C* **77** (2017) 466, arXiv: [1703.10485 \[hep-ex\]](#).
- [32] M. Cacciari, G. P. Salam and G. Soyez, *The anti- $k_t$  jet clustering algorithm*, *JHEP* **04** (2008) 063, arXiv: [0802.1189 \[hep-ph\]](#).
- [33] M. Cacciari, G. P. Salam and G. Soyez, *FastJet user manual*, *Eur. Phys. J. C* **72** (2012) 1896, arXiv: [1111.6097 \[hep-ph\]](#).
- [34] ATLAS Collaboration, *Jet energy scale measurements and their systematic uncertainties in proton–proton collisions at  $\sqrt{s} = 13$  TeV with the ATLAS detector*, *Phys. Rev. D* **96** (2017) 072002, arXiv: [1703.09665 \[hep-ex\]](#).
- [35] D. Krohn, J. Thaler and L.-T. Wang, *Jets with Variable R*, *JHEP* **06** (2009) 059, arXiv: [0903.0392 \[hep-ph\]](#).
- [36] ATLAS Collaboration, *Selection of jets produced in 13 TeV proton–proton collisions with the ATLAS detector*, ATL-CONF-2015-029, 2015, URL: <https://cds.cern.ch/record/2037702>.



- [37] ATLAS Collaboration, *Performance of pile-up mitigation techniques for jets in pp collisions at  $\sqrt{s} = 8$  TeV using the ATLAS detector*, *Eur. Phys. J. C* **76** (2016) 581, arXiv: [1510.03823](https://arxiv.org/abs/1510.03823) [hep-ex].
- [38] ATLAS Collaboration, *ATLAS flavour-tagging algorithms for the LHC Run 2 pp collision dataset*, *Eur. Phys. J. C* **83** (2023) 681, arXiv: [2211.16345](https://arxiv.org/abs/2211.16345) [physics.data-an].
- [39] ATLAS Collaboration, *ATLAS b-jet identification performance and efficiency measurement with  $t\bar{t}$  events in pp collisions at  $\sqrt{s} = 13$  TeV*, *Eur. Phys. J. C* **79** (2019) 970, arXiv: [1907.05120](https://arxiv.org/abs/1907.05120) [hep-ex].
- [40] ATLAS Collaboration, *Optimisation and performance studies of the ATLAS b-tagging algorithms for the 2017-18 LHC run*, ATL-PHYS-PUB-2017-013, 2017, URL: <https://cds.cern.ch/record/2273281>.
- [41] ATLAS Collaboration, *Performance of top-quark and W-boson tagging with ATLAS in Run 2 of the LHC*, *Eur. Phys. J. C* **79** (2019) 375, arXiv: [1808.07858](https://arxiv.org/abs/1808.07858) [hep-ex].
- [42] ATLAS Collaboration, *Electron and photon performance measurements with the ATLAS detector using the 2015–2017 LHC proton–proton collision data*, *JINST* **14** (2019) P12006, arXiv: [1908.00005](https://arxiv.org/abs/1908.00005) [hep-ex].
- [43] ATLAS Collaboration, *Electron reconstruction and identification in the ATLAS experiment using the 2015 and 2016 LHC proton–proton collision data at  $\sqrt{s} = 13$  TeV*, *Eur. Phys. J. C* **79** (2019) 639, arXiv: [1902.04655](https://arxiv.org/abs/1902.04655) [physics.ins-det].
- [44] ATLAS Collaboration, *Muon reconstruction and identification efficiency in ATLAS using the full Run 2 pp collision data set at  $\sqrt{s} = 13$  TeV*, *Eur. Phys. J. C* **81** (2021) 578, arXiv: [2012.00578](https://arxiv.org/abs/2012.00578) [hep-ex].
- [45] ATLAS Collaboration, *Measurement of the tau lepton reconstruction and identification performance in the ATLAS experiment using pp collisions at  $\sqrt{s} = 13$  TeV*, ATL-CONF-2017-029, 2017, URL: <https://cds.cern.ch/record/2261772>.
- [46] ATLAS Collaboration, *Reconstruction, Energy Calibration, and Identification of Hadronically Decaying Tau Leptons in the ATLAS Experiment for Run-2 of the LHC*, ATL-PHYS-PUB-2015-045, 2015, URL: <https://cds.cern.ch/record/2064383>.
- [47] ATLAS Collaboration, *Identification and energy calibration of hadronically decaying tau leptons with the ATLAS experiment in pp collisions at  $\sqrt{s} = 8$  TeV*, *Eur. Phys. J. C* **75** (2015) 303, arXiv: [1412.7086](https://arxiv.org/abs/1412.7086) [hep-ex].
- [48] ATLAS Collaboration, *Identification of hadronic tau lepton decays using neural networks in the ATLAS experiment*, ATL-PHYS-PUB-2019-033, 2019, URL: <https://cds.cern.ch/record/2688062>.
- [49] ATLAS Collaboration, *The performance of missing transverse momentum reconstruction and its significance with the ATLAS detector using  $140\text{ fb}^{-1}$  of  $\sqrt{s} = 13$  TeV pp collisions*, (2024), arXiv: [2402.05858](https://arxiv.org/abs/2402.05858) [hep-ex].
- [50] ATLAS Collaboration, *Object-based missing transverse momentum significance in the ATLAS Detector*, ATL-CONF-2018-038, 2018, URL: <https://cds.cern.ch/record/2630948>.

- [51] A. Elagin, P. Murat, A. Pranko and A. Safonov,  
*A new mass reconstruction technique for resonances decaying to  $\tau\tau$ ,*  
*Nucl. Instrum. Meth. A* **654** (2011) 481, arXiv: [1012.4686 \[hep-ex\]](#).
- [52] C. G. Lester and D. J. Summers,  
*Measuring masses of semi-invisibly decaying particle pairs produced at hadron colliders,*  
*Phys. Lett. B* **463** (1999) 99, arXiv: [hep-ph/9906349](#).
- [53] A. Barr, C. Lester and P. Stephens, *A variable for measuring masses at hadron colliders when missing energy is expected;  $m_{T2}$ : the truth behind the glamour,* *J. Phys. G* **29** (2003) 2343, arXiv: [hep-ph/0304226](#).
- [54] P. Konar, K. Kong, K. T. Matchev and M. Park,  
*Dark matter particle spectroscopy at the LHC: generalizing  $M_{T2}$  to asymmetric event topologies,*  
*JHEP* **04** (2010) 086, arXiv: [0911.4126 \[hep-ph\]](#).
- [55] C. G. Lester and B. Nachman, *Bisection-based asymmetric  $M_{T2}$  computation: a higher precision calculator than existing symmetric methods,* *JHEP* **03** (2015) 100, arXiv: [1411.4312 \[hep-ph\]](#).
- [56] D. R. Tovey,  
*On measuring the masses of pair-produced semi-invisibly decaying particles at hadron colliders,*  
*JHEP* **04** (2008) 034, arXiv: [0802.2879 \[hep-ph\]](#).
- [57] G. Karagiorgi, G. Kasieczka, S. Kravitz, B. Nachman and D. Shih,  
*Machine Learning in the Search for New Fundamental Physics,* (2021),  
arXiv: [2112.03769 \[hep-ph\]](#).
- [58] ATLAS Collaboration, *Recommendations for the Modeling of Smooth Backgrounds,*  
ATL-PHYS-PUB-2020-028, 2020, URL: <https://cds.cern.ch/record/2743717>.
- [59] ATLAS Collaboration,  
*Tools for estimating fake/non-prompt lepton backgrounds with the ATLAS detector at the LHC,*  
*JINST* **18** (2023) T11004, arXiv: [2211.16178 \[hep-ex\]](#).
- [60] J. S. Conway, ‘Incorporating Nuisance Parameters in Likelihoods for Multisource Spectra’,  
*PHYSTAT 2011*, 2011 115, arXiv: [1103.0354 \[physics.data-an\]](#).
- [61] A. L. Read, *Presentation of search results: the  $CL_S$  technique,* *J. Phys. G* **28** (2002) 2693.
- [62] G. Cowan, K. Cranmer, E. Gross and O. Vitells,  
*Asymptotic formulae for likelihood-based tests of new physics,* *Eur. Phys. J. C* **71** (2011) 1554,  
arXiv: [1007.1727 \[physics.data-an\]](#), Erratum: *Eur. Phys. J. C* **73** (2013) 2501.
- [63] U. Baur, I. Hinchliffe and D. Zeppenfeld, *Excited Quark Production at Hadron Colliders,*  
*Int. J. Mod. Phys. A* **2** (1987) 1285.
- [64] ATLAS Collaboration, *Search for new resonances in mass distributions of jet pairs using  $139\text{ fb}^{-1}$  of  $pp$  collisions at  $\sqrt{s} = 13\text{ TeV}$  with the ATLAS detector,* *JHEP* **03** (2020) 145, arXiv: [1910.08447 \[hep-ex\]](#).
- [65] ATLAS Collaboration, *Search for New Particles in Two-Jet Final States in 7 TeV Proton–Proton Collisions with the ATLAS Detector at the LHC,* *Phys. Rev. Lett.* **105** (2010) 161801, arXiv: [1008.2461 \[hep-ex\]](#).
- [66] CDF Collaboration,  
*Search for new particles decaying into dijets in proton-antiproton collisions at  $\sqrt{s} = 1.96\text{ TeV}$ ,*  
*Phys. Rev. D* **79** (2009) 112002, arXiv: [0812.4036 \[hep-ex\]](#).

- [67] ATLAS Collaboration, *Search for excited electrons singly produced in proton–proton collisions at  $\sqrt{s} = 13$  TeV with the ATLAS experiment at the LHC*, *Eur. Phys. J. C* **79** (2019) 803, arXiv: [1906.03204 \[hep-ex\]](#).
- [68] ATLAS Collaboration, *A search for an excited muon decaying to a muon and two jets in pp collisions at  $\sqrt{s} = 8$  TeV with the ATLAS detector*, *New J. Phys.* **18** (2016) 073021, arXiv: [1601.05627 \[hep-ex\]](#), Erratum: *New J. Phys.* **21** (2019) 109501.
- [69] ATLAS Collaboration, *Search for excited  $\tau$ -leptons and leptoquarks in the final state with  $\tau$ -leptons and jets in pp collisions at  $\sqrt{s} = 13$  TeV with the ATLAS detector*, *JHEP* **06** (2023) 199, arXiv: [2303.09444 \[hep-ex\]](#).
- [70] G. Altarelli, B. Mele and M. Ruiz-Altaba, *Searching for New Heavy Vector Bosons in  $p\bar{p}$  Colliders*, *Z. Phys. C* **45** (1989) 109, Erratum: *Z. Phys. C* **47** (1990) 676.
- [71] D. London and J. L. Rosner, *Extra gauge bosons in  $E_6$* , *Phys. Rev. D* **34** (1986) 1530.
- [72] C. T. Hill and S. J. Parke, *Top quark production: Sensitivity to new physics*, *Phys. Rev. D* **49** (1994) 4454, arXiv: [hep-ph/9312324](#).
- [73] C. T. Hill, *Topcolor assisted technicolor*, *Phys. Lett. B* **345** (1995) 483, arXiv: [hep-ph/9411426](#).
- [74] D. Pappadopulo, A. Thamm, R. Torre and A. Wulzer, *Heavy Vector Triplets: Bridging Theory and Data*, *JHEP* **09** (2014) 060, arXiv: [1402.4431 \[hep-ph\]](#).
- [75] R. S. Chivukula, A. G. Cohen and E. H. Simmons, *New strong interactions at the Tevatron?*, *Phys. Lett. B* **380** (1996) 92, arXiv: [hep-ph/9603311](#).
- [76] ATLAS Collaboration, *Search for high-mass dilepton resonances using  $139\text{fb}^{-1}$  of pp collision data collected at  $\sqrt{s} = 13$  TeV with the ATLAS detector*, *Phys. Lett. B* **796** (2019) 68, arXiv: [1903.06248 \[hep-ex\]](#).
- [77] ATLAS Collaboration, *Search for a heavy charged boson in events with a charged lepton and missing transverse momentum from pp collisions at  $\sqrt{s} = 13$  TeV with the ATLAS detector*, *Phys. Rev. D* **100** (2019) 052013, arXiv: [1906.05609 \[hep-ex\]](#).
- [78] ATLAS Collaboration, *Search for high-mass resonances in final states with a  $\tau$ -lepton and missing transverse momentum with the ATLAS detector*, (2024), arXiv: [2402.16576 \[hep-ex\]](#).
- [79] ATLAS Collaboration, *Search for additional heavy neutral Higgs and gauge bosons in the ditau final state produced in  $36\text{fb}^{-1}$  of pp collisions at  $\sqrt{s} = 13$  TeV with the ATLAS detector*, *JHEP* **01** (2018) 055, arXiv: [1709.07242 \[hep-ex\]](#).
- [80] ATLAS Collaboration, *Search for new phenomena in two-body invariant mass distributions using unsupervised machine learning for anomaly detection at  $\sqrt{s} = 13$  TeV with the ATLAS detector*, *Phys. Rev. Lett.* **132** (2024) 081801, arXiv: [2307.01612 \[hep-ex\]](#).
- [81] ATLAS Collaboration, *Search for resonances decaying into a weak vector boson and a Higgs boson in the fully hadronic final state produced in proton–proton collisions at  $\sqrt{s} = 13$  TeV with the ATLAS detector*, *Phys. Rev. D* **102** (2020) 112008, arXiv: [2007.05293 \[hep-ex\]](#).
- [82] ATLAS Collaboration, *Search for heavy resonances decaying into a Z or W boson and a Higgs boson in final states with leptons and b-jets in  $139\text{fb}^{-1}$  of pp collisions at  $\sqrt{s} = 13$  TeV with the ATLAS detector*, *JHEP* **06** (2023) 016, arXiv: [2207.00230 \[hep-ex\]](#).

- [83] A. J. Larkoski, I. Moutl and D. Neill, *Analytic Boosted Boson Discrimination*, *JHEP* **05** (2016) 117, arXiv: [1507.03018 \[hep-ph\]](#).
- [84] ATLAS Collaboration, *Observation of  $H \rightarrow b\bar{b}$  decays and  $VH$  production with the ATLAS detector*, *Phys. Lett. B* **786** (2018) 59, arXiv: [1808.08238 \[hep-ex\]](#).
- [85] ATLAS Collaboration, *Search for heavy diboson resonances in semileptonic final states in  $pp$  collisions at  $\sqrt{s} = 13$  TeV with the ATLAS detector*, *Eur. Phys. J. C* **80** (2020) 1165, arXiv: [2004.14636 \[hep-ex\]](#).
- [86] ATLAS Collaboration, *Search for diboson resonances in hadronic final states in  $139\text{fb}^{-1}$  of  $pp$  collisions at  $\sqrt{s} = 13$  TeV with the ATLAS detector*, *JHEP* **09** (2019) 091, arXiv: [1906.08589 \[hep-ex\]](#).
- [87] ATLAS Collaboration, *Search for resonant  $WZ$  production in the fully leptonic final state in proton–proton collisions at  $\sqrt{s} = 13$  TeV with the ATLAS detector*, *Eur. Phys. J. C* **83** (2023) 633, arXiv: [2207.03925 \[hep-ex\]](#).
- [88] ATLAS Collaboration, *Search for heavy resonances in the decay channel  $W^+W^- \rightarrow e\nu\mu\nu$  in  $pp$  collisions at  $\sqrt{s} = 13$  TeV using  $139\text{fb}^{-1}$  of data with the ATLAS detector*, ATLAS-CONF-2022-066, 2022, URL: <https://cds.cern.ch/record/2842518>.
- [89] ATLAS Collaboration, *Search for  $t\bar{t}$  resonances in fully hadronic final states in  $pp$  collisions at  $\sqrt{s} = 13$  TeV with the ATLAS detector*, *JHEP* **10** (2020) 061, arXiv: [2005.05138 \[hep-ex\]](#).
- [90] ATLAS Collaboration, *Search for vector-boson resonances decaying into a top quark and a bottom quark using  $pp$  collisions at  $\sqrt{s} = 13$  TeV with the ATLAS detector*, *JHEP* **12** (2023) 073, arXiv: [2308.08521 \[hep-ex\]](#).
- [91] ATLAS Collaboration, *Search for top-philic heavy resonances in  $pp$  collisions at  $\sqrt{s} = 13$  TeV with the ATLAS detector*, *Eur. Phys. J. C* **84** (2024) 157, arXiv: [2304.01678 \[hep-ex\]](#).
- [92] ATLAS Collaboration, *Search for heavy particles in the  $b$ -tagged dijet mass distribution with additional  $b$ -tagged jets in proton–proton collisions at  $\sqrt{s} = 13$  TeV with the ATLAS experiment*, *Phys. Rev. D* **105** (2022) 012001, arXiv: [2108.07586 \[hep-ex\]](#).
- [93] R. Edgar, D. Amidei, C. Grud and K. Sekhon, *Functional Decomposition: A new method for search and limit setting*, (2018), arXiv: [1805.04536 \[physics.data-an\]](#).
- [94] ATLAS Collaboration, *Search for a new  $Z'$  gauge boson in  $4\mu$  events with the ATLAS experiment*, *JHEP* **07** (2023) 090, arXiv: [2301.09342 \[hep-ex\]](#).
- [95] P. Baldi, K. Cranmer, T. Faucett, P. Sadowski and D. Whiteson, *Parameterized neural networks for high-energy physics*, *Eur. Phys. J. C* **76** (2016) 235, arXiv: [1601.07913 \[hep-ex\]](#).
- [96] ATLAS Collaboration, *Search for new phenomena in multi-body invariant masses in events with at least one isolated lepton and two jets using  $\sqrt{s} = 13$  TeV proton–proton collision data collected by the ATLAS detector*, *JHEP* **07** (2023) 202, arXiv: [2211.08945 \[hep-ex\]](#).
- [97] ATLAS Collaboration, *Search for dijet resonances in events with an isolated charged lepton using  $\sqrt{s} = 13$  TeV proton–proton collision data collected by the ATLAS detector*, *JHEP* **06** (2020) 151, arXiv: [2002.11325 \[hep-ex\]](#).

- [98] ATLAS Collaboration, *Pursuit of paired dijet resonances in the Run 2 dataset with ATLAS*, *Phys. Rev. D* **108** (2023) 112005, arXiv: 2307.14944 [hep-ex].
- [99] ATLAS Collaboration, *Search for new non-resonant phenomena in high-mass dilepton final states with the ATLAS detector*, *JHEP* **11** (2020) 005, arXiv: 2006.12946 [hep-ex],  
Erratum: *JHEP* **04** (2021) 142.
- [100] Y. Afik, J. Cohen, E. Gozani, E. Kajomovitz and Y. Rozen, *Establishing a Search for  $b \rightarrow s\ell^+\ell^-$  Anomalies at the LHC*, *JHEP* **08** (2018) 056, arXiv: 1805.11402 [hep-ph].
- [101] ATLAS Collaboration, *Search for New Phenomena in Final States with Two Leptons and One or No  $b$ -Tagged Jets at  $\sqrt{s} = 13$  TeV Using the ATLAS Detector*, *Phys. Rev. Lett.* **127** (2021) 141801, arXiv: 2105.13847 [hep-ex].
- [102] ATLAS Collaboration, *Search for new phenomena in dijet events using  $37\text{fb}^{-1}$  of  $pp$  collision data collected at  $\sqrt{s} = 13$  TeV with the ATLAS detector*, *Phys. Rev. D* **96** (2017) 052004, arXiv: 1703.09127 [hep-ex].
- [103] Super-Kamiokande Collaboration, *Measurement of atmospheric neutrino oscillation parameters by Super-Kamiokande I*, *Phys. Rev. D* **71** (2005) 112005, arXiv: hep-ex/0501064.
- [104] SNO Collaboration, *Direct Evidence for Neutrino Flavor Transformation from Neutral-Current Interactions in the Sudbury Neutrino Observatory*, *Phys. Rev. Lett.* **89** (2002) 011301, arXiv: nucl-ex/0204008.
- [105] E. Ma, *Pathways to naturally small neutrino masses*, *Phys. Rev. Lett.* **81** (1998) 1171, arXiv: hep-ph/9805219.
- [106] ATLAS Collaboration, *Search for Majorana neutrinos in same-sign  $WW$  scattering events from  $pp$  collisions at  $\sqrt{s} = 13$  TeV*, *Eur. Phys. J. C* **83** (2023) 824, arXiv: 2305.14931 [hep-ex].
- [107] ATLAS Collaboration, *Search for Heavy Neutral Leptons in Decays of  $W$  Bosons Using a Dilepton Displaced Vertex in  $\sqrt{s} = 13$  TeV  $pp$  Collisions with the ATLAS Detector*, *Phys. Rev. Lett.* **131** (2023) 061803, arXiv: 2204.11988 [hep-ex].
- [108] ATLAS Collaboration, *Search for heavy Majorana or Dirac neutrinos and right-handed  $W$  gauge bosons in final states with charged leptons and jets in  $pp$  collisions at  $\sqrt{s} = 13$  TeV with the ATLAS detector*, *Eur. Phys. J. C* **83** (2023) 1164, arXiv: 2304.09553 [hep-ex].
- [109] ATLAS Collaboration, *Search for type-III seesaw heavy leptons in dilepton final states in  $pp$  collisions at  $\sqrt{s} = 13$  TeV with the ATLAS detector*, *Eur. Phys. J. C* **81** (2021) 218, arXiv: 2008.07949 [hep-ex].
- [110] ATLAS Collaboration, *Search for type-III seesaw heavy leptons in leptonic final states in  $pp$  collisions at  $\sqrt{s} = 13$  TeV with the ATLAS detector*, *Eur. Phys. J. C* **82** (2022) 988, arXiv: 2202.02039 [hep-ex].
- [111] ATLAS Collaboration, *Search for new phenomena in three- or four-lepton events in  $pp$  collisions at  $\sqrt{s} = 13$  TeV with the ATLAS detector*, *Phys. Lett. B* **824** (2022) 136832, arXiv: 2107.00404 [hep-ex].
- [112] ATLAS Collaboration, *Performance of vertex reconstruction algorithms for detection of new long-lived particle decays within the ATLAS inner detector*, ATL-PHYS-PUB-2019-013, 2019, URL: <https://cds.cern.ch/record/2669425>.



- [113] J. C. Pati and A. Salam, *Lepton number as the fourth "color"*, [Phys. Rev. D \*\*10\*\* \(1974\) 275](#),  
Erratum: [Phys. Rev. D \*\*11\*\* \(1975\) 703](#).
- [114] R. N. Mohapatra and J. C. Pati, *"Natural" left-right symmetry*, [Phys. Rev. D \*\*11\*\* \(1975\) 2558](#).
- [115] G. Senjanovic and R. N. Mohapatra, *Exact left-right symmetry and spontaneous violation of parity*,  
[Phys. Rev. D \*\*12\*\* \(1975\) 1502](#).
- [116] C. Biggio and F. Bonnet, *Implementation of the Type III Seesaw Model in FeynRules/MadGraph  
and Prospects for Discovery with Early LHC Data*, [Eur. Phys. J. C \*\*72\*\* \(2012\) 1899](#),  
arXiv: [1107.3463 \[hep-ph\]](#).
- [117] L. Susskind, *Dynamics of spontaneous symmetry breaking in the Weinberg-Salam theory*,  
[Phys. Rev. D \*\*20\*\* \(1979\) 2619](#).
- [118] A. Djouadi and A. Lenz, *Sealing the fate of a fourth generation of fermions*,  
[Phys. Lett. B \*\*715\*\* \(2012\) 310](#), arXiv: [1204.1252 \[hep-ph\]](#).
- [119] O. Eberhardt et al., *Impact of a Higgs boson at a mass of 126 GeV on the standard model with  
three and four fermion generations*, [Phys. Rev. Lett. \*\*109\*\* \(2012\) 241802](#),  
arXiv: [1209.1101 \[hep-ph\]](#).
- [120] A. Lenz, *Constraints on a Fourth Generation of Fermions from Higgs Boson Searches*,  
[Adv. High Energy Phys. \*\*2013\*\* \(2013\) 910275](#).
- [121] P. H. Frampton, P. Q. Hung and M. Sher, *Quarks and leptons beyond the third generation*,  
[Phys. Rept. \*\*330\*\* \(2000\) 263](#), arXiv: [hep-ph/9903387](#).
- [122] C. T. Hill and E. H. Simmons, *Strong Dynamics and Electroweak Symmetry Breaking*,  
[Phys. Rept. \*\*381\*\* \(2003\) 235](#), arXiv: [hep-ph/0203079](#), [Erratum: [Phys.Rept. \*\*390\*\*, \(2004\) 553](#)].
- [123] S. Dimopoulos and J. Preskill, *Massless Composites With Massive Constituents*,  
[Nucl. Phys. B \*\*199\*\* \(1982\) 206](#).
- [124] D. B. Kaplan and H. Georgi, *SU(2) x U(1) Breaking by Vacuum Misalignment*,  
[Phys. Lett. B \*\*136\*\* \(1984\) 183](#).
- [125] D. B. Kaplan, H. Georgi and S. Dimopoulos, *Composite Higgs Scalars*,  
[Phys. Lett. B \*\*136\*\* \(1984\) 187](#).
- [126] J. L. Hewett and T. G. Rizzo, *Low-Energy Phenomenology of Superstring Inspired E(6) Models*,  
[Phys. Rept. \*\*183\*\* \(1989\) 193](#).
- [127] F. Gursev, P. Ramond and P. Sikivie, *A Universal Gauge Theory Model Based on E6*,  
[Phys. Lett. B \*\*60\*\* \(1976\) 177](#).
- [128] T. Asaka, W. Buchmüller and L. Covi, *Quarks and leptons between branes and bulk*,  
[Phys. Lett. B \*\*563\*\* \(2003\) 209](#), arXiv: [hep-ph/0304142](#).
- [129] T. Moroi and Y. Okada, *Radiative corrections to Higgs masses in the supersymmetric model with  
an extra family and anti-family*, [Mod. Phys. Lett. A \*\*7\*\* \(1992\) 187](#).
- [130] S. P. Martin, *A Supersymmetry Primer*, [Adv. Ser. Direct. High Energy Phys. \*\*18\*\* \(1998\) 1](#),  
arXiv: [hep-ph/9709356](#).
- [131] M. Endo, K. Hamaguchi, S. Iwamoto and N. Yokozaki, *Higgs mass and muon anomalous  
magnetic moment in supersymmetric models with vectorlike matters*,  
[Phys. Rev. D \*\*84\*\* \(2011\) 075017](#), arXiv: [1108.3071 \[hep-ph\]](#).

- [132] N. Kumar and S. P. Martin, *Vectorlike Leptons at the Large Hadron Collider*, *Phys. Rev. D* **92** (2015) 115018, arXiv: [1510.03456 \[hep-ph\]](#).
- [133] ATLAS Collaboration, *Search for third-generation vector-like leptons in pp collisions at  $\sqrt{s} = 13$  TeV with the ATLAS detector*, *JHEP* **07** (2023) 118, arXiv: [2303.05441 \[hep-ex\]](#).
- [134] Y. Freund and R. E. Schapire, *A Decision-Theoretic Generalization of On-Line Learning and an Application to Boosting*, *J. Comput. Syst. Sci.* **55** (1997) 119.
- [135] ATLAS Collaboration, *Search for single vector-like B quark production and decay via  $B \rightarrow bH(b\bar{b})$  in pp collisions at  $\sqrt{s} = 13$  TeV with the ATLAS detector*, *JHEP* **11** (2023) 168, arXiv: [2308.02595 \[hep-ex\]](#).
- [136] ATLAS Collaboration, *Search for single production of a vectorlike T quark decaying into a Higgs boson and top quark with fully hadronic final states using the ATLAS detector*, *Phys. Rev. D* **105** (2022) 092012, arXiv: [2201.07045 \[hep-ex\]](#).
- [137] ATLAS Collaboration, *Search for singly produced vector-like top partners in multilepton final states with  $139\text{fb}^{-1}$  of pp collision data at  $\sqrt{s} = 13$  TeV with the ATLAS detector*, (2023), arXiv: [2307.07584 \[hep-ex\]](#).
- [138] ATLAS Collaboration, *Search for pair-production of vector-like quarks in pp collision events at  $\sqrt{s} = 13$  TeV with at least one leptonically decaying Z boson and a third-generation quark with the ATLAS detector*, *Phys. Lett. B* **843** (2023) 138019, arXiv: [2210.15413 \[hep-ex\]](#).
- [139] ATLAS Collaboration, *Search for pair-produced vector-like top and bottom partners in events with large missing transverse momentum in pp collisions with the ATLAS detector*, *Eur. Phys. J. C* **83** (2023) 719, arXiv: [2212.05263 \[hep-ex\]](#).
- [140] ATLAS Collaboration, *Search for single production of vector-like T quarks decaying into Ht or Zt in pp collisions at  $\sqrt{s} = 13$  TeV with the ATLAS detector*, *JHEP* **08** (2023) 153, arXiv: [2305.03401 \[hep-ex\]](#).
- [141] J. Thaler and K. Van Tilburg, *Identifying Boosted Objects with N-subjettiness*, *JHEP* **03** (2011) 015, arXiv: [1011.2268 \[hep-ph\]](#).
- [142] ATLAS Collaboration, *Combination of the Searches for Pair-Produced Vectorlike Partners of the Third-Generation Quarks at  $\sqrt{s} = 13$  TeV with the ATLAS Detector*, *Phys. Rev. Lett.* **121** (2018) 211801, arXiv: [1808.02343 \[hep-ex\]](#).
- [143] S. Dimopoulos and L. Susskind, *Mass Without Scalars*, *Nucl. Phys. B* **155** (1979) 237, ed. by A. Zichichi.
- [144] H. Georgi and S. L. Glashow, *Unity of All Elementary-Particle Forces*, *Phys. Rev. Lett.* **32** (1974) 438.
- [145] R. Barbier et al., *R-parity-violating supersymmetry*, *Phys. Rept.* **420** (2005) 1, arXiv: [hep-ph/0406039](#).
- [146] B. Gripaios, M. Nardecchia and S. A. Renner, *Composite leptoquarks and anomalies in B-meson decays*, *JHEP* **05** (2015) 006, arXiv: [1412.1791 \[hep-ph\]](#).
- [147] BaBar Collaboration, *Measurement of an Excess of  $\bar{B} \rightarrow D^{(*)}\tau^{-}\bar{\nu}_{\tau}$  Decays and Implications for Charged Higgs Bosons*, *Phys. Rev. D* **88** (2013) 072012, arXiv: [1303.0571 \[hep-ex\]](#).



- [148] Belle Collaboration, *Observation of  $B^+ \rightarrow \bar{D}^*0\tau^+\nu_\tau$  and Evidence for  $B^+ \rightarrow \bar{D}^0\tau^+\nu_\tau$  at Belle*, *Phys. Rev. D* **82** (2010) 072005, arXiv: [1005.2302 \[hep-ex\]](#).
- [149] LHCb Collaboration, *Measurement of the ratios of branching fractions  $\mathcal{R}(D^*)$  and  $\mathcal{R}(D^0)$* , *Phys. Rev. Lett.* **131** (2023) 111802, arXiv: [2302.02886 \[hep-ex\]](#).
- [150] T. Aoyama et al., *The anomalous magnetic moment of the muon in the Standard Model*, *Phys. Rept.* **887** (2020) 1, arXiv: [2006.04822 \[hep-ph\]](#).
- [151] Muon g-2 Collaboration, *Final report of the E821 muon anomalous magnetic moment measurement at BNL*, *Phys. Rev. D* **73** (2006) 072003, arXiv: [hep-ex/0602035](#).
- [152] A. Greljo, P. Stangl and A. Eller Thomsen, *A model of muon anomalies*, *Phys. Lett. B* **820** (2021) 136554, arXiv: [2103.13991 \[hep-ph\]](#).
- [153] C. Cornella, J. Fuentes-Martín and G. Isidori, *Revisiting the vector leptoquark explanation of the B-physics anomalies*, *JHEP* **07** (2019) 168, arXiv: [1903.11517 \[hep-ph\]](#).
- [154] ATLAS Collaboration, *Search for pair production of third-generation scalar leptoquarks decaying into a top quark and a  $\tau$ -lepton in pp collisions at  $\sqrt{s} = 13$  TeV with the ATLAS detector*, *JHEP* **06** (2021) 179, arXiv: [2101.11582 \[hep-ex\]](#).
- [155] ATLAS Collaboration, *Search for a scalar partner of the top quark in the all-hadronic  $t\bar{t}$  plus missing transverse momentum final state at  $\sqrt{s} = 13$  TeV with the ATLAS detector*, *Eur. Phys. J. C* **80** (2020) 737, arXiv: [2004.14060 \[hep-ex\]](#).
- [156] ATLAS Collaboration, *Search for leptoquarks decaying into the  $b\tau$  final state in pp collisions at  $\sqrt{s} = 13$  TeV with the ATLAS detector*, *JHEP* **10** (2023) 001, arXiv: [2305.15962 \[hep-ex\]](#).
- [157] ATLAS Collaboration, *Search for pair production of third-generation leptoquarks decaying into a bottom quark and a  $\tau$ -lepton with the ATLAS detector*, *Eur. Phys. J. C* **83** (2023) 1075, arXiv: [2303.01294 \[hep-ex\]](#).
- [158] ATLAS Collaboration, *Search for new phenomena in final states with b-jets and missing transverse momentum in  $\sqrt{s} = 13$  TeV pp collisions with the ATLAS detector*, *JHEP* **05** (2021) 093, arXiv: [2101.12527 \[hep-ex\]](#).
- [159] ATLAS Collaboration, *Search for new phenomena in pp collisions in final states with tau leptons, b-jets, and missing transverse momentum with the ATLAS detector*, *Phys. Rev. D* **104** (2021) 112005, arXiv: [2108.07665 \[hep-ex\]](#).
- [160] ATLAS Collaboration, *Search for leptoquark pair production decaying into  $te^-\bar{t}e^+$  or  $t\mu^-\bar{t}\mu^+$  in multi-lepton final states in pp collisions at 13 TeV with the ATLAS detector*, (2023), arXiv: [2306.17642 \[hep-ex\]](#).
- [161] ATLAS Collaboration, *Search for pair-produced scalar and vector leptoquarks decaying into third-generation quarks and first- or second-generation leptons in pp collisions with the ATLAS detector*, *JHEP* **06** (2023) 188, arXiv: [2210.04517 \[hep-ex\]](#).
- [162] ATLAS Collaboration, *Search for pair production of scalar leptoquarks decaying into first- or second-generation leptons and top quarks in proton-proton collisions at  $\sqrt{s} = 13$  TeV with the ATLAS detector*, *Eur. Phys. J. C* **81** (2021) 313, arXiv: [2010.02098 \[hep-ex\]](#).

- [163] ATLAS Collaboration, *Search for pairs of scalar leptoquarks decaying into quarks and electrons or muons in  $\sqrt{s} = 13$  TeV  $pp$  collisions with the ATLAS detector*, *JHEP* **10** (2020) 112, arXiv: [2006.05872 \[hep-ex\]](#).
- [164] ATLAS Collaboration, *Combination of searches for pair-produced leptoquarks at  $\sqrt{s} = 13$  TeV with the ATLAS detector*, (2024), arXiv: [2401.11928 \[hep-ex\]](#).
- [165] ATLAS Collaboration, *Constraints on spin-0 dark matter mediators and invisible Higgs decays using ATLAS 13 TeV  $pp$  collision data with two top quarks and missing transverse momentum in the final state*, *Eur. Phys. J. C* **83** (2023) 503, arXiv: [2211.05426 \[hep-ex\]](#).
- [166] ATLAS Collaboration, *Search for leptoquark pair production decaying into  $t\ell^{-}\bar{\ell}^{+}$  in multilepton final states in  $pp$  collisions at 13 TeV with the ATLAS detector*, ATLAS-CONF-2022-052, 2022, URL: <https://cds.cern.ch/record/2816335>.
- [167] J. I. Illana and T. Riemann, *Charged lepton flavor violation from massive neutrinos in Z decays*, *Phys. Rev. D* **63** (2001) 053004, arXiv: [hep-ph/0010193](#).
- [168] ATLAS Collaboration, *Search for the charged-lepton-flavor-violating decay  $Z \rightarrow e\mu$  in  $pp$  collisions at  $\sqrt{s} = 13$  TeV with the ATLAS detector*, *Phys. Rev. D* **108** (2023) 032015, arXiv: [2204.10783 \[hep-ex\]](#).
- [169] ATLAS Collaboration, *Search for Lepton-Flavor Violation in Z-Boson Decays with  $\tau$  Leptons with the ATLAS Detector*, *Phys. Rev. Lett.* **127** (2021) 271801, arXiv: [2105.12491 \[hep-ex\]](#).
- [170] ATLAS Collaboration, *Search for charged-lepton-flavour violation in Z-boson decays with the ATLAS detector*, *Nature Phys.* **17** (2021) 819, arXiv: [2010.02566 \[hep-ex\]](#).
- [171] ATLAS Collaboration, *Search for lepton-flavour-violating decays of the Higgs and Z bosons with the ATLAS detector*, *Eur. Phys. J. C* **77** (2017) 70, arXiv: [1604.07730 \[hep-ex\]](#).
- [172] ATLAS Collaboration, *Search for lepton-flavour violation in high-mass dilepton final states using  $139\text{fb}^{-1}$  of  $pp$  collisions at  $\sqrt{s} = 13$  TeV with the ATLAS detector*, *JHEP* **10** (2023) 082, arXiv: [2307.08567 \[hep-ex\]](#).
- [173] G. Burdman, Z. Chacko, H.-S. Goh and R. Harnik, *Folded supersymmetry and the LEP paradox*, *JHEP* **02** (2007) 009, arXiv: [hep-ph/0609152](#).
- [174] D. Curtin and C. B. Verhaaren, *Discovering Uncolored Naturalness in Exotic Higgs Decays*, *JHEP* **12** (2015) 1, arXiv: [1506.06141 \[hep-ph\]](#).
- [175] ATLAS Collaboration, *Search for light long-lived neutral particles that decay to collimated pairs of leptons or light hadrons in  $pp$  collisions at  $\sqrt{s} = 13$  TeV with the ATLAS detector*, *JHEP* **06** (2023) 153, arXiv: [2206.12181 \[hep-ex\]](#).
- [176] ATLAS Collaboration, *Search for light long-lived neutral particles from Higgs boson decays via vector-boson-fusion production from  $pp$  collisions at  $\sqrt{s} = 13$  TeV with the ATLAS detector*, (2023), arXiv: [2311.18298 \[hep-ex\]](#).
- [177] ATLAS Collaboration, *Search for exotic decays of the Higgs boson into long-lived particles in  $pp$  collisions at  $\sqrt{s} = 13$  TeV using displaced vertices in the ATLAS inner detector*, *JHEP* **11** (2021) 229, arXiv: [2107.06092 \[hep-ex\]](#).

- [178] ATLAS Collaboration, *Search for neutral long-lived particles in pp collisions at  $\sqrt{s} = 13$  TeV that decay into displaced hadronic jets in the ATLAS calorimeter*, *JHEP* **06** (2022) 005, arXiv: [2203.01009 \[hep-ex\]](#).
- [179] ATLAS Collaboration, *Search for events with a pair of displaced vertices from long-lived neutral particles decaying into hadronic jets in the ATLAS muon spectrometer in pp collisions at  $\sqrt{s} = 13$  TeV*, *Phys. Rev. D* **106** (2022) 032005, arXiv: [2203.00587 \[hep-ex\]](#).
- [180] D. Curtin, R. Essig, S. Gori and J. Shelton, *Illuminating Dark Photons with High-Energy Colliders*, *JHEP* **02** (2015) 157, arXiv: [1412.0018 \[hep-ph\]](#).
- [181] A. Falkowski, J. T. Ruderman, T. Volansky and J. Zupan, *Hidden Higgs Decaying to Lepton Jets*, *JHEP* **05** (2010) 077, arXiv: [1002.2952 \[hep-ph\]](#).
- [182] A. Falkowski, J. T. Ruderman, T. Volansky and J. Zupan, *Discovering Higgs Boson Decays to Lepton Jets at Hadron Colliders*, *Phys. Rev. Lett.* **105** (2010) 241801, arXiv: [1007.3496 \[hep-ph\]](#).
- [183] ATLAS Collaboration, *A search for prompt lepton-jets in pp collisions at  $\sqrt{s} = 8$  TeV with the ATLAS detector*, *JHEP* **02** (2016) 062, arXiv: [1511.05542 \[hep-ex\]](#).
- [184] P. Ilten, Y. Soreq, M. Williams and W. Xue, *Serendipity in dark photon searches*, *JHEP* **06** (2018) 004, arXiv: [1801.04847 \[hep-ph\]](#).
- [185] ATLAS Collaboration, *Standalone vertex finding in the ATLAS muon spectrometer*, *JINST* **9** (2014) P02001, arXiv: [1311.7070 \[hep-ex\]](#).
- [186] E. Corbelli and P. Salucci, *The Extended Rotation Curve and the Dark Matter Halo of M33*, *Mon. Not. Roy. Astron. Soc.* **311** (2000) 441, arXiv: [astro-ph/9909252](#).
- [187] V. C. Rubin, N. Thonnard and W. K. Ford Jr., *Rotational properties of 21 SC galaxies with a large range of luminosities and radii, from NGC 4605 ( $R = 4$  kpc) to UGC 2885 ( $R = 122$  kpc)*, *Astrophys. J.* **238** (1980) 471.
- [188] K. G. Begeman, A. H. Broeils and R. H. Sanders, *Extended rotation curves of spiral galaxies: Dark haloes and modified dynamics*, *Mon. Not. Roy. Astron. Soc.* **249** (1991) 523.
- [189] G. Hinshaw et al., *Nine-Year Wilkinson Microwave Anisotropy Probe (WMAP) Observations: Cosmological Parameter Results*, *Astrophys. J. Suppl.* **208** (2013) 19, arXiv: [1212.5226 \[astro-ph.CO\]](#).
- [190] Planck Collaboration, *Planck 2018 results - I. Overview and the cosmological legacy of Planck*, *Astron. Astrophys.* **641** (2020) A1, arXiv: [1807.06205 \[astro-ph.CO\]](#).
- [191] V. Trimble, *Existence and Nature of Dark Matter in the Universe*, *Ann. Rev. Astron. Astrophys.* **25** (1987) 425.
- [192] G. Bertone, D. Hooper and J. Silk, *Particle dark matter: evidence, candidates and constraints*, *Phys. Rept.* **405** (2005) 279, arXiv: [hep-ph/0404175 \[hep-ph\]](#).
- [193] J. L. Feng, *Dark Matter Candidates from Particle Physics and Methods of Detection*, *Ann. Rev. Astron. Astrophys.* **48** (2010) 495, arXiv: [1003.0904](#).

- [194] J. Aalbers et al., *A next-generation liquid xenon observatory for dark matter and neutrino physics*, *J. Phys. G* **50** (2022) 013001, arXiv: 2203.02309 [physics.ins-det].
- [195] LUX-ZEPLIN Collaboration, *First Dark Matter Search Results from the LUX-ZEPLIN (LZ) Experiment*, *Phys. Rev. Lett.* **131** (2023) 041002, arXiv: 2207.03764 [hep-ex].
- [196] LUX Collaboration, *Results from a Search for Dark Matter in the Complete LUX Exposure*, *Phys. Rev. Lett.* **118** (2017) 021303, arXiv: 1608.07648 [astro-ph.CO].
- [197] PICO Collaboration, *Dark Matter Search Results from the Complete Exposure of the PICO-60 C<sub>3</sub>F<sub>8</sub> Bubble Chamber*, *Phys. Rev. D* **100** (2019) 022001, arXiv: 1902.04031 [astro-ph.CO].
- [198] PandaX-II Collaboration, *Search for Light Dark Matter-Electron Scattering in the PandaX-II Experiment*, *Phys. Rev. Lett.* **126** (2021) 211803, arXiv: 2101.07479 [hep-ex].
- [199] PandaX-II Collaboration, *Dark Matter Results From 54-Ton-Day Exposure of PandaX-II Experiment*, *Phys. Rev. Lett.* **119** (2017) 181302, arXiv: 1708.06917 [astro-ph.CO].
- [200] XENON Collaboration, *Search for New Physics in Electronic Recoil Data from XENONnT*, *Phys. Rev. Lett.* **129** (2022) 161805, arXiv: 2207.11330 [hep-ex].
- [201] XENON Collaboration, *First Dark Matter Search with Nuclear Recoils from the XENONnT Experiment*, *Phys. Rev. Lett.* **131** (2023) 041003, arXiv: 2303.14729 [hep-ex].
- [202] XENON Collaboration, *Constraining the spin-dependent WIMP-nucleon cross sections with XENON1T*, *Phys. Rev. Lett.* **122** (2019) 141301, arXiv: 1902.03234 [astro-ph.CO].
- [203] XENON Collaboration, *Search for Light Dark Matter Interactions Enhanced by the Migdal Effect or Bremsstrahlung in XENON1T*, *Phys. Rev. Lett.* **123** (2019) 241803, arXiv: 1907.12771 [hep-ex].
- [204] DarkSide-50 Collaboration, *Search for low-mass dark matter WIMPs with 12 ton-day exposure of DarkSide-50*, *Phys. Rev. D* **107** (2023) 063001, arXiv: 2207.11966 [hep-ex].
- [205] G. Angloher et al., *Results on light dark matter particles with a low-threshold CRESST-II detector*, *Eur. Phys. J. C* **76** (2016) 25, arXiv: 1509.01515 [astro-ph.CO].
- [206] M. Lai and on behalf of DEAP-3600 Collaboration, *Recent results from DEAP-3600*, *JINST* **18** (2023) C02046, arXiv: 2302.14484 [hep-ex].
- [207] DEAP-3600 Collaboration, *First Results from the DEAP-3600 Dark Matter Search with Argon at SNOLAB*, *Phys. Rev. Lett.* **121** (2018) 071801, arXiv: 1707.08042 [astro-ph.CO].
- [208] SuperCDMS Collaboration, *Results from the Super Cryogenic Dark Matter Search Experiment at Soudan*, *Phys. Rev. Lett.* **120** (2018) 061802, arXiv: 1708.08869 [hep-ex].
- [209] SuperCDMS Collaboration, *Low-mass dark matter search with CDMSlite*, *Phys. Rev. D* **97** (2018) 22002, arXiv: 1707.01632 [astro-ph.CO].

- [210] A. Acharyya et al., *Search for Ultraheavy Dark Matter from Observations of Dwarf Spheroidal Galaxies with VERITAS*, *Astrophys. J.* **945** (2023) 101, arXiv: 2302.08784 [astro-ph.HE].
- [211] H.E.S.S. Collaboration, *Search for Dark Matter Annihilation Signals in the H.E.S.S. Inner Galaxy Survey*, *Phys. Rev. Lett.* **129** (2022) 111101, arXiv: 2207.10471 [astro-ph.HE].
- [212] V. A. Acciari et al., *Combined searches for dark matter in dwarf spheroidal galaxies observed with the MAGIC telescopes, including new data from Coma Berenices and Draco*, *Phys. Dark. Univ.* **35** (2022) 100912, arXiv: 2111.15009 [astro-ph.HE].
- [213] A. Acharyya et al., *Sensitivity of the Cherenkov Telescope Array to a dark matter signal from the Galactic centre*, *JCAP* **01** (2021) 057, arXiv: 2007.16129 [astro-ph.HE].
- [214] A. U. Abeysekara et al., *A Search for Dark Matter in the Galactic Halo with HAWC*, *JCAP* **02** (2018) 049, arXiv: 1710.10288 [astro-ph.HE].
- [215] M. G. Aartsen et al., *Search for neutrinos from decaying dark matter with IceCube*, *Eur. Phys. J. C* **78** (2018) 831, arXiv: 1804.03848 [astro-ph.HE].
- [216] IceCube Collaboration, *Search for GeV-scale dark matter annihilation in the Sun with IceCube DeepCore*, *Phys. Rev. D* **105** (2022) 062004, arXiv: 2111.09970 [astro-ph.HE].
- [217] The Fermi-LAT and DES Collaborations, *Searching for Dark Matter Annihilation in Recently Discovered Milky Way Satellites with Fermi-LAT*, *Astrophys. J.* **834** (2017) 110, arXiv: 1611.03184 [astro-ph.HE].
- [218] The Fermi LAT Collaboration, *The Fermi Galactic Center GeV Excess and Implications for Dark Matter*, *Astrophys. J.* **840** (2017) 43, arXiv: 1704.03910 [astro-ph.HE].
- [219] G. Steigman and M. S. Turner, *Cosmological Constraints on the Properties of Weakly Interacting Massive Particles*, *Nucl. Phys. B* **253** (1985) 375.
- [220] G. R. Farrar and P. Fayet, *Phenomenology of the production, decay, and detection of new hadronic states associated with supersymmetry*, *Phys. Lett. B* **76** (1978) 575.
- [221] H. Goldberg, *Constraint on the Photino Mass from Cosmology*, *Phys. Rev. Lett.* **50** (1983) 1419, Erratum: *Phys. Rev. Lett.* **103** (2009) 099905.
- [222] J. Ellis, J. Hagelin, D. V. Nanopoulos, K. Olive and M. Srednicki, *Supersymmetric relics from the big bang*, *Nucl. Phys. B* **238** (1984) 453.
- [223] D. Abercrombie et al., *Dark Matter benchmark models for early LHC Run-2 Searches: Report of the ATLAS/CMS Dark Matter Forum*, *Phys. Dark. Univ.* **27** (2020) 100371, ed. by A. Boveia, C. Doglioni, S. Lowette, S. Malik and S. Mrenna, arXiv: 1507.00966 [hep-ex].
- [224] A. Boveia et al., *Recommendations on presenting LHC searches for missing transverse energy signals using simplified s-channel models of dark matter*, *Phys. Dark. Univ.* **27** (2020) 100365, ed. by O. Buchmueller et al., arXiv: 1603.04156 [hep-ex].
- [225] A. Albert et al., *Recommendations of the LHC Dark Matter Working Group: Comparing LHC searches for dark matter mediators in visible and invisible decay channels and calculations of the thermal relic density*, *Phys. Dark. Univ.* **26** (2019) 100377, arXiv: 1703.05703 [hep-ex].



- [226] T. Abe et al., *LHC Dark Matter Working Group: Next-generation spin-0 dark matter models*, *Phys. Dark. Univ.* **27** (2020) 100351, arXiv: 1810.09420 [hep-ex].
- [227] ATLAS Collaboration, *The quest to discover supersymmetry at the ATLAS experiment*, (2024), arXiv: 2403.02455 [hep-ex].
- [228] ATLAS Collaboration, *Search for new phenomena in events with an energetic jet and missing transverse momentum in pp collisions at  $\sqrt{s} = 13$  TeV with the ATLAS detector*, *Phys. Rev. D* **103** (2021) 112006, arXiv: 2102.10874 [hep-ex].
- [229] ATLAS Collaboration, *Search for dark matter in association with an energetic photon in pp collisions at  $\sqrt{s} = 13$  TeV with the ATLAS detector*, *JHEP* **02** (2021) 226, arXiv: 2011.05259 [hep-ex].
- [230] ATLAS Collaboration, *Search for associated production of a Z boson with an invisibly decaying Higgs boson or dark matter candidates at  $\sqrt{s} = 13$  TeV with the ATLAS detector*, *Phys. Lett. B* **829** (2022) 137066, arXiv: 2111.08372 [hep-ex].
- [231] J. Lindert et al., *Precise predictions for V+ jets dark matter backgrounds*, *Eur. Phys. J. C* **77** (2017) 829, arXiv: 1705.04664 [hep-ph].
- [232] ATLAS Collaboration, *Dark matter summary plots for s-channel, 2HDM+s and Dark Higgs models*, ATL-PHYS-PUB-2022-036, 2022, URL: <https://cds.cern.ch/record/2816368/>.
- [233] ATLAS Collaboration, *Search for Low-Mass Dijet Resonances Using Trigger-Level Jets with the ATLAS Detector in pp Collisions at  $\sqrt{s} = 13$  TeV*, *Phys. Rev. Lett.* **121** (2018) 081801, arXiv: 1804.03496 [hep-ex].
- [234] ATLAS Collaboration, *Search for low-mass resonances decaying into two jets and produced in association with a photon using pp collisions at  $\sqrt{s} = 13$  TeV with the ATLAS detector*, *Phys. Lett. B* **795** (2019) 56, arXiv: 1901.10917 [hep-ex].
- [235] ATLAS Collaboration, *Search for light resonances decaying to boosted quark pairs and produced in association with a photon or a jet in proton–proton collisions at  $\sqrt{s} = 13$  TeV with the ATLAS detector*, *Phys. Lett. B* **788** (2019) 316, arXiv: 1801.08769 [hep-ex].
- [236] M. Backović, A. Martini, K. Kong, O. Mattelaer and G. Mohlabeng, *MaddM: New dark matter tool in the LHC era*, *AIP Conf. Proc.* **1743** (2016) 060001, ed. by B. Szczerbinska et al., arXiv: 1509.03683 [hep-ph].
- [237] M. Duerr et al., *Hunting the dark Higgs*, *JHEP* **04** (2017) 143, arXiv: 1701.08780 [hep-ph].
- [238] M. Duerr, F. Kahlhoefer, K. Schmidt-Hoberg, T. Schwetz and S. Vogl, *How to save the WIMP: global analysis of a dark matter model with two s-channel mediators*, *JHEP* **09** (2016) 042, arXiv: 1606.07609 [hep-ph].
- [239] ATLAS Collaboration, *Search for Dark Matter Produced in Association with a Dark Higgs Boson Decaying into  $W^\pm W^\mp$  or ZZ in Fully Hadronic Final States from  $\sqrt{s} = 13$  TeV pp Collisions Recorded with the ATLAS Detector*, *Phys. Rev. Lett.* **126** (2021) 121802, arXiv: 2010.06548 [hep-ex].
- [240] ATLAS Collaboration, *Search for dark matter produced in association with a dark Higgs boson decaying into  $W^+W^-$  in the one-lepton final state at  $\sqrt{s} = 13$  TeV using  $139\text{fb}^{-1}$  of pp collisions recorded with the ATLAS detector*, *JHEP* **07** (2023) 116, arXiv: 2211.07175 [hep-ex].

- [241] ATLAS Collaboration, *Track assisted techniques for jet substructure*, ATL-PHYS-PUB-2018-012, 2018, URL: <https://cds.cern.ch/record/2630864>.
- [242] ATLAS Collaboration, *Observation of a new particle in the search for the Standard Model Higgs boson with the ATLAS detector at the LHC*, *Phys. Lett. B* **716** (2012) 1, arXiv: [1207.7214](https://arxiv.org/abs/1207.7214) [[hep-ex](#)].
- [243] CMS Collaboration, *Observation of a new boson at a mass of 125 GeV with the CMS experiment at the LHC*, *Phys. Lett. B* **716** (2012) 30, arXiv: [1207.7235](https://arxiv.org/abs/1207.7235) [[hep-ex](#)].
- [244] I. Antoniadis, M. Tuckmantel and F. Zwirner, *Phenomenology of a leptonic goldstino and invisible Higgs boson decays*, *Nucl. Phys. B* **707** (2005) 215, arXiv: [hep-ph/0410165](https://arxiv.org/abs/hep-ph/0410165) [[hep-ph](#)].
- [245] N. Arkani-Hamed, S. Dimopoulos, G. Dvali and J. March-Russell, *Neutrino masses from large extra dimensions*, *Phys. Rev. D* **65** (2001) 024032, arXiv: [hep-ph/9811448](https://arxiv.org/abs/hep-ph/9811448) [[hep-ph](#)].
- [246] A. Datta, K. Huitu, J. Laamanen and B. Mukhopadhyaya, *Linear collider signals of an invisible Higgs boson in theories of large extra dimensions*, *Phys. Rev. D* **70** (2004) 075003, arXiv: [hep-ph/0404056](https://arxiv.org/abs/hep-ph/0404056) [[hep-ph](#)].
- [247] S. Kanemura, S. Matsumoto, T. Nabeshima and N. Okada, *Can WIMP dark matter overcome the nightmare scenario?*, *Phys. Rev. D* **82** (2010) 055026, arXiv: [1005.5651](https://arxiv.org/abs/1005.5651) [[hep-ph](#)].
- [248] A. Djouadi, O. Lebedev, Y. Mambrini and J. Quevillon, *Implications of LHC searches for Higgs-portal dark matter*, *Phys. Lett. B* **709** (2012) 65, arXiv: [1112.3299](https://arxiv.org/abs/1112.3299) [[hep-ph](#)].
- [249] A. Djouadi, A. Falkowski, Y. Mambrini and J. Quevillon, *Direct Detection of Higgs-Portal Dark Matter at the LHC*, *Eur. Phys. J. C* **73** (2013) 2455, arXiv: [1205.3169](https://arxiv.org/abs/1205.3169) [[hep-ph](#)].
- [250] R. E. Shrock and M. Suzuki, *Invisible Decays of Higgs Bosons*, *Phys. Lett. B* **110** (1982) 250.
- [251] D. Choudhury and D. P. Roy, *Signatures of an invisibly decaying Higgs particle at LHC*, *Phys. Lett. B* **322** (1994) 368, arXiv: [hep-ph/9312347](https://arxiv.org/abs/hep-ph/9312347) [[hep-ph](#)].
- [252] O. J. P. Éboli and D. Zeppenfeld, *Observing an invisible Higgs boson*, *Phys. Lett. B* **495** (2000) 147, arXiv: [hep-ph/0009158](https://arxiv.org/abs/hep-ph/0009158) [[hep-ph](#)].
- [253] H. Davoudiasl, T. Han and H. E. Logan, *Discovering an invisibly decaying Higgs boson at hadron colliders*, *Phys. Rev. D* **71** (2005) 115007, arXiv: [hep-ph/0412269](https://arxiv.org/abs/hep-ph/0412269) [[hep-ph](#)].
- [254] R. M. Godbole, M. Guchait, K. Mazumdar, S. Moretti and D. P. Roy, *Search for 'invisible' Higgs signals at LHC via associated production with gauge bosons*, *Phys. Lett. B* **571** (2003) 184, arXiv: [hep-ph/0304137](https://arxiv.org/abs/hep-ph/0304137) [[hep-ph](#)].
- [255] D. Ghosh, R. Godbole, M. Guchait, K. Mohan and D. Sengupta, *Looking for an Invisible Higgs Signal at the LHC*, *Phys. Lett. B* **725** (2013) 344, arXiv: [1211.7015](https://arxiv.org/abs/1211.7015) [[hep-ph](#)].
- [256] G. Bélanger, B. Dumont, U. Ellwanger, J. F. Gunion and S. Kraml, *Status of invisible Higgs decays*, *Phys. Lett. B* **723** (2013) 340, arXiv: [1302.5694](https://arxiv.org/abs/1302.5694) [[hep-ph](#)].



- [257] D. Curtin et al., *Exotic decays of the 125 GeV Higgs boson*, *Phys. Rev. D* **90** (2014) 075004, arXiv: [1312.4992 \[hep-ph\]](#).
- [258] D. de Florian et al., *Handbook of LHC Higgs Cross Sections: 4. Deciphering the Nature of the Higgs Sector*, (2016), arXiv: [1610.07922 \[hep-ph\]](#).
- [259] K. Kudashkin, J. M. Lindert, K. Melnikov and C. Wever, *Higgs bosons with large transverse momentum at the LHC*, *Phys. Lett. B* **782** (2018) 210, arXiv: [1801.08226 \[hep-ph\]](#).
- [260] A. Djouadi, J. Kalinowski, M. Mühlleitner and M. Spira, *HDECAY: Twenty++ years after*, *Comput. Phys. Commun.* **238** (2019) 214, arXiv: [1801.09506 \[hep-ph\]](#).
- [261] M. Bonetti, K. Melnikov and L. Tancredi, *Higher order corrections to mixed QCD-EW contributions to Higgs boson production in gluon fusion*, *Phys. Rev. D* **97** (2018) 056017, arXiv: [1801.10403 \[hep-ph\]](#), Erratum: *Phys. Rev. D* **97** (2018) 099906(E).
- [262] F. Dulat, A. Lazopoulos and B. Mistlberger, *iHixs 2 – Inclusive Higgs cross sections*, *Comput. Phys. Commun.* **233** (2018) 243, arXiv: [1802.00827 \[hep-ph\]](#).
- [263] R. V. Harlander, J. Klappert, S. Liebler and L. Simon, *vh@nnlo-v2: new physics in Higgs Strahlung*, *JHEP* **05** (2018) 089, arXiv: [1802.04817 \[hep-ph\]](#).
- [264] M. Cacciari, F. A. Dreyer, A. Karlberg, G. P. Salam and G. Zanderighi, *Fully Differential Vector-Boson-Fusion Higgs Production at Next-to-Next-to-Leading Order*, *Phys. Rev. Lett.* **115** (2015) 082002, arXiv: [1506.02660 \[hep-ph\]](#), Erratum: *Phys. Rev. Lett.* **120** (2018) 139901.
- [265] ATLAS Collaboration, *Search for new phenomena with top quark pairs in final states with one lepton, jets, and missing transverse momentum in pp collisions at  $\sqrt{s} = 13$  TeV with the ATLAS detector*, *JHEP* **04** (2021) 174, arXiv: [2012.03799 \[hep-ex\]](#).
- [266] ATLAS Collaboration, *Search for new phenomena in events with two opposite-charge leptons, jets and missing transverse momentum in pp collisions at  $\sqrt{s} = 13$  TeV with the ATLAS detector*, *JHEP* **04** (2021) 165, arXiv: [2102.01444 \[hep-ex\]](#).
- [267] M. L. Graesser and J. Shelton, *Hunting Mixed Top Squark Decays*, *Phys. Rev. Lett.* **111** (2013) 121802, arXiv: [1212.4495 \[hep-ph\]](#).
- [268] ATLAS Collaboration, *Search for invisible Higgs-boson decays in events with vector-boson fusion signatures using  $139\text{ fb}^{-1}$  of proton–proton data recorded by the ATLAS experiment*, *JHEP* **08** (2022) 104, arXiv: [2202.07953 \[hep-ex\]](#).
- [269] ATLAS Collaboration, *Observation and measurement of Higgs boson decays to  $WW^*$  with the ATLAS detector*, *Phys. Rev. D* **92** (2015) 012006, arXiv: [1412.2641 \[hep-ex\]](#).
- [270] J. M. Lindert, S. Pozzorini and M. Schönherr, *Precise predictions for  $V + 2$  jet backgrounds in searches for invisible Higgs decays*, *JHEP* **01** (2023) 070, arXiv: [2204.07652 \[hep-ph\]](#).

- [271] ATLAS Collaboration, *Observation of electroweak production of two jets in association with an isolated photon and missing transverse momentum, and search for a Higgs boson decaying into invisible particles at 13 TeV with the ATLAS detector*, *Eur. Phys. J. C* **82** (2022) 105, arXiv: [2109.00925 \[hep-ex\]](#).
- [272] ATLAS Collaboration, *Combination of searches for invisible decays of the Higgs boson using  $139\text{fb}^{-1}$  of proton–proton collision data at  $\sqrt{s} = 13\text{ TeV}$  collected with the ATLAS experiment*, *Phys. Lett. B* **842** (2023) 137963, arXiv: [2301.10731 \[hep-ex\]](#).
- [273] J. F. Gunion and H. E. Haber, *CP-conserving two-Higgs-doublet model: The approach to the decoupling limit*, *Phys. Rev. D* **67** (2003) 075019, arXiv: [hep-ph/0207010](#).
- [274] ATLAS Collaboration, *Search for dark matter produced in association with a Standard Model Higgs boson decaying into  $b$ -quarks using the full Run 2 dataset from the ATLAS detector*, *JHEP* **11** (2021) 209, arXiv: [2108.13391 \[hep-ex\]](#).
- [275] ATLAS Collaboration, *Search for dark matter in events with missing transverse momentum and a Higgs boson decaying into two photons in  $pp$  collisions at  $\sqrt{s} = 13\text{ TeV}$  with the ATLAS detector*, *JHEP* **10** (2021) 013, arXiv: [2104.13240 \[hep-ex\]](#).
- [276] ATLAS Collaboration, *Search for dark matter produced in association with a Higgs boson decaying to tau leptons at  $\sqrt{s} = 13\text{ TeV}$  with the ATLAS detector*, *JHEP* **09** (2023) 189, arXiv: [2305.12938 \[hep-ex\]](#).
- [277] ATLAS Collaboration, *Search for dark matter produced in association with a single top quark in  $\sqrt{s} = 13\text{ TeV}$   $pp$  collisions with the ATLAS detector*, *Eur. Phys. J. C* **81** (2021) 860, arXiv: [2011.09308 \[hep-ex\]](#).
- [278] ATLAS Collaboration, *Search for dark matter produced in association with a single top quark and an energetic  $W$  boson in  $\sqrt{s} = 13\text{ TeV}$   $pp$  collisions with the ATLAS detector*, *Eur. Phys. J. C* **83** (2023) 603, arXiv: [2211.13138 \[hep-ex\]](#).
- [279] ATLAS Collaboration, *Search for charged Higgs bosons decaying into a top quark and a bottom quark at  $\sqrt{s} = 13\text{ TeV}$  with the ATLAS detector*, *JHEP* **06** (2021) 145, arXiv: [2102.10076 \[hep-ex\]](#).
- [280] ATLAS Collaboration, *Combination and summary of ATLAS dark matter searches interpreted in a 2HDM with a pseudo-scalar mediator using  $139\text{fb}^{-1}$  of  $\sqrt{s} = 13\text{ TeV}$   $pp$  collision data*, (2023), arXiv: [2306.00641 \[hep-ex\]](#).
- [281] ATLAS Collaboration, *Measurement of Higgs boson production in the diphoton decay channel in  $pp$  collisions at center-of-mass energies of 7 and 8 TeV with the ATLAS detector*, *Phys. Rev. D* **90** (2014) 112015, arXiv: [1408.7084 \[hep-ex\]](#).
- [282] M. Zaazoua, L. Truong, K. A. Assamagan and F. Fassi, *Higgs Portal Vector Dark Matter Interpretation: Review of Effective Field Theory Approach and Ultraviolet Complete Models*, *LHEP* **2022** (2022) 270, arXiv: [2107.01252 \[hep-ph\]](#).
- [283] G. Arcadi, A. Djouadi and M. Kado, *The Higgs-portal for vector dark matter and the effective field theory approach: A reappraisal*, *Phys. Lett. B* **805** (2020) 135427, arXiv: [2001.10750 \[hep-ph\]](#).
- [284] S. Baek, P. Ko and W.-I. Park, *Invisible Higgs decay width versus dark matter direct detection cross section in Higgs portal dark matter models*, *Phys. Rev. D* **90** (2014) 055014, arXiv: [1405.3530 \[hep-ph\]](#).

- [285] PandaX-4T Collaboration, *Dark Matter Search Results from the PandaX-4T Commissioning Run*, *Phys. Rev. Lett.* **127** (2021) 261802, arXiv: [2107.13438 \[hep-ex\]](#).
- [286] DarkSide Collaboration, *Low-Mass Dark Matter Search with the DarkSide-50 Experiment*, *Phys. Rev. Lett.* **121** (2018) 081307, arXiv: [1802.06994 \[astro-ph.HE\]](#).
- [287] J. Billard, E. Figueroa-Feliciano and L. Strigari, *Implication of neutrino backgrounds on the reach of next generation dark matter direct detection experiments*, *Phys. Rev. D* **89** (2014) 023524, arXiv: [1307.5458 \[hep-ph\]](#).
- [288] F. Ruppin, J. Billard, E. Figueroa-Feliciano and L. Strigari, *Complementarity of dark matter detectors in light of the neutrino background*, *Phys. Rev. D* **90** (2014) 083510, arXiv: [1408.3581 \[hep-ph\]](#).
- [289] M. J. Strassler and K. M. Zurek, *Echoes of a hidden valley at hadron colliders*, *Phys. Lett. B* **651** (2007) 374, arXiv: [hep-ph/0604261](#).
- [290] M. J. Strassler and K. M. Zurek, *Discovering the Higgs through highly-displaced vertices*, *Phys. Lett. B* **661** (2008) 263, arXiv: [hep-ph/0605193](#).
- [291] T. Han, Z. Si, K. M. Zurek and M. J. Strassler, *Phenomenology of hidden valleys at hadron colliders*, *JHEP* **07** (2008) 008, arXiv: [0712.2041 \[hep-ph\]](#).
- [292] P. Schwaller, D. Stolarski and A. Weiler, *Emerging Jets*, *JHEP* **05** (2015) 059, arXiv: [1502.05409 \[hep-ph\]](#).
- [293] ATLAS Collaboration, *Search for non-resonant production of semi-visible jets using Run 2 data in ATLAS*, *Phys. Lett. B* **848** (2024) 138324, arXiv: [2305.18037 \[hep-ex\]](#).
- [294] ATLAS Collaboration, *Search for Resonant Production of Dark Quarks in the Dijet Final State with the ATLAS Detector*, *JHEP* **02** (2024) 128, arXiv: [2311.03944 \[hep-ex\]](#).
- [295] T. Cohen, M. Lisanti, H. K. Lou and S. Mishra-Sharma, *LHC Searches for Dark Sector Showers*, *JHEP* **11** (2017) 196, arXiv: [1707.05326 \[hep-ph\]](#).
- [296] G. Albouy et al., *Theory, phenomenology, and experimental avenues for dark showers: a Snowmass 2021 report*, *Eur. Phys. J. C* **82** (2022) 1132, arXiv: [2203.09503 \[hep-ph\]](#).
- [297] M. Park and M. Zhang, *Tagging a jet from a dark sector with jet substructures at colliders*, *Phys. Rev. D* **100** (2019) 115009, arXiv: [1712.09279 \[hep-ph\]](#).
- [298] C. A. Stephan, *Almost-commutative geometries beyond the standard model*, *J. Phys. A* **39** (2006) 9657, arXiv: [hep-th/0509213](#).
- [299] F. Sannino and K. Tuominen, *Orientifold theory dynamics and symmetry breaking*, *Phys. Rev. D* **71** (2005) 051901, arXiv: [hep-ph/0405209](#).
- [300] R. N. Mohapatra and J. C. Pati, *Left-right gauge symmetry and an "isoconjugate" model of CP violation*, *Phys. Rev. D* **11** (1975) 566.
- [301] E. Farhi and R. L. Jaffe, *Strange matter*, *Phys. Rev. D* **30** (1984) 2379.
- [302] S. R. Coleman, *Q-balls*, *Nucl. Phys. B* **262** (1985) 263, Addendum: *Nucl. Phys. B* **269** (1986) 744.

- [303] P. A. M. Dirac, *The Theory of Magnetic Poles*, *Phys. Rev.* **74** (1948) 817.
- [304] ATLAS Collaboration, *Search for heavy long-lived multi-charged particles in the full LHC Run 2  $pp$  collision data at  $\sqrt{s} = 13$  TeV using the ATLAS detector*, *Phys. Lett. B* **847** (2023) 138316, arXiv: [2303.13613](#) [[hep-ex](#)].
- [305] ATLAS Collaboration, *Search for magnetic monopoles and stable particles with high electric charges in  $\sqrt{s} = 13$  TeV  $pp$  collisions with the ATLAS detector*, *JHEP* **11** (2023) 112, arXiv: [2308.04835](#) [[hep-ex](#)].
- [306] W.-Y. Song and W. Taylor, *Pair production of magnetic monopoles and stable high-electric-charge objects in proton–proton and heavy-ion collisions*, *J. Phys. G* **49** (2022) 045002, arXiv: [2107.10789](#) [[hep-ph](#)].
- [307] N. Arkani-Hamed, S. Dimopoulos and G. Dvali, *The Hierarchy problem and new dimensions at a millimeter*, *Phys. Lett. B* **429** (1998) 263, arXiv: [hep-ph/9803315](#).
- [308] L. Randall and R. Sundrum, *Large Mass Hierarchy from a Small Extra Dimension*, *Phys. Rev. Lett.* **83** (1999) 3370, arXiv: [hep-ph/9905221](#).
- [309] ATLAS Collaboration, *Search for new phenomena in events with a photon and missing transverse momentum in  $pp$  collisions at  $\sqrt{s} = 13$  TeV with the ATLAS detector*, *JHEP* **06** (2016) 059, arXiv: [1604.01306](#) [[hep-ex](#)].
- [310] B. C. Allanach et al., *Exploring Small Extra Dimensions at the Large Hadron Collider*, *JHEP* **12** (2002) 039, arXiv: [hep-ph/0211205](#).
- [311] ATLAS Collaboration, *Search for heavy particles decaying into top-quark pairs using lepton-plus-jets events in proton–proton collisions at  $\sqrt{s} = 13$  TeV with the ATLAS detector*, *Eur. Phys. J. C* **78** (2018) 565, arXiv: [1804.10823](#) [[hep-ex](#)].
- [312] ATLAS Collaboration, *Search for resonances decaying into photon pairs in  $139\text{ fb}^{-1}$  of  $pp$  collisions at  $\sqrt{s} = 13$  TeV with the ATLAS detector*, *Phys. Lett. B* **822** (2021) 136651, arXiv: [2102.13405](#) [[hep-ex](#)].
- [313] ATLAS Collaboration, *Search for resonant pair production of Higgs bosons in the  $b\bar{b}b\bar{b}$  final state using  $pp$  collisions at  $\sqrt{s} = 13$  TeV with the ATLAS detector*, *Phys. Rev. D* **105** (2022) 092002, arXiv: [2202.07288](#) [[hep-ex](#)].
- [314] ATLAS Collaboration, *Summary of diboson resonance searches at the ATLAS experiment using full Run-2 data*, ATL-PHYS-PUB-2023-007, 2023, URL: <https://cds.cern.ch/record/2853753/>.
- [315] G. F. Giudice and M. McCullough, *A Clockwork Theory*, *JHEP* **02** (2017) 036, arXiv: [1610.07962](#) [[hep-ph](#)].
- [316] G. F. Giudice, Y. Kats, M. McCullough, R. Torre and A. Urbano, *Clockwork/linear dilaton: structure and phenomenology*, *JHEP* **06** (2018) 009, arXiv: [1711.08437](#) [[hep-ph](#)].
- [317] ATLAS Collaboration, *Search for periodic signals in the dielectron and diphoton invariant mass spectra using  $139\text{ fb}^{-1}$  of  $pp$  collisions at  $\sqrt{s} = 13$  TeV with the ATLAS detector*, *JHEP* **10** (2023) 079, arXiv: [2305.10894](#) [[hep-ex](#)].
- [318] J. Morlet, G. Arens, E. Fourgeau and D. Giard, *Wave propagation and sampling theory; Part I, Complex signal and scattering in multilayered media*, *Geophysics* **47** (1982) 203, ISSN: 0016-8033.

- [319] D. M. Gingrich, *Quantum black holes with charge, color and spin at the LHC*, *J. Phys. G* **37** (2010) 105008, arXiv: [0912.0826 \[hep-ph\]](#).
- [320] X. Calmet, W. Gong and S. D. H. Hsu, *Colorful quantum black holes at the LHC*, *Phys. Lett. B* **668** (2008) 20, arXiv: [0806.4605 \[hep-ph\]](#).
- [321] L. A. Anchordoqui, J. L. Feng, H. Goldberg and A. D. Shapere, *Black holes from cosmic rays: Probes of extra dimensions and new limits on TeV-scale gravity*, *Phys. Rev. D* **65** (2002) 124027, arXiv: [hep-ph/0112247](#).
- [322] D.-C. Dai et al., *BlackMax: A black-hole event generator with rotation, recoil, split branes, and brane tension*, *Phys. Rev. D* **77** (2008) 076007, arXiv: [0711.3012 \[hep-ph\]](#).
- [323] ATLAS Collaboration, *Search for quantum black hole production in lepton+jet final states using proton–proton collisions at  $\sqrt{s} = 13$  TeV with the ATLAS detector*, *Phys. Rev. D* **109** (2024) 032010, arXiv: [2307.14967 \[hep-ex\]](#).
- [324] D. M. Gingrich, *Monte Carlo event generator for black hole production and decay in proton-proton collisions - QBH version 1.02*, *Comput. Phys. Commun.* **181** (2010) 1917, arXiv: [0911.5370 \[hep-ph\]](#).
- [325] ATLAS Collaboration, *Summary Plots for Heavy Particle Searches and Long-lived Particle Searches – March 2023*, ATL-PHYS-PUB-2023-008, 2023, URL: <https://cds.cern.ch/record/2853754>.
- [326] ATLAS Collaboration, *Search for new phenomena in the dijet mass distribution using pp collision data at  $\sqrt{s} = 8$  TeV with the ATLAS detector*, *Phys. Rev. D* **91** (2015) 052007, arXiv: [1407.1376 \[hep-ex\]](#).
- [327] ATLAS Collaboration, *Search for high-mass dilepton resonances in pp collisions at  $\sqrt{s} = 8$  TeV with the ATLAS detector*, *Phys. Rev. D* **90** (2014) 052005, arXiv: [1405.4123 \[hep-ex\]](#).
- [328] ATLAS Collaboration, *Search for type-III seesaw heavy leptons in pp collisions at  $\sqrt{s} = 8$  TeV with the ATLAS Detector*, *Phys. Rev. D* **92** (2015) 032001, arXiv: [1506.01839 \[hep-ex\]](#).
- [329] ATLAS Collaboration, *Search for pair and single production of new heavy quarks that decay to a Z boson and a third-generation quark in pp collisions at  $\sqrt{s} = 8$  TeV with the ATLAS detector*, *JHEP* **11** (2014) 104, arXiv: [1409.5500 \[hep-ex\]](#).
- [330] ATLAS Collaboration, *Searches for scalar leptoquarks in pp collisions at  $\sqrt{s} = 8$  TeV with the ATLAS detector*, *Eur. Phys. J. C* **76** (2016) 5, arXiv: [1508.04735 \[hep-ex\]](#).
- [331] ATLAS Collaboration, *Search for the lepton flavor violating decay  $Z \rightarrow e\mu$  in pp collisions at  $\sqrt{s} = 8$  TeV with the ATLAS detector*, *Phys. Rev. D* **90** (2014) 072010, arXiv: [1408.5774 \[hep-ex\]](#).
- [332] ATLAS Collaboration, *Search for long-lived neutral particles decaying into lepton jets in proton–proton collisions at  $\sqrt{s} = 8$  TeV with the ATLAS detector*, *JHEP* **11** (2014) 088, arXiv: [1409.0746 \[hep-ex\]](#).
- [333] ATLAS Collaboration, *Constraints on new phenomena via Higgs boson couplings and invisible decays with the ATLAS detector*, *JHEP* **11** (2015) 206, arXiv: [1509.00672 \[hep-ex\]](#).

- [334] ATLAS Collaboration, *Search for heavy long-lived multi-charged particles in pp collisions at  $\sqrt{s} = 8$  TeV using the ATLAS detector*, *Eur. Phys. J. C* **75** (2015) 362, arXiv: [1504.04188](https://arxiv.org/abs/1504.04188) [hep-ex].
- [335] ATLAS Collaboration, *Search for new phenomena in final states with an energetic jet and large missing transverse momentum in pp collisions at  $\sqrt{s} = 8$  TeV with the ATLAS detector*, *Eur. Phys. J. C* **75** (2015) 299, arXiv: [1502.01518](https://arxiv.org/abs/1502.01518) [hep-ex],  
Erratum: *Eur. Phys. J. C* **75** (2015) 408.
- [336] ATLAS Collaboration, *ATLAS Computing Acknowledgements*, ATL-SOFT-PUB-2023-001, 2023, URL: <https://cds.cern.ch/record/2869272>.



## The ATLAS Collaboration

G. Aad <sup>103</sup>, E. Aakvaag <sup>16</sup>, B. Abbott <sup>121</sup>, K. Abeling <sup>55</sup>, N.J. Abicht <sup>49</sup>, S.H. Abidi <sup>29</sup>, M. Aboeela <sup>44</sup>, A. Aboulhorma <sup>35e</sup>, H. Abramowicz <sup>152</sup>, H. Abreu <sup>151</sup>, Y. Abulaiti <sup>118</sup>, B.S. Acharya <sup>69a,69b,1</sup>, A. Ackermann <sup>63a</sup>, C. Adam Bourdarios <sup>4</sup>, L. Adamczyk <sup>86a</sup>, S.V. Addepalli <sup>26</sup>, M.J. Addison <sup>102</sup>, J. Adelman <sup>116</sup>, A. Adiguzel <sup>21c</sup>, T. Adye <sup>135</sup>, A.A. Affolder <sup>137</sup>, Y. Afik <sup>39</sup>, M.N. Agaras <sup>13</sup>, J. Agarwala <sup>73a,73b</sup>, A. Aggarwal <sup>101</sup>, C. Agheorghiesei <sup>27c</sup>, A. Ahmad <sup>36</sup>, F. Ahmadov <sup>38,y</sup>, W.S. Ahmed <sup>105</sup>, S. Ahuja <sup>96</sup>, X. Ai <sup>62e</sup>, G. Aielli <sup>76a,76b</sup>, A. Aikot <sup>164</sup>, M. Ait Tamlihat <sup>35e</sup>, B. Aitbenchikh <sup>35a</sup>, I. Aizenberg <sup>170</sup>, M. Akbiyik <sup>101</sup>, T.P.A. Åkesson <sup>99</sup>, A.V. Akimov <sup>37</sup>, D. Akiyama <sup>169</sup>, N.N. Akolkar <sup>24</sup>, S. Aktas <sup>21a</sup>, K. Al Houry <sup>41</sup>, G.L. Alberghi <sup>23b</sup>, J. Albert <sup>166</sup>, P. Albicocco <sup>53</sup>, G.L. Albouy <sup>60</sup>, S. Alderweireldt <sup>52</sup>, Z.L. Alegria <sup>122</sup>, M. Aleksa <sup>36</sup>, I.N. Aleksandrov <sup>38</sup>, C. Alexa <sup>27b</sup>, T. Alexopoulos <sup>10</sup>, F. Alfonsi <sup>23b</sup>, M. Algren <sup>56</sup>, M. Alhroob <sup>142</sup>, B. Ali <sup>133</sup>, H.M.J. Ali <sup>92</sup>, S. Ali <sup>149</sup>, S.W. Alibocus <sup>93</sup>, M. Aliev <sup>33c</sup>, G. Alimonti <sup>71a</sup>, W. Alkakhri <sup>55</sup>, C. Allaire <sup>66</sup>, B.M.M. Allbrooke <sup>147</sup>, J.F. Allen <sup>52</sup>, C.A. Allendes Flores <sup>138f</sup>, P.P. Allport <sup>20</sup>, A. Aloisio <sup>72a,72b</sup>, F. Alonso <sup>91</sup>, C. Alpigiani <sup>139</sup>, M. Alvarez Estevez <sup>100</sup>, A. Alvarez Fernandez <sup>101</sup>, M. Alves Cardoso <sup>56</sup>, M.G. Alviggi <sup>72a,72b</sup>, M. Aly <sup>102</sup>, Y. Amaral Coutinho <sup>83b</sup>, A. Ambler <sup>105</sup>, C. Amelung <sup>36</sup>, M. Amerl <sup>102</sup>, C.G. Ames <sup>110</sup>, D. Amidei <sup>107</sup>, K.J. Amirie <sup>156</sup>, S.P. Amor Dos Santos <sup>131a</sup>, K.R. Amos <sup>164</sup>, S. An <sup>84</sup>, V. Ananiev <sup>126</sup>, C. Anastopoulos <sup>140</sup>, T. Andeen <sup>11</sup>, J.K. Anders <sup>36</sup>, S.Y. Andrean <sup>47a,47b</sup>, A. Andreazza <sup>71a,71b</sup>, S. Angelidakis <sup>9</sup>, A. Angerami <sup>41,aa</sup>, A.V. Anisenkov <sup>37</sup>, A. Annovi <sup>74a</sup>, C. Antel <sup>56</sup>, M.T. Anthony <sup>140</sup>, E. Antipov <sup>146</sup>, M. Antonelli <sup>53</sup>, F. Anulli <sup>75a</sup>, M. Aoki <sup>84</sup>, T. Aoki <sup>154</sup>, J.A. Aparisi Pozo <sup>164</sup>, M.A. Aparo <sup>147</sup>, L. Aperio Bella <sup>48</sup>, C. Appelt <sup>18</sup>, A. Apyan <sup>26</sup>, S.J. Arbiol Val <sup>87</sup>, C. Arcangeletti <sup>53</sup>, A.T.H. Arce <sup>51</sup>, E. Arena <sup>93</sup>, J-F. Arguin <sup>109</sup>, S. Argyropoulos <sup>54</sup>, J.-H. Arling <sup>48</sup>, O. Arnaez <sup>4</sup>, H. Arnold <sup>115</sup>, G. Artoni <sup>75a,75b</sup>, H. Asada <sup>112</sup>, K. Asai <sup>119</sup>, S. Asai <sup>154</sup>, N.A. Asbah <sup>36</sup>, K. Assamagan <sup>29</sup>, R. Astalos <sup>28a</sup>, K.S.V. Astrand <sup>99</sup>, S. Atashi <sup>160</sup>, R.J. Atkin <sup>33a</sup>, M. Atkinson <sup>163</sup>, H. Atmani <sup>35f</sup>, P.A. Atlasiddha <sup>129</sup>, K. Augsten <sup>133</sup>, S. Auricchio <sup>72a,72b</sup>, A.D. Auriol <sup>20</sup>, V.A. Austrup <sup>102</sup>, G. Avolio <sup>36</sup>, K. Axiotis <sup>56</sup>, G. Azuelos <sup>109,ae</sup>, D. Babal <sup>28b</sup>, H. Bachacou <sup>136</sup>, K. Bachas <sup>153,p</sup>, A. Bachiu <sup>34</sup>, F. Backman <sup>47a,47b</sup>, A. Badea <sup>39</sup>, T.M. Baer <sup>107</sup>, P. Bagnaia <sup>75a,75b</sup>, M. Bahmani <sup>18</sup>, D. Bahner <sup>54</sup>, K. Bai <sup>124</sup>, J.T. Baines <sup>135</sup>, L. Baines <sup>95</sup>, O.K. Baker <sup>173</sup>, E. Bakos <sup>15</sup>, D. Bakshi Gupta <sup>8</sup>, V. Balakrishnan <sup>121</sup>, R. Balasubramanian <sup>115</sup>, E.M. Baldin <sup>37</sup>, P. Balek <sup>86a</sup>, E. Ballabene <sup>23b,23a</sup>, F. Balli <sup>136</sup>, L.M. Baltos <sup>63a</sup>, W.K. Balunas <sup>32</sup>, J. Balz <sup>101</sup>, E. Banas <sup>87</sup>, M. Bandieramonte <sup>130</sup>, A. Bandyopadhyay <sup>24</sup>, S. Bansal <sup>24</sup>, L. Barak <sup>152</sup>, M. Barakat <sup>48</sup>, E.L. Barberio <sup>106</sup>, D. Barberis <sup>57b,57a</sup>, M. Barbero <sup>103</sup>, M.Z. Barel <sup>115</sup>, K.N. Barends <sup>33a</sup>, T. Barillari <sup>111</sup>, M-S. Barisits <sup>36</sup>, T. Barklow <sup>144</sup>, P. Baron <sup>123</sup>, D.A. Baron Moreno <sup>102</sup>, A. Baroncelli <sup>62a</sup>, G. Barone <sup>29</sup>, A.J. Barr <sup>127</sup>, J.D. Barr <sup>97</sup>, F. Barreiro <sup>100</sup>, J. Barreiro Guimarães da Costa <sup>14a</sup>, U. Barron <sup>152</sup>, M.G. Barros Teixeira <sup>131a</sup>, S. Barsov <sup>37</sup>, F. Bartels <sup>63a</sup>, R. Bartoldus <sup>144</sup>, A.E. Barton <sup>92</sup>, P. Bartos <sup>28a</sup>, A. Basan <sup>101</sup>, M. Baselga <sup>49</sup>, A. Bassalat <sup>66,b</sup>, M.J. Basso <sup>157a</sup>, R. Bate <sup>165</sup>, R.L. Bates <sup>59</sup>, S. Batlamous <sup>100</sup>, B. Batool <sup>142</sup>, M. Battaglia <sup>137</sup>, D. Battulga <sup>18</sup>, M. Baucé <sup>75a,75b</sup>, M. Bauer <sup>36</sup>, P. Bauer <sup>24</sup>, L.T. Bazzano Hurrell <sup>30</sup>, J.B. Beacham <sup>51</sup>, T. Beau <sup>128</sup>, J.Y. Beaucamp <sup>91</sup>, P.H. Beauchemin <sup>159</sup>, P. Bechtel <sup>24</sup>, H.P. Beck <sup>19,o</sup>, K. Becker <sup>168</sup>, A.J. Beddall <sup>82</sup>, V.A. Bednyakov <sup>38</sup>, C.P. Bee <sup>146</sup>, L.J. Beemster <sup>15</sup>, T.A. Beermann <sup>36</sup>, M. Begalli <sup>83d</sup>, M. Begel <sup>29</sup>, A. Behera <sup>146</sup>, J.K. Behr <sup>48</sup>, J.F. Beirer <sup>36</sup>, F. Beisiegel <sup>24</sup>, M. Belfkir <sup>117b</sup>, G. Bella <sup>152</sup>, L. Bellagamba <sup>23b</sup>, A. Bellerive <sup>34</sup>, P. Bellos <sup>20</sup>, K. Beloborodov <sup>37</sup>, D. Bencheikroun <sup>35a</sup>, F. Bendebba <sup>35a</sup>, Y. Benhammou <sup>152</sup>,



K.C. Benkendorfer <sup>61</sup>, L. Beresford <sup>48</sup>, M. Beretta <sup>53</sup>, E. Bergeaas Kuutmann <sup>162</sup>, N. Berger <sup>4</sup>,  
 B. Bergmann <sup>133</sup>, J. Beringer <sup>17a</sup>, G. Bernardi <sup>5</sup>, C. Bernius <sup>144</sup>, F.U. Bernlochner <sup>24</sup>,  
 F. Bernon <sup>36,103</sup>, A. Berrocal Guardia <sup>13</sup>, T. Berry <sup>96</sup>, P. Berta <sup>134</sup>, A. Berthold <sup>50</sup>, S. Bethke <sup>111</sup>,  
 A. Betti <sup>75a,75b</sup>, A.J. Bevan <sup>95</sup>, N.K. Bhalla <sup>54</sup>, M. Bhamjee <sup>33c</sup>, S. Bhatta <sup>146</sup>,  
 D.S. Bhattacharya <sup>167</sup>, P. Bhattarai <sup>144</sup>, K.D. Bhide <sup>54</sup>, V.S. Bhopatkar <sup>122</sup>, R.M. Bianchi <sup>130</sup>,  
 G. Bianco <sup>23b,23a</sup>, O. Biebel <sup>110</sup>, R. Bielski <sup>124</sup>, M. Biglietti <sup>77a</sup>, C.S. Billingsley <sup>44</sup>, M. Bindi <sup>55</sup>,  
 A. Bingul <sup>21b</sup>, C. Bini <sup>75a,75b</sup>, A. Biondini <sup>93</sup>, C.J. Birch-sykes <sup>102</sup>, G.A. Bird <sup>32</sup>, M. Birman <sup>170</sup>,  
 M. Biros <sup>134</sup>, S. Biryukov <sup>147</sup>, T. Bisanz <sup>49</sup>, E. Bisceglie <sup>43b,43a</sup>, J.P. Biswal <sup>135</sup>, D. Biswas <sup>142</sup>,  
 I. Bloch <sup>48</sup>, A. Blue <sup>59</sup>, U. Blumenschein <sup>95</sup>, J. Blumenthal <sup>101</sup>, V.S. Bobrovnikov <sup>37</sup>,  
 M. Boehler <sup>54</sup>, B. Boehm <sup>167</sup>, D. Bogavac <sup>36</sup>, A.G. Bogdanchikov <sup>37</sup>, C. Bohm <sup>47a</sup>,  
 V. Boisvert <sup>96</sup>, P. Bokan <sup>36</sup>, T. Bold <sup>86a</sup>, M. Bomben <sup>5</sup>, M. Bona <sup>95</sup>, M. Boonekamp <sup>136</sup>,  
 C.D. Booth <sup>96</sup>, A.G. Borbély <sup>59</sup>, I.S. Bordulev <sup>37</sup>, H.M. Borecka-Bielska <sup>109</sup>, G. Borissov <sup>92</sup>,  
 D. Bortoletto <sup>127</sup>, D. Boscherini <sup>23b</sup>, M. Bosman <sup>13</sup>, J.D. Bossio Sola <sup>36</sup>, K. Bouaouda <sup>35a</sup>,  
 N. Bouchhar <sup>164</sup>, J. Boudreau <sup>130</sup>, E.V. Bouhova-Thacker <sup>92</sup>, D. Boumediene <sup>40</sup>,  
 R. Bouquet <sup>57b,57a</sup>, A. Boveia <sup>120</sup>, J. Boyd <sup>36</sup>, D. Boye <sup>29</sup>, I.R. Boyko <sup>38</sup>, J. Bracinik <sup>20</sup>,  
 N. Brahimí <sup>4</sup>, G. Brandt <sup>172</sup>, O. Brandt <sup>32</sup>, F. Braren <sup>48</sup>, B. Brau <sup>104</sup>, J.E. Brau <sup>124</sup>,  
 R. Brenner <sup>170</sup>, L. Brenner <sup>115</sup>, R. Brenner <sup>162</sup>, S. Bressler <sup>170</sup>, D. Britton <sup>59</sup>, D. Britzger <sup>111</sup>,  
 I. Brock <sup>24</sup>, G. Brooijmans <sup>41</sup>, E. Brost <sup>29</sup>, L.M. Brown <sup>166</sup>, L.E. Bruce <sup>61</sup>, T.L. Bruckler <sup>127</sup>,  
 P.A. Bruckman de Renstrom <sup>87</sup>, B. Brüers <sup>48</sup>, A. Bruni <sup>23b</sup>, G. Bruni <sup>23b</sup>, M. Bruschi <sup>23b</sup>,  
 N. Brusino <sup>75a,75b</sup>, T. Buanes <sup>16</sup>, Q. Buat <sup>139</sup>, D. Buchin <sup>111</sup>, A.G. Buckley <sup>59</sup>, O. Bulekov <sup>37</sup>,  
 B.A. Bullard <sup>144</sup>, S. Burdin <sup>93</sup>, C.D. Burgard <sup>49</sup>, A.M. Burger <sup>36</sup>, B. Burghgrave <sup>8</sup>,  
 O. Burlayenko <sup>54</sup>, J.T.P. Burr <sup>32</sup>, C.D. Burton <sup>11</sup>, J.C. Burzynski <sup>143</sup>, E.L. Busch <sup>41</sup>,  
 V. Büscher <sup>101</sup>, P.J. Bussey <sup>59</sup>, J.M. Butler <sup>25</sup>, C.M. Buttar <sup>59</sup>, J.M. Butterworth <sup>97</sup>,  
 W. Buttinger <sup>135</sup>, C.J. Buxo Vazquez <sup>108</sup>, A.R. Buzykaev <sup>37</sup>, S. Cabrera Urbán <sup>164</sup>,  
 L. Cadamuro <sup>66</sup>, D. Caforio <sup>58</sup>, H. Cai <sup>130</sup>, Y. Cai <sup>14a,14e</sup>, Y. Cai <sup>14c</sup>, V.M.M. Cairo <sup>36</sup>,  
 O. Cakir <sup>3a</sup>, N. Calace <sup>36</sup>, P. Calafiura <sup>17a</sup>, G. Calderini <sup>128</sup>, P. Calfayan <sup>68</sup>, G. Callea <sup>59</sup>,  
 L.P. Caloba <sup>83b</sup>, D. Calvet <sup>40</sup>, S. Calvet <sup>40</sup>, M. Calvetti <sup>74a,74b</sup>, R. Camacho Toro <sup>128</sup>,  
 S. Camarda <sup>36</sup>, D. Camarero Munoz <sup>26</sup>, P. Camarri <sup>76a,76b</sup>, M.T. Camerlingo <sup>72a,72b</sup>,  
 D. Cameron <sup>36</sup>, C. Camincher <sup>166</sup>, M. Campanelli <sup>97</sup>, A. Camplani <sup>42</sup>, V. Canale <sup>72a,72b</sup>,  
 A.C. Canbay <sup>3a</sup>, E. Canonero <sup>96</sup>, J. Cantero <sup>164</sup>, Y. Cao <sup>163</sup>, F. Capocasa <sup>26</sup>, M. Capua <sup>43b,43a</sup>,  
 A. Carbone <sup>71a,71b</sup>, R. Cardarelli <sup>76a</sup>, J.C.J. Cardenas <sup>8</sup>, F. Cardillo <sup>164</sup>, G. Carducci <sup>43b,43a</sup>,  
 T. Carli <sup>36</sup>, G. Carlino <sup>72a</sup>, J.I. Carlotto <sup>13</sup>, B.T. Carlson <sup>130,q</sup>, E.M. Carlson <sup>166,157a</sup>,  
 L. Carminati <sup>71a,71b</sup>, A. Carnelli <sup>136</sup>, M. Carnesale <sup>75a,75b</sup>, S. Caron <sup>114</sup>, E. Carquin <sup>138f</sup>,  
 S. Carrá <sup>71a</sup>, G. Carratta <sup>23b,23a</sup>, A.M. Carroll <sup>124</sup>, T.M. Carter <sup>52</sup>, M.P. Casado <sup>13,i</sup>,  
 M. Caspar <sup>48</sup>, F.L. Castillo <sup>4</sup>, L. Castillo Garcia <sup>13</sup>, V. Castillo Gimenez <sup>164</sup>, N.F. Castro <sup>131a,131e</sup>,  
 A. Catinaccio <sup>36</sup>, J.R. Catmore <sup>126</sup>, T. Cavaliere <sup>4</sup>, V. Cavaliere <sup>29</sup>, N. Cavalli <sup>23b,23a</sup>,  
 Y.C. Cekmecelioglu <sup>48</sup>, E. Celebi <sup>21a</sup>, S. Cella <sup>36</sup>, F. Celli <sup>127</sup>, M.S. Centonze <sup>70a,70b</sup>,  
 V. Cepaitis <sup>56</sup>, K. Cerny <sup>123</sup>, A.S. Cerqueira <sup>83a</sup>, A. Cerri <sup>147</sup>, L. Cerrito <sup>76a,76b</sup>, F. Cerutti <sup>17a</sup>,  
 B. Cervato <sup>142</sup>, A. Cervelli <sup>23b</sup>, G. Cesarini <sup>53</sup>, S.A. Cetin <sup>82</sup>, D. Chakraborty <sup>116</sup>, J. Chan <sup>171</sup>,  
 W.Y. Chan <sup>154</sup>, J.D. Chapman <sup>32</sup>, E. Chapon <sup>136</sup>, B. Chargeishvili <sup>150b</sup>, D.G. Charlton <sup>20</sup>,  
 M. Chatterjee <sup>19</sup>, C. Chauhan <sup>134</sup>, Y. Che <sup>14c</sup>, S. Chekanov <sup>6</sup>, S.V. Chekulaev <sup>157a</sup>,  
 G.A. Chelkov <sup>38,a</sup>, A. Chen <sup>107</sup>, B. Chen <sup>152</sup>, B. Chen <sup>166</sup>, H. Chen <sup>14c</sup>, H. Chen <sup>29</sup>,  
 J. Chen <sup>62c</sup>, J. Chen <sup>143</sup>, M. Chen <sup>127</sup>, S. Chen <sup>154</sup>, S.J. Chen <sup>14c</sup>, X. Chen <sup>62c,136</sup>,  
 X. Chen <sup>14b,ad</sup>, Y. Chen <sup>62a</sup>, C.L. Cheng <sup>171</sup>, H.C. Cheng <sup>64a</sup>, S. Cheong <sup>144</sup>, A. Cheplakov <sup>38</sup>,  
 E. Cheremushkina <sup>48</sup>, E. Cherepanova <sup>115</sup>, R. Cherkaoui El Moursli <sup>35e</sup>, E. Cheu <sup>7</sup>, K. Cheung <sup>65</sup>,  
 L. Chevalier <sup>136</sup>, V. Chiarella <sup>53</sup>, G. Chiarelli <sup>74a</sup>, N. Chiedde <sup>103</sup>, G. Chiodini <sup>70a</sup>,  
 A.S. Chisholm <sup>20</sup>, A. Chitan <sup>27b</sup>, M. Chitishvili <sup>164</sup>, M.V. Chizhov <sup>38</sup>, K. Choi <sup>11</sup>, Y. Chou <sup>139</sup>,

E.Y.S. Chow <sup>id114</sup>, K.L. Chu <sup>id170</sup>, M.C. Chu <sup>id64a</sup>, X. Chu <sup>id14a,14e</sup>, J. Chudoba <sup>id132</sup>,  
 J.J. Chwastowski <sup>id87</sup>, D. Cieri <sup>id111</sup>, K.M. Ciesla <sup>id86a</sup>, V. Cindro <sup>id94</sup>, A. Ciocio <sup>id17a</sup>, F. Ciroto <sup>id72a,72b</sup>,  
 Z.H. Citron <sup>id170</sup>, M. Citterio <sup>id71a</sup>, D.A. Ciubotaru <sup>id27b</sup>, A. Clark <sup>id56</sup>, P.J. Clark <sup>id52</sup>, C. Clarry <sup>id156</sup>,  
 J.M. Clavijo Columbie <sup>id48</sup>, S.E. Clawson <sup>id48</sup>, C. Clement <sup>id47a,47b</sup>, J. Clercx <sup>id48</sup>, Y. Coadou <sup>id103</sup>,  
 M. Cobal <sup>id69a,69c</sup>, A. Coccaro <sup>id57b</sup>, R.F. Coelho Barrue <sup>id131a</sup>, R. Coelho Lopes De Sa <sup>id104</sup>,  
 S. Coelli <sup>id71a</sup>, B. Cole <sup>id41</sup>, J. Collot <sup>id60</sup>, P. Conde Muiño <sup>id131a,131g</sup>, M.P. Connell <sup>id33c</sup>,  
 S.H. Connell <sup>id33c</sup>, E.I. Conroy <sup>id127</sup>, F. Conventi <sup>id72a,af</sup>, H.G. Cooke <sup>id20</sup>, A.M. Cooper-Sarkar <sup>id127</sup>,  
 F.A. Corchia <sup>id23b,23a</sup>, A. Cordeiro Oudot Choi <sup>id128</sup>, L.D. Corpe <sup>id40</sup>, M. Corradi <sup>id75a,75b</sup>,  
 F. Corriveau <sup>id105,w</sup>, A. Cortes-Gonzalez <sup>id18</sup>, M.J. Costa <sup>id164</sup>, F. Costanza <sup>id4</sup>, D. Costanzo <sup>id140</sup>,  
 B.M. Cote <sup>id120</sup>, G. Cowan <sup>id96</sup>, K. Cranmer <sup>id171</sup>, D. Cremonini <sup>id23b,23a</sup>, S. Crépe-Renaudin <sup>id60</sup>,  
 F. Crescioli <sup>id128</sup>, M. Cristinziani <sup>id142</sup>, M. Cristoforetti <sup>id78a,78b</sup>, V. Croft <sup>id115</sup>, J.E. Crosby <sup>id122</sup>,  
 G. Crosetti <sup>id43b,43a</sup>, A. Cueto <sup>id100</sup>, H. Cui <sup>id14a,14e</sup>, Z. Cui <sup>id7</sup>, W.R. Cunningham <sup>id59</sup>, F. Curcio <sup>id164</sup>,  
 J.R. Curran <sup>id52</sup>, P. Czodrowski <sup>id36</sup>, M.M. Czurylo <sup>id36</sup>, M.J. Da Cunha Sargedas De Sousa <sup>id57b,57a</sup>,  
 J.V. Da Fonseca Pinto <sup>id83b</sup>, C. Da Via <sup>id102</sup>, W. Dabrowski <sup>id86a</sup>, T. Dado <sup>id49</sup>, S. Dahbi <sup>id149</sup>,  
 T. Dai <sup>id107</sup>, D. Dal Santo <sup>id19</sup>, C. Dallapiccola <sup>id104</sup>, M. Dam <sup>id42</sup>, G. D'amen <sup>id29</sup>, V. D'Amico <sup>id110</sup>,  
 J. Damp <sup>id101</sup>, J.R. Dandoy <sup>id34</sup>, M. Danninger <sup>id143</sup>, V. Dao <sup>id36</sup>, G. Darbo <sup>id57b</sup>, S.J. Das <sup>id29,ag</sup>,  
 F. Dattola <sup>id48</sup>, S. D'Auria <sup>id71a,71b</sup>, A. D'avanzo <sup>id72a,72b</sup>, C. David <sup>id33a</sup>, T. Davidek <sup>id134</sup>,  
 B. Davis-Purcell <sup>id34</sup>, I. Dawson <sup>id95</sup>, H.A. Day-hall <sup>id133</sup>, K. De <sup>id8</sup>, R. De Asmundis <sup>id72a</sup>,  
 N. De Biase <sup>id48</sup>, S. De Castro <sup>id23b,23a</sup>, N. De Groot <sup>id114</sup>, P. de Jong <sup>id115</sup>, H. De la Torre <sup>id116</sup>,  
 A. De Maria <sup>id14c</sup>, A. De Salvo <sup>id75a</sup>, U. De Sanctis <sup>id76a,76b</sup>, F. De Santis <sup>id70a,70b</sup>, A. De Santo <sup>id147</sup>,  
 J.B. De Vivie De Regie <sup>id60</sup>, D.V. Dedovich <sup>id38</sup>, J. Degens <sup>id93</sup>, A.M. Deiana <sup>id44</sup>, F. Del Corso <sup>id23b,23a</sup>,  
 J. Del Peso <sup>id100</sup>, F. Del Rio <sup>id63a</sup>, L. Delagrangé <sup>id128</sup>, F. Deliot <sup>id136</sup>, C.M. Delitzsch <sup>id49</sup>,  
 M. Della Pietra <sup>id72a,72b</sup>, D. Della Volpe <sup>id56</sup>, A. Dell'Acqua <sup>id36</sup>, L. Dell'Asta <sup>id71a,71b</sup>, M. Delmastro <sup>id4</sup>,  
 P.A. Delsart <sup>id60</sup>, S. Demers <sup>id173</sup>, M. Demichev <sup>id38</sup>, S.P. Denisov <sup>id37</sup>, L. D'Eramo <sup>id40</sup>,  
 D. Derendarz <sup>id87</sup>, F. Derue <sup>id128</sup>, P. Dervan <sup>id93</sup>, K. Desch <sup>id24</sup>, C. Deutsch <sup>id24</sup>, F.A. Di Bello <sup>id57b,57a</sup>,  
 A. Di Ciaccio <sup>id76a,76b</sup>, L. Di Ciaccio <sup>id4</sup>, A. Di Domenico <sup>id75a,75b</sup>, C. Di Donato <sup>id72a,72b</sup>,  
 A. Di Girolamo <sup>id36</sup>, G. Di Gregorio <sup>id36</sup>, A. Di Luca <sup>id78a,78b</sup>, B. Di Micco <sup>id77a,77b</sup>, R. Di Nardo <sup>id77a,77b</sup>,  
 M. Diamantopoulou <sup>id34</sup>, F.A. Dias <sup>id115</sup>, T. Dias Do Vale <sup>id143</sup>, M.A. Diaz <sup>id138a,138b</sup>,  
 F.G. Diaz Capriles <sup>id24</sup>, M. Didenko <sup>id164</sup>, E.B. Diehl <sup>id107</sup>, S. Díez Cornell <sup>id48</sup>, C. Diez Pardo <sup>id142</sup>,  
 C. Dimitriadi <sup>id162,24</sup>, A. Dimitrievska <sup>id20</sup>, J. Dingfelder <sup>id24</sup>, I-M. Dinu <sup>id27b</sup>, S.J. Dittmeier <sup>id63b</sup>,  
 F. Dittus <sup>id36</sup>, M. Divisek <sup>id134</sup>, F. Djama <sup>id103</sup>, T. Djobava <sup>id150b</sup>, C. Doglioni <sup>id102,99</sup>, A. Dohnalova <sup>id28a</sup>,  
 J. Dolejsi <sup>id134</sup>, Z. Dolezal <sup>id134</sup>, K.M. Dona <sup>id39</sup>, M. Donadelli <sup>id83c</sup>, B. Dong <sup>id108</sup>, J. Donini <sup>id40</sup>,  
 A. D'Onofrio <sup>id72a,72b</sup>, M. D'Onofrio <sup>id93</sup>, J. Dopke <sup>id135</sup>, A. Doria <sup>id72a</sup>, N. Dos Santos Fernandes <sup>id131a</sup>,  
 P. Dougan <sup>id102</sup>, M.T. Dova <sup>id91</sup>, A.T. Doyle <sup>id59</sup>, M.A. Draguet <sup>id127</sup>, E. Dreyer <sup>id170</sup>,  
 I. Drivas-koulouris <sup>id10</sup>, M. Drnevich <sup>id118</sup>, M. Drozdova <sup>id56</sup>, D. Du <sup>id62a</sup>, T.A. du Pree <sup>id115</sup>,  
 F. Dubinin <sup>id37</sup>, M. Dubovsky <sup>id28a</sup>, E. Duchovni <sup>id170</sup>, G. Duckeck <sup>id110</sup>, O.A. Ducu <sup>id27b</sup>, D. Duda <sup>id52</sup>,  
 A. Dudarev <sup>id36</sup>, E.R. Duden <sup>id26</sup>, M. D'uffizi <sup>id102</sup>, L. Duflost <sup>id66</sup>, M. Dührssen <sup>id36</sup>, I. Duminica <sup>id27g</sup>,  
 A.E. Dumitriu <sup>id27b</sup>, M. Dunford <sup>id63a</sup>, S. Dungs <sup>id49</sup>, K. Dunne <sup>id47a,47b</sup>, A. Duperrin <sup>id103</sup>,  
 H. Duran Yildiz <sup>id3a</sup>, M. Düren <sup>id58</sup>, A. Durglishvili <sup>id150b</sup>, B.L. Dwyer <sup>id116</sup>, G.I. Dyckes <sup>id17a</sup>,  
 M. Dyndal <sup>id86a</sup>, B.S. Dziedzic <sup>id87</sup>, Z.O. Earnshaw <sup>id147</sup>, G.H. Eberwein <sup>id127</sup>, B. Eckerova <sup>id28a</sup>,  
 S. Eggebrecht <sup>id55</sup>, E. Egidio Purcino De Souza <sup>id128</sup>, L.F. Ehrke <sup>id56</sup>, G. Eigen <sup>id16</sup>, K. Einsweiler <sup>id17a</sup>,  
 T. Ekelof <sup>id162</sup>, P.A. Ekman <sup>id99</sup>, S. El Farkh <sup>id35b</sup>, Y. El Ghazali <sup>id35b</sup>, H. El Jarrari <sup>id36</sup>,  
 A. El Moussaouy <sup>id109</sup>, V. Ellajosyula <sup>id162</sup>, M. Ellert <sup>id162</sup>, F. Ellinghaus <sup>id172</sup>, N. Ellis <sup>id36</sup>,  
 J. Elmsheuser <sup>id29</sup>, M. Elsayy <sup>id117a</sup>, M. Elsing <sup>id36</sup>, D. Emelianov <sup>id135</sup>, Y. Enari <sup>id154</sup>, I. Ene <sup>id17a</sup>,  
 S. Epari <sup>id13</sup>, P.A. Erland <sup>id87</sup>, M. Errenst <sup>id172</sup>, M. Escalier <sup>id66</sup>, C. Escobar <sup>id164</sup>, E. Etzion <sup>id152</sup>,  
 G. Evans <sup>id131a</sup>, H. Evans <sup>id68</sup>, L.S. Evans <sup>id96</sup>, A. Ezhilov <sup>id37</sup>, S. Ezzarqtouni <sup>id35a</sup>, F. Fabbri <sup>id23b,23a</sup>,  
 L. Fabbri <sup>id23b,23a</sup>, G. Facini <sup>id97</sup>, V. Fadeyev <sup>id137</sup>, R.M. Fakhruddinov <sup>id37</sup>, D. Fakoudis <sup>id101</sup>,

S. Falciano <sup>75a</sup>, L.F. Falda Ulhoa Coelho <sup>36</sup>, P.J. Falke <sup>24</sup>, F. Fallavollita <sup>111</sup>, J. Faltova <sup>134</sup>,  
 C. Fan <sup>163</sup>, Y. Fan <sup>14a</sup>, Y. Fang <sup>14a,14e</sup>, M. Fanti <sup>71a,71b</sup>, M. Faraj <sup>69a,69b</sup>, Z. Farazpay <sup>98</sup>,  
 A. Farbin <sup>8</sup>, A. Farilla <sup>77a</sup>, T. Farooque <sup>108</sup>, S.M. Farrington <sup>52</sup>, F. Fassi <sup>35e</sup>, D. Fassouliotis <sup>9</sup>,  
 M. Faucci Giannelli <sup>76a,76b</sup>, W.J. Fawcett <sup>32</sup>, L. Fayard <sup>66</sup>, P. Federic <sup>134</sup>, P. Federicova <sup>132</sup>,  
 O.L. Fedin <sup>37,a</sup>, M. Feickert <sup>171</sup>, L. Feligioni <sup>103</sup>, D.E. Fellers <sup>124</sup>, C. Feng <sup>62b</sup>, M. Feng <sup>14b</sup>,  
 Z. Feng <sup>115</sup>, M.J. Fenton <sup>160</sup>, L. Ferencz <sup>48</sup>, R.A.M. Ferguson <sup>92</sup>, S.I. Fernandez Luengo <sup>138f</sup>,  
 P. Fernandez Martinez <sup>13</sup>, M.J.V. Fernoux <sup>103</sup>, J. Ferrando <sup>92</sup>, A. Ferrari <sup>162</sup>, P. Ferrari <sup>115,114</sup>,  
 R. Ferrari <sup>73a</sup>, D. Ferrere <sup>56</sup>, C. Ferretti <sup>107</sup>, F. Fiedler <sup>101</sup>, P. Fiedler <sup>133</sup>, A. Filipčić <sup>94</sup>,  
 E.K. Filmer <sup>1</sup>, F. Filthaut <sup>114</sup>, M.C.N. Fiolhais <sup>131a,131c,c</sup>, L. Fiorini <sup>164</sup>, W.C. Fisher <sup>108</sup>,  
 T. Fitschen <sup>102</sup>, P.M. Fitzhugh <sup>136</sup>, I. Fleck <sup>142</sup>, P. Fleischmann <sup>107</sup>, T. Flick <sup>172</sup>, M. Flores <sup>33d,ab</sup>,  
 L.R. Flores Castillo <sup>64a</sup>, L. Flores Sanz De Acedo <sup>36</sup>, F.M. Follega <sup>78a,78b</sup>, N. Fomin <sup>16</sup>,  
 J.H. Foo <sup>156</sup>, A. Formica <sup>136</sup>, A.C. Forti <sup>102</sup>, E. Fortin <sup>36</sup>, A.W. Fortman <sup>17a</sup>, M.G. Foti <sup>17a</sup>,  
 L. Fountas <sup>9j</sup>, D. Fournier <sup>66</sup>, H. Fox <sup>92</sup>, P. Francavilla <sup>74a,74b</sup>, S. Francescato <sup>61</sup>,  
 S. Franchellucci <sup>56</sup>, M. Franchini <sup>23b,23a</sup>, S. Franchino <sup>63a</sup>, D. Francis <sup>36</sup>, L. Franco <sup>114</sup>,  
 V. Franco Lima <sup>36</sup>, L. Franconi <sup>48</sup>, M. Franklin <sup>61</sup>, G. Frattari <sup>26</sup>, W.S. Freund <sup>83b</sup>, Y.Y. Frid <sup>152</sup>,  
 J. Friend <sup>59</sup>, N. Fritzsche <sup>50</sup>, A. Froch <sup>54</sup>, D. Froidevaux <sup>36</sup>, J.A. Frost <sup>127</sup>, Y. Fu <sup>62a</sup>,  
 S. Fuenzalida Garrido <sup>138f</sup>, M. Fujimoto <sup>103</sup>, K.Y. Fung <sup>64a</sup>, E. Furtado De Simas Filho <sup>83e</sup>,  
 M. Furukawa <sup>154</sup>, J. Fuster <sup>164</sup>, A. Gabrielli <sup>23b,23a</sup>, A. Gabrielli <sup>156</sup>, P. Gadow <sup>36</sup>,  
 G. Gagliardi <sup>57b,57a</sup>, L.G. Gagnon <sup>17a</sup>, S. Gaid <sup>161</sup>, S. Galantzan <sup>152</sup>, E.J. Gallas <sup>127</sup>,  
 B.J. Gallop <sup>135</sup>, K.K. Gan <sup>120</sup>, S. Ganguly <sup>154</sup>, Y. Gao <sup>52</sup>, F.M. Garay Walls <sup>138a,138b</sup>, B. Garcia <sup>29</sup>,  
 C. García <sup>164</sup>, A. Garcia Alonso <sup>115</sup>, A.G. Garcia Caffaro <sup>173</sup>, J.E. García Navarro <sup>164</sup>,  
 M. Garcia-Sciveres <sup>17a</sup>, G.L. Gardner <sup>129</sup>, R.W. Gardner <sup>39</sup>, N. Garelli <sup>159</sup>, D. Garg <sup>80</sup>,  
 R.B. Garg <sup>144,m</sup>, J.M. Gargan <sup>52</sup>, C.A. Garner <sup>156</sup>, C.M. Garvey <sup>33a</sup>, P. Gaspar <sup>83b</sup>, V.K. Gassmann <sup>159</sup>,  
 G. Gaudio <sup>73a</sup>, V. Gautam <sup>13</sup>, P. Gauzzi <sup>75a,75b</sup>, I.L. Gavrilenko <sup>37</sup>, A. Gavriyuk <sup>37</sup>, C. Gay <sup>165</sup>,  
 G. Gaycken <sup>48</sup>, E.N. Gazis <sup>10</sup>, A.A. Geanta <sup>27b</sup>, C.M. Gee <sup>137</sup>, A. Gekow <sup>120</sup>, C. Gemme <sup>57b</sup>,  
 M.H. Genest <sup>60</sup>, A.D. Gentry <sup>113</sup>, S. George <sup>96</sup>, W.F. George <sup>20</sup>, T. Geralis <sup>46</sup>,  
 P. Gessinger-Befurt <sup>36</sup>, M.E. Geyik <sup>172</sup>, M. Ghani <sup>168</sup>, K. Ghorbanian <sup>95</sup>, A. Ghosal <sup>142</sup>,  
 A. Ghosh <sup>160</sup>, A. Ghosh <sup>7</sup>, B. Giacobbe <sup>23b</sup>, S. Giagu <sup>75a,75b</sup>, T. Giani <sup>115</sup>, P. Giannetti <sup>74a</sup>,  
 A. Giannini <sup>62a</sup>, S.M. Gibson <sup>96</sup>, M. Gignac <sup>137</sup>, D.T. Gil <sup>86b</sup>, A.K. Gilbert <sup>86a</sup>, B.J. Gilbert <sup>41</sup>,  
 D. Gillberg <sup>34</sup>, G. Gilles <sup>115</sup>, L. Ginabat <sup>128</sup>, D.M. Gingrich <sup>2,ae</sup>, M.P. Giordani <sup>69a,69c</sup>,  
 P.F. Giraud <sup>136</sup>, G. Giugliarelli <sup>69a,69c</sup>, D. Giugni <sup>71a</sup>, F. Giuli <sup>36</sup>, I. Gkialas <sup>9j</sup>, L.K. Gladilin <sup>37</sup>,  
 C. Glasman <sup>100</sup>, G.R. Gledhill <sup>124</sup>, G. Glemža <sup>48</sup>, M. Glisic <sup>124</sup>, I. Gnesi <sup>43b,f</sup>, Y. Go <sup>29</sup>,  
 M. Goblirsch-Kolb <sup>36</sup>, B. Gocke <sup>49</sup>, D. Godin <sup>109</sup>, B. Gokturk <sup>21a</sup>, S. Goldfarb <sup>106</sup>, T. Golling <sup>56</sup>,  
 M.G.D. Gololo <sup>33g</sup>, D. Golubkov <sup>37</sup>, J.P. Gombas <sup>108</sup>, A. Gomes <sup>131a,131b</sup>, G. Gomes Da Silva <sup>142</sup>,  
 A.J. Gomez Delegido <sup>164</sup>, R. Gonçalo <sup>131a,131c</sup>, L. Gonella <sup>20</sup>, A. Gongadze <sup>150c</sup>, F. Gonnella <sup>20</sup>,  
 J.L. Gonski <sup>144</sup>, R.Y. González Andana <sup>52</sup>, S. González de la Hoz <sup>164</sup>, R. Gonzalez Lopez <sup>93</sup>,  
 C. Gonzalez Renteria <sup>17a</sup>, M.V. Gonzalez Rodrigues <sup>48</sup>, R. Gonzalez Suarez <sup>162</sup>,  
 S. Gonzalez-Sevilla <sup>56</sup>, L. Goossens <sup>36</sup>, B. Gorini <sup>36</sup>, E. Gorini <sup>70a,70b</sup>, A. Gorišek <sup>94</sup>,  
 T.C. Gosart <sup>129</sup>, A.T. Goshaw <sup>51</sup>, M.I. Gostkin <sup>38</sup>, S. Goswami <sup>122</sup>, C.A. Gottardo <sup>36</sup>,  
 S.A. Gotz <sup>110</sup>, M. Gouighri <sup>35b</sup>, V. Goumarre <sup>48</sup>, A.G. Goussiou <sup>139</sup>, N. Govender <sup>33c</sup>,  
 I. Grabowska-Bold <sup>86a</sup>, K. Graham <sup>34</sup>, E. Gramstad <sup>126</sup>, S. Grancagnolo <sup>70a,70b</sup>, C.M. Grant <sup>1,136</sup>,  
 P.M. Gravila <sup>27f</sup>, F.G. Gravili <sup>70a,70b</sup>, H.M. Gray <sup>17a</sup>, M. Greco <sup>70a,70b</sup>, C. Grefe <sup>24</sup>,  
 I.M. Gregor <sup>48</sup>, K.T. Greif <sup>160</sup>, P. Grenier <sup>144</sup>, S.G. Grewe <sup>111</sup>, A.A. Grillo <sup>137</sup>, K. Grimm <sup>31</sup>,  
 S. Grinstein <sup>13,s</sup>, J.-F. Grivaz <sup>66</sup>, E. Gross <sup>170</sup>, J. Grosse-Knetter <sup>55</sup>, J.C. Grundy <sup>127</sup>,  
 L. Guan <sup>107</sup>, C. Gubbels <sup>165</sup>, J.G.R. Guerrero Rojas <sup>164</sup>, G. Guerrieri <sup>69a,69c</sup>, F. Guescini <sup>111</sup>,  
 R. Gugel <sup>101</sup>, J.A.M. Guhit <sup>107</sup>, A. Guida <sup>18</sup>, E. Guilloton <sup>168</sup>, S. Guindon <sup>36</sup>, F. Guo <sup>14a,14e</sup>,  
 J. Guo <sup>62c</sup>, L. Guo <sup>48</sup>, Y. Guo <sup>107</sup>, R. Gupta <sup>48</sup>, R. Gupta <sup>130</sup>, S. Gurbuz <sup>24</sup>, S.S. Gurdasani <sup>54</sup>,

G. Gustavino [id<sup>36</sup>](#), M. Guth [id<sup>56</sup>](#), P. Gutierrez [id<sup>121</sup>](#), L.F. Gutierrez Zagazeta [id<sup>129</sup>](#), M. Gutsche [id<sup>50</sup>](#), C. Gutschow [id<sup>97</sup>](#), C. Gwenlan [id<sup>127</sup>](#), C.B. Gwilliam [id<sup>93</sup>](#), E.S. Haaland [id<sup>126</sup>](#), A. Haas [id<sup>118</sup>](#), M. Habedank [id<sup>48</sup>](#), C. Haber [id<sup>17a</sup>](#), H.K. Hadavand [id<sup>8</sup>](#), A. Hadeef [id<sup>50</sup>](#), S. Hadzic [id<sup>111</sup>](#), A.I. Hagan [id<sup>92</sup>](#), J.J. Hahn [id<sup>142</sup>](#), E.H. Haines [id<sup>97</sup>](#), M. Haleem [id<sup>167</sup>](#), J. Haley [id<sup>122</sup>](#), J.J. Hall [id<sup>140</sup>](#), G.D. Hallewell [id<sup>103</sup>](#), L. Halser [id<sup>19</sup>](#), K. Hamano [id<sup>166</sup>](#), M. Hamer [id<sup>24</sup>](#), G.N. Hamity [id<sup>52</sup>](#), E.J. Hampshire [id<sup>96</sup>](#), J. Han [id<sup>62b</sup>](#), K. Han [id<sup>62a</sup>](#), L. Han [id<sup>14c</sup>](#), L. Han [id<sup>62a</sup>](#), S. Han [id<sup>17a</sup>](#), Y.F. Han [id<sup>156</sup>](#), K. Hanagaki [id<sup>84</sup>](#), M. Hance [id<sup>137</sup>](#), D.A. Hangal [id<sup>41</sup>](#), H. Hanif [id<sup>143</sup>](#), M.D. Hank [id<sup>129</sup>](#), J.B. Hansen [id<sup>42</sup>](#), P.H. Hansen [id<sup>42</sup>](#), K. Hara [id<sup>158</sup>](#), D. Harada [id<sup>56</sup>](#), T. Harenberg [id<sup>172</sup>](#), S. Harkusha [id<sup>37</sup>](#), M.L. Harris [id<sup>104</sup>](#), Y.T. Harris [id<sup>127</sup>](#), J. Harrison [id<sup>13</sup>](#), N.M. Harrison [id<sup>120</sup>](#), P.F. Harrison [id<sup>168</sup>](#), N.M. Hartman [id<sup>111</sup>](#), N.M. Hartmann [id<sup>110</sup>](#), Y. Hasegawa [id<sup>141</sup>](#), S. Hassan [id<sup>16</sup>](#), R. Hauser [id<sup>108</sup>](#), C.M. Hawkes [id<sup>20</sup>](#), R.J. Hawkins [id<sup>36</sup>](#), Y. Hayashi [id<sup>154</sup>](#), S. Hayashida [id<sup>112</sup>](#), D. Hayden [id<sup>108</sup>](#), C. Hayes [id<sup>107</sup>](#), R.L. Hayes [id<sup>115</sup>](#), C.P. Hays [id<sup>127</sup>](#), J.M. Hays [id<sup>95</sup>](#), H.S. Hayward [id<sup>93</sup>](#), F. He [id<sup>62a</sup>](#), M. He [id<sup>14a,14e</sup>](#), Y. He [id<sup>155</sup>](#), Y. He [id<sup>48</sup>](#), Y. He [id<sup>97</sup>](#), N.B. Heatley [id<sup>95</sup>](#), V. Hedberg [id<sup>99</sup>](#), A.L. Heggelund [id<sup>126</sup>](#), N.D. Hehir [id<sup>95,\\*</sup>](#), C. Heidegger [id<sup>54</sup>](#), K.K. Heidegger [id<sup>54</sup>](#), W.D. Heidorn [id<sup>81</sup>](#), J. Heilman [id<sup>34</sup>](#), S. Heim [id<sup>48</sup>](#), T. Heim [id<sup>17a</sup>](#), J.G. Heinlein [id<sup>129</sup>](#), J.J. Heinrich [id<sup>124</sup>](#), L. Heinrich [id<sup>111,ac</sup>](#), J. Hejbal [id<sup>132</sup>](#), A. Held [id<sup>171</sup>](#), S. Hellesund [id<sup>16</sup>](#), C.M. Helling [id<sup>165</sup>](#), S. Hellman [id<sup>47a,47b</sup>](#), R.C.W. Henderson [id<sup>92</sup>](#), L. Henkelmann [id<sup>32</sup>](#), A.M. Henriques Correia [id<sup>36</sup>](#), H. Herde [id<sup>99</sup>](#), Y. Hernández Jiménez [id<sup>146</sup>](#), L.M. Herrmann [id<sup>24</sup>](#), T. Herrmann [id<sup>50</sup>](#), G. Herten [id<sup>54</sup>](#), R. Hertenberger [id<sup>110</sup>](#), L. Hervas [id<sup>36</sup>](#), M.E. Hesping [id<sup>101</sup>](#), N.P. Hessey [id<sup>157a</sup>](#), E. Hill [id<sup>156</sup>](#), S.J. Hillier [id<sup>20</sup>](#), J.R. Hinds [id<sup>108</sup>](#), F. Hinterkeuser [id<sup>24</sup>](#), M. Hirose [id<sup>125</sup>](#), S. Hirose [id<sup>158</sup>](#), D. Hirschbuehl [id<sup>172</sup>](#), T.G. Hitchings [id<sup>102</sup>](#), B. Hiti [id<sup>94</sup>](#), J. Hobbs [id<sup>146</sup>](#), R. Hobincu [id<sup>27e</sup>](#), N. Hod [id<sup>170</sup>](#), M.C. Hodgkinson [id<sup>140</sup>](#), B.H. Hodgkinson [id<sup>127</sup>](#), A. Hoecker [id<sup>36</sup>](#), D.D. Hofer [id<sup>107</sup>](#), J. Hofer [id<sup>48</sup>](#), T. Holm [id<sup>24</sup>](#), M. Holzbock [id<sup>111</sup>](#), L.B.A.H. Hommels [id<sup>32</sup>](#), B.P. Honan [id<sup>102</sup>](#), J. Hong [id<sup>62c</sup>](#), T.M. Hong [id<sup>130</sup>](#), B.H. Hooberman [id<sup>163</sup>](#), W.H. Hopkins [id<sup>6</sup>](#), Y. Horii [id<sup>112</sup>](#), S. Hou [id<sup>149</sup>](#), A.S. Howard [id<sup>94</sup>](#), J. Howarth [id<sup>59</sup>](#), J. Hoya [id<sup>6</sup>](#), M. Hrabovsky [id<sup>123</sup>](#), A. Hrynevich [id<sup>48</sup>](#), T. Hryn'ova [id<sup>4</sup>](#), P.J. Hsu [id<sup>65</sup>](#), S.-C. Hsu [id<sup>139</sup>](#), T. Hsu [id<sup>66</sup>](#), M. Hu [id<sup>17a</sup>](#), Q. Hu [id<sup>62a</sup>](#), S. Huang [id<sup>64b</sup>](#), X. Huang [id<sup>14a,14e</sup>](#), Y. Huang [id<sup>140</sup>](#), Y. Huang [id<sup>101</sup>](#), Y. Huang [id<sup>14a</sup>](#), Z. Huang [id<sup>102</sup>](#), Z. Hubacek [id<sup>133</sup>](#), M. Huebner [id<sup>24</sup>](#), F. Huegging [id<sup>24</sup>](#), T.B. Huffman [id<sup>127</sup>](#), C.A. Hugli [id<sup>48</sup>](#), M. Huhtinen [id<sup>36</sup>](#), S.K. Huiberts [id<sup>16</sup>](#), R. Hulsken [id<sup>105</sup>](#), N. Huseynov [id<sup>12</sup>](#), J. Huston [id<sup>108</sup>](#), J. Huth [id<sup>61</sup>](#), R. Hyneman [id<sup>144</sup>](#), G. Iacobucci [id<sup>56</sup>](#), G. Iakovidis [id<sup>29</sup>](#), I. Ibragimov [id<sup>142</sup>](#), L. Iconomidou-Fayard [id<sup>66</sup>](#), J.P. Iddon [id<sup>36</sup>](#), P. Iengo [id<sup>72a,72b</sup>](#), R. Iguchi [id<sup>154</sup>](#), T. Iizawa [id<sup>127</sup>](#), Y. Ikegami [id<sup>84</sup>](#), N. Ilic [id<sup>156</sup>](#), H. Imam [id<sup>35a</sup>](#), M. Ince Lezki [id<sup>56</sup>](#), T. Ingebretsen Carlson [id<sup>47a,47b</sup>](#), G. Introzzi [id<sup>73a,73b</sup>](#), M. Iodice [id<sup>77a</sup>](#), V. Ippolito [id<sup>75a,75b</sup>](#), R.K. Irwin [id<sup>93</sup>](#), M. Ishino [id<sup>154</sup>](#), W. Islam [id<sup>171</sup>](#), C. Issever [id<sup>18,48</sup>](#), S. Istin [id<sup>21a,ai</sup>](#), H. Ito [id<sup>169</sup>](#), R. Iuppa [id<sup>78a,78b</sup>](#), A. Ivina [id<sup>170</sup>](#), J.M. Izen [id<sup>45</sup>](#), V. Izzo [id<sup>72a</sup>](#), P. Jacka [id<sup>132,133</sup>](#), P. Jackson [id<sup>1</sup>](#), B.P. Jaeger [id<sup>143</sup>](#), C.S. Jagfeld [id<sup>110</sup>](#), G. Jain [id<sup>157a</sup>](#), P. Jain [id<sup>54</sup>](#), K. Jakobs [id<sup>54</sup>](#), T. Jakoubek [id<sup>170</sup>](#), J. Jamieson [id<sup>59</sup>](#), K.W. Janas [id<sup>86a</sup>](#), M. Javurkova [id<sup>104</sup>](#), L. Jeanty [id<sup>124</sup>](#), J. Jejelava [id<sup>150a,z</sup>](#), P. Jenni [id<sup>54,g</sup>](#), C.E. Jessiman [id<sup>34</sup>](#), C. Jia [id<sup>62b</sup>](#), J. Jia [id<sup>146</sup>](#), X. Jia [id<sup>61</sup>](#), X. Jia [id<sup>14a,14e</sup>](#), Z. Jia [id<sup>14c</sup>](#), C. Jiang [id<sup>52</sup>](#), S. Jiggins [id<sup>48</sup>](#), J. Jimenez Pena [id<sup>13</sup>](#), S. Jin [id<sup>14c</sup>](#), A. Jinaru [id<sup>27b</sup>](#), O. Jinnouchi [id<sup>155</sup>](#), P. Johansson [id<sup>140</sup>](#), K.A. Johns [id<sup>7</sup>](#), J.W. Johnson [id<sup>137</sup>](#), D.M. Jones [id<sup>147</sup>](#), E. Jones [id<sup>48</sup>](#), P. Jones [id<sup>32</sup>](#), R.W.L. Jones [id<sup>92</sup>](#), T.J. Jones [id<sup>93</sup>](#), H.L. Joos [id<sup>55,36</sup>](#), R. Joshi [id<sup>120</sup>](#), J. Jovicevic [id<sup>15</sup>](#), X. Ju [id<sup>17a</sup>](#), J.J. Junggeburth [id<sup>104</sup>](#), T. Junkermann [id<sup>63a</sup>](#), A. Juste Rozas [id<sup>13,s</sup>](#), M.K. Juzek [id<sup>87</sup>](#), S. Kabana [id<sup>138e</sup>](#), A. Kaczmarska [id<sup>87</sup>](#), M. Kado [id<sup>111</sup>](#), H. Kagan [id<sup>120</sup>](#), M. Kagan [id<sup>144</sup>](#), A. Kahn [id<sup>41</sup>](#), A. Kahn [id<sup>129</sup>](#), C. Kahra [id<sup>101</sup>](#), T. Kaji [id<sup>154</sup>](#), E. Kajomovitz [id<sup>151</sup>](#), N. Kakati [id<sup>170</sup>](#), I. Kalaitzidou [id<sup>54</sup>](#), C.W. Kalderon [id<sup>29</sup>](#), N.J. Kang [id<sup>137</sup>](#), D. Kar [id<sup>33g</sup>](#), K. Karava [id<sup>127</sup>](#), M.J. Kareem [id<sup>157b</sup>](#), E. Karentzos [id<sup>54</sup>](#), I. Karkanas [id<sup>153</sup>](#), O. Karkout [id<sup>115</sup>](#), S.N. Karpov [id<sup>38</sup>](#), Z.M. Karpova [id<sup>38</sup>](#), V. Kartvelishvili [id<sup>92</sup>](#), A.N. Karyukhin [id<sup>37</sup>](#), E. Kasimi [id<sup>153</sup>](#), J. Katzy [id<sup>48</sup>](#), S. Kaur [id<sup>34</sup>](#), K. Kawade [id<sup>141</sup>](#), M.P. Kawale [id<sup>121</sup>](#), C. Kawamoto [id<sup>88</sup>](#), T. Kawamoto [id<sup>62a</sup>](#), E.F. Kay [id<sup>36</sup>](#), F.I. Kaya [id<sup>159</sup>](#), S. Kazakos [id<sup>108</sup>](#), V.F. Kazanin [id<sup>37</sup>](#), Y. Ke [id<sup>146</sup>](#), J.M. Keaveney [id<sup>33a</sup>](#), R. Keeler [id<sup>166</sup>](#), G.V. Kehris [id<sup>61</sup>](#), J.S. Keller [id<sup>34</sup>](#), A.S. Kelly [id<sup>97</sup>](#), J.J. Kempster [id<sup>147</sup>](#), P.D. Kennedy [id<sup>101</sup>](#), O. Kepka [id<sup>132</sup>](#), B.P. Kerridge [id<sup>135</sup>](#), S. Kersten [id<sup>172</sup>](#),



B.P. Kerševan <sup>94</sup>, L. Keszeghova <sup>28a</sup>, S. Ketabchi Haghghat <sup>156</sup>, R.A. Khan <sup>130</sup>, A. Khanov <sup>122</sup>,  
 A.G. Kharlamov <sup>37</sup>, T. Kharlamova <sup>37</sup>, E.E. Khoda <sup>139</sup>, M. Kholodenko <sup>37</sup>, T.J. Khoo <sup>18</sup>,  
 G. Khoriauli <sup>167</sup>, J. Khubua <sup>150b</sup>, Y.A.R. Khwaira <sup>66</sup>, B. Kibirige<sup>33g</sup>, A. Kilgallon <sup>124</sup>,  
 D.W. Kim <sup>47a,47b</sup>, Y.K. Kim <sup>39</sup>, N. Kimura <sup>97</sup>, M.K. Kingston <sup>55</sup>, A. Kirchoff <sup>55</sup>, C. Kirfel <sup>24</sup>,  
 F. Kirfel <sup>24</sup>, J. Kirk <sup>135</sup>, A.E. Kiryunin <sup>111</sup>, C. Kitsaki <sup>10</sup>, O. Kivernyk <sup>24</sup>, M. Klassen <sup>159</sup>,  
 C. Klein <sup>34</sup>, L. Klein <sup>167</sup>, M.H. Klein <sup>44</sup>, S.B. Klein <sup>56</sup>, U. Klein <sup>93</sup>, P. Klimek <sup>36</sup>,  
 A. Klimentov <sup>29</sup>, T. Klioutchnikova <sup>36</sup>, P. Kluit <sup>115</sup>, S. Kluth <sup>111</sup>, E. Kneringer <sup>79</sup>,  
 T.M. Knight <sup>156</sup>, A. Knue <sup>49</sup>, R. Kobayashi <sup>88</sup>, D. Kobylanski <sup>170</sup>, S.F. Koch <sup>127</sup>,  
 M. Kocian <sup>144</sup>, P. Kodyš <sup>134</sup>, D.M. Koeck <sup>124</sup>, P.T. Koenig <sup>24</sup>, T. Koffas <sup>34</sup>, O. Kolay <sup>50</sup>,  
 I. Koletsou <sup>4</sup>, T. Komarek <sup>123</sup>, K. Köneke <sup>54</sup>, A.X.Y. Kong <sup>1</sup>, T. Kono <sup>119</sup>, N. Konstantinidis <sup>97</sup>,  
 P. Kontaxakis <sup>56</sup>, B. Konya <sup>99</sup>, R. Kopeliansky <sup>41</sup>, S. Koperny <sup>86a</sup>, K. Korcyl <sup>87</sup>, K. Kordas <sup>153,e</sup>,  
 A. Korn <sup>97</sup>, S. Korn <sup>55</sup>, I. Korolkov <sup>13</sup>, N. Korotkova <sup>37</sup>, B. Kortman <sup>115</sup>, O. Kortner <sup>111</sup>,  
 S. Kortner <sup>111</sup>, W.H. Kostecka <sup>116</sup>, V.V. Kostyukhin <sup>142</sup>, A. Kotsokechagia <sup>136</sup>, A. Kotwal <sup>51</sup>,  
 A. Koulouris <sup>36</sup>, A. Kourkoumeli-Charalampidi <sup>73a,73b</sup>, C. Kourkoumelis <sup>9</sup>, E. Kourlitis <sup>111,ac</sup>,  
 O. Kovanda <sup>124</sup>, R. Kowalewski <sup>166</sup>, W. Kozanecki <sup>136</sup>, A.S. Kozhin <sup>37</sup>, V.A. Kramarenko <sup>37</sup>,  
 G. Kramberger <sup>94</sup>, P. Kramer <sup>101</sup>, M.W. Krasny <sup>128</sup>, A. Krasznahorkay <sup>36</sup>, J.W. Kraus <sup>172</sup>,  
 J.A. Kremer <sup>48</sup>, T. Kresse <sup>50</sup>, J. Kretschmar <sup>93</sup>, K. Kreul <sup>18</sup>, P. Krieger <sup>156</sup>,  
 S. Krishnamurthy <sup>104</sup>, M. Krivos <sup>134</sup>, K. Krizka <sup>20</sup>, K. Kroeninger <sup>49</sup>, H. Kroha <sup>111</sup>, J. Kroll <sup>132</sup>,  
 J. Kroll <sup>129</sup>, K.S. Krowpman <sup>108</sup>, U. Kruchonak <sup>38</sup>, H. Krüger <sup>24</sup>, N. Krumnack<sup>81</sup>, M.C. Kruse <sup>51</sup>,  
 O. Kuchinskaia <sup>37</sup>, S. Kuday <sup>3a</sup>, S. Kuehn <sup>36</sup>, R. Kuesters <sup>54</sup>, T. Kuhl <sup>48</sup>, V. Kukhtin <sup>38</sup>,  
 Y. Kulchitsky <sup>37,a</sup>, S. Kuleshov <sup>138d,138b</sup>, M. Kumar <sup>33g</sup>, N. Kumari <sup>48</sup>, P. Kumari <sup>157b</sup>,  
 A. Kupco <sup>132</sup>, T. Kupfer<sup>49</sup>, A. Kupich <sup>37</sup>, O. Kuprash <sup>54</sup>, H. Kurashige <sup>85</sup>, L.L. Kurchaninov <sup>157a</sup>,  
 O. Kurdysh <sup>66</sup>, Y.A. Kurochkin <sup>37</sup>, A. Kurova <sup>37</sup>, M. Kuze <sup>155</sup>, A.K. Kvam <sup>104</sup>, J. Kvita <sup>123</sup>,  
 T. Kwan <sup>105</sup>, N.G. Kyriacou <sup>107</sup>, L.A.O. Laatu <sup>103</sup>, C. Lacasta <sup>164</sup>, F. Lacava <sup>75a,75b</sup>,  
 H. Lacker <sup>18</sup>, D. Lacour <sup>128</sup>, N.N. Lad <sup>97</sup>, E. Ladygin <sup>38</sup>, A. Lafarge <sup>40</sup>, B. Laforge <sup>128</sup>,  
 T. Lagouri <sup>173</sup>, F.Z. Lahbabi <sup>35a</sup>, S. Lai <sup>55</sup>, I.K. Lakomic <sup>86a</sup>, J.E. Lambert <sup>166</sup>, S. Lammers <sup>68</sup>,  
 W. Lampl <sup>7</sup>, C. Lampoudis <sup>153,e</sup>, G. Lamprinoudis<sup>101</sup>, A.N. Lancaster <sup>116</sup>, E. Lançon <sup>29</sup>,  
 U. Landgraf <sup>54</sup>, M.P.J. Landon <sup>95</sup>, V.S. Lang <sup>54</sup>, O.K.B. Langrekken <sup>126</sup>, A.J. Lankford <sup>160</sup>,  
 F. Lanni <sup>36</sup>, K. Lantzsch <sup>24</sup>, A. Lanza <sup>73a</sup>, A. Lapertosa <sup>57b,57a</sup>, J.F. Laporte <sup>136</sup>, T. Lari <sup>71a</sup>,  
 F. Lasagni Manghi <sup>23b</sup>, M. Lassnig <sup>36</sup>, V. Latonova <sup>132</sup>, A. Laudrain <sup>101</sup>, A. Laurier <sup>151</sup>,  
 S.D. Lawlor <sup>140</sup>, Z. Lawrence <sup>102</sup>, R. Lazaridou<sup>168</sup>, M. Lazzaroni <sup>71a,71b</sup>, B. Le<sup>102</sup>,  
 E.M. Le Boulicaut <sup>51</sup>, L.T. Le Pottier <sup>17a</sup>, B. Leban <sup>23b,23a</sup>, A. Lebedev <sup>81</sup>, M. LeBlanc <sup>102</sup>,  
 F. Ledroit-Guillon <sup>60</sup>, A.C.A. Lee<sup>97</sup>, S.C. Lee <sup>149</sup>, S. Lee <sup>47a,47b</sup>, T.F. Lee <sup>93</sup>, L.L. Leeuw <sup>33c</sup>,  
 H.P. Lefebvre <sup>96</sup>, M. Lefebvre <sup>166</sup>, C. Leggett <sup>17a</sup>, G. Lehmann Miotto <sup>36</sup>, M. Leigh <sup>56</sup>,  
 W.A. Leight <sup>104</sup>, W. Leinonen <sup>114</sup>, A. Leisos <sup>153,r</sup>, M.A.L. Leite <sup>83c</sup>, C.E. Leitgeb <sup>18</sup>,  
 R. Leitner <sup>134</sup>, K.J.C. Leney <sup>44</sup>, T. Lenz <sup>24</sup>, S. Leone <sup>74a</sup>, C. Leonidopoulos <sup>52</sup>, A. Leopold <sup>145</sup>,  
 C. Leroy <sup>109</sup>, R. Les <sup>108</sup>, C.G. Lester <sup>32</sup>, M. Levchenko <sup>37</sup>, J. Levêque <sup>4</sup>, L.J. Levinson <sup>170</sup>,  
 G. Levrini<sup>23b,23a</sup>, M.P. Lewicki <sup>87</sup>, C. Lewis <sup>139</sup>, D.J. Lewis <sup>4</sup>, A. Li <sup>5</sup>, B. Li <sup>62b</sup>, C. Li <sup>62a</sup>,  
 C-Q. Li <sup>111</sup>, H. Li <sup>62a</sup>, H. Li <sup>62b</sup>, H. Li <sup>14c</sup>, H. Li <sup>14b</sup>, H. Li <sup>62b</sup>, J. Li <sup>62c</sup>, K. Li <sup>139</sup>,  
 L. Li <sup>62c</sup>, M. Li <sup>14a,14e</sup>, Q.Y. Li <sup>62a</sup>, S. Li <sup>14a,14e</sup>, S. Li <sup>62d,62c,d</sup>, T. Li <sup>5</sup>, X. Li <sup>105</sup>, Z. Li <sup>127</sup>,  
 Z. Li <sup>105</sup>, Z. Li <sup>14a,14e</sup>, S. Liang<sup>14a,14e</sup>, Z. Liang <sup>14a</sup>, M. Liberatore <sup>136</sup>, B. Liberti <sup>76a</sup>, K. Lie <sup>64c</sup>,  
 J. Lieber Marin <sup>83e</sup>, H. Lien <sup>68</sup>, K. Lin <sup>108</sup>, R.E. Lindley <sup>7</sup>, J.H. Lindon <sup>2</sup>, E. Lipeles <sup>129</sup>,  
 A. Lipniacka <sup>16</sup>, A. Lister <sup>165</sup>, J.D. Little <sup>4</sup>, B. Liu <sup>14a</sup>, B.X. Liu <sup>143</sup>, D. Liu <sup>62d,62c</sup>,  
 E.H.L. Liu <sup>20</sup>, J.B. Liu <sup>62a</sup>, J.K.K. Liu <sup>32</sup>, K. Liu <sup>62d</sup>, K. Liu <sup>62d,62c</sup>, M. Liu <sup>62a</sup>, M.Y. Liu <sup>62a</sup>,  
 P. Liu <sup>14a</sup>, Q. Liu <sup>62d,139,62c</sup>, X. Liu <sup>62a</sup>, X. Liu <sup>62b</sup>, Y. Liu <sup>14d,14e</sup>, Y.L. Liu <sup>62b</sup>, Y.W. Liu <sup>62a</sup>,  
 J. Llorente Merino <sup>143</sup>, S.L. Lloyd <sup>95</sup>, E.M. Lobodzinska <sup>48</sup>, P. Loch <sup>7</sup>, T. Lohse <sup>18</sup>,  
 K. Lohwasser <sup>140</sup>, E. Loiacono <sup>48</sup>, M. Lokajicek <sup>132,\*</sup>, J.D. Lomas <sup>20</sup>, J.D. Long <sup>163</sup>,

I. Longarini [id160](#), L. Longo [id70a,70b](#), R. Longo [id163](#), I. Lopez Paz [id67](#), A. Lopez Solis [id48](#),  
 N. Lorenzo Martinez [id4](#), A.M. Lory [id110](#), G. Löschcke Centeno [id147](#), O. Loseva [id37](#), X. Lou [id47a,47b](#),  
 X. Lou [id14a,14e](#), A. Lounis [id66](#), P.A. Love [id92](#), G. Lu [id14a,14e](#), M. Lu [id66](#), S. Lu [id129](#), Y.J. Lu [id65](#),  
 H.J. Lubatti [id139](#), C. Luci [id75a,75b](#), F.L. Lucio Alves [id14c](#), F. Luehring [id68](#), I. Luise [id146](#),  
 O. Lukianchuk [id66](#), O. Lundberg [id145](#), B. Lund-Jensen [id145](#), N.A. Luongo [id6](#), M.S. Lutz [id36](#),  
 A.B. Lux [id25](#), D. Lynn [id29](#), R. Lysak [id132](#), E. Lytken [id99](#), V. Lyubushkin [id38](#), T. Lyubushkina [id38](#),  
 M.M. Lyukova [id146](#), M.Firdaus M. Soberi [id52](#), H. Ma [id29](#), K. Ma [id62a](#), L.L. Ma [id62b](#), W. Ma [id62a](#),  
 Y. Ma [id122](#), D.M. Mac Donnell [id166](#), G. Maccarrone [id53](#), J.C. MacDonald [id101](#),  
 P.C. Machado De Abreu Farias [id83e](#), R. Madar [id40](#), T. Madula [id97](#), J. Maeda [id85](#), T. Maeno [id29](#),  
 H. Maguire [id140](#), V. Maiboroda [id136](#), A. Maio [id131a,131b,131d](#), K. Maj [id36a](#), O. Majersky [id48](#),  
 S. Majewski [id124](#), N. Makovec [id66](#), V. Maksimovic [id15](#), B. Malaescu [id128](#), Pa. Malecki [id87](#),  
 V.P. Maleev [id37](#), F. Malek [id60,n](#), M. Mali [id94](#), D. Malito [id96](#), U. Mallik [id80](#), S. Maltezos [id10](#),  
 S. Malyukov [id38](#), J. Mamuzic [id13](#), G. Mancini [id53](#), M.N. Mancini [id26](#), G. Manco [id73a,73b](#),  
 J.P. Mandalia [id95](#), I. Mandić [id94](#), L. Manhaes de Andrade Filho [id83a](#), I.M. Maniatis [id170](#),  
 J. Manjarres Ramos [id90](#), D.C. Mankad [id170](#), A. Mann [id110](#), S. Manzoni [id36](#), L. Mao [id62c](#),  
 X. Mapekula [id33c](#), A. Marantis [id153,r](#), G. Marchiori [id5](#), M. Marcisovsky [id132](#), C. Marcon [id71a](#),  
 M. Marinescu [id20](#), S. Marium [id48](#), M. Marjanovic [id121](#), A. Markhoos [id54](#), M. Markovitch [id66](#),  
 E.J. Marshall [id92](#), Z. Marshall [id17a](#), S. Marti-Garcia [id164](#), T.A. Martin [id168](#), V.J. Martin [id52](#),  
 B. Martin dit Latour [id16](#), L. Martinelli [id75a,75b](#), M. Martinez [id13,s](#), P. Martinez Agullo [id164](#),  
 V.I. Martinez Outschoorn [id104](#), P. Martinez Suarez [id13](#), S. Martin-Haugh [id135](#), G. Martinovicova [id134](#),  
 V.S. Martoiu [id27b](#), A.C. Martyniuk [id97](#), A. Marzin [id36](#), D. Mascione [id78a,78b](#), L. Masetti [id101](#),  
 T. Mashimo [id154](#), J. Masik [id102](#), A.L. Maslennikov [id37](#), P. Massarotti [id72a,72b](#), P. Mastrandrea [id74a,74b](#),  
 A. Mastroberardino [id43b,43a](#), T. Masubuchi [id154](#), T. Mathisen [id162](#), J. Matousek [id134](#), N. Matsuzawa [id154](#),  
 J. Maurer [id27b](#), A.J. Maury [id66](#), B. Maček [id94](#), D.A. Maximov [id37](#), A.E. May [id102](#), R. Mazini [id149](#),  
 I. Maznas [id116](#), M. Mazza [id108](#), S.M. Mazza [id137](#), E. Mazzeo [id71a,71b](#), C. Mc Ginn [id29](#),  
 J.P. Mc Gowan [id166](#), S.P. Mc Kee [id107](#), C.C. McCracken [id165](#), E.F. McDonald [id106](#),  
 A.E. McDougall [id115](#), J.A. Mcfayden [id147](#), R.P. McGovern [id129](#), G. Mchedlidze [id150b](#),  
 R.P. Mckenzie [id33g](#), T.C. Mclachlan [id48](#), D.J. Mclaughlin [id97](#), S.J. McMahon [id135](#),  
 C.M. Mccpartland [id93](#), R.A. McPherson [id166,w](#), S. Mehlhase [id110](#), A. Mehta [id93](#), D. Melini [id164](#),  
 B.R. Mellado Garcia [id33g](#), A.H. Melo [id55](#), F. Meloni [id48](#), A.M. Mendes Jacques Da Costa [id102](#),  
 H.Y. Meng [id156](#), L. Meng [id92](#), S. Menke [id111](#), M. Mentink [id36](#), E. Meoni [id43b,43a](#), G. Mercado [id116](#),  
 C. Merlassino [id69a,69c](#), L. Merola [id72a,72b](#), C. Meroni [id71a,71b](#), J. Metcalfe [id6](#), A.S. Mete [id6](#),  
 C. Meyer [id68](#), J-P. Meyer [id136](#), R.P. Middleton [id135](#), L. Mijović [id52](#), G. Mikenberg [id170](#),  
 M. Mikestikova [id132](#), M. Mikuž [id94](#), H. Mildner [id101](#), A. Milic [id36](#), D.W. Miller [id39](#), E.H. Miller [id144](#),  
 L.S. Miller [id34](#), A. Milov [id170](#), D.A. Milstead [id47a,47b](#), T. Min [id14c](#), A.A. Minaenko [id37](#),  
 I.A. Minashvili [id150b](#), L. Mince [id59](#), A.I. Mincer [id118](#), B. Mindur [id86a](#), M. Mineev [id38](#), Y. Mino [id88](#),  
 L.M. Mir [id13](#), M. Miralles Lopez [id59](#), M. Mironova [id17a](#), A. Mishima [id154](#), M.C. Missio [id114](#),  
 A. Mitra [id168](#), V.A. Mitsou [id164](#), Y. Mitsumori [id112](#), O. Miu [id156](#), P.S. Miyagawa [id95](#),  
 T. Mkrtchyan [id63a](#), M. Mlinarevic [id97](#), T. Mlinarevic [id97](#), M. Mlynarikova [id36](#), S. Mobius [id19](#),  
 P. Mogg [id110](#), M.H. Mohamed Farook [id113](#), A.F. Mohammed [id14a,14e](#), S. Mohapatra [id41](#),  
 G. Mokgatitswane [id33g](#), L. Moleri [id170](#), B. Mondal [id142](#), S. Mondal [id133](#), K. Mönig [id48](#),  
 E. Monnier [id103](#), L. Monsonis Romero [id164](#), J. Montejo Berlingen [id13](#), M. Montella [id120](#),  
 F. Montekali [id77a,77b](#), F. Monticelli [id91](#), S. Monzani [id69a,69c](#), N. Morange [id66](#),  
 A.L. Moreira De Carvalho [id48](#), M. Moreno Llácer [id164](#), C. Moreno Martinez [id56](#), P. Morettini [id57b](#),  
 S. Morgenstern [id36](#), M. Morii [id61](#), M. Morinaga [id154](#), F. Morodei [id75a,75b](#), L. Morvaj [id36](#),  
 P. Moschovakos [id36](#), B. Moser [id36](#), M. Mosidze [id150b](#), T. Moskalets [id54](#), P. Moskvitina [id114](#),  
 J. Moss [id31,k](#), A. Moussa [id35d](#), E.J.W. Moyse [id104](#), O. Mtintsilana [id33g](#), S. Muanza [id103](#),














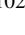

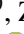

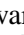
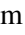

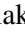


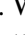

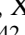





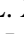


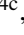
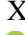




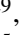

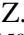








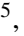





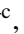






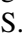









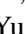

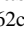






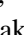

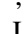






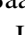
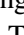


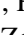
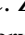




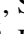
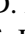

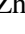
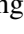

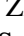






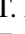
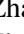



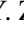
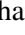

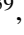
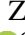

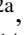
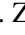
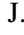
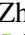
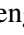








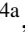



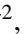

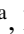




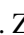


J. Mueller <sup>130</sup>, D. Muenstermann <sup>92</sup>, R. Müller <sup>19</sup>, G.A. Mullier <sup>162</sup>, A.J. Mullin<sup>32</sup>, J.J. Mullin<sup>129</sup>, D.P. Mungo <sup>156</sup>, D. Munoz Perez <sup>164</sup>, F.J. Munoz Sanchez <sup>102</sup>, M. Murin <sup>102</sup>, W.J. Murray <sup>168,135</sup>, M. Muškinja <sup>94</sup>, C. Mwewa <sup>29</sup>, A.G. Myagkov <sup>37,a</sup>, A.J. Myers <sup>8</sup>, G. Myers <sup>107</sup>, M. Myska <sup>133</sup>, B.P. Nachman <sup>17a</sup>, O. Nackenhorst <sup>49</sup>, K. Nagai <sup>127</sup>, K. Nagano <sup>84</sup>, J.L. Nagle <sup>29,ag</sup>, E. Nagy <sup>103</sup>, A.M. Nairz <sup>36</sup>, Y. Nakahama <sup>84</sup>, K. Nakamura <sup>84</sup>, K. Nakkalil <sup>5</sup>, H. Nanjo <sup>125</sup>, R. Narayan <sup>44</sup>, E.A. Narayanan <sup>113</sup>, I. Naryshkin <sup>37</sup>, M. Naseri <sup>34</sup>, S. Nasri <sup>117b</sup>, C. Nass <sup>24</sup>, G. Navarro <sup>22a</sup>, J. Navarro-Gonzalez <sup>164</sup>, R. Nayak <sup>152</sup>, A. Nayaz <sup>18</sup>, P.Y. Nechaeva <sup>37</sup>, S. Nechaeva <sup>23b,23a</sup>, F. Nechansky <sup>48</sup>, L. Nedic <sup>127</sup>, T.J. Neep <sup>20</sup>, A. Negri <sup>73a,73b</sup>, M. Negrini <sup>23b</sup>, C. Nellist <sup>115</sup>, C. Nelson <sup>105</sup>, K. Nelson <sup>107</sup>, S. Nemecek <sup>132</sup>, M. Nessi <sup>36,h</sup>, M.S. Neubauer <sup>163</sup>, F. Neuhaus <sup>101</sup>, J. Neundorf <sup>48</sup>, R. Newhouse <sup>165</sup>, P.R. Newman <sup>20</sup>, C.W. Ng <sup>130</sup>, Y.W.Y. Ng <sup>48</sup>, B. Ngair <sup>117a</sup>, H.D.N. Nguyen <sup>109</sup>, R.B. Nickerson <sup>127</sup>, R. Nicolaidou <sup>136</sup>, J. Nielsen <sup>137</sup>, M. Niemeyer <sup>55</sup>, J. Niermann <sup>55</sup>, N. Nikiforou <sup>36</sup>, V. Nikolaenko <sup>37,a</sup>, I. Nikolic-Audit <sup>128</sup>, K. Nikolopoulos <sup>20</sup>, P. Nilsson <sup>29</sup>, I. Ninca <sup>48</sup>, H.R. Nindhito <sup>56</sup>, G. Ninio <sup>152</sup>, A. Nisati <sup>75a</sup>, N. Nishu <sup>2</sup>, R. Nisius <sup>111</sup>, J-E. Nitschke <sup>50</sup>, E.K. Nkadimeng <sup>33g</sup>, T. Nobe <sup>154</sup>, D.L. Noel <sup>32</sup>, T. Nommensen <sup>148</sup>, M.B. Norfolk <sup>140</sup>, R.R.B. Norisam <sup>97</sup>, B.J. Norman <sup>34</sup>, M. Noury <sup>35a</sup>, J. Novak <sup>94</sup>, T. Novak <sup>48</sup>, L. Novotny <sup>133</sup>, R. Novotny <sup>113</sup>, L. Nozka <sup>123</sup>, K. Ntekas <sup>160</sup>, N.M.J. Nunes De Moura Junior <sup>83b</sup>, J. Ocariz <sup>128</sup>, A. Ochi <sup>85</sup>, I. Ochoa <sup>131a</sup>, S. Oerdek <sup>48,t</sup>, J.T. Offermann <sup>39</sup>, A. Ogrodnik <sup>134</sup>, A. Oh <sup>102</sup>, C.C. Ohm <sup>145</sup>, H. Oide <sup>84</sup>, R. Oishi <sup>154</sup>, M.L. Ojeda <sup>48</sup>, Y. Okumura <sup>154</sup>, L.F. Oleiro Seabra <sup>131a</sup>, S.A. Olivares Pino <sup>138d</sup>, G. Oliveira Correa <sup>13</sup>, D. Oliveira Damazio <sup>29</sup>, D. Oliveira Goncalves <sup>83a</sup>, J.L. Oliver <sup>160</sup>, Ö.O. Öncel <sup>54</sup>, A.P. O'Neill <sup>19</sup>, A. Onofre <sup>131a,131e</sup>, P.U.E. Onyisi <sup>11</sup>, M.J. Oreglia <sup>39</sup>, G.E. Orellana <sup>91</sup>, D. Orestano <sup>77a,77b</sup>, N. Orlando <sup>13</sup>, R.S. Orr <sup>156</sup>, V. O'Shea <sup>59</sup>, L.M. Osojnak <sup>129</sup>, R. Ospanov <sup>62a</sup>, G. Otero y Garzon <sup>30</sup>, H. Otono <sup>89</sup>, P.S. Ott <sup>63a</sup>, G.J. Ottino <sup>17a</sup>, M. Ouchrif <sup>35d</sup>, F. Ould-Saada <sup>126</sup>, T. Ovsiannikova <sup>139</sup>, M. Owen <sup>59</sup>, R.E. Owen <sup>135</sup>, K.Y. Oyulmaz <sup>21a</sup>, V.E. Ozcan <sup>21a</sup>, F. Ozturk <sup>87</sup>, N. Ozturk <sup>8</sup>, S. Ozturk <sup>82</sup>, H.A. Pacey <sup>127</sup>, A. Pacheco Pages <sup>13</sup>, C. Padilla Aranda <sup>13</sup>, G. Padovano <sup>75a,75b</sup>, S. Pagan Griso <sup>17a</sup>, G. Palacino <sup>68</sup>, A. Palazzo <sup>70a,70b</sup>, J. Pampel <sup>24</sup>, J. Pan <sup>173</sup>, T. Pan <sup>64a</sup>, D.K. Panchal <sup>11</sup>, C.E. Pandini <sup>115</sup>, J.G. Panduro Vazquez <sup>96</sup>, H.D. Pandya <sup>1</sup>, H. Pang <sup>14b</sup>, P. Pani <sup>48</sup>, G. Panizzo <sup>69a,69c</sup>, L. Panwar <sup>128</sup>, L. Paolozzi <sup>56</sup>, S. Parajuli <sup>163</sup>, A. Paramonov <sup>6</sup>, C. Paraskevopoulos <sup>53</sup>, D. Paredes Hernandez <sup>64b</sup>, A. Pareti <sup>73a,73b</sup>, K.R. Park <sup>41</sup>, T.H. Park <sup>156</sup>, M.A. Parker <sup>32</sup>, F. Parodi <sup>57b,57a</sup>, E.W. Parrish <sup>116</sup>, V.A. Parrish <sup>52</sup>, J.A. Parsons <sup>41</sup>, U. Parzefall <sup>54</sup>, B. Pascual Dias <sup>109</sup>, L. Pascual Dominguez <sup>152</sup>, E. Pasqualucci <sup>75a</sup>, S. Passaggio <sup>57b</sup>, F. Pastore <sup>96</sup>, P. Patel <sup>87</sup>, U.M. Patel <sup>51</sup>, J.R. Pater <sup>102</sup>, T. Pauly <sup>36</sup>, C.I. Pazos <sup>159</sup>, J. Pearkes <sup>144</sup>, M. Pedersen <sup>126</sup>, R. Pedro <sup>131a</sup>, S.V. Peleganchuk <sup>37</sup>, O. Penc <sup>36</sup>, E.A. Pender <sup>52</sup>, G.D. Penn <sup>173</sup>, K.E. Pensi <sup>110</sup>, M. Penzin <sup>37</sup>, B.S. Peralva <sup>83d</sup>, A.P. Pereira Peixoto <sup>139</sup>, L. Pereira Sanchez <sup>144</sup>, D.V. Perepelitsa <sup>29,ag</sup>, E. Perez Codina <sup>157a</sup>, M. Perganti <sup>10</sup>, H. Pernegger <sup>36</sup>, O. Perrin <sup>40</sup>, K. Peters <sup>48</sup>, R.F.Y. Peters <sup>102</sup>, B.A. Petersen <sup>36</sup>, T.C. Petersen <sup>42</sup>, E. Petit <sup>103</sup>, V. Petousis <sup>133</sup>, C. Petridou <sup>153,e</sup>, T. Petru <sup>134</sup>, A. Petrukhin <sup>142</sup>, M. Pettee <sup>17a</sup>, N.E. Pettersson <sup>36</sup>, A. Petukhov <sup>37</sup>, K. Petukhova <sup>134</sup>, R. Pezoa <sup>138f</sup>, L. Pezzotti <sup>36</sup>, G. Pezzullo <sup>173</sup>, T.M. Pham <sup>171</sup>, T. Pham <sup>106</sup>, P.W. Phillips <sup>135</sup>, G. Piacquadio <sup>146</sup>, E. Pianori <sup>17a</sup>, F. Piazza <sup>124</sup>, R. Piegai <sup>30</sup>, D. Pietreanu <sup>27b</sup>, A.D. Pilkington <sup>102</sup>, M. Pinamonti <sup>69a,69c</sup>, J.L. Pinfeld <sup>2</sup>, B.C. Pinheiro Pereira <sup>131a</sup>, A.E. Pinto Pinoargote <sup>101,136</sup>, L. Pintucci <sup>69a,69c</sup>, K.M. Piper <sup>147</sup>, A. Pirttikoski <sup>56</sup>, D.A. Pizzi <sup>34</sup>, L. Pizzimento <sup>64b</sup>, A. Pizzini <sup>115</sup>, M.-A. Pleier <sup>29</sup>, V. Plesanovs<sup>54</sup>, V. Pleskot <sup>134</sup>, E. Plotnikova<sup>38</sup>, G. Poddar <sup>95</sup>, R. Poettgen <sup>99</sup>, L. Poggioli <sup>128</sup>, I. Pokharel <sup>55</sup>, S. Polacek <sup>134</sup>, G. Polesello <sup>73a</sup>, A. Poley <sup>143,157a</sup>, A. Polini <sup>23b</sup>, C.S. Pollard <sup>168</sup>, Z.B. Pollock <sup>120</sup>, E. Pompa Pacchi <sup>75a,75b</sup>, D. Ponomarenko <sup>114</sup>, L. Pontecorvo <sup>36</sup>, S. Popa <sup>27a</sup>, G.A. Popeneciu <sup>27d</sup>, A. Poreba <sup>36</sup>, D.M. Portillo Quintero <sup>157a</sup>,

S. Pospisil <sup>133</sup>, M.A. Postill <sup>140</sup>, P. Postolache <sup>27c</sup>, K. Potamianos <sup>168</sup>, P.A. Potepa <sup>86a</sup>,  
 I.N. Potrap <sup>38</sup>, C.J. Potter <sup>32</sup>, H. Potti <sup>1</sup>, J. Poveda <sup>164</sup>, M.E. Pozo Astigarraga <sup>36</sup>,  
 A. Prades Ibanez <sup>164</sup>, J. Pretel <sup>54</sup>, D. Price <sup>102</sup>, M. Primavera <sup>70a</sup>, M.A. Principe Martin <sup>100</sup>,  
 R. Privara <sup>123</sup>, T. Procter <sup>59</sup>, M.L. Proffitt <sup>139</sup>, N. Proklova <sup>129</sup>, K. Prokofiev <sup>64c</sup>, G. Proto <sup>111</sup>,  
 J. Proudfoot <sup>6</sup>, M. Przybycien <sup>86a</sup>, W.W. Przygoda <sup>86b</sup>, A. Psallidas <sup>46</sup>, J.E. Puddefoot <sup>140</sup>,  
 D. Pudzha <sup>37</sup>, D. Pyatiizbyantseva <sup>37</sup>, J. Qian <sup>107</sup>, D. Qichen <sup>102</sup>, Y. Qin <sup>13</sup>, T. Qiu <sup>52</sup>,  
 A. Quadt <sup>55</sup>, M. Queitsch-Maitland <sup>102</sup>, G. Quetant <sup>56</sup>, R.P. Quinn <sup>165</sup>, G. Rabanal Bolanos <sup>61</sup>,  
 D. Rafanoharana <sup>54</sup>, F. Ragusa <sup>71a,71b</sup>, J.L. Rainbolt <sup>39</sup>, J.A. Raine <sup>56</sup>, S. Rajagopalan <sup>29</sup>,  
 E. Ramakoti <sup>37</sup>, I.A. Ramirez-Berend <sup>34</sup>, K. Ran <sup>48,14e</sup>, N.P. Rapheeha <sup>33g</sup>, H. Rasheed <sup>27b</sup>,  
 V. Raskina <sup>128</sup>, D.F. Rassloff <sup>63a</sup>, A. Rastogi <sup>17a</sup>, S. Rave <sup>101</sup>, B. Ravina <sup>55</sup>, I. Ravinovich <sup>170</sup>,  
 M. Raymond <sup>36</sup>, A.L. Read <sup>126</sup>, N.P. Readioff <sup>140</sup>, D.M. Rebutzi <sup>73a,73b</sup>, G. Redlinger <sup>29</sup>,  
 A.S. Reed <sup>111</sup>, K. Reeves <sup>26</sup>, J.A. Reidelsturz <sup>172</sup>, D. Reikher <sup>152</sup>, A. Rej <sup>49</sup>, C. Rembser <sup>36</sup>,  
 M. Renda <sup>27b</sup>, M.B. Rendel <sup>111</sup>, F. Renner <sup>48</sup>, A.G. Rennie <sup>160</sup>, A.L. Rescia <sup>48</sup>, S. Resconi <sup>71a</sup>,  
 M. Ressegotti <sup>57b,57a</sup>, S. Rettie <sup>36</sup>, J.G. Reyes Rivera <sup>108</sup>, E. Reynolds <sup>17a</sup>, O.L. Rezanova <sup>37</sup>,  
 P. Reznicek <sup>134</sup>, H. Riani <sup>35d</sup>, N. Ribaric <sup>92</sup>, E. Ricci <sup>78a,78b</sup>, R. Richter <sup>111</sup>, S. Richter <sup>47a,47b</sup>,  
 E. Richter-Was <sup>86b</sup>, M. Ridel <sup>128</sup>, S. Ridouani <sup>35d</sup>, P. Rieck <sup>118</sup>, P. Riedler <sup>36</sup>, E.M. Riefel <sup>47a,47b</sup>,  
 J.O. Rieger <sup>115</sup>, M. Rijssenbeek <sup>146</sup>, M. Rimoldi <sup>36</sup>, L. Rinaldi <sup>23b,23a</sup>, T.T. Rinn <sup>29</sup>,  
 M.P. Rinnagel <sup>110</sup>, G. Ripellino <sup>162</sup>, I. Riu <sup>13</sup>, J.C. Rivera Vergara <sup>166</sup>, F. Rizatdinova <sup>122</sup>,  
 E. Rizvi <sup>95</sup>, B.R. Roberts <sup>17a</sup>, S.H. Robertson <sup>105,w</sup>, D. Robinson <sup>32</sup>, C.M. Robles Gajardo <sup>138f</sup>,  
 M. Robles Manzano <sup>101</sup>, A. Robson <sup>59</sup>, A. Rocchi <sup>76a,76b</sup>, C. Roda <sup>74a,74b</sup>, S. Rodriguez Bosca <sup>36</sup>,  
 Y. Rodriguez Garcia <sup>22a</sup>, A. Rodriguez Rodriguez <sup>54</sup>, A.M. Rodríguez Vera <sup>116</sup>, S. Roe <sup>36</sup>,  
 J.T. Roemer <sup>160</sup>, A.R. Roepe-Gier <sup>137</sup>, J. Roggel <sup>172</sup>, O. Røhne <sup>126</sup>, R.A. Rojas <sup>104</sup>,  
 C.P.A. Roland <sup>128</sup>, J. Roloff <sup>29</sup>, A. Romaniouk <sup>37</sup>, E. Romano <sup>73a,73b</sup>, M. Romano <sup>23b</sup>,  
 A.C. Romero Hernandez <sup>163</sup>, N. Rompotis <sup>93</sup>, L. Roos <sup>128</sup>, S. Rosati <sup>75a</sup>, B.J. Rosser <sup>39</sup>,  
 E. Rossi <sup>127</sup>, E. Rossi <sup>72a,72b</sup>, L.P. Rossi <sup>61</sup>, L. Rossini <sup>54</sup>, R. Rosten <sup>120</sup>, M. Rotaru <sup>27b</sup>,  
 B. Rottler <sup>54</sup>, C. Rougier <sup>90</sup>, D. Rousseau <sup>66</sup>, D. Rouso <sup>48</sup>, A. Roy <sup>163</sup>, S. Roy-Garand <sup>156</sup>,  
 A. Rozanov <sup>103</sup>, Z.M.A. Rozario <sup>59</sup>, Y. Rozen <sup>151</sup>, A. Rubio Jimenez <sup>164</sup>, A.J. Ruby <sup>93</sup>,  
 V.H. Ruelas Rivera <sup>18</sup>, T.A. Ruggeri <sup>1</sup>, A. Ruggiero <sup>127</sup>, A. Ruiz-Martinez <sup>164</sup>, A. Rummler <sup>36</sup>,  
 Z. Rurikova <sup>54</sup>, N.A. Rusakovich <sup>38</sup>, H.L. Russell <sup>166</sup>, G. Russo <sup>75a,75b</sup>, J.P. Rutherford <sup>7</sup>,  
 S. Rutherford Colmenares <sup>32</sup>, K. Rybacki <sup>92</sup>, M. Rybar <sup>134</sup>, E.B. Rye <sup>126</sup>, A. Ryzhov <sup>44</sup>,  
 J.A. Sabater Iglesias <sup>56</sup>, P. Sabatini <sup>164</sup>, H.F.W. Sadrozinski <sup>137</sup>, F. Safai Tehrani <sup>75a</sup>,  
 B. Safarzadeh Samani <sup>135</sup>, S. Saha <sup>1</sup>, M. Sahinsoy <sup>111</sup>, A. Saibel <sup>164</sup>, M. Saimpert <sup>136</sup>,  
 M. Saito <sup>154</sup>, T. Saito <sup>154</sup>, A. Sala <sup>71a,71b</sup>, D. Salamani <sup>36</sup>, A. Salnikov <sup>144</sup>, J. Salt <sup>164</sup>,  
 A. Salvador Salas <sup>152</sup>, D. Salvatore <sup>43b,43a</sup>, F. Salvatore <sup>147</sup>, A. Salzburger <sup>36</sup>, D. Sammel <sup>54</sup>,  
 E. Sampson <sup>92</sup>, D. Sampsonidis <sup>153,e</sup>, D. Sampsonidou <sup>124</sup>, J. Sánchez <sup>164</sup>,  
 V. Sanchez Sebastian <sup>164</sup>, H. Sandaker <sup>126</sup>, C.O. Sander <sup>48</sup>, J.A. Sandesara <sup>104</sup>, M. Sandhoff <sup>172</sup>,  
 C. Sandoval <sup>22b</sup>, D.P.C. Sankey <sup>135</sup>, T. Sano <sup>88</sup>, A. Sansoni <sup>53</sup>, L. Santi <sup>75a,75b</sup>, C. Santoni <sup>40</sup>,  
 H. Santos <sup>131a,131b</sup>, A. Santra <sup>170</sup>, K.A. Saoucha <sup>161</sup>, J.G. Saraiva <sup>131a,131d</sup>, J. Sardain <sup>7</sup>,  
 O. Sasaki <sup>84</sup>, K. Sato <sup>158</sup>, C. Sauer <sup>63b</sup>, F. Sauerburger <sup>54</sup>, E. Sauvan <sup>4</sup>, P. Savard <sup>156,ae</sup>,  
 R. Sawada <sup>154</sup>, C. Sawyer <sup>135</sup>, L. Sawyer <sup>98</sup>, I. Sayago Galvan <sup>164</sup>, C. Sbarra <sup>23b</sup>, A. Sbrizzi <sup>23b,23a</sup>,  
 T. Scanlon <sup>97</sup>, J. Schaarschmidt <sup>139</sup>, U. Schäfer <sup>101</sup>, A.C. Schaffer <sup>66,44</sup>, D. Schaile <sup>110</sup>,  
 R.D. Schamberger <sup>146</sup>, C. Scharf <sup>18</sup>, M.M. Schefer <sup>19</sup>, V.A. Schegelsky <sup>37</sup>, D. Scheirich <sup>134</sup>,  
 F. Schenck <sup>18</sup>, M. Schernau <sup>160</sup>, C. Scheulen <sup>55</sup>, C. Schiavi <sup>57b,57a</sup>, M. Schioppa <sup>43b,43a</sup>,  
 B. Schlag <sup>144,m</sup>, K.E. Schleicher <sup>54</sup>, S. Schlenker <sup>36</sup>, J. Schmeing <sup>172</sup>, M.A. Schmidt <sup>172</sup>,  
 K. Schmieden <sup>101</sup>, C. Schmitt <sup>101</sup>, N. Schmitt <sup>101</sup>, S. Schmitt <sup>48</sup>, L. Schoeffel <sup>136</sup>,  
 A. Schoening <sup>63b</sup>, P.G. Scholer <sup>34</sup>, E. Schopf <sup>127</sup>, M. Schott <sup>101</sup>, J. Schovancova <sup>36</sup>,  
 S. Schramm <sup>56</sup>, T. Schroer <sup>56</sup>, H-C. Schultz-Coulon <sup>63a</sup>, M. Schumacher <sup>54</sup>, B.A. Schumm <sup>137</sup>,

Ph. Schune <sup>136</sup>, A.J. Schuy <sup>139</sup>, H.R. Schwartz <sup>137</sup>, A. Schwartzman <sup>144</sup>, T.A. Schwarz <sup>107</sup>,  
 Ph. Schwemling <sup>136</sup>, R. Schwienhorst <sup>108</sup>, A. Sciandra <sup>29</sup>, G. Sciolla <sup>26</sup>, F. Scuri <sup>74a</sup>,  
 C.D. Sebastiani <sup>93</sup>, K. Sedlaczek <sup>116</sup>, P. Seema <sup>18</sup>, S.C. Seidel <sup>113</sup>, A. Seiden <sup>137</sup>,  
 B.D. Seidlitz <sup>41</sup>, C. Seitz <sup>48</sup>, J.M. Seixas <sup>83b</sup>, G. Sekhniaidze <sup>72a</sup>, L. Selem <sup>60</sup>,  
 N. Semprini-Cesari <sup>23b,23a</sup>, D. Sengupta <sup>56</sup>, V. Senthilkumar <sup>164</sup>, L. Serin <sup>66</sup>, L. Serkin <sup>69a,69b</sup>,  
 M. Sessa <sup>76a,76b</sup>, H. Severini <sup>121</sup>, F. Sforza <sup>57b,57a</sup>, A. Sfyrla <sup>56</sup>, Q. Sha <sup>14a</sup>, E. Shabalina <sup>55</sup>,  
 A.H. Shah <sup>32</sup>, R. Shaheen <sup>145</sup>, J.D. Shahinian <sup>129</sup>, D. Shaked Renous <sup>170</sup>, L.Y. Shan <sup>14a</sup>,  
 M. Shapiro <sup>17a</sup>, A. Sharma <sup>36</sup>, A.S. Sharma <sup>165</sup>, P. Sharma <sup>80</sup>, P.B. Shatalov <sup>37</sup>, K. Shaw <sup>147</sup>,  
 S.M. Shaw <sup>102</sup>, A. Shcherbakova <sup>37</sup>, Q. Shen <sup>62c,5</sup>, D.J. Sheppard <sup>143</sup>, P. Sherwood <sup>97</sup>, L. Shi <sup>97</sup>,  
 X. Shi <sup>14a</sup>, C.O. Shimmin <sup>173</sup>, J.D. Shinner <sup>96</sup>, I.P.J. Shipsey <sup>127</sup>, S. Shirabe <sup>89</sup>,  
 M. Shiyakova <sup>38,u</sup>, J. Shlomi <sup>170</sup>, M.J. Shochet <sup>39</sup>, J. Shojaii <sup>106</sup>, D.R. Shope <sup>126</sup>,  
 B. Shrestha <sup>121</sup>, S. Shrestha <sup>120,ah</sup>, E.M. Shrif <sup>33g</sup>, M.J. Shroff <sup>166</sup>, P. Sicho <sup>132</sup>,  
 A.M. Sickles <sup>163</sup>, E. Sideras Haddad <sup>33g</sup>, A.C. Sidley <sup>115</sup>, A. Sidoti <sup>23b</sup>, F. Siegert <sup>50</sup>,  
 Dj. Sijacki <sup>15</sup>, F. Sili <sup>91</sup>, J.M. Silva <sup>52</sup>, M.V. Silva Oliveira <sup>29</sup>, S.B. Silverstein <sup>47a</sup>, S. Simion <sup>66</sup>,  
 R. Simoniello <sup>36</sup>, E.L. Simpson <sup>102</sup>, H. Simpson <sup>147</sup>, L.R. Simpson <sup>107</sup>, N.D. Simpson <sup>99</sup>,  
 S. Simsek <sup>82</sup>, S. Sindhu <sup>55</sup>, P. Sinervo <sup>156</sup>, S. Singh <sup>156</sup>, S. Sinha <sup>48</sup>, S. Sinha <sup>102</sup>,  
 M. Sioli <sup>23b,23a</sup>, I. Siral <sup>36</sup>, E. Sitnikova <sup>48</sup>, J. Sjölin <sup>47a,47b</sup>, A. Skaf <sup>55</sup>, E. Skorda <sup>20</sup>,  
 P. Skubic <sup>121</sup>, M. Slawinska <sup>87</sup>, V. Smakhtin <sup>170</sup>, B.H. Smart <sup>135</sup>, S.Yu. Smirnov <sup>37</sup>, Y. Smirnov <sup>37</sup>,  
 L.N. Smirnova <sup>37,a</sup>, O. Smirnova <sup>99</sup>, A.C. Smith <sup>41</sup>, D.R. Smith <sup>160</sup>, E.A. Smith <sup>39</sup>,  
 H.A. Smith <sup>127</sup>, J.L. Smith <sup>102</sup>, R. Smith <sup>144</sup>, M. Smizanska <sup>92</sup>, K. Smolek <sup>133</sup>, A.A. Snesarev <sup>37</sup>,  
 S.R. Snider <sup>156</sup>, H.L. Snoek <sup>115</sup>, S. Snyder <sup>29</sup>, R. Sobie <sup>166,w</sup>, A. Soffer <sup>152</sup>,  
 C.A. Solans Sanchez <sup>36</sup>, E.Yu. Soldatov <sup>37</sup>, U. Soldevila <sup>164</sup>, A.A. Solodkov <sup>37</sup>, S. Solomon <sup>26</sup>,  
 A. Soloshenko <sup>38</sup>, K. Solovieva <sup>54</sup>, O.V. Solovyanov <sup>40</sup>, P. Sommer <sup>36</sup>, A. Sonay <sup>13</sup>,  
 W.Y. Song <sup>157b</sup>, A. Sopczak <sup>133</sup>, A.L. Soppio <sup>97</sup>, F. Sopkova <sup>28b</sup>, J.D. Sorenson <sup>113</sup>,  
 I.R. Sotarriva Alvarez <sup>155</sup>, V. Sothilingam <sup>63a</sup>, O.J. Soto Sandoval <sup>138c,138b</sup>, S. Sottocornola <sup>68</sup>,  
 R. Soualah <sup>161</sup>, Z. Soumami <sup>35e</sup>, D. South <sup>48</sup>, N. Soybelman <sup>170</sup>, S. Spagnolo <sup>70a,70b</sup>,  
 M. Spalla <sup>111</sup>, D. Sperlich <sup>54</sup>, G. Spigo <sup>36</sup>, S. Spinali <sup>92</sup>, D.P. Spiteri <sup>59</sup>, M. Spousta <sup>134</sup>,  
 E.J. Staats <sup>34</sup>, R. Stamen <sup>63a</sup>, A. Stampekis <sup>20</sup>, M. Standke <sup>24</sup>, E. Stanecka <sup>87</sup>,  
 W. Stanek-Maslouska <sup>48</sup>, M.V. Stange <sup>50</sup>, B. Stanislaus <sup>17a</sup>, M.M. Stanitzki <sup>48</sup>, B. Stapf <sup>48</sup>,  
 E.A. Starchenko <sup>37</sup>, G.H. Stark <sup>137</sup>, J. Stark <sup>90</sup>, P. Staroba <sup>132</sup>, P. Starovoitov <sup>63a</sup>, S. Stärz <sup>105</sup>,  
 R. Staszewski <sup>87</sup>, G. Stavropoulos <sup>46</sup>, J. Steentoft <sup>162</sup>, P. Steinberg <sup>29</sup>, B. Stelzer <sup>143,157a</sup>,  
 H.J. Stelzer <sup>130</sup>, O. Stelzer-Chilton <sup>157a</sup>, H. Stenzel <sup>58</sup>, T.J. Stevenson <sup>147</sup>, G.A. Stewart <sup>36</sup>,  
 J.R. Stewart <sup>122</sup>, M.C. Stockton <sup>36</sup>, G. Stoicea <sup>27b</sup>, M. Stolarski <sup>131a</sup>, S. Stonjek <sup>111</sup>,  
 A. Straessner <sup>50</sup>, J. Strandberg <sup>145</sup>, S. Strandberg <sup>47a,47b</sup>, M. Stratmann <sup>172</sup>, M. Strauss <sup>121</sup>,  
 T. Streblner <sup>103</sup>, P. Strizenec <sup>28b</sup>, R. Ströhmer <sup>167</sup>, D.M. Strom <sup>124</sup>, R. Stroynowski <sup>44</sup>,  
 A. Strubig <sup>47a,47b</sup>, S.A. Stucci <sup>29</sup>, B. Stugu <sup>16</sup>, J. Stupak <sup>121</sup>, N.A. Styles <sup>48</sup>, D. Su <sup>144</sup>,  
 S. Su <sup>62a</sup>, W. Su <sup>62d</sup>, X. Su <sup>62a</sup>, D. Suchy <sup>28a</sup>, K. Sugizaki <sup>154</sup>, V.V. Sulin <sup>37</sup>, M.J. Sullivan <sup>93</sup>,  
 D.M.S. Sultan <sup>127</sup>, L. Sultanaliyeva <sup>37</sup>, S. Sultansoy <sup>3b</sup>, T. Sumida <sup>88</sup>, S. Sun <sup>107</sup>, S. Sun <sup>171</sup>,  
 O. Sunneborn Gudnadottir <sup>162</sup>, N. Sur <sup>103</sup>, M.R. Sutton <sup>147</sup>, H. Suzuki <sup>158</sup>, M. Svatos <sup>132</sup>,  
 M. Swiatlowski <sup>157a</sup>, T. Swirski <sup>167</sup>, I. Sykora <sup>28a</sup>, M. Sykora <sup>134</sup>, T. Sykora <sup>134</sup>, D. Ta <sup>101</sup>,  
 K. Tackmann <sup>48,t</sup>, A. Taffard <sup>160</sup>, R. Tafirout <sup>157a</sup>, J.S. Tafoya Vargas <sup>66</sup>, Y. Takubo <sup>84</sup>,  
 M. Talby <sup>103</sup>, A.A. Talyshv <sup>37</sup>, K.C. Tam <sup>64b</sup>, N.M. Tamir <sup>152</sup>, A. Tanaka <sup>154</sup>, J. Tanaka <sup>154</sup>,  
 R. Tanaka <sup>66</sup>, M. Tanasini <sup>57b,57a</sup>, Z. Tao <sup>165</sup>, S. Tapia Araya <sup>138f</sup>, S. Tapprogge <sup>101</sup>,  
 A. Tarek Abouelfadl Mohamed <sup>108</sup>, S. Tarem <sup>151</sup>, K. Tariq <sup>14a</sup>, G. Tarna <sup>27b</sup>, G.F. Tartarelli <sup>71a</sup>,  
 M.J. Tartarin <sup>90</sup>, P. Tas <sup>134</sup>, M. Tasevsky <sup>132</sup>, E. Tassi <sup>43b,43a</sup>, A.C. Tate <sup>163</sup>, G. Tateno <sup>154</sup>,  
 Y. Tayalati <sup>35e,v</sup>, G.N. Taylor <sup>106</sup>, W. Taylor <sup>157b</sup>, A.S. Tee <sup>171</sup>, R. Teixeira De Lima <sup>144</sup>,  
 P. Teixeira-Dias <sup>96</sup>, J.J. Teoh <sup>156</sup>, K. Terashi <sup>154</sup>, J. Terron <sup>100</sup>, S. Terzo <sup>13</sup>, M. Testa <sup>53</sup>,

R.J. Teuscher [id](#)<sup>156,w</sup>, A. Thaler [id](#)<sup>79</sup>, O. Theiner [id](#)<sup>56</sup>, N. Themistokleous [id](#)<sup>52</sup>, T. Theveneaux-Pelzer [id](#)<sup>103</sup>, O. Thielmann [id](#)<sup>172</sup>, D.W. Thomas<sup>96</sup>, J.P. Thomas [id](#)<sup>20</sup>, E.A. Thompson [id](#)<sup>17a</sup>, P.D. Thompson [id](#)<sup>20</sup>, E. Thomson [id](#)<sup>129</sup>, R.E. Thornberry<sup>44</sup>, Y. Tian [id](#)<sup>55</sup>, V. Tikhomirov [id](#)<sup>37,a</sup>, Yu.A. Tikhonov [id](#)<sup>37</sup>, S. Timoshenko<sup>37</sup>, D. Timoshyn [id](#)<sup>134</sup>, E.X.L. Ting [id](#)<sup>1</sup>, P. Tipton [id](#)<sup>173</sup>, S.H. Tlou [id](#)<sup>33g</sup>, K. Todome [id](#)<sup>155</sup>, S. Todorova-Nova [id](#)<sup>134</sup>, S. Todt<sup>50</sup>, M. Togawa [id](#)<sup>84</sup>, J. Tojo [id](#)<sup>89</sup>, S. Tokár [id](#)<sup>28a</sup>, K. Tokushuku [id](#)<sup>84</sup>, O. Toldaiev [id](#)<sup>68</sup>, R. Tombs [id](#)<sup>32</sup>, M. Tomoto [id](#)<sup>84,112</sup>, L. Tompkins [id](#)<sup>144,m</sup>, K.W. Topolnicki [id](#)<sup>86b</sup>, E. Torrence [id](#)<sup>124</sup>, H. Torres [id](#)<sup>90</sup>, E. Torró Pastor [id](#)<sup>164</sup>, M. Toscani [id](#)<sup>30</sup>, C. Toscirri [id](#)<sup>39</sup>, M. Tost [id](#)<sup>11</sup>, D.R. Tovey [id](#)<sup>140</sup>, A. Traeet<sup>16</sup>, I.S. Trandafir [id](#)<sup>27b</sup>, T. Trefzger [id](#)<sup>167</sup>, A. Tricoli [id](#)<sup>29</sup>, I.M. Trigger [id](#)<sup>157a</sup>, S. Trincaz-Duvoid [id](#)<sup>128</sup>, D.A. Trischuk [id](#)<sup>26</sup>, B. Trocmé [id](#)<sup>60</sup>, L. Truong [id](#)<sup>33c</sup>, M. Trzebinski [id](#)<sup>87</sup>, A. Trzupke [id](#)<sup>87</sup>, F. Tsai [id](#)<sup>146</sup>, M. Tsai [id](#)<sup>107</sup>, A. Tsiamis [id](#)<sup>153,e</sup>, P.V. Tsiareshka<sup>37</sup>, S. Tsigaridas [id](#)<sup>157a</sup>, A. Tsirigotis [id](#)<sup>153,r</sup>, V. Tsiskaridze [id](#)<sup>156</sup>, E.G. Tskhadadze [id](#)<sup>150a</sup>, M. Tsopoulou [id](#)<sup>153</sup>, Y. Tsujikawa [id](#)<sup>88</sup>, I.I. Tsukerman [id](#)<sup>37</sup>, V. Tsulaia [id](#)<sup>17a</sup>, S. Tsuno [id](#)<sup>84</sup>, K. Tsuru [id](#)<sup>119</sup>, D. Tsybychev [id](#)<sup>146</sup>, Y. Tu [id](#)<sup>64b</sup>, A. Tudorache [id](#)<sup>27b</sup>, V. Tudorache [id](#)<sup>27b</sup>, A.N. Tuna [id](#)<sup>61</sup>, S. Turchikhin [id](#)<sup>57b,57a</sup>, I. Turk Cakir [id](#)<sup>3a</sup>, R. Turra [id](#)<sup>71a</sup>, T. Turtuvshin [id](#)<sup>38,x</sup>, P.M. Tuts [id](#)<sup>41</sup>, S. Tzamarias [id](#)<sup>153,e</sup>, E. Tzovara [id](#)<sup>101</sup>, F. Ukegawa [id](#)<sup>158</sup>, P.A. Ulloa Poblete [id](#)<sup>138c,138b</sup>, E.N. Umaka [id](#)<sup>29</sup>, G. Unal [id](#)<sup>36</sup>, A. Undrus [id](#)<sup>29</sup>, G. Unel [id](#)<sup>160</sup>, J. Urban [id](#)<sup>28b</sup>, P. Urquijo [id](#)<sup>106</sup>, P. Urrejola [id](#)<sup>138a</sup>, G. Usai [id](#)<sup>8</sup>, R. Ushioda [id](#)<sup>155</sup>, M. Usman [id](#)<sup>109</sup>, Z. Uysal [id](#)<sup>82</sup>, V. Vacek [id](#)<sup>133</sup>, B. Vachon [id](#)<sup>105</sup>, T. Vafeiadis [id](#)<sup>36</sup>, A. Vaitkus [id](#)<sup>97</sup>, C. Valderanis [id](#)<sup>110</sup>, E. Valdes Santurio [id](#)<sup>47a,47b</sup>, M. Valente [id](#)<sup>157a</sup>, S. Valentinetti [id](#)<sup>23b,23a</sup>, A. Valero [id](#)<sup>164</sup>, E. Valiente Moreno [id](#)<sup>164</sup>, A. Vallier [id](#)<sup>90</sup>, J.A. Valls Ferrer [id](#)<sup>164</sup>, D.R. Van Arneman [id](#)<sup>115</sup>, T.R. Van Daalen [id](#)<sup>139</sup>, A. Van Der Graaf [id](#)<sup>49</sup>, P. Van Gemmeren [id](#)<sup>6</sup>, M. Van Rijnbach [id](#)<sup>126</sup>, S. Van Stroud [id](#)<sup>97</sup>, I. Van Vulpen [id](#)<sup>115</sup>, P. Vana [id](#)<sup>134</sup>, M. Vanadia [id](#)<sup>76a,76b</sup>, W. Vandelli [id](#)<sup>36</sup>, E.R. Vandewall [id](#)<sup>122</sup>, D. Vannicola [id](#)<sup>152</sup>, L. Vannoli [id](#)<sup>53</sup>, R. Vari [id](#)<sup>75a</sup>, E.W. Varnes [id](#)<sup>7</sup>, C. Varni [id](#)<sup>17b</sup>, T. Varol [id](#)<sup>149</sup>, D. Varouchas [id](#)<sup>66</sup>, L. Varriale [id](#)<sup>164</sup>, K.E. Varvell [id](#)<sup>148</sup>, M.E. Vasile [id](#)<sup>27b</sup>, L. Vaslin<sup>84</sup>, G.A. Vasquez [id](#)<sup>166</sup>, A. Vasyukov [id](#)<sup>38</sup>, R. Vavricka<sup>101</sup>, F. Vazeille [id](#)<sup>40</sup>, T. Vazquez Schroeder [id](#)<sup>36</sup>, J. Veatch [id](#)<sup>31</sup>, V. Vecchio [id](#)<sup>102</sup>, M.J. Veen [id](#)<sup>104</sup>, I. Veliscek [id](#)<sup>29</sup>, L.M. Veloce [id](#)<sup>156</sup>, F. Veloso [id](#)<sup>131a,131c</sup>, S. Veneziano [id](#)<sup>75a</sup>, A. Ventura [id](#)<sup>70a,70b</sup>, S. Ventura Gonzalez [id](#)<sup>136</sup>, A. Verbytskyi [id](#)<sup>111</sup>, M. Verducci [id](#)<sup>74a,74b</sup>, C. Vergis [id](#)<sup>95</sup>, M. Verissimo De Araujo [id](#)<sup>83b</sup>, W. Verkerke [id](#)<sup>115</sup>, J.C. Vermeulen [id](#)<sup>115</sup>, C. Vernieri [id](#)<sup>144</sup>, M. Vessella [id](#)<sup>104</sup>, M.C. Vetterli [id](#)<sup>143,ae</sup>, A. Vgenopoulos [id](#)<sup>153,e</sup>, N. Viaux Maira [id](#)<sup>138f</sup>, T. Vickey [id](#)<sup>140</sup>, O.E. Vickey Boeriu [id](#)<sup>140</sup>, G.H.A. Viehhauser [id](#)<sup>127</sup>, L. Vignani [id](#)<sup>63b</sup>, M. Villa [id](#)<sup>23b,23a</sup>, M. Villaplana Perez [id](#)<sup>164</sup>, E.M. Villhauer<sup>52</sup>, E. Vilucchi [id](#)<sup>53</sup>, M.G. Vincter [id](#)<sup>34</sup>, G.S. Virdee [id](#)<sup>20</sup>, A. Visibile<sup>115</sup>, C. Vittori [id](#)<sup>36</sup>, I. Vivarelli [id](#)<sup>23b,23a</sup>, E. Voevodina [id](#)<sup>111</sup>, F. Vogel [id](#)<sup>110</sup>, J.C. Voigt [id](#)<sup>50</sup>, P. Vokac [id](#)<sup>133</sup>, Yu. Volkotrub [id](#)<sup>86b</sup>, J. Von Ahnen [id](#)<sup>48</sup>, E. Von Toerne [id](#)<sup>24</sup>, B. Vormwald [id](#)<sup>36</sup>, V. Vorobel [id](#)<sup>134</sup>, K. Vorobev [id](#)<sup>37</sup>, M. Vos [id](#)<sup>164</sup>, K. Voss [id](#)<sup>142</sup>, M. Vozak [id](#)<sup>115</sup>, L. Vozdecky [id](#)<sup>121</sup>, N. Vranjes [id](#)<sup>15</sup>, M. Vranjes Milosavljevic [id](#)<sup>15</sup>, M. Vreeswijk [id](#)<sup>115</sup>, N.K. Vu [id](#)<sup>62d,62c</sup>, R. Vuillermet [id](#)<sup>36</sup>, O. Vujinovic [id](#)<sup>101</sup>, I. Vukotic [id](#)<sup>39</sup>, S. Wada [id](#)<sup>158</sup>, C. Wagner<sup>104</sup>, J.M. Wagner [id](#)<sup>17a</sup>, W. Wagner [id](#)<sup>172</sup>, S. Wahdan [id](#)<sup>172</sup>, H. Wahlberg [id](#)<sup>91</sup>, M. Wakida [id](#)<sup>112</sup>, J. Walder [id](#)<sup>135</sup>, R. Walker [id](#)<sup>110</sup>, W. Walkowiak [id](#)<sup>142</sup>, A. Wall [id](#)<sup>129</sup>, E.J. Wallin [id](#)<sup>99</sup>, T. Wamorkar [id](#)<sup>6</sup>, A.Z. Wang [id](#)<sup>137</sup>, C. Wang [id](#)<sup>101</sup>, C. Wang [id](#)<sup>11</sup>, H. Wang [id](#)<sup>17a</sup>, J. Wang [id](#)<sup>64c</sup>, R.-J. Wang [id](#)<sup>101</sup>, R. Wang [id](#)<sup>61</sup>, R. Wang [id](#)<sup>6</sup>, S.M. Wang [id](#)<sup>149</sup>, S. Wang [id](#)<sup>62b</sup>, S. Wang [id](#)<sup>14a</sup>, T. Wang [id](#)<sup>62a</sup>, W.T. Wang [id](#)<sup>80</sup>, W. Wang [id](#)<sup>14a</sup>, X. Wang [id](#)<sup>14c</sup>, X. Wang [id](#)<sup>163</sup>, X. Wang [id](#)<sup>62c</sup>, Y. Wang [id](#)<sup>62d</sup>, Y. Wang [id](#)<sup>14c</sup>, Z. Wang [id](#)<sup>107</sup>, Z. Wang [id](#)<sup>62d,51,62c</sup>, Z. Wang [id](#)<sup>107</sup>, A. Warburton [id](#)<sup>105</sup>, R.J. Ward [id](#)<sup>20</sup>, N. Warrack [id](#)<sup>59</sup>, S. Waterhouse [id](#)<sup>96</sup>, A.T. Watson [id](#)<sup>20</sup>, H. Watson [id](#)<sup>59</sup>, M.F. Watson [id](#)<sup>20</sup>, E. Watton [id](#)<sup>59,135</sup>, G. Watts [id](#)<sup>139</sup>, B.M. Waugh [id](#)<sup>97</sup>, J.M. Webb [id](#)<sup>54</sup>, C. Weber [id](#)<sup>29</sup>, H.A. Weber [id](#)<sup>18</sup>, M.S. Weber [id](#)<sup>19</sup>, S.M. Weber [id](#)<sup>63a</sup>, C. Wei [id](#)<sup>62a</sup>, Y. Wei [id](#)<sup>127</sup>, A.R. Weidberg [id](#)<sup>127</sup>, E.J. Weik [id](#)<sup>118</sup>, J. Weingarten [id](#)<sup>49</sup>, M. Weirich [id](#)<sup>101</sup>, C. Weiser [id](#)<sup>54</sup>, C.J. Wells [id](#)<sup>48</sup>, T. Wenaus [id](#)<sup>29</sup>, B. Wendland [id](#)<sup>49</sup>, T. Wengler [id](#)<sup>36</sup>, N.S. Wenke<sup>111</sup>, N. Wermes [id](#)<sup>24</sup>, M. Wessels [id](#)<sup>63a</sup>, A.M. Wharton [id](#)<sup>92</sup>, A.S. White [id](#)<sup>61</sup>, A. White [id](#)<sup>8</sup>, M.J. White [id](#)<sup>1</sup>, D. Whiteson [id](#)<sup>160</sup>, L. Wickremasinghe [id](#)<sup>125</sup>, W. Wiedenmann [id](#)<sup>171</sup>, M. Wielers [id](#)<sup>135</sup>,



C. Wigglesworth , D.J. Wilbern<sup>121</sup>, H.G. Wilkens , J.J.H. Wilkinson , D.M. Williams , H.H. Williams<sup>129</sup>, S. Williams , S. Willocq , B.J. Wilson , P.J. Windischhofer , F.I. Winkel , F. Winklmeier , B.T. Winter , J.K. Winter , M. Wittgen<sup>144</sup>, M. Wobisch , T. Wojtkowski<sup>60</sup>, Z. Wolffs , J. Wollrath<sup>160</sup>, M.W. Wolter , H. Wolters , M.C. Wong<sup>137</sup>, E.L. Woodward , S.D. Worm , B.K. Wosiek , K.W. Woźniak , S. Wozniowski , K. Wraight , C. Wu , M. Wu , M. Wu , S.L. Wu , X. Wu , Y. Wu , Z. Wu , J. Wuerzinger , T.R. Wyatt , B.M. Wynne , S. Xella , L. Xia , M. Xia , J. Xiang , M. Xie , X. Xie , S. Xin , A. Xiong , J. Xiong , D. Xu , H. Xu , L. Xu , R. Xu , T. Xu , Y. Xu , Z. Xu , Z. Xu , B. Yabsley , S. Yacoob , Y. Yamaguchi , E. Yamashita , H. Yamauchi , T. Yamazaki , Y. Yamazaki , J. Yan , S. Yan , Z. Yan , H.J. Yang , H.T. Yang , S. Yang , T. Yang , X. Yang , X. Yang , Y. Yang , Y. Yang , Z. Yang , W-M. Yao , H. Ye , H. Ye , J. Ye , S. Ye , X. Ye , Y. Yeh , I. Yeletsikh , B.K. Yeo , M.R. Yexley , T.P. Yildirim , P. Yin , K. Yorita , S. Younas , C.J.S. Young , C. Young , C. Yu , Y. Yu , M. Yuan , R. Yuan , L. Yue , M. Zaazoua , B. Zabinski , E. Zaid<sup>52</sup>, Z.K. Zak , T. Zakareishvili , N. Zakharchuk , S. Zambito , J.A. Zamora Saa , J. Zang , D. Zanzi , O. Zaplatilek , C. Zeitnitz , H. Zeng , J.C. Zeng , D.T. Zenger Jr , O. Zenin , T. Ženiš , S. Zenz , S. Zerradi , D. Zerwas , M. Zhai , D.F. Zhang , J. Zhang , J. Zhang , K. Zhang , L. Zhang , L. Zhang , P. Zhang , R. Zhang , S. Zhang , S. Zhang , T. Zhang , X. Zhang , X. Zhang , Y. Zhang , Y. Zhang , Y. Zhang , Z. Zhang , Z. Zhang , H. Zhao , T. Zhao , Y. Zhao , Z. Zhao , Z. Zhao , A. Zhemchugov , J. Zheng , K. Zheng , X. Zheng , Z. Zheng , D. Zhong , B. Zhou , H. Zhou , N. Zhou , Y. Zhou , Y. Zhou<sup>7</sup>, C.G. Zhu , J. Zhu , Y. Zhu , Y. Zhu , X. Zhuang , K. Zhukov , N.I. Zimine , J. Zinsser , M. Ziolkowski , L. Živković , A. Zoccoli , K. Zoch , T.G. Zorbas , O. Zormpa , W. Zou , L. Zwalinski .

<sup>1</sup>Department of Physics, University of Adelaide, Adelaide; Australia.

<sup>2</sup>Department of Physics, University of Alberta, Edmonton AB; Canada.

<sup>3</sup>(<sup>a</sup>)Department of Physics, Ankara University, Ankara; (<sup>b</sup>)Division of Physics, TOBB University of Economics and Technology, Ankara; Türkiye.

<sup>4</sup>LAPP, Université Savoie Mont Blanc, CNRS/IN2P3, Annecy; France.

<sup>5</sup>APC, Université Paris Cité, CNRS/IN2P3, Paris; France.

<sup>6</sup>High Energy Physics Division, Argonne National Laboratory, Argonne IL; United States of America.

<sup>7</sup>Department of Physics, University of Arizona, Tucson AZ; United States of America.

<sup>8</sup>Department of Physics, University of Texas at Arlington, Arlington TX; United States of America.

<sup>9</sup>Physics Department, National and Kapodistrian University of Athens, Athens; Greece.

<sup>10</sup>Physics Department, National Technical University of Athens, Zografou; Greece.

<sup>11</sup>Department of Physics, University of Texas at Austin, Austin TX; United States of America.

<sup>12</sup>Institute of Physics, Azerbaijan Academy of Sciences, Baku; Azerbaijan.

<sup>13</sup>Institut de Física d'Altes Energies (IFAE), Barcelona Institute of Science and Technology, Barcelona; Spain.

<sup>14</sup>(<sup>a</sup>)Institute of High Energy Physics, Chinese Academy of Sciences, Beijing; (<sup>b</sup>)Physics Department, Tsinghua University, Beijing; (<sup>c</sup>)Department of Physics, Nanjing University, Nanjing; (<sup>d</sup>)School of Science, Shenzhen Campus of Sun Yat-sen University; (<sup>e</sup>)University of Chinese Academy of Science (UCAS), Beijing; China.

- <sup>15</sup>Institute of Physics, University of Belgrade, Belgrade; Serbia.
- <sup>16</sup>Department for Physics and Technology, University of Bergen, Bergen; Norway.
- <sup>17</sup>(<sup>a</sup>)Physics Division, Lawrence Berkeley National Laboratory, Berkeley CA;(<sup>b</sup>)University of California, Berkeley CA; United States of America.
- <sup>18</sup>Institut für Physik, Humboldt Universität zu Berlin, Berlin; Germany.
- <sup>19</sup>Albert Einstein Center for Fundamental Physics and Laboratory for High Energy Physics, University of Bern, Bern; Switzerland.
- <sup>20</sup>School of Physics and Astronomy, University of Birmingham, Birmingham; United Kingdom.
- <sup>21</sup>(<sup>a</sup>)Department of Physics, Bogazici University, Istanbul;(<sup>b</sup>)Department of Physics Engineering, Gaziantep University, Gaziantep;(<sup>c</sup>)Department of Physics, Istanbul University, Istanbul; Türkiye.
- <sup>22</sup>(<sup>a</sup>)Facultad de Ciencias y Centro de Investigaciones, Universidad Antonio Nariño, Bogotá;(<sup>b</sup>)Departamento de Física, Universidad Nacional de Colombia, Bogotá; Colombia.
- <sup>23</sup>(<sup>a</sup>)Dipartimento di Fisica e Astronomia A. Righi, Università di Bologna, Bologna;(<sup>b</sup>)INFN Sezione di Bologna; Italy.
- <sup>24</sup>Physikalisches Institut, Universität Bonn, Bonn; Germany.
- <sup>25</sup>Department of Physics, Boston University, Boston MA; United States of America.
- <sup>26</sup>Department of Physics, Brandeis University, Waltham MA; United States of America.
- <sup>27</sup>(<sup>a</sup>)Transilvania University of Brasov, Brasov;(<sup>b</sup>)Horia Hulubei National Institute of Physics and Nuclear Engineering, Bucharest;(<sup>c</sup>)Department of Physics, Alexandru Ioan Cuza University of Iasi, Iasi;(<sup>d</sup>)National Institute for Research and Development of Isotopic and Molecular Technologies, Physics Department, Cluj-Napoca;(<sup>e</sup>)National University of Science and Technology Politehnica, Bucharest;(<sup>f</sup>)West University in Timisoara, Timisoara;(<sup>g</sup>)Faculty of Physics, University of Bucharest, Bucharest; Romania.
- <sup>28</sup>(<sup>a</sup>)Faculty of Mathematics, Physics and Informatics, Comenius University, Bratislava;(<sup>b</sup>)Department of Subnuclear Physics, Institute of Experimental Physics of the Slovak Academy of Sciences, Kosice; Slovak Republic.
- <sup>29</sup>Physics Department, Brookhaven National Laboratory, Upton NY; United States of America.
- <sup>30</sup>Universidad de Buenos Aires, Facultad de Ciencias Exactas y Naturales, Departamento de Física, y CONICET, Instituto de Física de Buenos Aires (IFIBA), Buenos Aires; Argentina.
- <sup>31</sup>California State University, CA; United States of America.
- <sup>32</sup>Cavendish Laboratory, University of Cambridge, Cambridge; United Kingdom.
- <sup>33</sup>(<sup>a</sup>)Department of Physics, University of Cape Town, Cape Town;(<sup>b</sup>)iThemba Labs, Western Cape;(<sup>c</sup>)Department of Mechanical Engineering Science, University of Johannesburg, Johannesburg;(<sup>d</sup>)National Institute of Physics, University of the Philippines Diliman (Philippines);(<sup>e</sup>)University of South Africa, Department of Physics, Pretoria;(<sup>f</sup>)University of Zululand, KwaDlangezwa;(<sup>g</sup>)School of Physics, University of the Witwatersrand, Johannesburg; South Africa.
- <sup>34</sup>Department of Physics, Carleton University, Ottawa ON; Canada.
- <sup>35</sup>(<sup>a</sup>)Faculté des Sciences Ain Chock, Réseau Universitaire de Physique des Hautes Energies - Université Hassan II, Casablanca;(<sup>b</sup>)Faculté des Sciences, Université Ibn-Tofail, Kénitra;(<sup>c</sup>)Faculté des Sciences Semlalia, Université Cadi Ayyad, LPHEA-Marrakech;(<sup>d</sup>)LPMR, Faculté des Sciences, Université Mohamed Premier, Oujda;(<sup>e</sup>)Faculté des sciences, Université Mohammed V, Rabat;(<sup>f</sup>)Institute of Applied Physics, Mohammed VI Polytechnic University, Ben Guerir; Morocco.
- <sup>36</sup>CERN, Geneva; Switzerland.
- <sup>37</sup>Affiliated with an institute covered by a cooperation agreement with CERN.
- <sup>38</sup>Affiliated with an international laboratory covered by a cooperation agreement with CERN.
- <sup>39</sup>Enrico Fermi Institute, University of Chicago, Chicago IL; United States of America.
- <sup>40</sup>LPC, Université Clermont Auvergne, CNRS/IN2P3, Clermont-Ferrand; France.
- <sup>41</sup>Nevis Laboratory, Columbia University, Irvington NY; United States of America.



- <sup>42</sup>Niels Bohr Institute, University of Copenhagen, Copenhagen; Denmark.
- <sup>43</sup>(<sup>a</sup>)Dipartimento di Fisica, Università della Calabria, Rende; (<sup>b</sup>)INFN Gruppo Collegato di Cosenza, Laboratori Nazionali di Frascati; Italy.
- <sup>44</sup>Physics Department, Southern Methodist University, Dallas TX; United States of America.
- <sup>45</sup>Physics Department, University of Texas at Dallas, Richardson TX; United States of America.
- <sup>46</sup>National Centre for Scientific Research "Demokritos", Agia Paraskevi; Greece.
- <sup>47</sup>(<sup>a</sup>)Department of Physics, Stockholm University; (<sup>b</sup>)Oskar Klein Centre, Stockholm; Sweden.
- <sup>48</sup>Deutsches Elektronen-Synchrotron DESY, Hamburg and Zeuthen; Germany.
- <sup>49</sup>Fakultät Physik, Technische Universität Dortmund, Dortmund; Germany.
- <sup>50</sup>Institut für Kern- und Teilchenphysik, Technische Universität Dresden, Dresden; Germany.
- <sup>51</sup>Department of Physics, Duke University, Durham NC; United States of America.
- <sup>52</sup>SUPA - School of Physics and Astronomy, University of Edinburgh, Edinburgh; United Kingdom.
- <sup>53</sup>INFN e Laboratori Nazionali di Frascati, Frascati; Italy.
- <sup>54</sup>Physikalisches Institut, Albert-Ludwigs-Universität Freiburg, Freiburg; Germany.
- <sup>55</sup>II. Physikalisches Institut, Georg-August-Universität Göttingen, Göttingen; Germany.
- <sup>56</sup>Département de Physique Nucléaire et Corpusculaire, Université de Genève, Genève; Switzerland.
- <sup>57</sup>(<sup>a</sup>)Dipartimento di Fisica, Università di Genova, Genova; (<sup>b</sup>)INFN Sezione di Genova; Italy.
- <sup>58</sup>II. Physikalisches Institut, Justus-Liebig-Universität Giessen, Giessen; Germany.
- <sup>59</sup>SUPA - School of Physics and Astronomy, University of Glasgow, Glasgow; United Kingdom.
- <sup>60</sup>LPSC, Université Grenoble Alpes, CNRS/IN2P3, Grenoble INP, Grenoble; France.
- <sup>61</sup>Laboratory for Particle Physics and Cosmology, Harvard University, Cambridge MA; United States of America.
- <sup>62</sup>(<sup>a</sup>)Department of Modern Physics and State Key Laboratory of Particle Detection and Electronics, University of Science and Technology of China, Hefei; (<sup>b</sup>)Institute of Frontier and Interdisciplinary Science and Key Laboratory of Particle Physics and Particle Irradiation (MOE), Shandong University, Qingdao; (<sup>c</sup>)School of Physics and Astronomy, Shanghai Jiao Tong University, Key Laboratory for Particle Astrophysics and Cosmology (MOE), SKLPPC, Shanghai; (<sup>d</sup>)Tsung-Dao Lee Institute, Shanghai; (<sup>e</sup>)School of Physics and Microelectronics, Zhengzhou University; China.
- <sup>63</sup>(<sup>a</sup>)Kirchhoff-Institut für Physik, Ruprecht-Karls-Universität Heidelberg, Heidelberg; (<sup>b</sup>)Physikalisches Institut, Ruprecht-Karls-Universität Heidelberg, Heidelberg; Germany.
- <sup>64</sup>(<sup>a</sup>)Department of Physics, Chinese University of Hong Kong, Shatin, N.T., Hong Kong; (<sup>b</sup>)Department of Physics, University of Hong Kong, Hong Kong; (<sup>c</sup>)Department of Physics and Institute for Advanced Study, Hong Kong University of Science and Technology, Clear Water Bay, Kowloon, Hong Kong; China.
- <sup>65</sup>Department of Physics, National Tsing Hua University, Hsinchu; Taiwan.
- <sup>66</sup>IJCLab, Université Paris-Saclay, CNRS/IN2P3, 91405, Orsay; France.
- <sup>67</sup>Centro Nacional de Microelectrónica (IMB-CNM-CSIC), Barcelona; Spain.
- <sup>68</sup>Department of Physics, Indiana University, Bloomington IN; United States of America.
- <sup>69</sup>(<sup>a</sup>)INFN Gruppo Collegato di Udine, Sezione di Trieste, Udine; (<sup>b</sup>)ICTP, Trieste; (<sup>c</sup>)Dipartimento Politecnico di Ingegneria e Architettura, Università di Udine, Udine; Italy.
- <sup>70</sup>(<sup>a</sup>)INFN Sezione di Lecce; (<sup>b</sup>)Dipartimento di Matematica e Fisica, Università del Salento, Lecce; Italy.
- <sup>71</sup>(<sup>a</sup>)INFN Sezione di Milano; (<sup>b</sup>)Dipartimento di Fisica, Università di Milano, Milano; Italy.
- <sup>72</sup>(<sup>a</sup>)INFN Sezione di Napoli; (<sup>b</sup>)Dipartimento di Fisica, Università di Napoli, Napoli; Italy.
- <sup>73</sup>(<sup>a</sup>)INFN Sezione di Pavia; (<sup>b</sup>)Dipartimento di Fisica, Università di Pavia, Pavia; Italy.
- <sup>74</sup>(<sup>a</sup>)INFN Sezione di Pisa; (<sup>b</sup>)Dipartimento di Fisica E. Fermi, Università di Pisa, Pisa; Italy.
- <sup>75</sup>(<sup>a</sup>)INFN Sezione di Roma; (<sup>b</sup>)Dipartimento di Fisica, Sapienza Università di Roma, Roma; Italy.
- <sup>76</sup>(<sup>a</sup>)INFN Sezione di Roma Tor Vergata; (<sup>b</sup>)Dipartimento di Fisica, Università di Roma Tor Vergata, Roma; Italy.

- 77<sup>(a)</sup> INFN Sezione di Roma Tre; <sup>(b)</sup> Dipartimento di Matematica e Fisica, Università Roma Tre, Roma; Italy.
- 78<sup>(a)</sup> INFN-TIFPA; <sup>(b)</sup> Università degli Studi di Trento, Trento; Italy.
- 79 Universität Innsbruck, Department of Astro and Particle Physics, Innsbruck; Austria.
- 80 University of Iowa, Iowa City IA; United States of America.
- 81 Department of Physics and Astronomy, Iowa State University, Ames IA; United States of America.
- 82 İstinye University, Sariyer, Istanbul; Türkiye.
- 83<sup>(a)</sup> Departamento de Engenharia Elétrica, Universidade Federal de Juiz de Fora (UFJF), Juiz de Fora; <sup>(b)</sup> Universidade Federal do Rio De Janeiro COPPE/EE/IF, Rio de Janeiro; <sup>(c)</sup> Instituto de Física, Universidade de São Paulo, São Paulo; <sup>(d)</sup> Rio de Janeiro State University, Rio de Janeiro; <sup>(e)</sup> Federal University of Bahia, Bahia; Brazil.
- 84 KEK, High Energy Accelerator Research Organization, Tsukuba; Japan.
- 85 Graduate School of Science, Kobe University, Kobe; Japan.
- 86<sup>(a)</sup> AGH University of Krakow, Faculty of Physics and Applied Computer Science, Krakow; <sup>(b)</sup> Marian Smoluchowski Institute of Physics, Jagiellonian University, Krakow; Poland.
- 87 Institute of Nuclear Physics Polish Academy of Sciences, Krakow; Poland.
- 88 Faculty of Science, Kyoto University, Kyoto; Japan.
- 89 Research Center for Advanced Particle Physics and Department of Physics, Kyushu University, Fukuoka ; Japan.
- 90 L2IT, Université de Toulouse, CNRS/IN2P3, UPS, Toulouse; France.
- 91 Instituto de Física La Plata, Universidad Nacional de La Plata and CONICET, La Plata; Argentina.
- 92 Physics Department, Lancaster University, Lancaster; United Kingdom.
- 93 Oliver Lodge Laboratory, University of Liverpool, Liverpool; United Kingdom.
- 94 Department of Experimental Particle Physics, Jožef Stefan Institute and Department of Physics, University of Ljubljana, Ljubljana; Slovenia.
- 95 School of Physics and Astronomy, Queen Mary University of London, London; United Kingdom.
- 96 Department of Physics, Royal Holloway University of London, Egham; United Kingdom.
- 97 Department of Physics and Astronomy, University College London, London; United Kingdom.
- 98 Louisiana Tech University, Ruston LA; United States of America.
- 99 Fysiska institutionen, Lunds universitet, Lund; Sweden.
- 100 Departamento de Física Teórica C-15 and CIAFF, Universidad Autónoma de Madrid, Madrid; Spain.
- 101 Institut für Physik, Universität Mainz, Mainz; Germany.
- 102 School of Physics and Astronomy, University of Manchester, Manchester; United Kingdom.
- 103 CPPM, Aix-Marseille Université, CNRS/IN2P3, Marseille; France.
- 104 Department of Physics, University of Massachusetts, Amherst MA; United States of America.
- 105 Department of Physics, McGill University, Montreal QC; Canada.
- 106 School of Physics, University of Melbourne, Victoria; Australia.
- 107 Department of Physics, University of Michigan, Ann Arbor MI; United States of America.
- 108 Department of Physics and Astronomy, Michigan State University, East Lansing MI; United States of America.
- 109 Group of Particle Physics, University of Montreal, Montreal QC; Canada.
- 110 Fakultät für Physik, Ludwig-Maximilians-Universität München, München; Germany.
- 111 Max-Planck-Institut für Physik (Werner-Heisenberg-Institut), München; Germany.
- 112 Graduate School of Science and Kobayashi-Maskawa Institute, Nagoya University, Nagoya; Japan.
- 113 Department of Physics and Astronomy, University of New Mexico, Albuquerque NM; United States of America.
- 114 Institute for Mathematics, Astrophysics and Particle Physics, Radboud University/Nikhef, Nijmegen;

Netherlands.

<sup>115</sup>Nikhef National Institute for Subatomic Physics and University of Amsterdam, Amsterdam; Netherlands.

<sup>116</sup>Department of Physics, Northern Illinois University, DeKalb IL; United States of America.

<sup>117</sup>(<sup>a</sup>)New York University Abu Dhabi, Abu Dhabi;(<sup>b</sup>)United Arab Emirates University, Al Ain; United Arab Emirates.

<sup>118</sup>Department of Physics, New York University, New York NY; United States of America.

<sup>119</sup>Ochanomizu University, Otsuka, Bunkyo-ku, Tokyo; Japan.

<sup>120</sup>Ohio State University, Columbus OH; United States of America.

<sup>121</sup>Homer L. Dodge Department of Physics and Astronomy, University of Oklahoma, Norman OK; United States of America.

<sup>122</sup>Department of Physics, Oklahoma State University, Stillwater OK; United States of America.

<sup>123</sup>Palacký University, Joint Laboratory of Optics, Olomouc; Czech Republic.

<sup>124</sup>Institute for Fundamental Science, University of Oregon, Eugene, OR; United States of America.

<sup>125</sup>Graduate School of Science, Osaka University, Osaka; Japan.

<sup>126</sup>Department of Physics, University of Oslo, Oslo; Norway.

<sup>127</sup>Department of Physics, Oxford University, Oxford; United Kingdom.

<sup>128</sup>LPNHE, Sorbonne Université, Université Paris Cité, CNRS/IN2P3, Paris; France.

<sup>129</sup>Department of Physics, University of Pennsylvania, Philadelphia PA; United States of America.

<sup>130</sup>Department of Physics and Astronomy, University of Pittsburgh, Pittsburgh PA; United States of America.

<sup>131</sup>(<sup>a</sup>)Laboratório de Instrumentação e Física Experimental de Partículas - LIP, Lisboa;(<sup>b</sup>)Departamento de Física, Faculdade de Ciências, Universidade de Lisboa, Lisboa;(<sup>c</sup>)Departamento de Física, Universidade de Coimbra, Coimbra;(<sup>d</sup>)Centro de Física Nuclear da Universidade de Lisboa, Lisboa;(<sup>e</sup>)Departamento de Física, Universidade do Minho, Braga;(<sup>f</sup>)Departamento de Física Teórica y del Cosmos, Universidad de Granada, Granada (Spain);(<sup>g</sup>)Departamento de Física, Instituto Superior Técnico, Universidade de Lisboa, Lisboa; Portugal.

<sup>132</sup>Institute of Physics of the Czech Academy of Sciences, Prague; Czech Republic.

<sup>133</sup>Czech Technical University in Prague, Prague; Czech Republic.

<sup>134</sup>Charles University, Faculty of Mathematics and Physics, Prague; Czech Republic.

<sup>135</sup>Particle Physics Department, Rutherford Appleton Laboratory, Didcot; United Kingdom.

<sup>136</sup>IRFU, CEA, Université Paris-Saclay, Gif-sur-Yvette; France.

<sup>137</sup>Santa Cruz Institute for Particle Physics, University of California Santa Cruz, Santa Cruz CA; United States of America.

<sup>138</sup>(<sup>a</sup>)Departamento de Física, Pontificia Universidad Católica de Chile, Santiago;(<sup>b</sup>)Millennium Institute for Subatomic physics at high energy frontier (SAPHIR), Santiago;(<sup>c</sup>)Instituto de Investigación Multidisciplinario en Ciencia y Tecnología, y Departamento de Física, Universidad de La Serena;(<sup>d</sup>)Universidad Andres Bello, Department of Physics, Santiago;(<sup>e</sup>)Instituto de Alta Investigación, Universidad de Tarapacá, Arica;(<sup>f</sup>)Departamento de Física, Universidad Técnica Federico Santa María, Valparaíso; Chile.

<sup>139</sup>Department of Physics, University of Washington, Seattle WA; United States of America.

<sup>140</sup>Department of Physics and Astronomy, University of Sheffield, Sheffield; United Kingdom.

<sup>141</sup>Department of Physics, Shinshu University, Nagano; Japan.

<sup>142</sup>Department Physik, Universität Siegen, Siegen; Germany.

<sup>143</sup>Department of Physics, Simon Fraser University, Burnaby BC; Canada.

<sup>144</sup>SLAC National Accelerator Laboratory, Stanford CA; United States of America.

<sup>145</sup>Department of Physics, Royal Institute of Technology, Stockholm; Sweden.

- <sup>146</sup>Departments of Physics and Astronomy, Stony Brook University, Stony Brook NY; United States of America.
- <sup>147</sup>Department of Physics and Astronomy, University of Sussex, Brighton; United Kingdom.
- <sup>148</sup>School of Physics, University of Sydney, Sydney; Australia.
- <sup>149</sup>Institute of Physics, Academia Sinica, Taipei; Taiwan.
- <sup>150</sup><sup>(a)</sup>E. Andronikashvili Institute of Physics, Iv. Javakhishvili Tbilisi State University, Tbilisi;<sup>(b)</sup>High Energy Physics Institute, Tbilisi State University, Tbilisi;<sup>(c)</sup>University of Georgia, Tbilisi; Georgia.
- <sup>151</sup>Department of Physics, Technion, Israel Institute of Technology, Haifa; Israel.
- <sup>152</sup>Raymond and Beverly Sackler School of Physics and Astronomy, Tel Aviv University, Tel Aviv; Israel.
- <sup>153</sup>Department of Physics, Aristotle University of Thessaloniki, Thessaloniki; Greece.
- <sup>154</sup>International Center for Elementary Particle Physics and Department of Physics, University of Tokyo, Tokyo; Japan.
- <sup>155</sup>Department of Physics, Tokyo Institute of Technology, Tokyo; Japan.
- <sup>156</sup>Department of Physics, University of Toronto, Toronto ON; Canada.
- <sup>157</sup><sup>(a)</sup>TRIUMF, Vancouver BC;<sup>(b)</sup>Department of Physics and Astronomy, York University, Toronto ON; Canada.
- <sup>158</sup>Division of Physics and Tomonaga Center for the History of the Universe, Faculty of Pure and Applied Sciences, University of Tsukuba, Tsukuba; Japan.
- <sup>159</sup>Department of Physics and Astronomy, Tufts University, Medford MA; United States of America.
- <sup>160</sup>Department of Physics and Astronomy, University of California Irvine, Irvine CA; United States of America.
- <sup>161</sup>University of Sharjah, Sharjah; United Arab Emirates.
- <sup>162</sup>Department of Physics and Astronomy, University of Uppsala, Uppsala; Sweden.
- <sup>163</sup>Department of Physics, University of Illinois, Urbana IL; United States of America.
- <sup>164</sup>Instituto de Física Corpuscular (IFIC), Centro Mixto Universidad de Valencia - CSIC, Valencia; Spain.
- <sup>165</sup>Department of Physics, University of British Columbia, Vancouver BC; Canada.
- <sup>166</sup>Department of Physics and Astronomy, University of Victoria, Victoria BC; Canada.
- <sup>167</sup>Fakultät für Physik und Astronomie, Julius-Maximilians-Universität Würzburg, Würzburg; Germany.
- <sup>168</sup>Department of Physics, University of Warwick, Coventry; United Kingdom.
- <sup>169</sup>Waseda University, Tokyo; Japan.
- <sup>170</sup>Department of Particle Physics and Astrophysics, Weizmann Institute of Science, Rehovot; Israel.
- <sup>171</sup>Department of Physics, University of Wisconsin, Madison WI; United States of America.
- <sup>172</sup>Fakultät für Mathematik und Naturwissenschaften, Fachgruppe Physik, Bergische Universität Wuppertal, Wuppertal; Germany.
- <sup>173</sup>Department of Physics, Yale University, New Haven CT; United States of America.
- <sup>a</sup> Also Affiliated with an institute covered by a cooperation agreement with CERN.
- <sup>b</sup> Also at An-Najah National University, Nablus; Palestine.
- <sup>c</sup> Also at Borough of Manhattan Community College, City University of New York, New York NY; United States of America.
- <sup>d</sup> Also at Center for High Energy Physics, Peking University; China.
- <sup>e</sup> Also at Center for Interdisciplinary Research and Innovation (CIRI-AUTH), Thessaloniki; Greece.
- <sup>f</sup> Also at Centro Studi e Ricerche Enrico Fermi; Italy.
- <sup>g</sup> Also at CERN, Geneva; Switzerland.
- <sup>h</sup> Also at Département de Physique Nucléaire et Corpusculaire, Université de Genève, Genève; Switzerland.
- <sup>i</sup> Also at Departament de Física de la Universitat Autònoma de Barcelona, Barcelona; Spain.
- <sup>j</sup> Also at Department of Financial and Management Engineering, University of the Aegean, Chios; Greece.

- k* Also at Department of Physics, California State University, Sacramento; United States of America.
- l* Also at Department of Physics, King's College London, London; United Kingdom.
- m* Also at Department of Physics, Stanford University, Stanford CA; United States of America.
- n* Also at Department of Physics, Stellenbosch University; South Africa.
- o* Also at Department of Physics, University of Fribourg, Fribourg; Switzerland.
- p* Also at Department of Physics, University of Thessaly; Greece.
- q* Also at Department of Physics, Westmont College, Santa Barbara; United States of America.
- r* Also at Hellenic Open University, Patras; Greece.
- s* Also at Institutio Catalana de Recerca i Estudis Avancats, ICREA, Barcelona; Spain.
- t* Also at Institut für Experimentalphysik, Universität Hamburg, Hamburg; Germany.
- u* Also at Institute for Nuclear Research and Nuclear Energy (INRNE) of the Bulgarian Academy of Sciences, Sofia; Bulgaria.
- v* Also at Institute of Applied Physics, Mohammed VI Polytechnic University, Ben Guerir; Morocco.
- w* Also at Institute of Particle Physics (IPP); Canada.
- x* Also at Institute of Physics and Technology, Mongolian Academy of Sciences, Ulaanbaatar; Mongolia.
- y* Also at Institute of Physics, Azerbaijan Academy of Sciences, Baku; Azerbaijan.
- z* Also at Institute of Theoretical Physics, Ilia State University, Tbilisi; Georgia.
- aa* Also at Lawrence Livermore National Laboratory, Livermore; United States of America.
- ab* Also at National Institute of Physics, University of the Philippines Diliman (Philippines); Philippines.
- ac* Also at Technical University of Munich, Munich; Germany.
- ad* Also at The Collaborative Innovation Center of Quantum Matter (CICQM), Beijing; China.
- ae* Also at TRIUMF, Vancouver BC; Canada.
- af* Also at Università di Napoli Parthenope, Napoli; Italy.
- ag* Also at University of Colorado Boulder, Department of Physics, Colorado; United States of America.
- ah* Also at Washington College, Chestertown, MD; United States of America.
- ai* Also at Yeditepe University, Physics Department, Istanbul; Türkiye.
- \* Deceased